University of Alberta

STUDY OF THE EXCAVATION EFFECTS ON BURIED PIPELINES

By

MING HE ©

A thesis submitted to the Faculty of Graduate Studies and Research in partial fulfillment of the requirements for the degree of Master of Science

in

Structural Engineering

Department of Civil and Environmental Engineering

Edmonton, Alberta

Spring 2007

Your file Votre référence
ISBN: 978-0-494-29966-1
Our file Notre référence
ISBN: 978-0-494-29966-1

ABSTRACT

Ground movements will induce strains in pipes and pose a risk to the integrity of the pipeline. To solve this problem, one mitigation method is to excavate the buried pipeline located in hazardous area and to relieve the strain accumulated in the pipeline due to the soil movements. A series of tests were conducted using commonly excavation procedure to excavate the pipe under different conditions. In order to investigate the effect of soil condition, frozen versus loose soil, the tests were conducted both in summer and winter. The pipe was excavated under zero and 50% SMYS to study the effect of internal pressure on the excavation process. The maximum values of strains and deformations and the conditions resulting in the maximum excavation effects are analyzed. The effect of soil condition and internal pressure were investigated. By using ABAQUS program, a finite element model was also developed to model the pipe-soil interaction and the excavation procedure. Soil properties were obtained by conducting a series of geotechnical tests on soil samples collected from the field. The finite element results agreed quite well with the test results.

ACKNOWLEDGEMENTS

The author would like to thank Dr. J.J. Roger Cheng for his guidance throughout this project. The author also acknowledges the financial and technical support from the industrial sponsor TransCanada Pipelines Limited.

Many people have contributed to the success of this project. Dr. Mohammad R. Behbahanifard had provided direct assistance and support. Thanks to the geotechnical professors, Dr. Dave H. Chan, Dr. David C. Sego and the fellow graduate students, Zuo Long Chou, Bing Song and other students. The assistance from the technical staff in the I.F. Morrison Laboratory and Soil Mechanics Laboratory of the University of Alberta is also gratefully acknowledged.

Finally, the author would like to appreciate the encouragement and love from the author's family, wife Ying and daughter Jennifer.

TABLE OF CONTENTS

1 **INTRODUCTION** 1

1.1 **Statement of the Problem** 1

1.2 **Objectives and Scope** 2

1.3 **Background Information** 3

2 **EXPERIMENTAL PROGRAM** 8

2.1 **Test Specimen** 8

2.2 **Instrumentation** 8

2.2.1 Strain Gauge and Thermistor Layouts 8

2.2.2 Sealing Gland 9

2.2.3 Wiring 10

2.2.4 Digital Video Recorder 11

2.2.5 Internal Pressure 11

2.3 **Data Acquisition System** 11

2.4 **Measurement of Temperature** 12

2.5 **Test Arrangement** 12

2.6 **Test Procedures** 13

2.7 **Position of Excavator in the Tests** 14

2.8 **Temperature Measured During the Tests** 15

2.9 **Soil Condition** 15

3 **TEST RESULTS AND DATA ANALYSIS OF SUMMER EXCAVATION TESTS** 42

3.1 **Results of Summer Excavation Test** 42

3.1.1 Section 1 42

3.1.1.1 Hoop strains at the 0° 42

3.1.1.2 Hoop strains at the 180° 43

3.1.1.3 Hoop strains at the 90° 44

3.1.1.4 Longitudinal strains at the 0° and 180°..... 44

3.1.2 Section 2..... 45

3.1.2.1 Longitudinal strains at the 0° and 180°..... 45

3.1.3 Section 3..... 46

3.1.3.1 Hoop strains at the 0°..... 46

3.1.3.2 Hoop strains at the 180°..... 46

3.1.3.3 Hoop strains at the 45°..... 47

3.1.3.4 Hoop strains at the 315°..... 48

3.1.3.5 Hoop strains at the 90°..... 48

3.1.3.6 Hoop strains at the 270°..... 49

3.1.3.7 Longitudinal strains at the 0°..... 50

3.1.4 Section 4..... 50

3.1.4.1 Longitudinal strains at the 0° and 180° **50**

3.1.5 Section 5..... 51

3.1.5.1 Hoop strains at the 0°..... 51

3.1.5.2 Hoop strains at the 180°..... 52

3.1.5.3 Hoop strains at the 45°..... 53

3.1.5.4 Hoop strains at the 315°..... 53

3.1.5.5 Hoop strains at the 90°..... 54

3.1.5.6 Hoop strains at the 270°..... 55

3.1.5.7 Longitudinal strains at the 0°..... 55

3.1.6 Section 6..... 56

3.1.7 Section 7..... 57

3.1.7.1 Hoop strains at the 0°..... 57

3.1.7.2 Hoop strains at the 180°..... 58

3.1.7.3 Hoop strains at the 90°..... 58

3.1.7.4 Longitudinal strains at the 0° and 180° 59

3.1.8 Summary of Summer Test Results 60

3.2 Data Analysis of Summer Excavation Tests 60

3.2.1 Summer Un-pressurized Test 61

3.2.1.1 Hoop strains 61

3.2.1.2 Ovalization 61

3.2.1.3 Longitudinal strains 62

3.2.2 Comparison of Summer Un-pressurized Test 1 and 2 63

3.2.2.1 Hoop strains 63

3.2.2.2 Ovalization 64

3.2.2.3 Longitudinal strains 64

3.2.3 Summer Pressurized Test 65

3.2.3.1 Hoop strains 65

3.2.3.2 Ovalization 66

3.2.3.3 Longitudinal strains 67

3.2.4 Comparison of Summer Un-Pressurized and Pressurized Tests 67

3.2.4.1 Hoop strains 67

3.2.4.2 Ovalization 68

3.2.4.3 Longitudinal strains 68

3.3 Impact Factor 69

4 TEST RESULTS AND DATA ANALYSIS OF WINTER EXCAVATION TESTS 118

4.1 Winter Pressurized Test 118

4.1.1 Test Results of Pressurized Test 118

4.1.1.1 Strains from low-speed data acquisition system 118

4.1.1.2 Comparison of strains obtained from high-speed and low-speed data acquisition system 119
4.1.1.3 Ovalization 121
4.2 Winter Un-pressurized Test 122
4.2.1 Test Results of Un-pressurized Test 122
4.2.1.1 Section 1 122
4.2.1.2 Section 2 and Section 3 123
4.2.1.3 Section 4 and Section 5 127
4.2.1.4 Section 6 129
4.2.1.5 Section 7 130
4.2.2 Comparison of Hoop Strain in High-speed and Low-speed 131
4.3 Comparison of Winter Pressurized Test and Winter Un-pressurized Test 133
4.3.1 Hoop strains 133
4.3.2 Ovalization 134
4.3.3 Longitudinal Strains 135
4.4 Impact Factor 135

5 COMPARISONS OF SUMMER AND WINTER TESTS 169
5.1 Comparisons of Summer Tests and Winter Tests 169
5.1.1 Hoop strain 169
5.1.2 Ovalization 170
5.1.3 Longitudinal Strain 171
5.2 Summary of Summer and Winter Excavation Tests 171
5.3 Conclusions of Summer and Winter Excavation Tests 178

6 SOIL TESTS 191

6.1 Introduction..... 191
6.2 Soil Tests..... 191
6.2.1 Soil Classification Tests..... 191
6.2.2 Triaxial Tests..... 192
6.3 Test Data Analysis..... 193
6.3.1 Soil Classification..... 193
6.3.2 Determination of Modulus of Elasticity..... 193
6.3.3 Determination of Shear Strength..... 194
6.3.4 Other Soil Parameters from CU Triaxial Test..... 194

7 FINITE ELEMENT ANALYSIS..... 201
7.1 Introduction..... 201
7.2 Description of Models..... 201
7.2.1 Mesh Selection..... 201
7.2.2 Elements..... 203
7.2.3 Material Models..... 203
7.2.4 Multi-point constraints (MPC)..... 210
7.2.5 Boundary Condition..... 211
7.2.6 Loading Condition – Excavator..... 212
7.2.7 Excavation – Removal of Soil..... 213
7.2.8 Steps to Simulate Excavation Process..... 213

8 DISCUSSION OF EXPERIMENTAL AND NUMERICAL RESULTS..... 226
8.1 Comparison of Test and FEA Results..... 226
8.2 Discuss of the Results of Test and FEA..... 226
8.2.1 Hoop Strain..... 226
8.2.3 Deformation..... 227
8.2.3 Longitudinal Strain..... 228
8.3 *Factors Influencing the Simulation in the FEA Model*..... 228

9 SUMMARY, CONCLUSIONS AND RECOMMENDATIONS..... 247

9.1 Summary..... 247

9.2 Conclusions..... 248

9.3 Recommendations..... 250

REFERENCES..... 252

LIST OF TABLES

Table 2.1	Summary of arrangement of strain gauges.....	16
Table 2.2	The calibration factors of four extensometers used for measuring ovalization.....	18
Table 2.3	Excavator position of summer un-pressurized test (test 1).....	18
Table 2.4	Excavator position of summer un-pressurized test (test 2).....	19
Table 2.5	Excavator position of summer pressurized test.....	19
Table 2.6	Position of excavator in winter un-pressurized test.....	20
Table 2.7	Temperature measured in the summer excavation tests.....	21
Table 3.1	Summary result of hoop strain in summer un-pressurized test 1.....	71
Table 3.2	Summary results of ovalization measured at Section 6 in summer un-pressurized test 1.....	72
Table 3.3	Maximum deformation measured in summer un-pressurized tests.....	72
Table 3.4	Summary result of longitudinal strain in summer un-pressurized test 1	73
Table 3.5	Comparison of hoop strain between summer un-pressurized test 1 and 2.....	74
Table 3.6	Comparison of ovalization between summer un-pressurized test 1 and 2.....	74
Table 3.7	Comparison of longitudinal strain between summer un-pressurized test 1 and 2.....	75
Table 3.8	Summary of the hoop strain in summer pressurized test.....	75
Table 3.9	Summary of the deformation measured at section 6 in summer pressurized test.....	77
Table 3.10	Summary of the longitudinal strain in summer pressurized test.....	78
Table 3.11	Comparison of maximum hoop strain between summer un-pressurized test and pressurized test.....	79
Table 3.12	Comparison of maximum vertical and horizontal deformation between summer un-pressurized test and pressurized test (unit: mm).....	80

Table 3.13 Comparison of maximum diagonal deformation between summer un-pressurized test and pressurized test..... 80
Table 3.14 Comparison of maximum ovalization between summer un-pressurized test and pressurized test..... 80
Table 3.15 Comparison of maximum longitudinal strain between summer un-pressurized test and pressurized test..... 81

Table 4.1 Comparison of maximum hoop strains captured by high-speed and low-speed DAS in winter pressurized test..... 137
Table 4.2 Comparison of maximum hoop strains captured by high-speed and low-speed DAS in winter un-pressurized test..... 137
Table 4.3 Comparison of the maximum strain and ovalization between winter pressurized test and un-pressurized test..... 138

Table 5.1 Summaries of maximum hoop strains, ovalization and longitudinal strain in summer excavation tests..... 180
Table 5.2 Summaries of maximum hoop strains, ovalization and longitudinal strain in winter excavation tests..... 180
Table 5.3 Effects of Internal Pressure in Summer Tests..... 181
Table 5.4 Effects of Internal Pressure in Winter Tests..... 182
Table 5.5 Summary of the maximum hoop strain, ovalization and longitudinal strain in summer and winter tests..... 183
Table 5.6 Comparison of maximum strain and ovalization in summer and winter test under critical condition 1..... 184
Table 5.7 Summary of impact factors..... 185
Table 5.8 Summaries of maximum hoop strains, ovalization and longitudinal strain in summer and winter excavation tests..... 185
Table 5.9 Critical conditions in summer tests..... 186
Table 5.10 Critical conditions in winter tests..... 186

Table 6.1 Modulus of elasticity determined in CU triaxial tests..... 195

Table 6.2 Other soil parameters determined from CU triaxial test..... 195

Table 8.1 Comparison of maximum hoop strain between test and FEA..... 230
Table 8.2 Comparison of maximum deformation between test and FEA..... 230
Table 8.3 Comparison of maximum longitudinal strain between test and FEA under critical condition 1..... 230
Table 8.4 Comparison of maximum longitudinal strain between test and FEA under critical condition 2..... 231

LIST OF FIGURES

Figure 1.1	Assumed soil pressure distribution (Spangler and Handy, 1982).....	6
Figure 1.2	Influence of external and internal pressure on the deformation of the cross-section of pipeline (Spangler and Handy, 1982).....	6
Figure 1.3	Load effect of excavator.....	7
Figure 2.1	Specimen before modification.....	22
Figure 2.2	Specimen after modification.....	22
Figure 2.3	Instrumentation section layouts.....	23
Figure 2.4	Strain gauge layouts at sections 1, 2, 3 and 4.....	24
Figure 2.5	Strain gauge layouts at sections 5, 6 and 7.....	25
Figure 2.6	Composition of device for measuring ovalization.....	26
Figure 2.7	Extensometers, device for measuring ovalization being calibrated in the I.F. Morrison Structural Laboratory at the University of Alberta	27
Figure 2.8	Calibration curve------relationship between strain and deformation...	27
Figure 2.9	Initial tension strain set-up of device for measuring ovalization.....	28
Figure 2.10	Extensometers, device for measuring ovalization installed at section 6.....	28
Figure 2.11	Thermistor being waterproofed.....	29
Figure 2.12	Sealing gland.....	29
Figure 2.13	Reducer was fitted in the opening in the pipe.....	30
Figure 2.14	Sealing gland was put into the opening.....	30
Figure 2.15	Secure the gland body.....	31
Figure 2.16	The sealing gland was connected with the internal strain gauge inside the pipeline.....	31
Figure 2.17	Outside of sealing gland after wiring.....	32
Figure 2.18	Excavator used in summer test------Komatsu Avance PC 220LC.....	32
Figure 1.19	Excavator used in winter excavation test------ DEERE 270C LC.....	33
Figure 2.20	Excavator position---excavation length.....	33
Figure 2.21	Excavator position---left side and right side.....	34

Figure 2.22 Schematic diagram of the position of excavator in summer tests (Top view)..... 35
Figure 2.23 Schematic diagram of the position of excavator in winter un-pressurized test (Top view)..... 36
Figure 2.24 Excavation process in summer..... 36
Figure 2.25 Exposed portion of the pipeline after excavation in summer..... 37
Figure 2.26 Removal of the side soil in winter excavation test..... 37
Figure 2.27 Removal of the top soil in winter excavation test..... 38
Figure 2.28 The excavated pipeline after winter un-pressurized test..... 39
Figure 2.29 Temperature history in winter pressurized excavation test..... 40
Figure 2.30 Temperature history in winter un-pressurized excavation test..... 40
Figure 2.31 Frozen line observed in winter excavation test..... 41

Figure 3.1 Results of hoop strain at the top (0°) of section 1 in summer test 1, 2, & 3 (low speed data)..... 82
Figure 3.2 Results of hoop strain at the bottom (180°) of section 1 in summer test 1, 2, & 3 (low speed data)..... 83
Figure 3.3 Results of hoop strain at the side (90°) of section 1 in summer test 1, 2, & 3 (low speed data)..... 84
Figure 3.4 Results of longitudinal strain at the top (0°) and bottom (180°) of section 1 in summer test 1, 2, & 3 (low speed data)..... 85
Figure 3.5 Results of longitudinal strain at the top (0°) and bottom (180°) of section 2 in summer test 1, 2, & 3 (low speed data)..... 86
Figure 3.6 Results of hoop strain at the top (0°) of section 3 in summer test 1, 2, & 3 (low speed data)..... 87
Figure 3.7 Results of hoop strain at the bottom (180°) of section 3 in summer test 1, 2, & 3 (low speed data)..... 88
Figure 3.8 Results of hoop strain (45°) of section 3 in summer test 1, 2, & 3 (low speed data)..... 89
Figure 3.9 Results of hoop strain (315°) of section 3 in summer test 1, 2, & 3 (low speed data)..... 90

Figure 3.10 Results of hoop strain at the side (90°) of section 3 in summer test 1, 2, & 3 (low speed data)..... 91
Figure 3.11 Results of hoop strain at the side (270°) of section 3 in summer test 1, 2, & 3 (low speed data)..... 92
Figure 3.12 Results of longitudinal strain at the top (0°) of section 3 in summer test 1, 2, & 3 (low speed data)..... 93
Figure 3.13 Results of longitudinal strain at the top (0°) and bottom (180°) of section 4 in summer test 1, 2, & 3 (low speed data)..... 94
Figure 3.14 Results of hoop strain at the top (0°) of section 5 in summer test 1, 2, & 3 (low speed data)..... 95
Figure 3.15 Results of hoop strain at the bottom (180°) of section 5 in summer test 1, 2, & 3 (low speed data)..... 96
Figure 3.16 Results of hoop strain (45°) of section 5 in summer test 1, 2, & 3 (low speed data)..... 97
Figure 3.17 Results of hoop strain (315°) of section 5 in summer test 1, 2, & 3 (low speed data)..... 98
Figure 3.18 Results of hoop strain at the side (90°) of section 5 in summer test 1, 2, & 3 (low speed data)..... 99
Figure 3.19 Results of hoop strain at the side (270°) of section 5 in summer test 1, 2, & 3 (low speed data)..... 100
Figure 3.20 Results of longitudinal strain at the top (0°) of section 5 in summer test 1, 2, & 3 (low speed data)..... 101
Figure 3.21 Results of deformation (vertical and horizontal) of section 6 in summer test 1, 2, & 3 (low speed data)..... 102
Figure 3.22 Results of deformation (diagonal) of section 6 in summer test 1, 2, & 3 (static readings)..... 103
Figure 3.23 Results of hoop strain at the top (0°) of section 7 in summer test 1, 2, & 3 (low speed data)..... 104
Figure 3.24 Results of hoop strain at the bottom (180°) of section 7 in summer test 1, 2, & 3 (low speed data)..... 105

Figure 3.25 Results of hoop strain at the side (90°) of section 7 in summer test 1, 2, & 3 (low speed data)..... 106
Figure 3.26 Results of longitudinal strain at the top (0°) and the bottom (180°) of section 7 in summer test 1, 2, & 3 (low speed data)..... 107
Figure 3.27 Maximum hoop strain in summer un-pressurized test 1 at buried state..... 108
Figure 3.28 Maximum hoop strain in summer un-pressurized test at exposed state..... 108
Figure 3.29 Maximum deformation and ovalization in summer un-pressurized test 1..... 109
Figure 3.30 Schematic diagram of longitudinal deformation in excavation process..... 110
Figure 3.31 Maximum longitudinal strain in summer un-pressurized test 1 at buried state..... 111
Figure 3 32 Maximum longitudinal strain in summer un-pressurized test 1 at exposed state..... 111
Figure 3.33 Maximum hoop strain in summer pressurized test---Situation 1..... 112
Figure 3.34 Maximum hoop strain in summer pressurized test---Situation 2..... 112
Figure 3.35 Maximum hoop strain in summer pressurized test---Situation 3..... 112
Figure 3.36 Maximum longitudinal strain in summer pressurized test at buried state..... 113
Figure 3.37 Maximum longitudinal strain in summer pressurized test at exposed state..... 113
Figure 3.38 Comparison of maximum hoop strains between summer un-pressurized and pressurized tests..... 114
Figure 3.39 Comparison of maximum ovalization between summer un-pressurized and pressurized tests..... 115
Figure 3.40 Comparison of maximum longitudinal strains between summer un-pressurized and pressurized tests..... 116
Figure 3.41 Impact factors of hoop strain in summer un-pressurized tests..... 117
Figure 3.42 Impact factors of longitudinal strain in summer un-pressurized tests.. 117

Figure 4.1 Hoop strain at the top (0°) of section 1 in winter pressurized test, low speed..... 139
Figure 4.2 Hoop strain at the right side (90°) of section 1 in winter pressurized test, low speed..... 139
Figure 4.3 Hoop strain at the bottom (180°) of section 1 in winter pressurized test, low speed..... 140
Figure 4.4 Longitudinal strain at the top (0°) and bottom (180°) of section 1 in winter pressurized test, low speed..... 140
Figure 4.5 Longitudinal strain at the top (0°) and bottom (180°) of section 2 in winter test 1, low speed..... 141
Figure 4.6 Longitudinal strain at the top (0°) of section 3 in winter pressurized test, low speed..... 141
Figure 4.7 Hoop strain at the top (0°) of section 2 (high speed) and section 3 (low speed) in winter pressurized test..... 142
Figure 4.8 Hoop strain at the 30° of section 2 (high speed) and the 45° of section 3 (low speed) in winter pressurized test..... 142
Figure 4.9 Hoop strain at the 60° of section 2 (high speed) and the 45° of section 3 (low speed) in winter pressurized test..... 143
Figure 4.10 Hoop strain at the right side (90°) of section 2 (high speed) and section 3 (low speed) in winter pressurized test..... 143
Figure 4.11 Hoop strain at the bottom (180°) of section 2 (high speed) and section 3 (low speed) in winter pressurized test..... 144
Figure 4.12 Hoop strain at the left side (270°) of section 2 (high speed) and section 3 (low speed) in winter pressurized test..... 144
Figure 4.13 Hoop strain at the 315° of section 2 (high speed) and section 3 (low speed) in winter pressurized test..... 145

Figure 4.14 Comparison of maximum hoop strains in high-speed and low-speed in winter pressurized test..... 145
Figure 4.15 Deformation in vertical and horizontal direction at section 6 (low speed) in winter pressurized test..... 146
Figure 4.16 Deformation in diagonal direction at section 6 (low speed) in winter pressurized test..... 146
Figure 4.17 Hoop strain at the bottom (180°) of section 1 in winter un-pressurized test, low speed..... 147
Figure 4.18 Longitudinal strain at bottom (180°) of section 1 in winter un-pressurized test, low speed..... 147
Figure 4.19 Longitudinal strain at the top (0°) and bottom (180°) of section 2 in winter un-pressurized test, low speed..... 148
Figure 4.20 Longitudinal strain at bottom (180°) of section 3 in winter un-pressurized test, low speed..... 148
Figure 4.21 Hoop strain at the top (0°) of section 2 (high speed) and section 3 (low speed) in winter un-pressurized test..... 149
Figure 4.22 Hoop strain at the 30° of section 2 (high speed) and the 45° of section 3 (low speed) in winter un-pressurized test..... 149
Figure 4.23 Hoop strain at the 60° of section 2 (high speed) and the 45° of section 3 (low speed) in winter un-pressurized test..... 150
Figure 4.24 Hoop strain at the right side (90°) of section 2 (high speed) and section 3 (low speed) in winter un-pressurized test..... 150
Figure 4.25 Hoop strain at the bottom (180°) of section 2 (high speed) and section 3 (low speed) in winter un-pressurized test..... 151
Figure 4.26 Hoop strain at the left side (270°) of section 2 (high speed) and section 3 (low speed) in winter un-pressurized test..... 151
Figure 4.27 Hoop strain at the 315° of section 2 (high speed) and section 3 (low speed) in winter un-pressurized test..... 152
Figure 4.28 Longitudinal strain at the top (0°) and bottom (180°) of section 4 in winter un-pressurized test, low speed..... 152

Figure 4.29 Longitudinal strain at the top (0°) of section 5 in winter un-pressurized test, low speed..... 153
Figure 4.30 Hoop strain at the top (0°) of section 4 (high speed) and section 5 (low speed) in winter un-pressurized test..... 153
Figure 4.31 Hoop strain at the 45° of section 4 (high speed) and section 5 (low speed) in winter un-pressurized test..... 154
Figure 4.32 Hoop strain at the 45° of section 4 (high speed) and the 315° of section 5 (low speed) in winter un-pressurized test..... 154
Figure 4.33 Hoop strain at the right side (90°) of section 4 (high speed) and section 5 (low speed) in winter un-pressurized test..... 155
Figure 4.34 Hoop strain at the bottom (180°) of section 4 (high speed) and section 5 (low speed) in winter un-pressurized test..... 155
Figure 4.35 Hoop strain at the left side (270°) of section 4 (high speed) and section 5 (low speed) in winter un-pressurized test..... 156
Figure 4.36 Deformation in vertical and horizontal direction at section 6 (low speed) in winter un-pressurized test..... 156
Figure 4.37 Deformation in diagonal direction at section 6 (low speed) in winter un-pressurized test..... 157
Figure 4.38 Hoop strain at the top (0°) of section 7 in winter un-pressurized test, low speed..... 157
Figure 4.39 Hoop strain at the right side (90°) of section 7 in winter un-pressurized test, low speed..... 158
Figure 4.40 Hoop strain at the bottom (180°) of section 7 in winter un-pressurized test, low speed..... 158
Figure 4.41 Longitudinal strain at the top (0°) and bottom (180°) of section 7 in winter un-pressurized test, low speed..... 159
Figure 4.42 Comparison of maximum hoop strain in high speed and low speed in winter un-pressurized test at buried state..... 160

Figure 4.43 Transient hoop strain at 45° position of section 4 at second of 5638 captured by high speed DAS in winter un-pressurized test..... 161
Figure 4.44 Transient hoop strain at right side of section 4 (90°) at second of 5633 captured by high speed DAS in winter un-pressurized test..... 161
Figure 4.45 Transient hoop strain at left side of section 4 (270°) at second of 6816 captured by high speed DAS in winter un-pressurized test..... 162
Figure 4.46 Comparison of maximum hoop strain in high speed and low speed in winter un-pressurized test at exposed state..... 162
Figure 4.47 Comparison of hoop strain reversal captured by high speed and low speed DAS in winter un-pressurized test..... 163
Figure 4.48 Hoop strain reversal at 30° of section 2 and 45° of section 3 at second of 4976 in high speed and low speed in winter un-pressurized test..... 163
Figure 4.49 Hoop strain reversal at right side (90°) of section 2 and section 3 at second of 4976in high speed and low speed in winter un-pressurized test..... 164
Figure 4.50 Hoop strain reversal at left side (270°) of section 2 and section 3 at second of 6067 in high speed and low speed in winter un-pressurized test..... 164
Figure 4.51 Hoop strain reversal at the 315° position of section 2 and section 3 at second of 3896 in high speed and low speed in winter un-pressurized test..... 165
Figure 4.52 Comparison of maximum hoop strain of winter pressurized test and un-pressurized test (high speed)..... 165
Figure 4.53 Comparison of maximum hoop strain of winter pressurized test and un-pressurized test (low speed)..... 166
Figure 4.54 Comparison of maximum ovalization of winter pressurized test and un-pressurized test at buried state..... 166

Figure 4.55 Comparison of maximum longitudinal strain of winter pressurized test and un-pressurized test in the instrumented section that the excavator is directly sitting on..... 167
Figure 4.56 Impact factors of hoop strain (high speed) in winter un-pressurized test..... 167
Figure 4.57 Impact factors of hoop strain (low speed) in winter un-pressurized test..... 168
Figure 4.58 Impact factors of longitudinal strain in winter un-pressurized test..... 168

Figure 5.1 Comparison of maximum hoop strain in summer test (low speed) and winter test (low speed and high speed)..... 187
Figure 5.2 Comparison of maximum ovalization in summer test and winter test. 188
Figure 5.3 Comparison of maximum longitudinal strain in summer test and winter test..... 189
Figure 5.4 Critical conditions (summer or winter)..... 190
Figure 5.5 Critical conditions (winter)..... 190

Figure 6.1 Grain size curve..... 196
Figure 6.2 Soil sample taken from excavation field for CU triaxial test..... 197
Figure 6.3 CU triaxial test setup..... 198
Figure 6.4 Soil sample after CU triaxial test..... 198
Figure 6.5 Soil classification..... 199
Figure 6.6 Results of CU triaxial tests..... 199
Figure 6.7 Effective stress failure envelops for CU triaxial tests..... 200

Figure 7.1 Contours of equal vertical stress under a loaded area of width B according to Boussinesq analysis (Spangler, 1982)..... 216
Figure 7.2 Dimension of the mesh in X-Z plane (only left part was shown and the right part is symmetry)..... 217
Figure 7.3 Whole meshes in X-Z plane..... 218
Figure 7.4 Whole meshes in X-Z plane after excavation..... 218

Figure 7.5 Mesh in Y-Z plane (X=0)..... 219
Figure 7.6 Porous elastic volumetric behaviour..... 219
Figure 7.7 Clay yield surface in the p-t plane..... 220
Figure 7.8 Clay yield surface sections in the Π-plane..... 220
Figure 7.9 Modulus of elasticity E, varied with depth of soil (n=1.3475, K=1278)..... 221
Figure 7.10 Determination of M, slope of critical state line by CU triaxial test.... 221
Figure 7.11 Normal consolidation and overconsolidation..... 222
Figure 7.12 MPC around the circumferential direction..... 222
Figure 7.13 Excavator positions during excavation process..... 223
Figure 7.14 Critical positions of excavator during excavation process..... 223
Figure 7.15 Four loading cases in a period of digging..... 225

Figure 8.1 Comparison of hoop strain at top of section 1 between test and FEA results..... 232
Figure 8.2 Comparison of hoop strain at right side of section 1 between test and FEA results..... 232
Figure 8.3 Comparison of hoop strain at bottom of section 1 between test and FEA results..... 233
Figure 8.4 Comparison of longitudinal strain at top and bottom of section 1 between test and FEA results..... 233
Figure 8.5 Comparison of longitudinal strain at top and bottom of section 2 between test and FEA results..... 234
Figure 8.6 Comparison of hoop strain at top of section 3 between test and FEA results..... 234
Figure 8.7 Comparison of hoop strain at right side of section 3 between test and FEA results..... 235
Figure 8.8 Comparison of hoop strain at bottom of section 3 between test and FEA results..... 235
Figure 8.9 Comparison of hoop strain at left side of section 3 between test and FEA results..... 236

Figure 8.10 Comparison of longitudinal strain at top of section 3 between test and FEA results..... 236
Figure 8.11 Comparison of longitudinal strain at top and bottom of section 4 between test and FEA results..... 237
Figure 8.12 Comparison of hoop strain at top of section 5 between test and FEA results..... 237
Figure 8.13 Comparison of hoop strain at right side of section 5 between test and FEA results..... 238
Figure 8.14 Comparison of hoop strain at bottom of section 5 between test and FEA results..... 238
Figure 8.15 Comparison of hoop strain at left side of section 5 between test and FEA results..... 239
Figure 8.16 Comparison of longitudinal strain at top of section 5 between test and FEA results..... 239
Figure 8.17 Comparison of deformation in vertical and horizontal direction at section 6 between test and FEA results..... 240
Figure 8.18 Comparison of hoop strain at top of section 7 between test and FEA results..... 240
Figure 8.19 Comparison of hoop strain at right side of section 7 between test and FEA results..... 241
Figure 8.20 Comparison of hoop strain at bottom of section 7 between test and FEA results..... 241
Figure 8.21 Comparison of longitudinal strain at top and bottom of section 7 between test and FEA results..... 242
Figure 8.22 Typical process of deformation in excavation..... 246

LIST OF SYMBOLS

a	value of the equivalent pressure stress at critical state
a_0	hardening parameter
A	average area of each node with axial spring
C_C	compression index
C_S	swelling index
e_0	initial void ratio
e^{el}	deviatoric part of the total elastic strain
E	modulus of elasticity
E_i	initial tangent modulus
G	shear modulus
k'	modulus of subgrade reaction
K	ratio of the flow stress in triaxial tension to the flow stress in triaxial compression or modulus number
K_0	coefficient of earth pressure at rest
LL	liquid limit
J^{el}	elastic part of the volume ratio between the current and reference configurations
J^{pl}	inelastic volume change
M	material parameter defining the slope of the critical state lines
n	exponent determining the rate of variation of E_i and σ_3'
p	equivalent pressure stress

p_0 initial value of the equivalent pressure stress

p_a atmospheric pressure

p_t^{el} "elastic tensile strength" of the material

R_p overconsoildation ratio

S deviatoric stress

β "capping" parameter used to provide a different shaped yield ellipse on the wet side of critical state

ε_{vol}^{el} elastic part of volume strain

φ' Mohr-Coulomb friction angle

κ logarithmic bulk modulus

λ logarithmic hardening constant defined in the *CLAY PLASTICITY option

v Poisson ratio

σ_3 the minor principal stress or minor effective principal stress

σ_v vertical normal stress

1 INTRODUCTION

1.1 Statement of the Problem

There are two main geotechnical mechanisms that cause ground movement and produce strains in buried pipelines in Alberta (Rizkalla et al., 1993). Slope instability of river valleys is the primary mechanism, and the other one is differential thaw settlement. Ground movements will induce strains in pipes and pose a risk to the integrity of the pipeline. To solve this problem, one mitigation method is to excavate the buried pipeline located in a hazardous area and to relieve the strain accumulated in the pipeline due to the soil movements (Braun et al., 1998).

As a part of the integrity program, the in-line inspection is often followed by the defect assessment and determination of the excavation location. The defects can be confirmed and repaired in the field through excavation. Dent is a kind of defect which may contain cracks. During an excavation process, the excavator creates additional strains and deformations in the pipeline. In some situations the additional strains due to excavation might trigger the formation of a wrinkle or even a fracture in the pipeline. The cracks are likely to grow through the wall during excavation (McCoy et al., 2004). Therefore, for a pipeline located in a hazardous area which might contain some kind of defects, the effects of excavation in this process are very important safety issues.

In addition, due to potential damage to the pipe caused by excavation, the operation pressure might need to be limited during excavation. Therefore, the amount of oil or gas transported will decrease to bring about economical loss. How to make a correct assessment of the excavation effects and determine a safe internal pressure under excavation has become a necessity for the economical consideration.

With the exploration of oil and gas resources into the Canadian North, the pipelines have increasingly become exposed to the extreme harsh environments. The regular maintenance of the pipeline has to take into account of the soil condition, season and the feasibility of using heavy machines. The excavation might be performed under frozen soil condition in winter. The effect of excavation on the buried pipeline in frozen soil can be significant; for example, the dynamic effects caused by the digging of excavator on the frozen, hard soil.

In summary, the investigation of effects of excavation on the buried pipelines is important for the safe and economical operation and maintenance of buried pipelines.

1.2 Objectives and Scope

In order to investigate the effects of excavation on the buried pipeline, a series of tests were conducted on a full-scale buried pipe specimen in the field. Test parameters, such as seasonal condition (summer or winter), type of soil, magnitude of internal pressure, type of excavator, procedure of excavation and temperature change, were considered in the program to study the magnitude and distribution of stresses, strains and deformations in a pipeline during an excavation. Of course, soil cover depth and pipe diameter and thickness are also important variables for consideration in the test program.

The experimental work is complemented by the finite element analysis that provides a numerical simulation of the behaviour of the tested specimen. The goal of the numerical study is to develop a finite element model validated using field test results, and to facilitate the extension of the experimental database to various pipeline specifications in the future.

The primary objectives of this study can be summarized as follows:

1. To determine the additional strains and deformations imposed on a pipeline during the excavation process;
2. To investigate the behaviour of pipeline under different excavation parameters, mainly soil condition and internal pressure;
3. To capture the dynamic effects on a buried pipeline during the excavation process;
4. To develop a finite element model to simulate the excavation process and validate it with field tests.

1.3 Background Information

The impact due to the excavation machine is defined as accidental loads in the Canadian Standard, Oil and Gas Pipeline System (CSA Z662, 2003). The required minimum buried depth is specified in the Standard to minimize the stresses in the buried pipe and the effects of the impact load.

A significant amount of research has been done on the loads on underground conduits by Spangler and Handy (1982). Based on the field loading experiment, the assumed soil pressure distribution is shown graphically in Figure 1.1 for flexible pipe buried under ground. The vertical load may be determined by Marston's theory of load on conduit (Spangler and Handy, 1982). The vertical reaction is distributed over the width of bedding of the pipe. The horizontal pressure is assumed distributed parabolically and determined using the modulus of passive resistance (e) or modulus of soil reaction (E') and horizontal deflection of the pipe. The formula for computing the horizontal deflection (may be considered the same as the vertical deflection) is

$$\Delta_x = D_l \frac{KW_c r^3}{EI + 0.061E'r^3} \qquad [1.1]$$

in which

Δ_x = horizontal deflection

D_l = deflection lag factor

K = a bedding constant

W_c = vertical load per unit length

r = mean radius of the pipe

E = modulus of elasticity of pipe material

I = moment of inertia per unit length of cross section of pipe wall

$E' = er$ = modulus of soil reaction

e = modulus of passive resistance of enveloping soil

In addition to supporting dead loads imposed by earth cover, buried pipes can also be exposed to superimposed concentrated or distributed live loads. Large concentrated loads, such as those caused by truck-wheel, railway car, locomotive, and aircraft at airports are of most practical interest (ALA, 2001). The live loads transferred to the pipe from different vehicles are specified with the height of cover (ALA, 2001). Live load due to traffic, usually a static concentrated surface load, is calculated using Boussinesq equation as recommended by Spangler and Handy (1982). Under the effect of earth and surface loads, the through-wall bending stress in the buried pipe is estimated according to (ALA, 2001):

$$\sigma_{bw} = 4E(\frac{\Delta y}{D})(\frac{t}{D}) \qquad [1.2]$$

where:

σ_{bw} = through bending stress

E = modulus of elasticity of pipe

Δy = vertical deflection of pipe which can be determined using the formula similar to equation [1.1], for detail see reference (ALA, 2001)

t = pipe wall thickness

D = outside diameter of pipe.

The impact factor of moving vehicle ranges from 1.5 to 2.0 (Spangler and Handy, 1982). An impact factor 1.5 is given to account for bumps and irregularities in the travel surface (ALA, 2001). The impact loads due to the large weight falling can also be found and determined according to this guideline.

The influence of internal pressure is shown in Figure 1.2 (Spangler and Handy, 1982). The internal pressure can re-round the shape with an intermediate ellipse between a circle and the deflected shape under external load (*i.e.*, filling soil) alone.

There are various methods for predicting the structural behaviour of flexible conduit and the in-depth analysis of the strength and weakness of these methods are conducted and summarized by Moser (2001). In particular, the research at Utah State University (Moser, 2001) has shown that the finite element method (FEM) is an effective method in predicting the behaviour of large-diameter HDPE (High Density Polyethylene) pipes.

No research has been found regarding the effect of excavator during excavation process. The excavator usually sits on the pipe during the excavation process. The excavator weight is a main load. As shown in Figure 1.3, the operation of excavator may also produce dynamic loads because of the rocking and movement of bucket and boom.

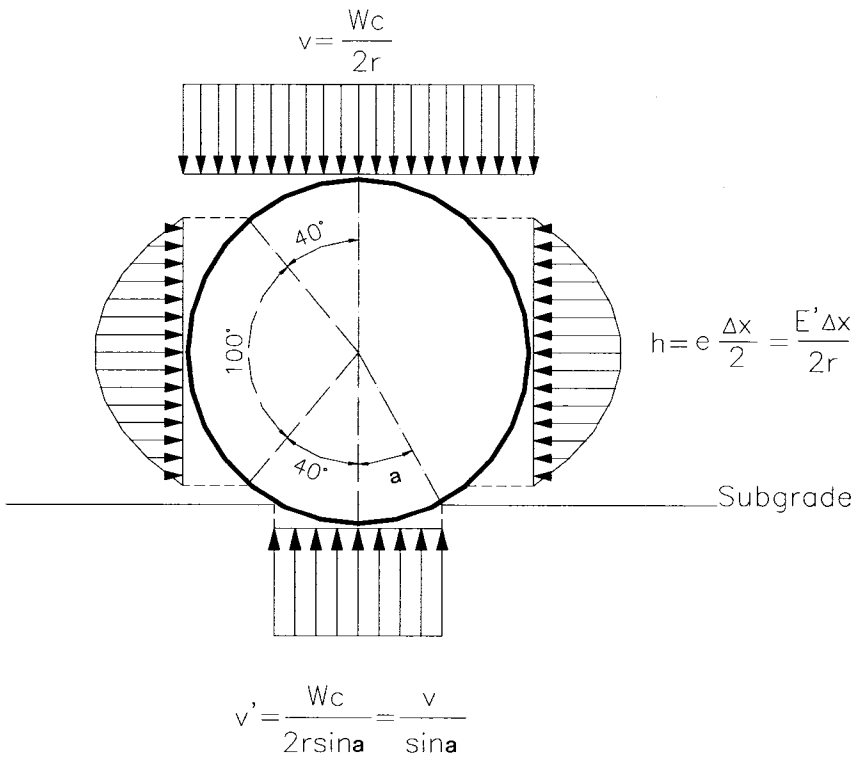

Figure 1.1 Assumed soil pressure distribution (Spangler and Handy, 1982)

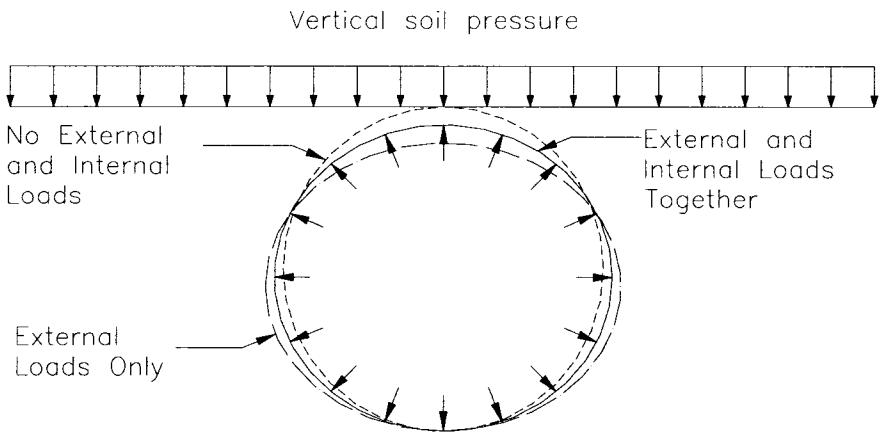

Figure 1.2 Influence of external and internal pressure on the deformation of the cross-section of pipeline (Spangler and Handy, 1982)

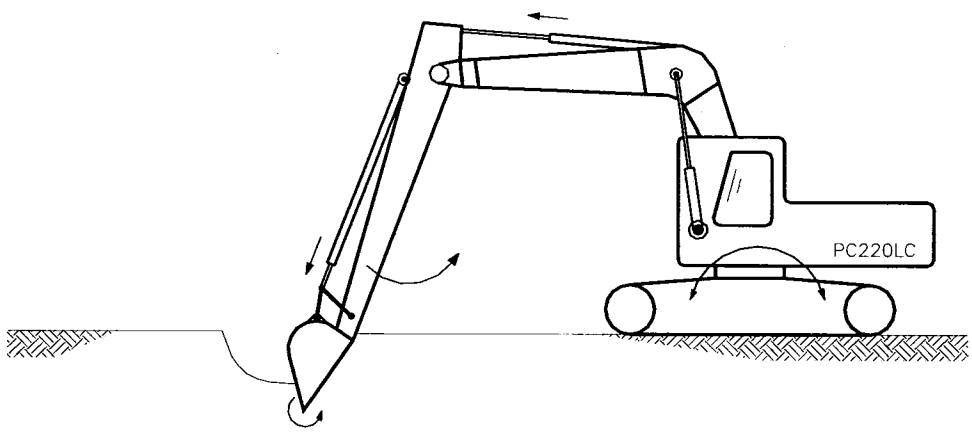

Figure 1.3 Load effect of excavator

2 EXPERIMENTAL PROGRAM

2.1 Test Specimen

The test specimen was modified from a pipe segment (Figure 2.1), which had been used for an air testing, by removing the central blind flange and re-welding the two joints together at the TCPL (TansCanada Pipelines Ltd.) Spruce Grove Fabrication Facility. The test specimen after modification is shown in Figure 2.2.

Nominal diameter of the specimen is 914.4 mm (36 inch), thickness is 13.7 mm and grade 483 MPa. The total length of the specimen is 27.57 m. There is a line of fittings along the specimen from previous air testing program, as shown in Figure 2.1, and two of them were used to fit sealing glands that will be discussed later.

2.2 Instrumentation

2.2.1 Strain Gauge and Thermistor Layouts

The schematic detail of the instrumentation used in this test is shown in Figure 2.3. A total of 80 strain gauges were mounted on seven different cross sections (Sections 1 to 7) along the specimen. As shown in Figure 2.3, Sections 1, 2, 3, 4, 5 and 7 were used to measure hoop and longitudinal strains at inside and outside of the pipe. Section 6 was used to measure the ovalization of the pipe during the excavation process. Details of all the strain gauges that were used in this test are summarized in Table 2.1.

Four different strain gauge layouts (A, B, C and D) were used in Sections 1, 2, 3, 4, 5 and 7, as shown in Figures 2.4 and 2.5. A total of sixty strain gauges were used to measure the hoop strains both inside and outside the pipe. In addition, a total of sixteen strain gauges were mounted on the top and bottom of the pipe to capture the longitudinal

strains (six strain gauges were used on the inside and ten strain gauges were used on the outside of the pipe).

Four custom made extensometers were used to measure the ovalization of the pipe at Section 6, as shown in Figure 2.5. The extensometer consists of a very thin plate (bronze foil) in series with a pair of springs, which were arranged in parallel, as shown in Figure 2.6. The stiffness of the spring and the foil were selected based on the expected deformation of the pipe during the experiment. A strain gauge was mounted on the foil. The deformation against the strain induced in the foil was calibrated in the lab (Figure 2.7). A typical calibration curve of the extensometer is shown in Figure 2.8, and the calibration factors of four extensometers are summarized in Table 2.2. Four spring-foil system was installed in the radial direction of Section 6 to capture the ovalization as shown in Figures 2.9 and 2.10.

Four thermistors (Figure 2.11) were mounted at two different sections along the pipe to measure the temperature on the inside (T1 and T2) and outside (T3 and T4) of the pipe during the excavation. The locations of the thermistors are shown in Figure 2.3.

2.2.2 Sealing Gland

The wires, which were connected to the internal strain gauges and thermistors, had to be taken out from inside of the pipe to the outside data acquisition system. There were some openings, which were used to conduct air tests, in the specimen that can be used for this purpose (see Figure 2.1). The water-tightness during test was achieved by installing sealing gland at the opening since the specimen will be tested with internal pressure. The sealing gland used was HD37-450 (60CU) PG4AG, 24/84 (see Figure 2.12). Gland Type was PG4-375-G.

The sealing gland had high density feed-through with an outside diameter of 9.53 mm (0.375") and a length of 114.3 mm (4.5"). There were 60 copper wire conductors in each sealing gland. The length of conductor outside the pipeline was 610 mm (24 inches) and internal length was 2134 mm (84 inches). Its internal ends were connected to the internal wire from strain gauges and its external ends were connected to the wires that were connected to a data acquisition system. The sealant was grafoil and its pressure rating was 22 MPa (3200 psi) at 20°C.

Two sealing glands were used in the specimen. One was installed 235 mm before Section 2 and the second one was 185 mm before Section 4. The first one was used to take out all the wires from Sections 1, 2 and 3 and the second one to take out all the wires from Sections 4, 5, 6 and 7.

Figures 2.13 to 2.17 show the installation procedure of sealing glands. The sealing glands were applied with torque around 90 to 100 ft-lbs. Water test up to 11.5 MPa was conducted to verify the water tightness at shop.

2.2.3 Wiring

The wiring consists of the following steps:

- Connecting the internal conductor of sealing glands with the wires from internal strain gauges and thermistors (shown in Figure 2.16).
- Connecting the external conductors of the sealing glands with the wires to a data acquisition system.
- Connecting the external strain gauges and thermistors to the data acquisition system
- Waterproofing all the external and internal joints.

2.2.4 Digital Video Recorder

During the excavation test, a digital video recorder was used to record the position of excavator with time. There were four little flags on the surface of the ground along the specimen to mark the positions of Sections 1, 2, 4 and 7.

2.2.5 Internal Pressure

During pressurized test, the pipeline specimen was filled with water and pressurized to 7.24 MPa (1050 psi). The pressure was maintained at constant throughout the test. The pressure was measured with a pressure transducer.

2.3 Data Acquisition System

Both high-speed and low-speed data acquisition systems were used to collect dynamic and static strain readings during the excavation, respectively. The high-speed data acquisition system had 24 channels and was set up to collect strain at a sampling rate of about 100 readings per second. The low-speed data acquisition system was able to record one data per second.

Twenty-four hoop strain gauges at Sections 2 and 4 were connected to the high speed data acquisition system. The rest of the gauges (fifty-six strain gauges) were connected to the low speed data acquisition system.

As shown in Figure 2.3, Sections 2 and 3 and also Sections 4 and 5 were selected at a distance of D/2, where D is the outside diameter of the specimen, apart from each other in order to be able to make a comparison between low-speed and high-speed strain readings during the excavation process.

2.4 Measurement of Temperature

The thermistor resistances were measured with a multi-meter. Conversion formula or table can be used to convert resistance to temperature. The following formula provided by Optimum Instruments Inc. is used:

$$X = Ln(R)$$

$$T = C_0+X*(C_1+X*(C_2+X*(C_3+X*(C_4+X*C_5))))$$

$$C_0 = 448.378448925865115$$

$$C_1 = -95.859120175003461$$

$$C_2 = 8.361953542603310$$

$$C_3 = -0.434098177910065$$

$$C_4 = 0.011182629079790$$

$$C_5 = -0.000094138790516$$

where R is the resistance of the thermistor in ohm, T is temperature in Celsius.

2.5 Test Arrangement

There were three summer excavation tests conducted on Oct. 14 and 15, 2004. Summer test 1 and test 2 were conducted with zero internal pressure. Summer test 3 had the internal pressure of 7.24 MPa (1050 psi), which can produce a hoop stress of 241.5 MPa that corresponds to 50% of the specified minimum yield strength (SMYS).

Two winter excavation tests were done from March 22 to March 24, 2005. Winter test 1 was a pressurized test with internal pressure of 7.24 MPa (producing a hoop stress of 50% SMYS) and winter test 2 was an un-pressurized test with zero internal pressure.

2.6 Test Procedures

The excavator used for the summer tests was a Komatsu Avance PC 220LC as shown in Figure 2.18. The operating weight was 24,510 kg or 240 kN and the ground pressure was 36.3 kPa. The track length on ground was 3845 mm and width was 800 mm. Overall width of the excavator was 3380 mm. The excavator used in the winter excavation tests was a DEERE 270C LC as shown in Figure 2.19. The operating weight was 28,518 kg or 279 kN and the ground pressure was 40.2 kPa. The track length on ground was 4050 mm and width was 800 mm. Overall width of the excavator was 3390 mm.

Each test was conducted using similar procedures. Firstly, the specimen was laid into the ditch and backfilled with soil. The layout of the specimen is shown in Figure 2.3. Secondly, the excavator moved far away from the buried specimen. Thirdly, the initial readings of all the instrumentation were taken by the data acquisition systems. Then the excavator moved back and sat on Sections 2 and 3 to start the excavation.

The excavation zone is shown in Figure 2.20. For all tests, the excavation started approximately from 2 meters before Section 1 to about 2 meters after Section 4, giving a total excavation length of about 13 m. On average, the excavator was able to excavate a length of about 2.6 meters at each position with a ditch depth of about 2 meters. A complete excavation was conducted by excavator sitting on five distinct positions, i.e. at Section 2, at the middle of Sections 2 and 4, at Section 4, at the middle of Sections 4 and 7, and at Section 7. At each position, the excavator can be either at left side or at right side of the pipeline as shown in Figure 2.21. The left side or right side is determined as you stand at Section 1 (starting section) and face towards Section 7 (end section).

After the excavation had completed, the data acquisition systems were stopped and the excavator began to backfill the specimen and prepare for the next test.

In the first winter pressurized test, because a fitting between Sections 1 and 2 failed, the test was not finished. The excavation area was about 3 m before and 1.4 m after Section 1, giving a total excavated length of about 4.4 m. In the second winter excavation test, the excavated area from the first pressurized test was backfilled with original soil. The excavation procedure was similar to that in the summer tests. However, to protect the sealing gland from the damage caused by excavation of frozen soil, the top soil of the section around the sealing gland (Section 2 and Section 4) was not removed.

2.7 Position of Excavator in the Tests

The positions of the excavator are recorded through the digital video recorder and presented in Tables 2.3, 2.4 and 2.5 for summer tests. Time in column 2 of these tables is relative to the moment of start of the excavation. The excavator positions in summer tests are schematically shown in Figure 2.22.

The positions of the excavator in the winter un-pressurized test are presented in Table 2.6, and are schematically shown in Figure 2.23. For the winter pressurized test, the excavator stayed only at Section 2.

The excavation process was shown in the Figures 2.24 and 2.25 for summer tests and in Figures 2.26 to 2.28 for winter tests, respectively.

2.8 Temperature Measured During the Tests

The temperature measured in summer tests is shown in Table 2.7. The temperature history in winter tests 1 and 2 is presented in Figure 2.29 and Figure 2.30 respectively.

2.9 Soil Condition

As shown in Figure 2.29 and Figure 2.30, the temperature of the specimen in winter test was below zero degree (from −0.1 to −2.4°C) both at the top and bottom of the pipe. Therefore, the soil was frozen during the winter excavation tests. According to the observation in the field, the frozen line is about 1.5 m below the ground surface as shown schematically in Figure 2.31.

Table 2.1 Summary of arrangement of strain gauges

(a) Internal strain gauges

No.	Section	Gauge No.	Position	Direction	DAS Type
1	1	25	0°	Hoop	Low Speed
2		27	90°	Hoop	Low Speed
3		29	180°	Hoop	Low Speed
4		61	0°	Longitudinal	Low Speed
5		63	180°	Longitudinal	Low Speed
6	2	1	0°	Hoop	High Speed
7		3	30°	Hoop	High Speed
8		5	60°	Hoop	High Speed
9		7	90°	Hoop	High Speed
10		9	180°	Hoop	High Speed
11		11	270°	Hoop	High Speed
12		13	315°	Hoop	High Speed
13		64	0°	Longitudinal	Low Speed
14		67	180°	Longitudinal	Low Speed
15	3	31	0°	Hoop	Low Speed
16		33	45°	Hoop	Low Speed
17		35	90°	Hoop	Low Speed
18		37	180°	Hoop	Low Speed
19		39	270°	Hoop	Low Speed
20		41	315°	Hoop	Low Speed
21		68	0°	Longitudinal	Low Speed
22	4	15	0°	Hoop	High Speed
23		17	45°	Hoop	High Speed
24		19	90°	Hoop	High Speed
25		21	180°	Hoop	High Speed
26		23	270°	Hoop	High Speed
27		69	0°	Longitudinal	Low Speed
28		72	180°	Longitudinal	Low Speed
29	5	43	0°	Hoop	Low Speed
30		45	45°	Hoop	Low Speed
31		47	90°	Hoop	Low Speed
32		49	180°	Hoop	Low Speed
33		51	270°	Hoop	Low Speed
34		53	315°	Hoop	Low Speed
35		73	0°	Longitudinal	Low Speed
36	7	55	0°	Hoop	Low Speed
37		57	90°	Hoop	Low Speed
38		59	180°	Hoop	Low Speed
39		74	0°	Longitudinal	Low Speed
40		76	180°	Longitudinal	Low Speed

(b) External strain gauges

No.	Section	Gauge No.	Position	Direction	DAS Type
41	1	26	0°	Hoop	Low Speed
42		28	90°	Hoop	Low Speed
43		30	180°	Hoop	Low Speed
44		62	180°	Longitudinal	Low Speed
45	2	2	0°	Hoop	High Speed
46		4	30°	Hoop	High Speed
47		6	60°	Hoop	High Speed
48		8	90°	Hoop	High Speed
49		10	180°	Hoop	High Speed
50		12	270°	Hoop	High Speed
51		14	315°	Hoop	High Speed
52		65	0°	Longitudinal	Low Speed
53		66	180°	Longitudinal	Low Speed
54	3	32	0°	Hoop	Low Speed
55		34	45°	Hoop	Low Speed
56		36	90°	Hoop	Low Speed
57		38	180°	Hoop	Low Speed
58		40	270°	Hoop	Low Speed
59		42	315°	Hoop	Low Speed
60	4	16	0°	Hoop	High Speed
61		18	45°	Hoop	High Speed
62		20	90°	Hoop	High Speed
63		22	180°	Hoop	High Speed
64		24	270°	Hoop	High Speed
65		70	0°	Longitudinal	Low Speed
66		71	180°	Longitudinal	Low Speed
67	5	44	0°	Hoop	Low Speed
68		46	45°	Hoop	Low Speed
69		48	90°	Hoop	Low Speed
70		50	180°	Hoop	Low Speed
71		52	270°	Hoop	Low Speed
72		54	315°	Hoop	Low Speed
73	6	77	0°	Radial	Low Speed
74		78	45°	Radial	Low Speed
75		79	90°	Radial	Low Speed
76		80	315°	Radial	Low Speed
77	7	56	0°	Hoop	Low Speed
78		58	90°	Hoop	Low Speed
79		60	180°	Hoop	Low Speed
80		75	180°	Longitudinal	Low Speed

Table 2.2 The calibration factors of four extensometers used for measuring ovalization

DMD #	Slope (με/mm)	R^2	Initial Length of Spring (mm)
1	38.220	0.9983	42.68
2	37.989	0.9990	42.67
3	35.770	0.9990	42.27
4	45.559	0.9997	43.04

Table 2.3 Excavator position of summer un-pressurized test (test 1)

No.	Time (seconds)	Action of Excavator	Location of Excavator		Excavating Zone
			Left	Right	
1		Move on to pipe			
2	0	Start to Excavate	2		About 2~3m before Sect.1
3	390	Move		2	
4	890	Pause			
5	1050	Re-start			
		Back		Mid. of 2~4	
6	1430	Move	Mid. of 2~4		
7	1680	Back	4		
8	2055	Move		4	
9	2270	Back		Mid. of 4~7	
10	2553	Move	Mid. of 4~7		
11	2755	Back	7		
12	3065	Move		7	
13	3305	Back		After 7	
14	3409	End of excavation		After 7	About 2~3m aft. Sect.4

Note: Move—from one side to another side
Back—Move backwards

Table 2.4 Excavator position of summer un-pressurized test (test 2)

No.	Time (seconds)	Action of Excavator	Location of Excavator		Excavating Zone
			Left	Right	
1		Stay far away			
2		Move on to pipe			
3	0	Start to excavate	2		About 2~3m before Sect.
4	201	Pause			
5	292	Re-start			
6	332	Back	2~4		
7	525	Move		2~4	
8	852	Back		4	
9	1110	Move	4		
10	1244	Back	4~7		
11	1533	Move		4~7	
12	1679	Back		4~7	
13	2011	Move	7		
14	2032	Back	7		
15	2402	Move		7	
16	2558	End			About 2~3m aft. Sect.4

Note: Move---from one side to another side
Back---Move backwards

Table 2.5 Excavator position of summer pressurized test

No.	Time (seconds)	Action of Excavator	Location of Excavator		Excavating Zone
			Left	Right	
1		Far behind sect.7. Move on to pipe			
2	0	Start to excavate	2		About 3m before Sect.
3	27	Back	2~4		
4	487	Move		2~4	
5	727	Back		4	
6	1018	Move	4		
7	1161	Back	4~7		
8	1393	Move		4~7	
9	1521	Back		7	
10	1848	Move	7		
11	2031	End			About 2~3m aft. Sect.4

Note: Move---from one side to another side
Back---Move backwards

Table 2.6 Position of excavator in winter un-pressurized test

No.	Time (second)	Action of Excavator	Position of Excavator Left	Right
1	0			
2	191	Start	2	
3	973	Moved		2
4	1861	Moved	4	
5	2743	Moved		4
6	3378	Moved	4~7	
7	4483	Moved		4~7
8	5120	Moved		7
9	6403	Moved	7	
10	7294	End		

Table 2.7 Temperature measured in the summer excavation test

	Gauges No.	Time				Temperature Change
		11:07	12:45	12:55	13:50	
Excavation	T1	10.53°	---	10.55°	10.92°	0.02°
Summer	T2	9.65°	---	9.61°	9.61°	-0.04°
Test 1	T3	10.51°	10.49°	---	10.64°	-0.02°
Oct. 14, 2004	T4	9.53°	9.51°	---	9.49°	-0.02°

	Gauges No.	Time				Temperature Change
		15:00	15:02	15:24	15:43	
Excavation	T1	10.98°	10.94°	10.79°	10.70°	-0.28°
Summer	T2	9.57°	9.57°	9.57°	---	0.00°
Test 2	T3	10.38°	10.36°	10.36°	10.34°	-0.04°
Oct. 14, 2004	T4	9.49°	9.49°	9.47°	9.47°	-0.02°

	Gauges No.	Time				Temperature Change
		8:14	9:25	9:30	9:37	
Excavation	T1	10.06°	10.15°	10.15°	10.15°	0.08°
Summer	T2	9.40°	9.32°	9.32°	9.36°	-0.04°
Test 3	T3	10.04°	10.04°	10.04°	10.04°	-0.00°
Oct. 15, 2004	T4	9.32°	9.26°	9.28°	9.28°	-0.04°

Notes:

T1: Internal gauge at top of pipe
T2: Internal gauge at bottom of pipe
T3: External gauge at top of pipe
T4: Eternal gauge at bottom of pipe

Figure 2.1 Specimen before modification

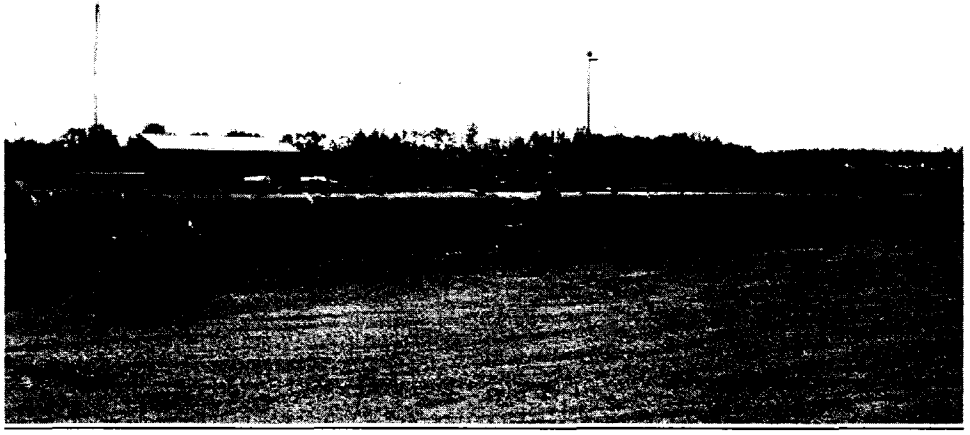

Figure 2.2 Specimen after modification

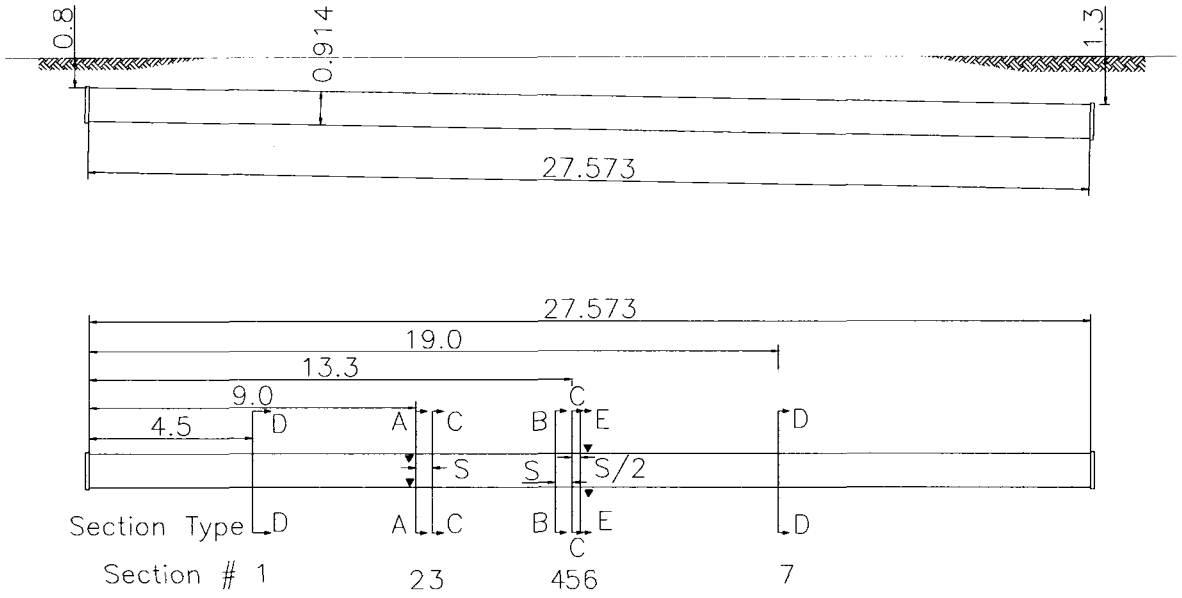

Figure 2.3 Instrumentation section layouts

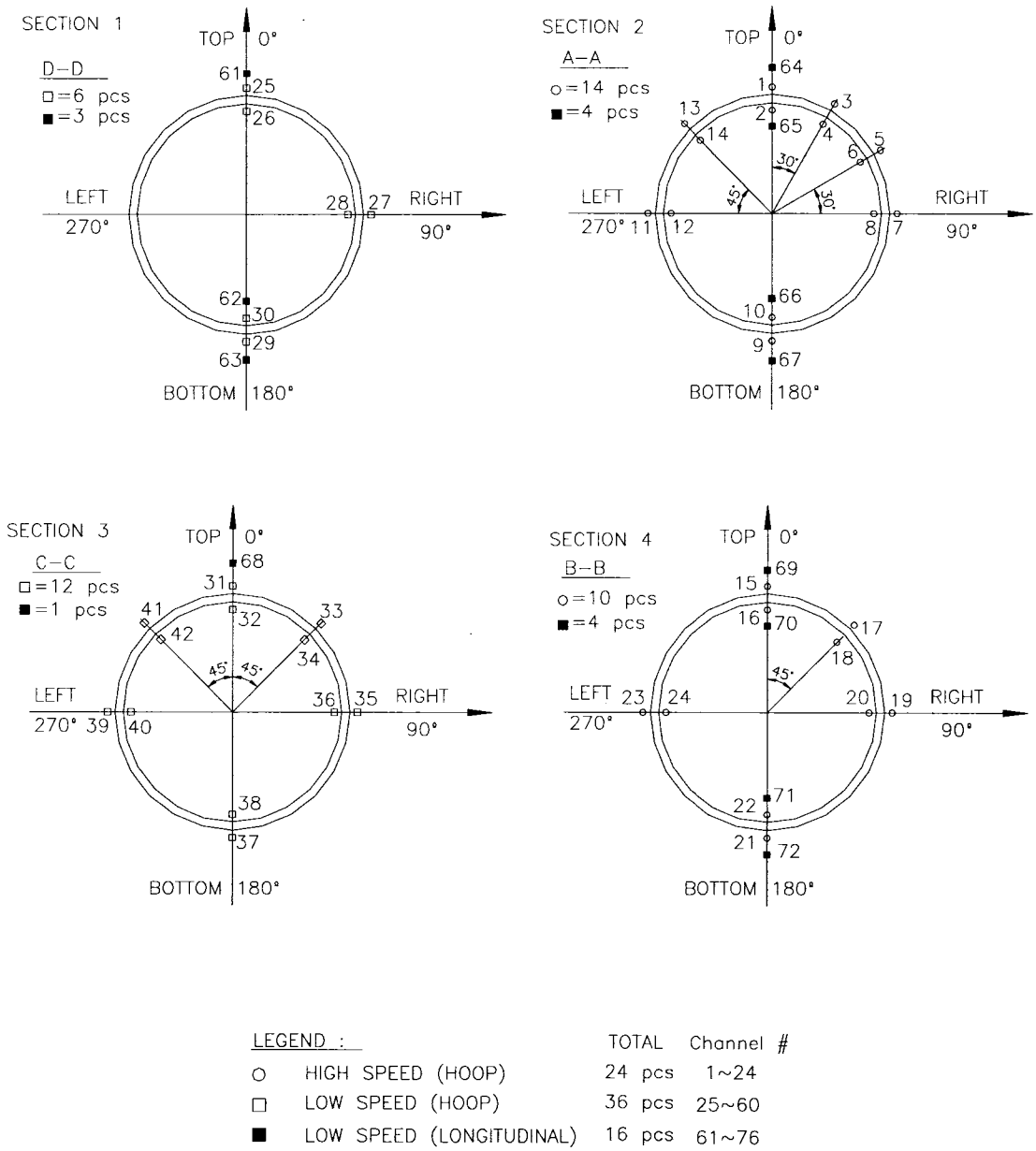

LEGEND :		TOTAL	Channel #
○	HIGH SPEED (HOOP)	24 pcs	1~24
□	LOW SPEED (HOOP)	36 pcs	25~60
■	LOW SPEED (LONGITUDINAL)	16 pcs	61~76

Figure 2.4 Strain gauge layouts at Sections 1, 2, 3 and 4

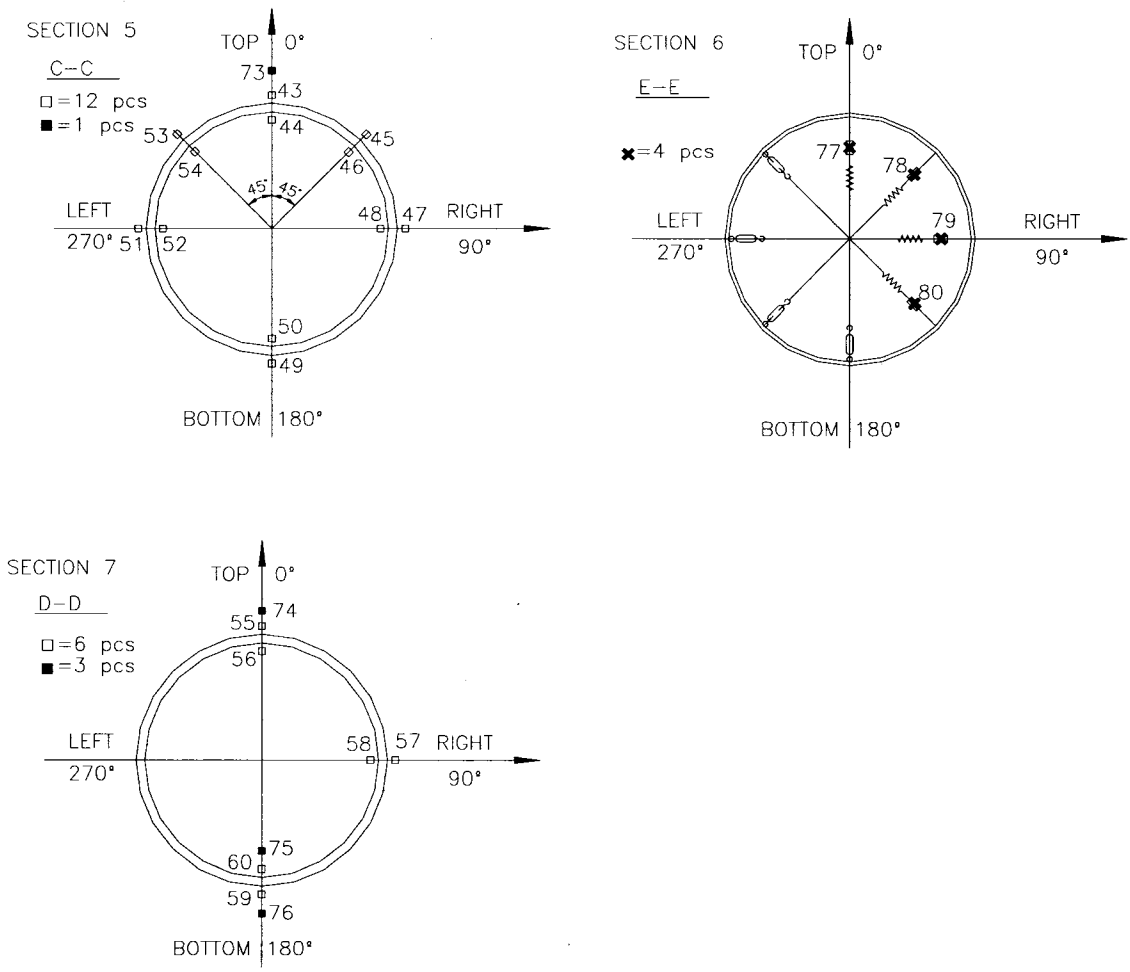

LEGEND :		TOTAL	Channel #
○	HIGH SPEED (HOOP)	24 pcs	1~24
□	LOW SPEED (HOOP)	36 pcs	25~60
■	LOW SPEED (LONGITUDINAL)	16 pcs	61~76
✖	LOW SPEED (RADIAL)	4 pcs	77~80

Figure 2.5 Strain gauge layouts at Sections 5, 6 and 7

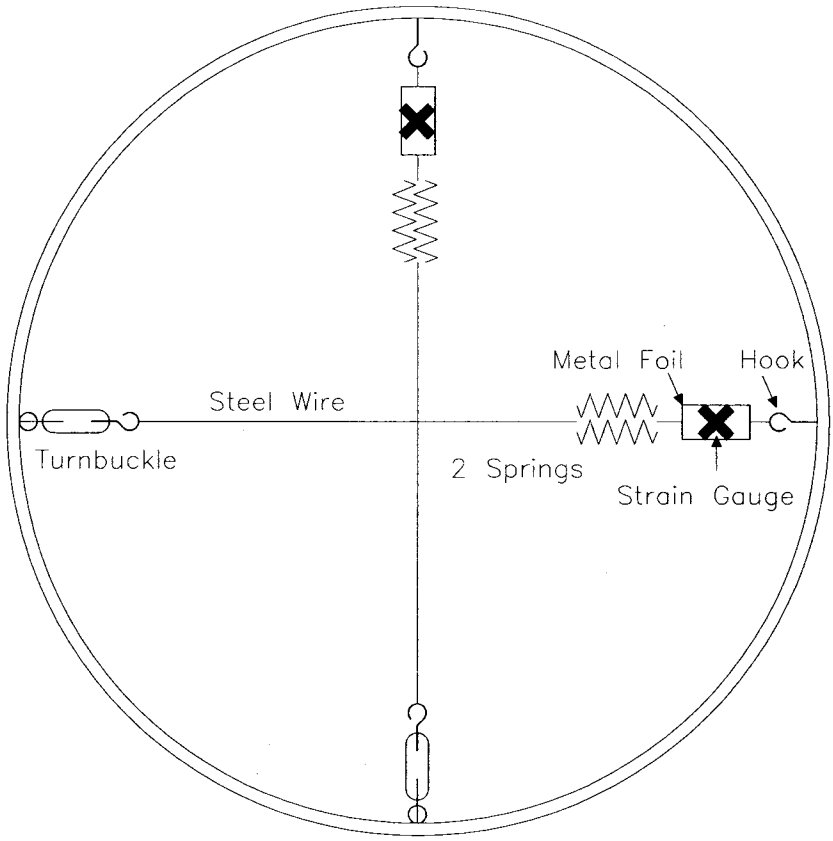

Figure 2.6 Composition of device for measuring ovalization

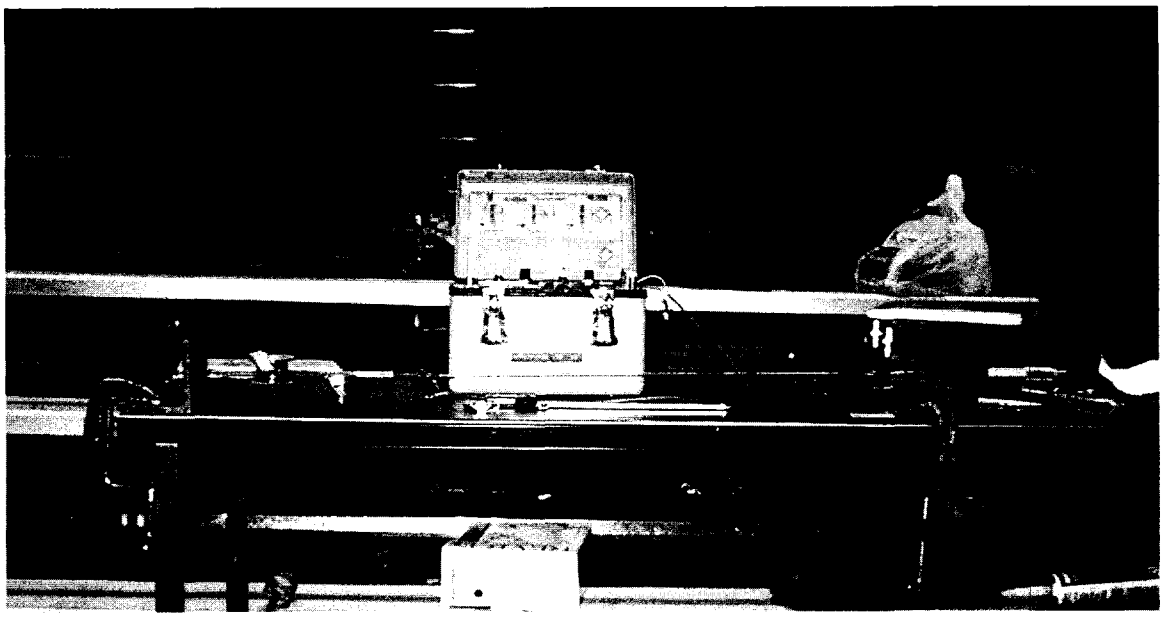

Figure 2.7 Extensometers, device for measuring ovalization being calibrated

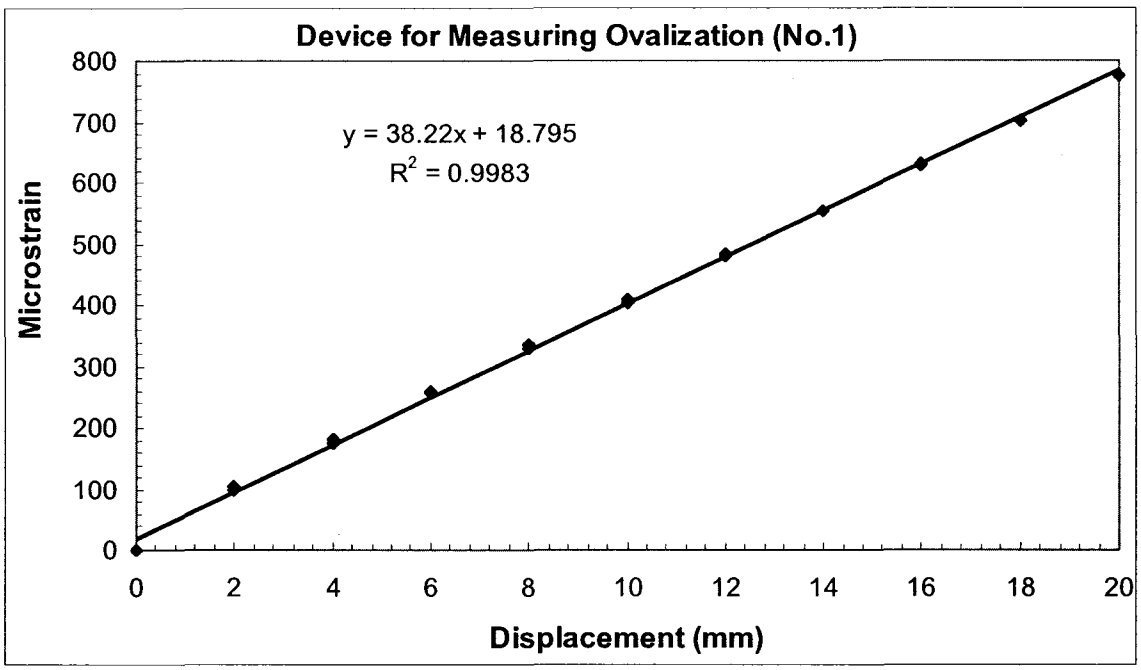

Figure 2.8 Calibration curve – relationship between strain and deformation

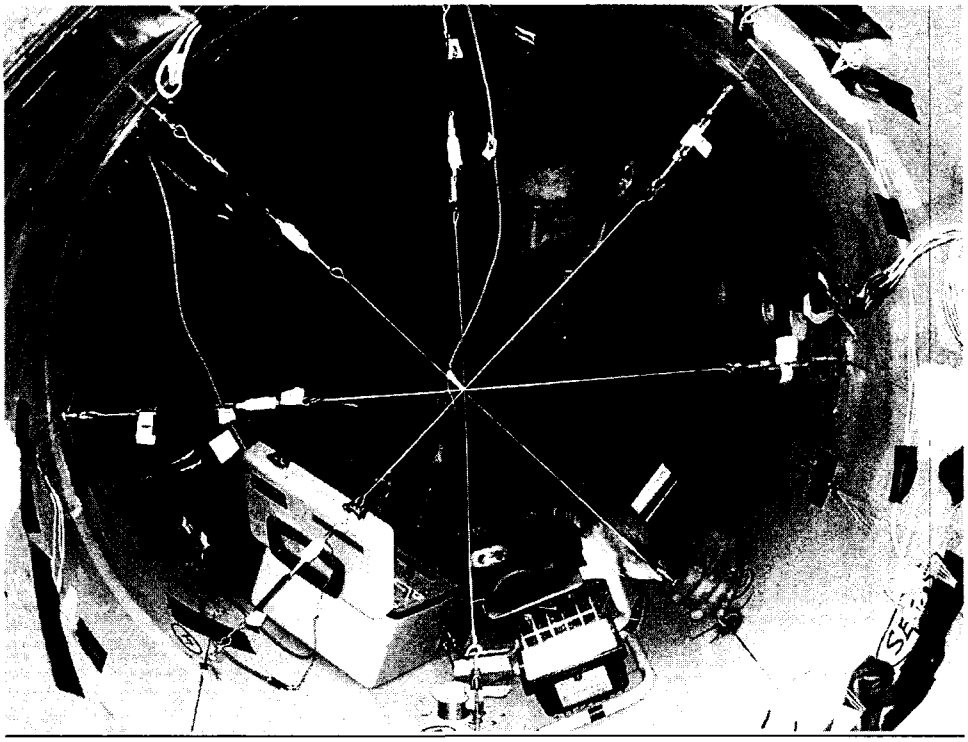

Figure 2.9 Initial tension strain set-up of device for measuring ovalization

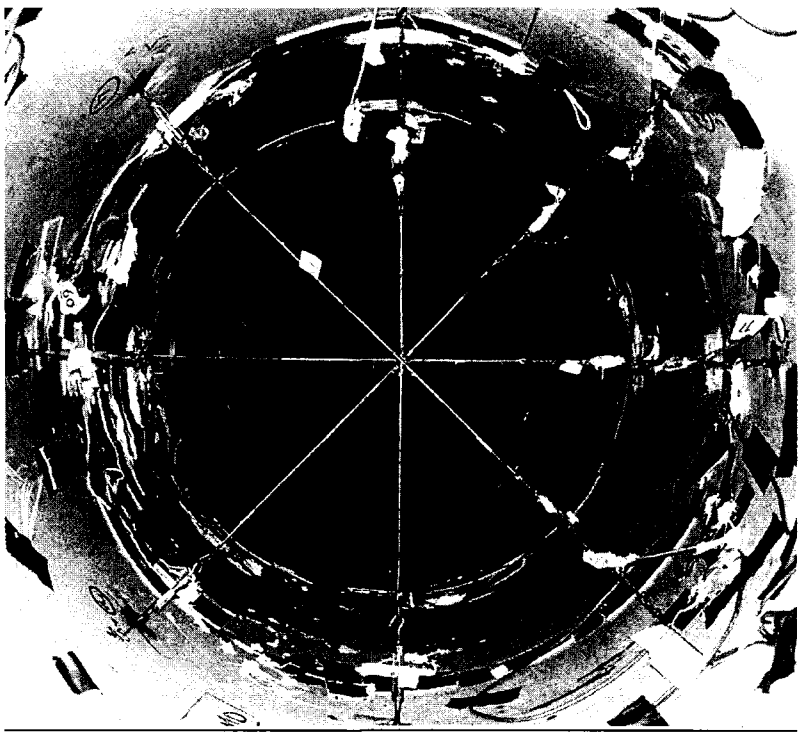

Figure 2.10 Extensometers , device for measuring ovalization installed at Section 6

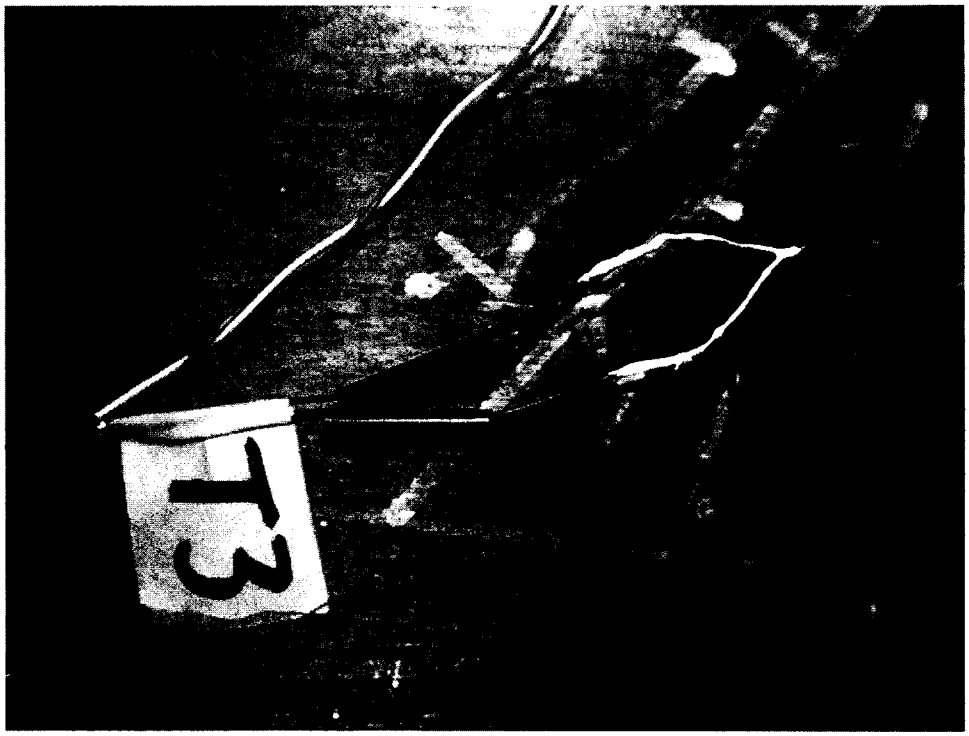

Figure 2.11 Thermistor being waterproofed

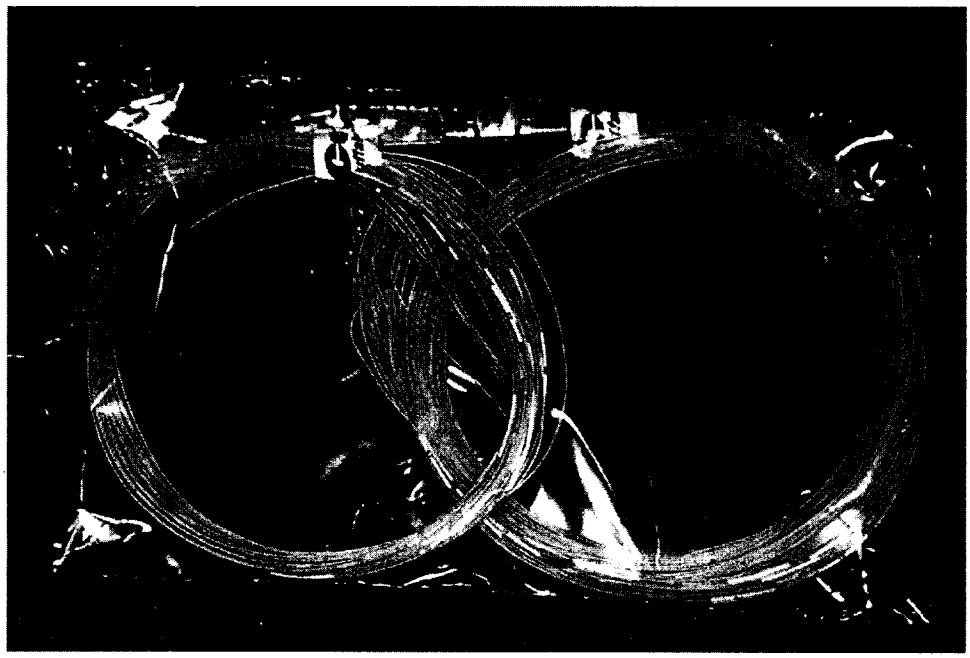

Figure 2.12 Sealing gland

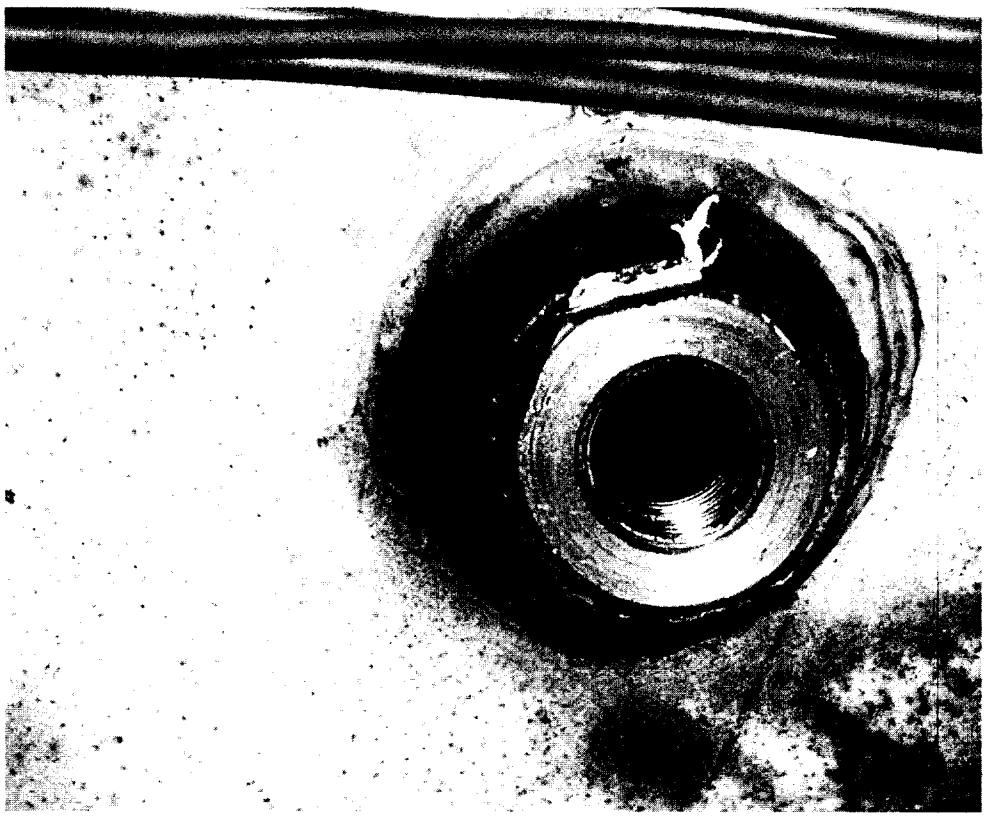

Figure 2.13 Reducer was fitted in the opening in the pipe

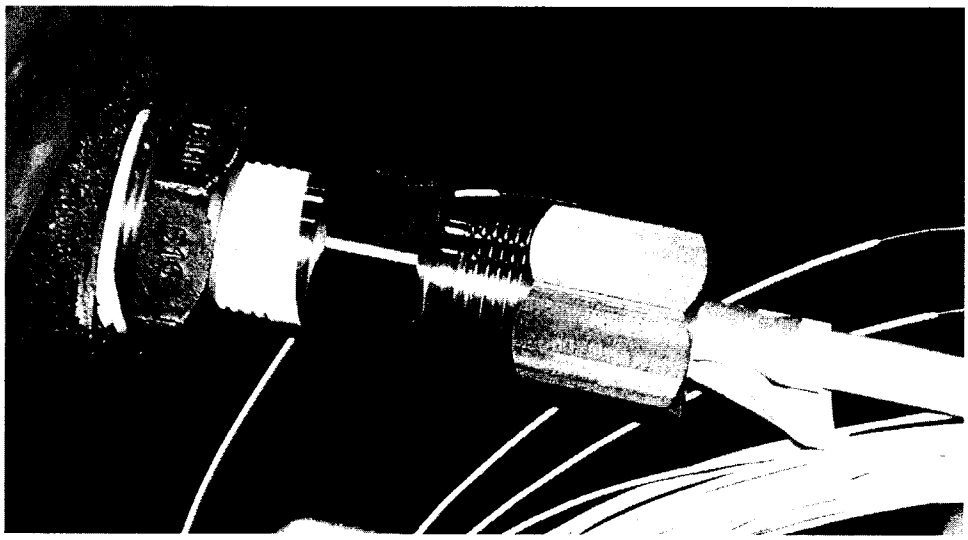

Figure 2.14 Sealing gland was put into the opening

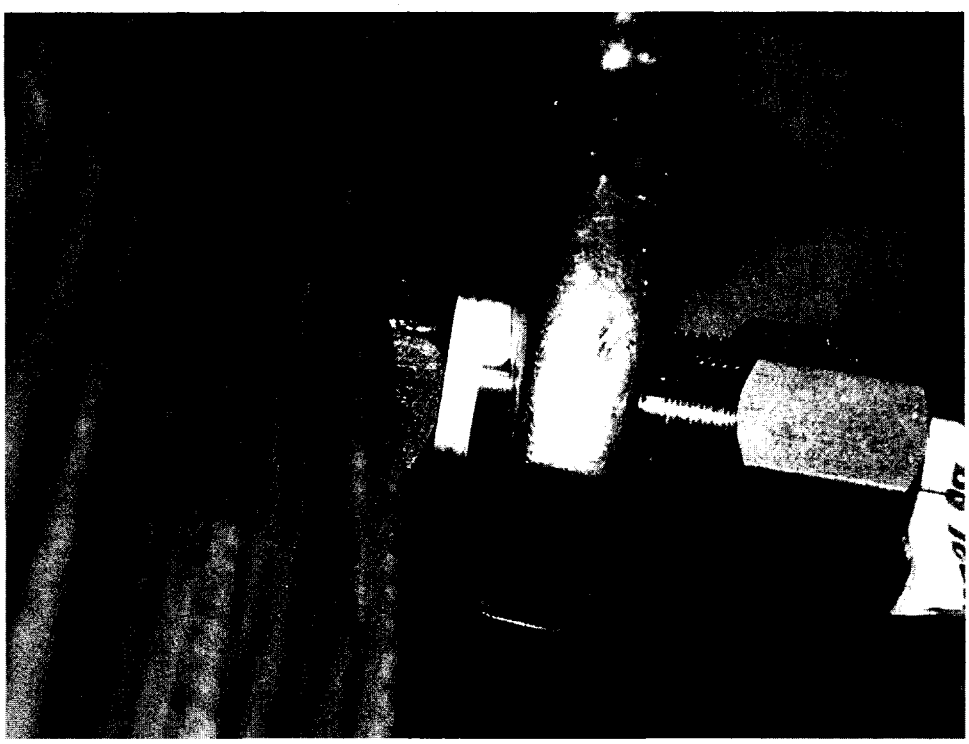

Figure 2.15 Secure the gland body

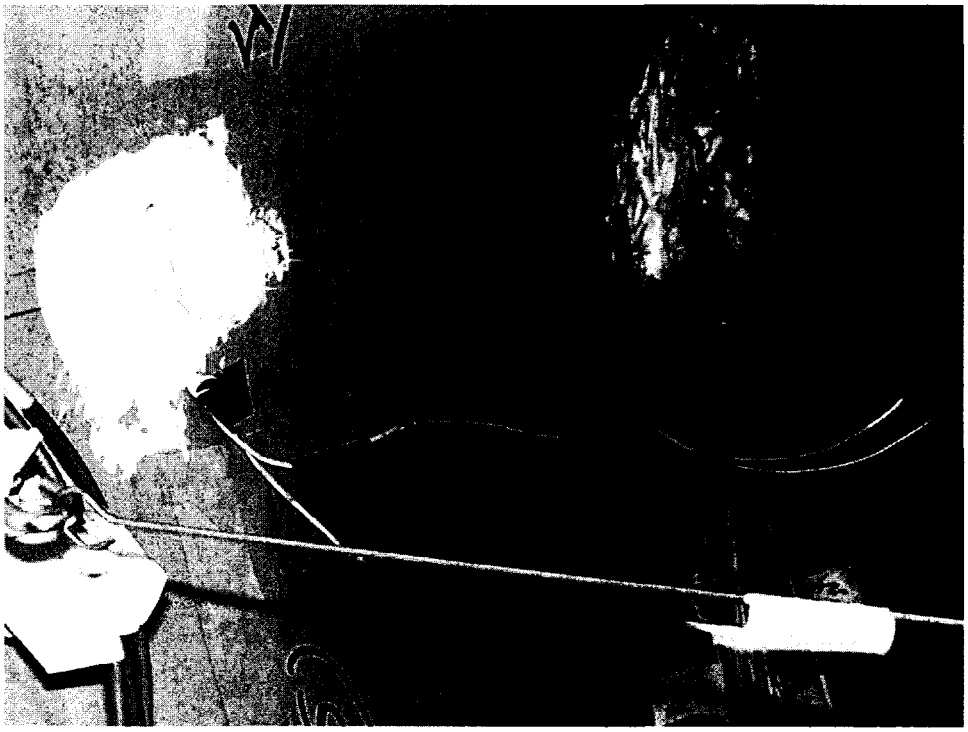

Figure 2.16 The sealing gland was connected with the internal strain gauge inside the pipeline

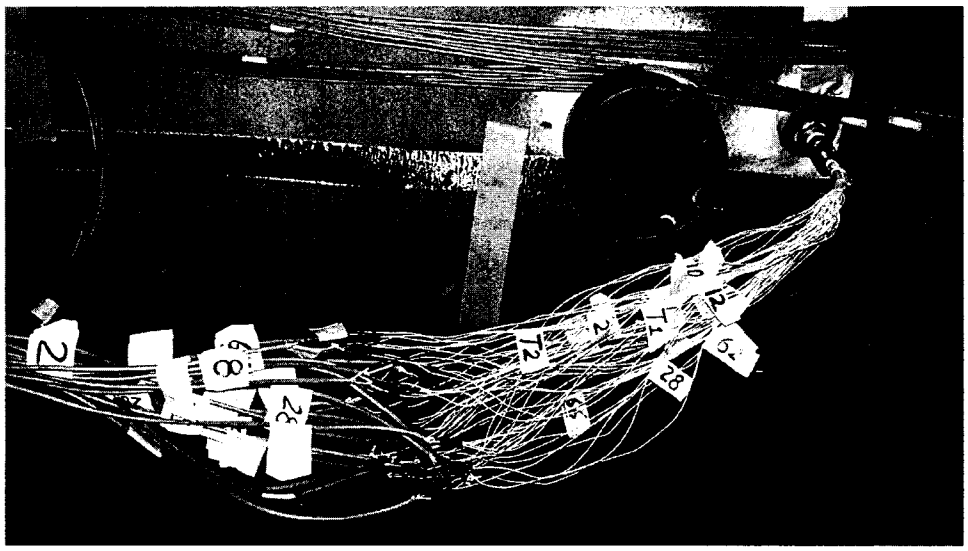

Figure 2.17 Outside of sealing gland after wiring

Figure 2.18 Excavator used in summer test
– Komatsu Avance PC 220LC

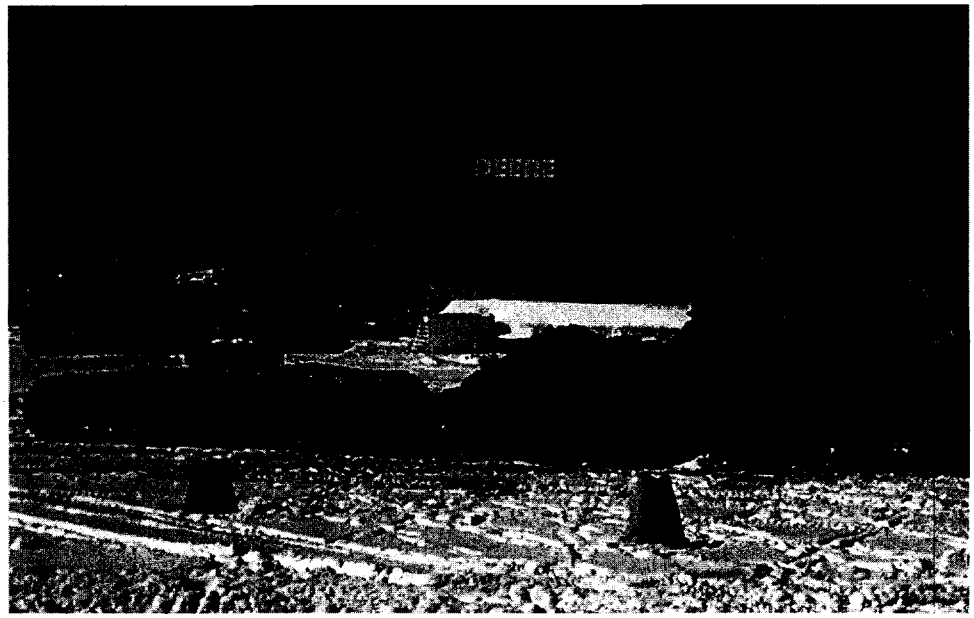

Figure 2.19 Excavator used in winter excavation test – DEERE 270C LC

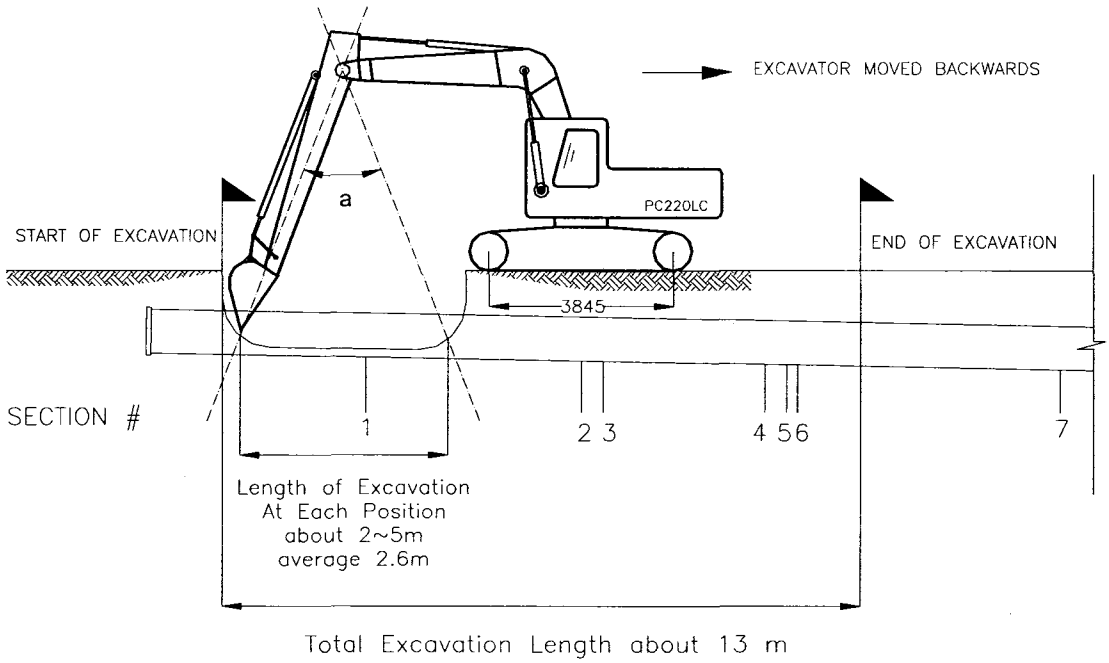

Figure 2.20 Excavator position – excavation length

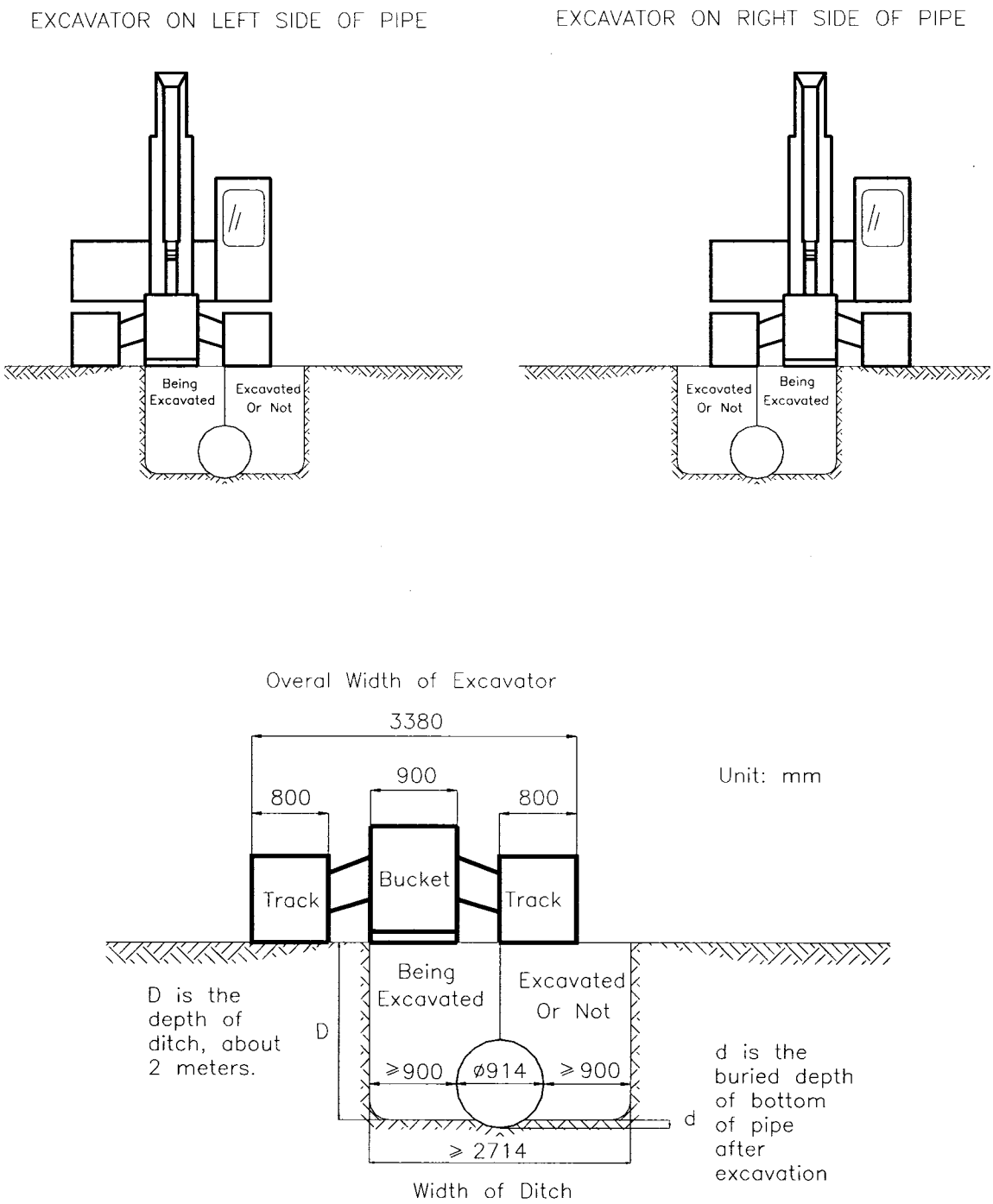

Figure 2.21 Excavator position---left side and right side

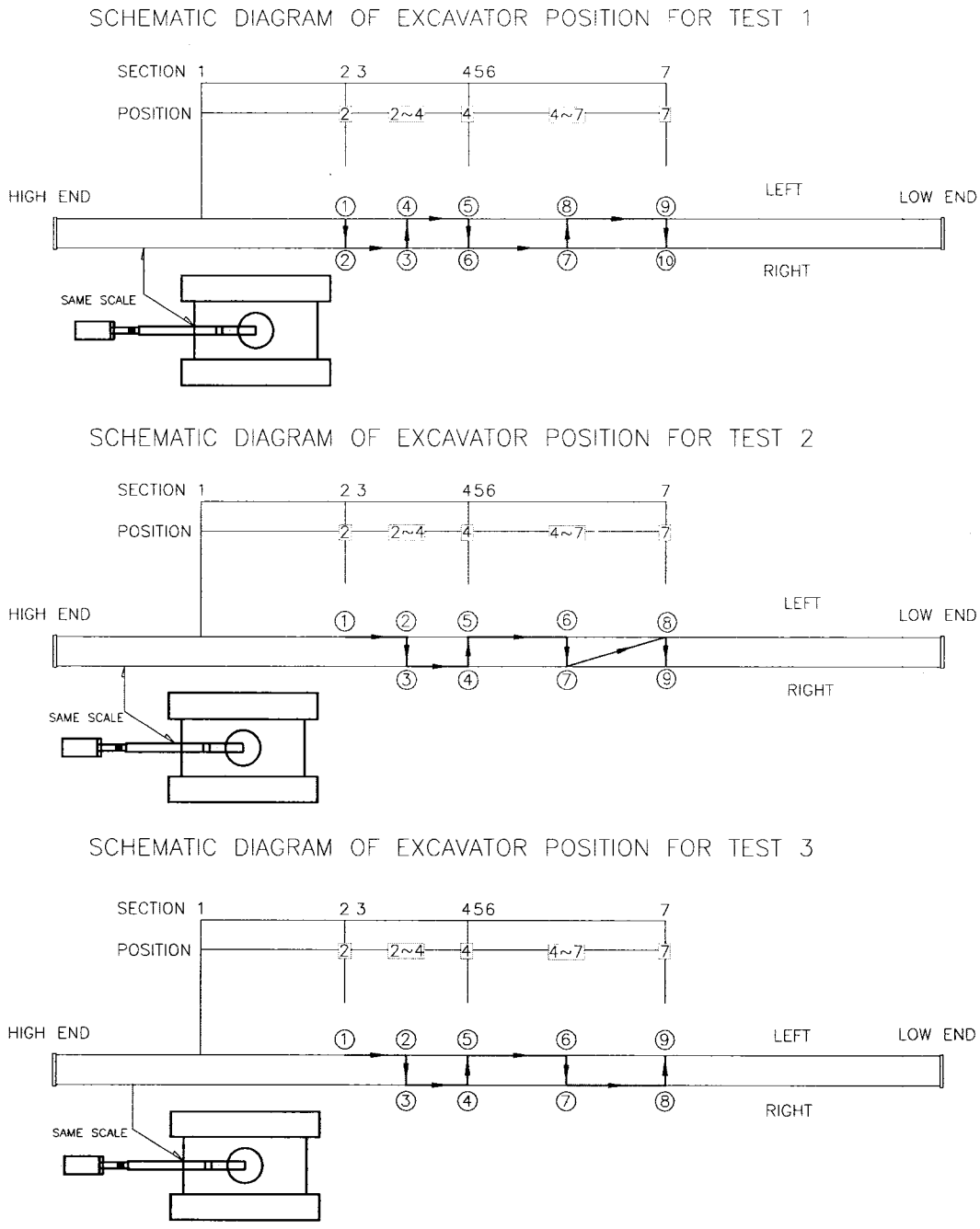

Figure 2.22 Schematic diagram of the position of excavator in summer tests

(Top view)

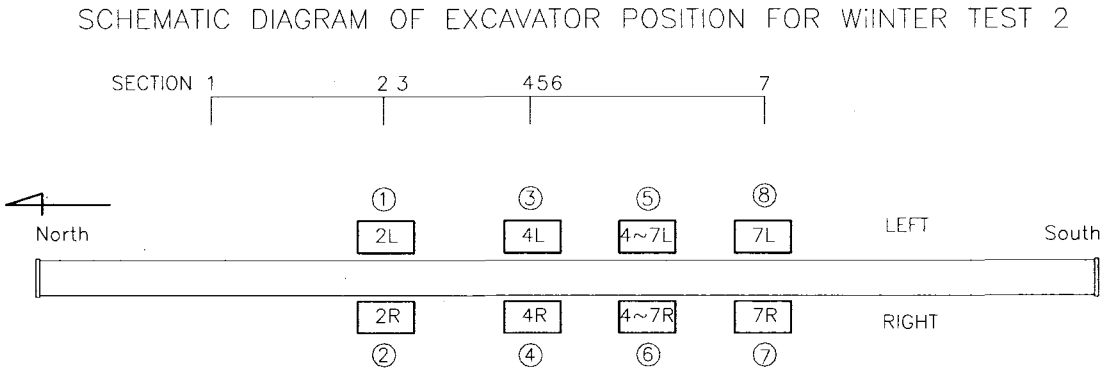

Figure 2.23 Schematic diagram of the position of excavator in winter un-pressurized test (Top view)

Figure 2.24 Excavation process in summer

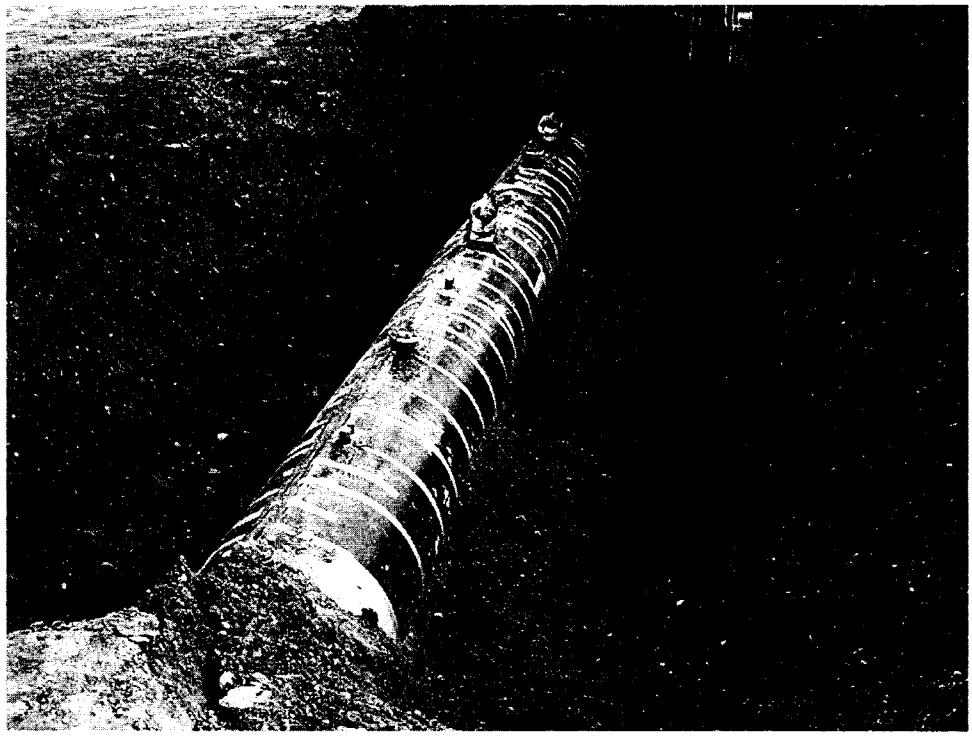

Figure 2.25 Exposed portion of the pipeline after excavation in summer

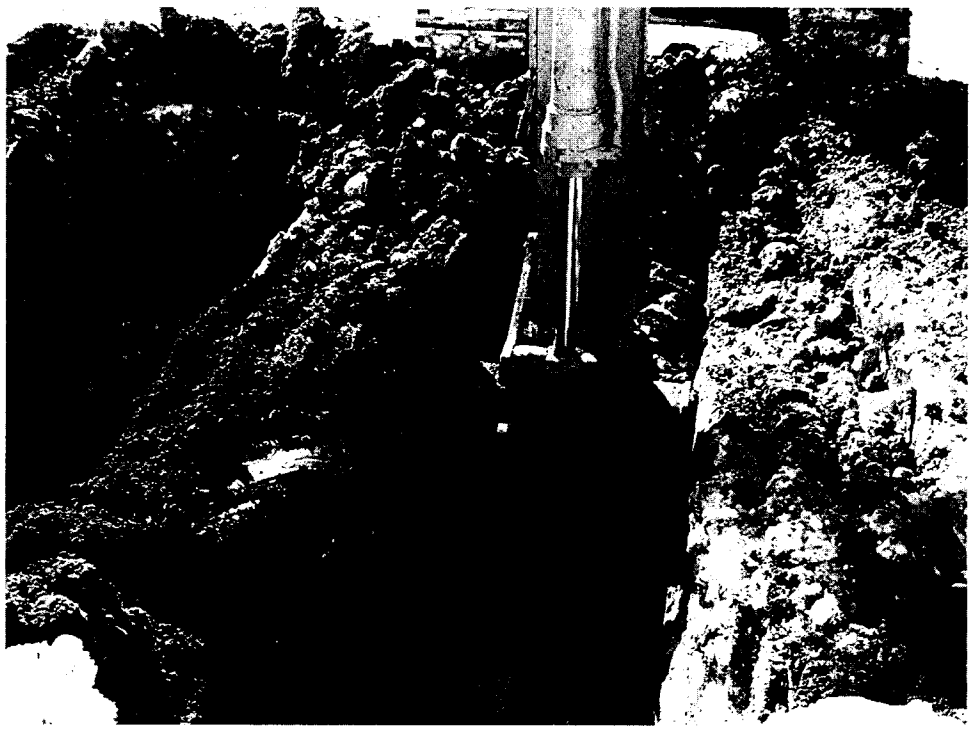

Figure 2.26 Removal of the side soil in winter excavation test

Figure 2.27 Removal of the top soil in winter excavation test

Figure 2.28 The excavated pipeline after winter un-pressurized test

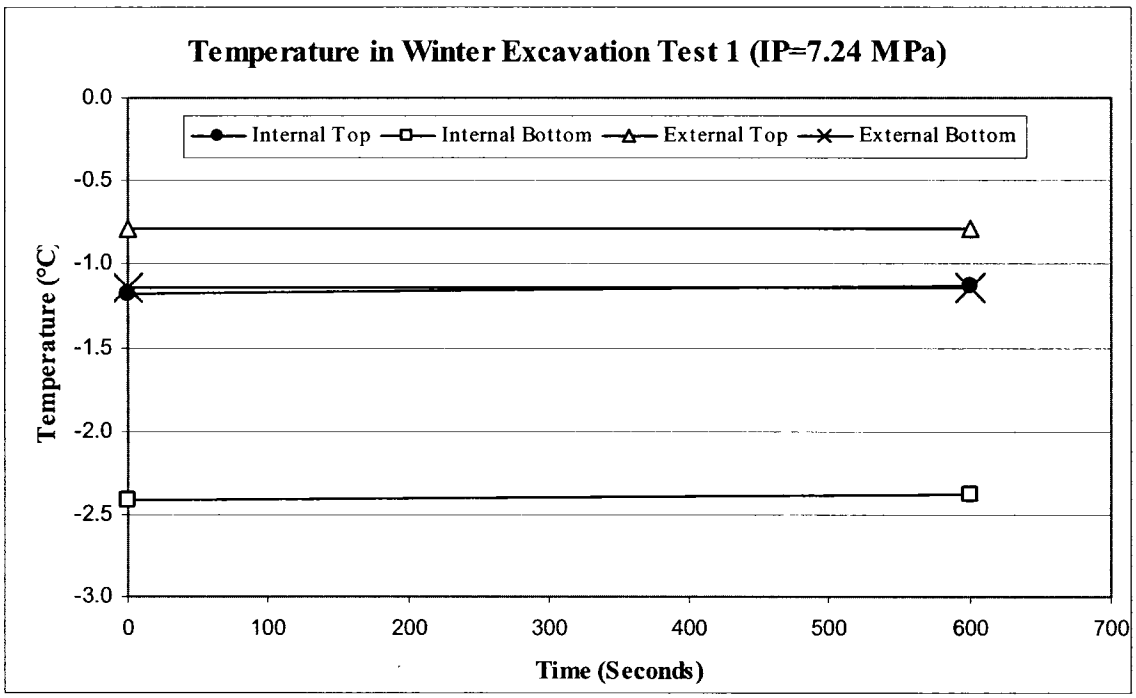

Figure 2.29 Temperature history in winter pressurized excavation test

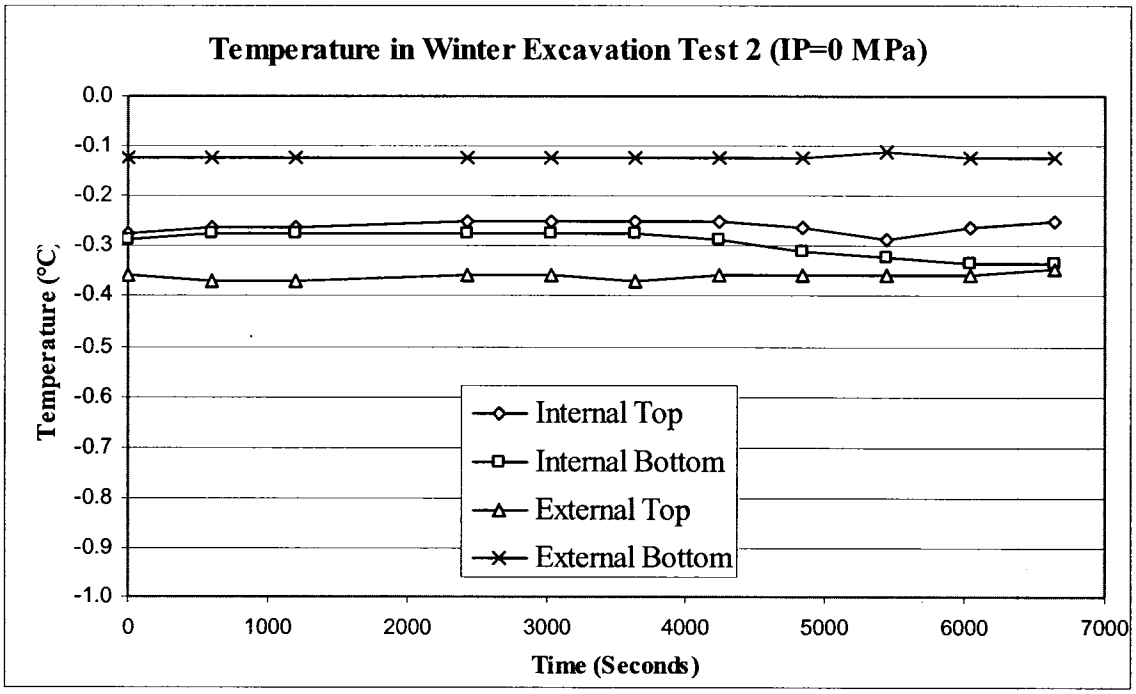

Figure 2.30 Temperature history in winter un-pressurized excavation test

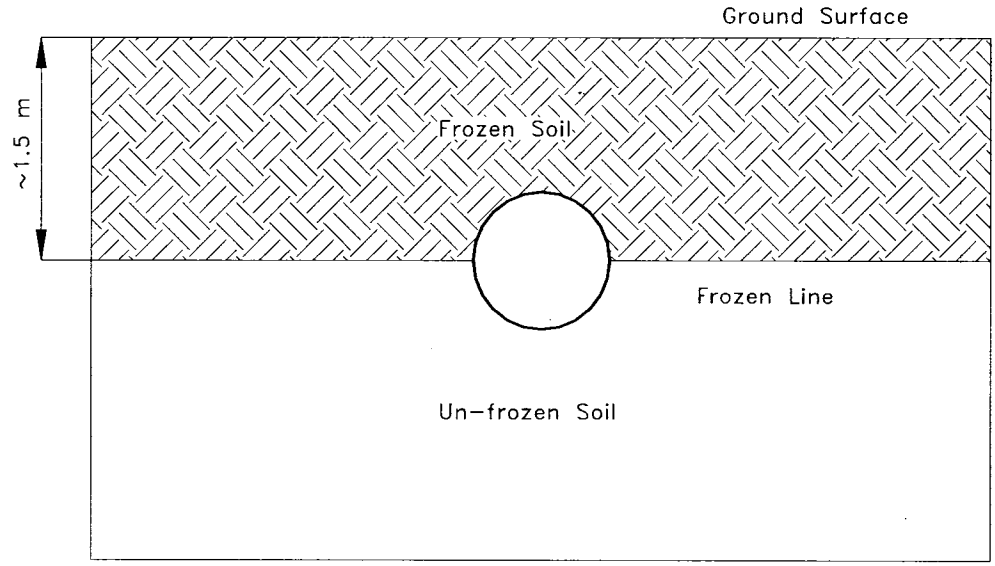

Figure 2.31 Frozen line observed in winter excavation test

3 TEST RESULTS AND DATA ANALYSIS OF SUMMER EXCAVATION TESTS

3.1 Results of Summer Excavation Test

The stain histories of summer excavation test 1, test 2 and test 3 are shown in from Figure 3.1 to Figure 3.26. The horizontal axis is time in second. The vertical axis is strain (unit: micro-strain) for Sections 1, 2, 3, 4, 5 and 7 and deformation (unit: millimeter) for Section 6. The positions of excavator at a specific time during the excavation are shown with the instrumented section number. At each position, the excavator can be either at left or right side.

Unfortunately, the LABVIEW program for high-speed data acquisition system encountered technical problems in summer tests. The high-speed data were found not reliable and will not be presented here. Therefore, only the low speed data were analyzed.

3.1.1 Section 1

3.1.1.1 Hoop strains at the 0°

History of hoop strain at the top (0°) of Section 1 during tests 1, 2, and 3 is shown in Figure 3.1. As expected, there is a good agreement between test 1 and test 2. The magnitude of hoop strain is reduced as a result of internal pressure in test 3.

For un-pressurized tests, the maximum hoop strain was +82με (inside) and -81με (outside) when the excavator was at Section 2. When excavator was at Section 7, the end position of excavation, the maximum hoop strain was -48με (inside) and +48με (outside). For test 3, when excavator was at Section 7, the maximum hoop strain was -33με (inside) +21με (outside), which were 69% (inside) and 44% (outside) of the magnitude of maximum hoop strain in un-pressurized tests at this location of excavator.

By comparing the inside and outside hoop strains, it can be concluded that the pipe cross-section is under a localized bending in all the three tests. For un-pressurized pipe at a specific location of the excavator, the middle of Sections 2 and 4, the sign of the inside hoop strain changed from positive to negative while the sign of the outside hoop strain changed from negative to positive. However in test 3, the sign of the cross-section bending does not change obviously with the location of excavator.

3.1.1.2 Hoop strains at the 180°

History of hoop strain at the bottom (180°) of Section 1 during tests 1, 2, and 3 is shown in Figure 3.2. As expected, there is a good agreement between test 1 and test 2. The magnitude of hoop strain is reduced as a result of internal pressure in test 3.

For un-pressurized tests, the maximum hoop strain was +127με (outside) and -128με (inside) when the excavator was at Section 7, the end position of excavation. For test 3, when excavator was at Section 7, the maximum hoop strain was +73με (outside) and -76με (inside), which is 57% (outside) and 59% (inside) of the magnitude of maximum hoop strain in un-pressurized tests.

By comparing the inside and outside hoop strains, it can be concluded that the pipe cross-section is under a localized bending in all the three tests. For three tests at a specific location of the excavator, the middle of Sections 2 and 4, the sign of the inside hoop strain changed from positive to negative while the sign of the outside hoop strain changed from negative to positive.

3.1.1.3 Hoop strains at the 90°

History of hoop strain at the side (90°) of Section 1 during tests 1, 2, and 3 is shown in Figure 3.3. As expected, there is a good agreement between test 1 and test 2. The magnitude of hoop strain is reduced as a result of internal pressure in test 3.

For un-pressurized tests, the maximum hoop strain was +92με (inside) and -50με (outside) when the excavator was at Section 7, the end position of excavation. For test 3, when excavator was at Section 7, the maximum hoop strain was +55με (inside) and -27με (outside), which is 60% (inside) and 54% (outside) of the magnitude of maximum hoop strain in un-pressurized tests.

By comparing the inside and outside hoop strains, it can be concluded that the pipe cross-section is under a localized bending in all the three tests. For un-pressurized pipe at a specific location of the excavator, the middle of Sections 2 and 4, the sign of the outside hoop strain changed from positive to negative while the sign of the inside hoop strain changed from negative to positive. However in test 3, the sign of the cross-section bending strains didn't change with the location of excavator.

3.1.1.4 Longitudinal strains at the 0° and 180°

History of longitudinal strain at the top (0°) and the bottom (180°) of Section 1 during tests 1, 2, and 3 is shown in Figure 3.4. As expected, there is a good agreement between test 1 and test 2.

For un-pressurized tests, the maximum longitudinal strain was +36με (top) and -37με (bottom) when the excavator was at Section 4. For test 3, when excavator was also at Section 4, the longitudinal strain attains the maximum of +39με (top) and -33με

(bottom), which was 108% (top) and 89% (bottom) of the magnitude of maximum longitudinal strain in un-pressurized tests.

By comparing the top and bottom longitudinal strains, it can be concluded that the pipe is under a longitudinal bending in all the three tests. At a specific location of the excavator, for instance, for test 1 this location is Section 2, the sign of the bottom longitudinal strain changed from positive to negative while the sign of the top longitudinal strain changed from negative to positive. When the excavator was at Section 7, the longitudinal strains in all the three tests decreased gradually and approached to zero.

3.1.2 Section 2

3.1.2.1 Longitudinal strains at the 0° and 180°

History of longitudinal strain at the top (0°) and the bottom (180°) of Section 2 during tests 1, 2, and 3 is shown in Figure 3.5. As expected, there is a good agreement between test 1 and test 2.

For un-pressurized tests, the maximum longitudinal strain was -106με (top) and +69με (bottom) when the excavator was at Section 2. For test 3, the maximum longitudinal strain was -39με (top) and +39με (bottom) when the excavator was at middle of Sections 2 and 4, which was 37% (top) and 57% (bottom) of the magnitude of maximum longitudinal strain in un-pressurized tests. When the excavator was at section 7, for un-pressurized tests the maximum longitudinal strain was +52με (top) and -59με (bottom); for test 3, the longitudinal maximum strain was +52με (top) and -45με (bottom), which was 100% (top) and 76% (bottom) of the magnitude of maximum longitudinal strain in un-pressurized tests at this location of excavator.

By comparing the top and bottom longitudinal strains, it can be concluded that the pipe is under a longitudinal bending in all the three tests. At a specific location of the excavator, for instance, for test 1 this location is Section 4, the sign of the bottom longitudinal strain changed from positive to negative while the sign of the top longitudinal strain changed from negative to positive.

3.1.3 Section 3

3.1.3.1 Hoop strains at the 0°

History of hoop strain at the top (0°) of Section 3 during tests 1, 2, and 3 is shown in Figure 3.6. As expected, there is a good agreement between test 1 and test 2. The magnitude of hoop strain is reduced as a result of internal pressure in test 3.

For un-pressurized tests, the maximum hoop strain was -122με (outside) when the excavator was at Section 2. The maximum hoop strain was -21με (outside) for test 3, which is 17% of the magnitude of maximum hoop strain in un-pressurized tests.

For un-pressurized pipe at a specific location of the excavator, the middle of Section 4 and 7, the sign of the outside hoop strain changed from negative to positive.

3.1.3.2 Hoop strains at the 180°

History of hoop strain at the bottom (180°) of Section 3 during tests 1, 2, and 3 is shown in Figure 3.7. As expected, there is a good agreement between test 1 and test 2. The magnitude of hoop strain is reduced as a result of internal pressure in test 3.

For un-pressurized tests, the maximum hoop strain was -134με (outside) and +116με (inside) when the excavator was at Section 2. When the excavator was at Section 7, the maximum hoop strain was +144με (outside) and -122με (inside). For test 3, the maximum hoop strain was +77με (outside) and -76με (inside) when excavator was at

Section 7, which is 53% (outside) and 62% (inside) of the magnitude of maximum hoop strain in un-pressurized tests at the same location of excavator.

By comparing the inside and outside hoop strains, it can be concluded that the pipe cross-section is under a localized bending in all the three tests. For three tests at a specific location of the excavator, for example, for un-pressurized tests this location is Section 4, the sign of the inside hoop strain changed from positive to negative while the sign of the outside hoop strain changed from negative to positive.

3.1.3.3 Hoop strains at the 45°

History of hoop strain (45°) of Section 3 during tests 1, 2, and 3 is shown in Figure 3.8. As expected, there is a good agreement between test 1 and test 2. The magnitude of hoop strain is reduced as a result of internal pressure in test 3.

For un-pressurized tests, the maximum hoop strain was +54με (outside) and -67με (inside) when the excavator was at the middle of Sectiona 2 and 4. For test 3, at this location of excavator, the maximum hoop strain was +23με (inside) and -34με (outside), which is 43% (positive) and 51% (negative)of the magnitude of maximum hoop strain in un-pressurized tests.

By comparing the inside and outside hoop strains, it can be concluded that the pipe cross-section is under a localized bending in all the three tests. The hoop strain changes significantly with the movement of excavator from left to right or from right to left.

3.1.3.4 Hoop strains at the 315°

History of hoop strain (315°) of Section 3 during tests 1, 2, and 3 is shown in Figure 3.9. As expected, there is a good agreement between test 1 and test 2. The magnitude of hoop strain is reduced as a result of internal pressure in test 3.

For un-pressurized tests, the maximum hoop strain was +63με (outside) and -59με (inside) when the excavator was at section 2. For test 3, the maximum hoop strain was +37με (inside) and -23με (outside), which is 59% (positive) and 39% (negative) of the magnitude of maximum hoop strain in un-pressurized tests.

By comparing the inside and outside hoop strains, it can be concluded that the pipe cross-section is under a localized bending in all the three tests. The hoop strain changes significantly with the movement of excavator from left to right or from right to left.

3.1.3.5 Hoop strains at the 90°

History of hoop strain at the side (90°) of Section 3 during tests 1, 2, and 3 is shown in Figure 3.10. As expected, there is a good agreement between test 1 and test 2. The magnitude of hoop strain is reduced as a result of internal pressure in test 3.

For un-pressurized tests, the maximum hoop strain was -134με (inside) and +118με (outside) when the excavator was at Section 2. When the excavator was at section 7, the end position of excavation, the maximum hoop strain was +83με (inside) and -79με (outside). For test 3, when excavator was at Section 7, the maximum hoop strain was +46με (inside) and -42με (outside), which was 55% (inside) and 53% (outside) of the magnitude of maximum hoop strain in un-pressurized tests at the same excavator position.

By comparing the inside and outside hoop strains, it can be concluded that the pipe cross-section is under a localized bending in all the three tests. For un-pressurized pipe at a specific location of the excavator, Section 4, the sign of the outside hoop strain changed from positive to negative while the sign of the inside hoop strain changed from negative to positive. In test 3, the sign of the cross-section bending strains didn't change significantly.

3.1.3.6 Hoop strains at the 270°

History of hoop strain at the side (270°) of Section 3 during tests 1, 2 and 3 is shown in Figure 3.11. As expected, there is a good agreement between test 1 and test 2. The magnitude of hoop strain is reduced as a result of internal pressure in test 3.

For un-pressurized tests, the maximum hoop strain was +111με (outside) and -118με (inside) when the excavator was at the middle of Sections 2 and 4 respectively. When the excavator was at Section 7, the maximum hoop strain was +76με (inside) and -74με (outside). For test 3, the maximum hoop strain was +41με (inside) and -35με (outside) when the excavator was at Section 7, which is 54% (inside) and 47% (outside) of the magnitude of maximum hoop strain in un-pressurized tests at the same excavator position.

By comparing the inside and outside hoop strains, it can be concluded that the pipe cross-section is under a localized bending in all the three tests. For three tests at a specific location of the excavator, for example for test 1 this was the middle of Sections 4 and 7, the sign of the outside hoop strain changed from positive to negative while the sign of the inside hoop strain changed from negative to positive.

3.1.3.7 Longitudinal strains at the 0°

History of longitudinal strain at the top (0°) of Section 3 during tests 1, 2 and 3 is shown in Figure 3.12. As expected, there is a good agreement between test 1 and test 2.

For un-pressurized tests, the maximum longitudinal strain was -89με (top) when the excavator was at Section 2. For test 3, the longitudinal strain attains the maximum of -41με (top) when excavator was at the middle of Sections 2 and 4, which is 46% (top) of the magnitude of maximum longitudinal strain in un-pressurized tests. For tests without internal pressure, the maximum longitudinal strain was +48με (top) when the excavator was at Section 7. At this excavator location, for test 3, the maximum longitudinal strain was +51με (top), which was 106% (top) of the maximum longitudinal strain in un-pressurized tests.

At a specific location of the excavator, for instance, for test 1 this location is Section 4, the sign of the top longitudinal strain changed from negative to positive in all the three tests.

3.1.4 Section 4

3.1.4.1 Longitudinal strains at the 0° and 180°

History of longitudinal strain at the top (0°) and the bottom (180°) of Section 4 during tests 1, 2, and 3 is shown in Figure 3.13. As expected, there is a good agreement between test 1 and test 2.

For un-pressurized tests, the maximum longitudinal strain was -108με (top) and +56με (bottom) when the excavator was at Section 4. For test 3, the longitudinal maximum strain was -47με (top) and +56με (bottom) at this location of excavator, which was 44% (top) and 100% (bottom) of the magnitude of maximum longitudinal strain in

un-pressurized tests. For un-pressurized tests, the maximum longitudinal strain was +26με (top) and -47με (bottom) when the excavator was at Section 7. For test 3, the longitudinal maximum strain was +46με (top) and -21με (bottom) at this location of excavator, which was 177% (top) and 45% (bottom) of the magnitude of maximum longitudinal strain in un-pressurized tests at this location of excavator.

By comparing the top and bottom longitudinal strains, it can be concluded that the pipe is under a longitudinal bending in all the three tests. At a specific location of the excavator, for instance, for test 1 this location is Section 7, the sign of the bottom longitudinal strain changed from positive to negative while the sign of the top longitudinal strain changed from negative to positive.

3.1.5 Section 5

3.1.5.1 Hoop strains at the 0°

History of hoop strain at the top (0°) of Section 5 during tests 1, 2, and 3 is shown in Figure 3.14. As expected, there is a good agreement between test 1 and test 2. The magnitude of hoop strain is reduced as a result of internal pressure in test 3.

For un-pressurized tests, the maximum hoop strain was -142με (outside) and +176με (inside) when the excavator was at Section 4. When the excavator was at Section 7, the maximum hoop strain was +27με (outside) and -32με (inside). For test 3, when excavator was at Section 7, the maximum hoop strain was +12με (outside) and -23με (inside), which is 44% (outside) and 72% (inside) of the magnitude of maximum hoop strain in un-pressurized tests.

By comparing the inside and outside hoop strains, it can be concluded that the pipe cross-section is under a localized bending in all the three tests. For un-pressurized

pipe at a specific location of the excavator, Section 7, the sign of the inside hoop strain changed from positive to negative while the sign of the outside hoop strain changed from negative to positive. For test 3, the sign of the cross-section bending strains changed when the excavator moved on and left Section 4.

3.1.5.2 Hoop strains at the 180°

History of hoop strain at the bottom (180°) of Section 5 during tests 1, 2, and 3 is shown in Figure 3.15. As expected, there is a good agreement between test 1 and test 2. The magnitude of hoop strain is reduced as a result of internal pressure in test 3.

For un-pressurized tests, the maximum hoop strain was -144με (outside) and +114με (inside) when the excavator was at Section 4. When the excavator was at Section 7, the maximum hoop strain was +84με (outside) and -93με (inside). For test 3, the maximum hoop strain was +65με (outside) and -60με (inside) when excavator was at Section 7, which was 77% (outside) and 65% (inside) of the magnitude of maximum hoop strain in un-pressurized tests at the same location of excavator.

By comparing the inside and outside hoop strains, it can be concluded that the pipe cross-section is under a localized bending in all the three tests. For un-pressurized tests at a specific location of the excavator, for instance in test 1 this location was Section 7, the sign of the inside hoop strain changed from positive to negative while the sign of the outside hoop strain changed from negative to positive. However, in test 3, the sign of the cross-section bending didn't change with the location of excavator.

3.1.5.3 Hoop strains at the 45°

History of hoop strain (45°) of Section 5 during tests 1, 2, and 3 is shown in Figure 3.16. As expected, there is a good agreement between test 1 and test 2. The magnitude of hoop strain is reduced as a result of internal pressure in test 3.

For un-pressurized tests, the maximum hoop strain was +64με and -54με (inside) when the excavator was at the middle of Sections 2 and 4, and at the middle Sections 4 and 7 respectively. For test 3, the maximum hoop strain was +21με (outside) and -33με (inside) when the excavator was at Section 7, which was 33% (positive) and 61% (negative) of the magnitude of maximum hoop strain in un-pressurized tests.

By comparing the inside and outside hoop strains, it can be concluded that the pipe cross-section is under a localized bending in all the three tests. The hoop strain changed significantly with the movement of excavator from left to right or from right to left.

3.1.5.4 Hoop strains at the 315°

History of hoop strain (315°) of Section 5 during tests 1, 2, and 3 is shown in Figure 3.17. As expected, there is a good agreement between test 1 and test 2. The magnitude of hoop strain is reduced as a result of internal pressure in test 3.

For un-pressurized tests, the maximum hoop strain was +81με (outside) and -98με (inside) when the excavator was at the middle Sections 4 and 7 in test 2. For test 3, the maximum hoop strain was +23με (inside) and -22με (outside) when the excavator was at the middle of Sections 2 and 4, which is 28% (positive) and 22% (negative) of the magnitude of maximum hoop strain in un-pressurized tests.

By comparing the inside and outside hoop strains, it can be concluded that the pipe cross-section is under a localized bending in all the three tests. The hoop strain changed significantly with the movement of excavator from left to right or from right to left.

3.1.5.5 Hoop strains at the 90°

History of hoop strain at the side (90°) of Section 5 during tests 1, 2, and 3 is shown in Figure 3.18. As expected, there is a good agreement between test 1 and test 2. The magnitude of hoop strain is reduced as a result of internal pressure in test 3.

For un-pressurized tests, the maximum hoop strain was -143με (inside) and +116με (outside) when the excavator was at Section 4. When the excavator was at Section 7, the end position of excavation, the maximum hoop strain was +37με (inside) and -44με (outside). In test 3, when excavator was at Section 7, the maximum hoop strain was +36με (inside) and -43με (outside), which is 97% (inside) and 98% (outside) of the magnitude of maximum hoop strain in un-pressurized tests at the same excavator position.

By comparing the inside and outside hoop strains, it can be concluded that the pipe cross-section is under a localized bending in all the three tests. For un-pressurized pipe at a specific location of the excavator, Section 7, the sign of the outside hoop strain changed from positive to negative while the sign of the inside hoop strain changed from negative to positive. In test 3, the sign of the cross-section bending strains changed when the excavator moved on and left Section 4.

3.1.5.6 Hoop strains at the 270°

History of hoop strain at the side (270°) of Section 5 during tests 1, 2, and 3 is shown in Figure 3.19. As expected, there is a good agreement between test 1 and test 2. The magnitude of hoop strain is reduced as a result of internal pressure in test 3.

For un-pressurized tests, the maximum hoop strain was -134με (inside) and +110με (outside) when the excavator was at Section 4. When the excavator was at Section 7, the end position of excavation, the maximum hoop strain was +40με (inside) and -39με (outside). For test 3, when excavator was at Section 7, the maximum hoop strain was +35με (inside) and -34με (outside), which is 88% (inside) and 87% (outside) of the magnitude of maximum hoop strain in un-pressurized tests at the same excavator position.

By comparing the inside and outside hoop strains, it can be concluded that the pipe cross-section is under a localized bending in all the three tests. For un-pressurized pipe at a specific location of the excavator, Section 7, the sign of the outside hoop strain changed from positive to negative while the sign of the inside hoop strain changed from negative to positive. In test 3, the sign of the cross-section bending strains also changed when the excavator moved on and left Section 4.

3.1.5.7 Longitudinal strains at the 0°

History of longitudinal strain at the top (0°) of Section 5 during tests 1, 2, and 3 is shown in Figure 3.20. As expected, there is a good agreement between test 1 and test 2.

For un-pressurized tests, the maximum longitudinal strain was -126με (top) when the excavator was at Section 4. For test 3, the longitudinal strain attains the maximum of -51με (top) when excavator was at Section 4, which is 40% of the magnitude of maximum

longitudinal strain in un-pressurized tests. For un-pressurized tests, the maximum longitudinal strain was +20με (top) when the excavator was at Section 7. For test 3, the maximum longitudinal strain was +43με (top) when excavator was at Section 7, which was 215% of the maximum longitudinal strain in un-pressurized tests.

At a specific location of the excavator, for instance, for test 1 and test 2 this location is Section 7, the sign of the top longitudinal strain changed from negative to positive in all the three tests.

3.1.6 Section 6

History of deformation in the vertical and horizontal directions of Section 6 during tests 1, 2, and 3 is shown in Figure 3.21. As expected, there is a good agreement between test 1 and test 2. The magnitude of deformation is reduced as a result of internal pressure in test 3.

For un-pressurized tests, the maximum deformation was -2.77 mm (vertical) and +2.60 mm (horizontal) when the excavator was at Section 4. In test 3, the maximum deformation at this location of excavator was -0.46 mm (vertical) and +0.48 mm (horizontal), which is 17% (vertical) and 18% (horizontal) of the magnitude of maximum deformation in un-pressurized tests. When excavator was at Section 7, the end position of excavation, the maximum deformation was +1.24 mm (vertical) and -0.97 mm (horizontal) in un-pressurized tests. For test 3, when excavator was at Section 7, the maximum deformation was +0.71 mm (vertical) and -0.42 mm (horizontal), which is 57% (vertical) and 43% (horizontal) of the magnitude of maximum deformation in un-pressurized tests.

By comparing the vertical and horizontal deformation, it can be concluded that the pipe cross-section experienced a process of flattening and re-rounding in all the three tests. For un-pressurized pipe at a specific location of the excavator, for instance for test 1 this location was Section 7, the sign of the vertical deformation changed from negative to positive while the sign of the horizontal deformation changed from positive to negative. In test 3, the sign of the vertical and horizontal deformation changed when the excavator moved on and away from Section 4

History of diagonal deformation of Section 6 during tests 1, 2, and 3 is shown in Figure 3.22. As expected, there is a good agreement between test 1 and test 2.

For un-pressurized tests, the maximum deformation was +1.27 mm and -0.93 mm when the excavator was at the middle of Sections 2 and 4 and at the middle Sections 4 and 7 respectively. In test 3, the maximum deformation was +0.26 mm and -0.13 mm when the excavator was at Section 7 and, at the middle Sections 4 and 7 respectively. This is 20% (positive) and 14% (negative) of the magnitude of maximum deformation in un-pressurized tests.

As shown in the figure, the diagonal deformation changed significantly with the movement of excavator from left to right or from right to left.

3.1.7 Section 7

3.1.7.1 Hoop strains at the 0°

History of hoop strain at the top (0°) of Section 7 during tests 1, 2, and 3 is shown in Figure 3.23. As expected, there is a good agreement between test 1 and test 2. The magnitude of hoop strain is reduced as a result of internal pressure in test 3.

For un-pressurized tests, the maximum hoop strain was +195με (inside) and -132με (outside) when the excavator was at Section 7. For test 3, when excavator was at Section 7, the maximum hoop strain was +32με (inside) and -27με (outside), which is 16% (inside) and 20% (outside) of the magnitude of maximum hoop strain in un-pressurized tests.

By comparing the inside and outside hoop strains, it can be concluded that the pipe cross-section is under a localized bending in all the three tests. For un-pressurized pipe the sign of the outside and inside hoop strain didn't changed. However in test 3, the sign of the cross-section bending strains changed when the excavator moved on Section 7.

3.1.7.2 Hoop strains at the 180°

History of hoop strain at the bottom (180°) of Section 7 during tests 1, 2, and 3 is shown in Figure 3.24. As expected, there is a good agreement between test 1 and test 2. The magnitude of hoop strain is reduced as a result of internal pressure in test 3.

For un-pressurized tests, the maximum hoop strain was -140με (outside) when the excavator was at Section 7. For test 3, when excavator was at Section 7, the maximum hoop strain was -14με (outside), which is 10% of the magnitude of maximum hoop strain in un-pressurized tests.

As shown in the figure, for un-pressurized pipe the sign of the outside and inside hoop strain didn't changed. However in test 3, the sign of the cross-section bending strains changed when the excavator moved on Section 7.

3.1.7.3 Hoop strains at the 90°

History of hoop strain at the side (90°) of Section 7 during tests 1, 2, and 3 is shown in Figure 3.25. As expected, there is a good agreement between test 1 and test 2.

The magnitude of hoop strain is reduced as a result of internal pressure in test 3.

For un-pressurized tests, the maximum hoop strain was +118με (outside) and -130με (inside) when the excavator was at Section 7. For test 3, when excavator was at Section 7, the maximum hoop strain was +12με (inside) and -23με (outside), which is 12% (outside) and 18% (inside) of the magnitude of maximum hoop strain in un-pressurized tests.

By comparing the inside and outside hoop strains, it can be concluded that the pipe cross-section is under a localized bending in all the three tests. For un-pressurized pipe the sign of the outside and inside hoop strain didn't changed. However in test 3, the sign of the cross-section bending strains changed when the excavator moved on Section 7.

3.1.7.4 Longitudinal strains at the 0° and 180°

History of longitudinal strain at the top (0°) and the bottom (180°) of Section 7 during tests 1, 2, and 3 is shown in Figure 3.26. As expected, there is a good agreement between test 1 and test 2.

For un-pressurized tests, the maximum longitudinal strain was -124με (top) and +72με (bottom) when the excavator was at Section 7. For test 3, when excavator was at Section 7, the longitudinal strain attains the maximum of -58με (top) and +66με (bottom), which was 47% (top) and 92% (bottom) of the magnitude of maximum longitudinal strain in un-pressurized tests.

By comparing the top and bottom longitudinal strains in all the three tests, it can be concluded that the pipe is under a longitudinal bending. At a specific location of the excavator, for instance, for test 1 this location is Section 4, the sign of the top longitudinal

strain changed from positive to negative while the sign of the bottom longitudinal strain changed from negative to positive.

3.1.8 Summary of Summer Test Results

In summary, based on analysis of the strain and deformation history in the process of excavation, it can be concluded that the pipe cross-section is under a localized bending in all the tests by comparing the inside and outside hoop strains. By comparing the top and bottom longitudinal strains, the pipeline is under a longitudinal bending in all the three tests. The signs of the strains changed at a specific position of excavator. There is a good agreement between test 1 and test 2. The magnitude of hoop strain and deformation is reduced as a result of internal pressure.

3.2 Data Analysis of Summer Excavation Tests

As presented in the plots of the history of strains and deformation of the specimen in the whole process of summer excavation, the strains and deformation changed with the position of excavator. The strains and deformation are analyzed position by position. All the strain and deformation were measured by referring to the "zero strain or deformation". In the un-pressurized test, this is when the specimen was (1) buried, (2) filled with water, (3) internal pressure was zero, and (4) excavator was not in the field and had no effects. In the pressurized test, this is when the specimen was (1) buried, (2) filled with water, (3) internal pressure was 7.24 MPa, and (4) excavator was not in the field and had no effects.

3.2.1 Summer Un-pressurized Test

3.2.1.1 Hoop strains

In Table 3.1 is shown the summary results of hoop strains of summer excavation test 1.

When the pipeline was buried, the maximum hoop strains occurred in the section of pipeline that the excavator was just sitting above. The maximum strains of Sections 3, 5 and 7 under this condition are shown in Figure 3.27. The maximum hoop strain was +195με at top and -144με at bottom.

With the excavation of excavator the instrumented Sections 1, 3 and 5 got exposed sequentially. At a specific position of excavator, the sign of the hoop strain changed. For Section 1, this position was about the middle of Sections 2 and 4. For Sections 3 and 5, this was around Section 4 and Section 7 respectively. The hoop strain increased and attained another maximum when the excavator moved backwards to Section 7, the end position of excavation. Under this condition the maximum strains of Sections 1, 3 and 5 are shown in Figure 3.28. As shown in this figure, the maximum hoop strain was +144με and -120με at bottom. The bottom was the most critical position comparing the strains at the top or side.

3.2.1.2 Ovalization

The vertical and horizontal deformation and the corresponding ovalization measured at Section 6 are presented in Table 3.2.

As shown in the table, the maximum deformation was -2.77 mm in vertical direction and 2.60 mm in horizontal direction. This happened when excavator was just sitting above this Section 6. The sign indicates the flattening in vertical direction and

expanding in horizontal direction. Hence, the maximum additional ovalization due to the excavation was

$$(|d_h| + |d_v|)/D = (2.60+2.77)\ \text{mm}/914\text{mm} = 0.59\%.$$

When excavator was at the final position of excavator, the maximum ovalization was -0.24%. The negative sign represented that the cross section deformed in the opposite direction as shown in Figure 3.29.

As shown in Table 3.3, the maximum deformation in the diagonal directions is 1.27 mm or –0.93 mm. Therefore, the deformation in vertical and horizontal directions is more critical.

3.2.1.3 Longitudinal strains

The summary results of longitudinal strains are presented in Table 3.4.

A schematic diagram of longitudinal deformation of the specimen is shown in Figure 3.30 at subsequent specific positions of excavator in the excavation process. The weight of excavator and the force due to the removal of soil to produce an upward load relative to the original buried state is all demonstrated together with the deformation. Basically, the specimen was experiencing the global bending in the longitudinal direction.

As that in hoop strain, the maximum longitudinal strains occurred in the instrumented section of the specimen the excavator was just sitting on. The maximum longitudinal strains are shown in Figure 3.31. The magnitude of negative strains at the top was greater than the positive strain at the bottom. The ratio of top over bottom is about 1.86~2.06 times.

Due to the excavation, another maximum longitudinal strain happened at the exposed sections, Sections 1 and 2 as shown in Figure 3.32. For Section 1, the maximum

longitudinal strains occurred when the excavator was at Section 4. The longitudinal strains reached the maximum value, +36με at top and -37με at bottom until they reduced. The maximum longitudinal strains were measured at Section 2 when the excavator was at Section 7. They were +52με at top and -59με at bottom. The magnitude of longitudinal strains at the top and bottom was almost equal.

3.2.2 Comparison of Summer Un-pressurized Test 1 and 2

As shown in the results of the history of strain and deformation in summer tests, the un-pressurized test 1 and test 2 agreed very well. The data of summer excavation test 2 was analyzed in the same way as test 1. The results were summarized and compared with test 1 as follows.

3.2.2.1 Hoop strains

The maximum hoop strains occurred at Sections 3, 5 and 7 where the excavator was just sitting. Another maximum hoop strain was measured at the exposed sections, Sections 1, 3 and 5 when the excavator was at Section 7. For the specific section under these two critical conditions, the maximum hoop strains in test 1 and test 2 are presented in Table 3.5. From this table, it is found:

1. Under critical condition 1, the maximum hoop strain was +195με and -144με in test 1. They were +195με and -124με in test 2, which are 100 % (positive) and 86% (negative) of the maximum hoop strain in test 1.
2. Under critical condition 2, the maximum hoop strains in test 1 and 2 at the exposed sections (i.e., Sections 1, 3 and 5) of specimen are very close. The maximum hoop strain was +144με and -120με at bottom in test 1. They were +144με and -128με in

test 2, which are 100 % (positive) and 106% (negative) of the maximum hoop strain in test 1.

3.2.2.2 Ovalization

In Table 3.6 were compared the maximum vertical and horizontal deformation in test 1 and test 2 at the two critical conditions. Under critical condition 1, the maximum ovalization was 0.59% in test 1 and 0.31% in test 2. Under critical condition 2, the maximum ovalization was -0.24% for test 1 and -0.21% for test 2. The deformation under the two critical conditions is opposite. The cross-section re-rounded with the removal of soil as shown in Figure 3.29. The difference existed because of the different compaction and excavator positions.

The deformations in diagonal directions of test 1 and 2 were presented in Table 3.3. As shown in this table, they are smaller than the deformation in vertical and horizontal directions. Hence, the maximum deformation occurred in the vertical and horizontal directions.

3.2.2.3 Longitudinal strains

In Table 3.7 are given the maximum longitudinal strains of test 1 and test 2 for Sections 1, 2, 3, 4, 5 and 7.

Comparing the maximum strain in test 1 and test 2, it is found that the maximum longitudinal strains of test 1 and 2 occurred at the same condition as discussed before, i.e. the critical condition 1 and critical condition 2. The maximum longitudinal strains in the two tests are very close. Under critical condition 1, the maximum negative strain was -126με in test 1 and -117με in test 2. The maximum positive strains was +72με for both

tests. Under critical condition 2, the maximum negative strain was -59με in test 1 and -52με in test 2. The maximum positive strains are +52με in test 1 and +36με in test 2.

The schematic diagram of longitudinal deformation in excavation process is shown in Figure 3.30 and the maximum strains in Figure 3.31 and Figure 3.32.

3.2.3 Summer Pressurized Test

3.2.3.1 Hoop strains

The results of maximum hoop strains in summer pressurized test (test 3) are presented in Table 3.8.

At buried state the hoop strains measured in the instrumented sections was more complicated in pressurized test due to the combining action of excavator and internal pressure. The cross section under the excavator may get flatten and meanwhile the neighboring section may get re-round due to the internal pressure. The reason of re-rounding is different against that in critical condition 2. The following three situations caused the maximum hoop strains in pressurized test:

1. The first situation is that the maximum hoop strain at top and bottom is negative outside and positive inside while the maximum hoop strain at two sides is positive outside and negative inside. This resulted from the action of excavator to flatten the pipe cross section. The instrumented sections where the maximum strains measured were still buried. The maximum hoop strains are shown in Figure 3.33.
2. The second situation is that the maximum hoop strain at top and bottom is positive outside and negative inside while the maximum hoop strain at two sides is negative outside and positive inside. This is caused by the action of internal pressure to re-

round the pipe cross section. The instrumented sections where the maximum strains measured were also buried. The maximum hoop strains are shown in Figure 3.34.

3. The third situation is that the maximum hoop strain at top and bottom is positive outside and negative inside while the maximum hoop strain at two sides is negative outside and positive inside. This is because the pipe was re-rounded due to the removal of the overburden. The maximum hoop strains are shown in Figure 3.35.

The maximum hoop strains were +32με and -28με in situation 1. They were +30με and -34με in situation 2. So the maximum strain in buried state was +32 and -34με. The maximum hoop strains were +77με and –76με in situation 3. Therefore the maximum hoop strains happened at the bottom of the specimen under critical condition 2.

3.2.3.2 Ovalization

The maximum and average deformation in vertical, horizontal and diagonal directions are presented in Table 3.9. As shown in this table, the average deformation in vertical direction was positive and gradually increased with the backward movement of the excavator. But it became negative when the excavator was at Section 4 (Sections 4 and 6 are very close). After the excavator moved back, it returned to positive again and attained the maximum positive deformation when the excavator was at Section 7. On the contrary, the deformation in horizontal direction was opposite in this process. Therefore, in the whole process of excavation, the cross section 6 was re-rounded first due to the internal pressure before the excavator moved on it. Then it was flattened as the excavator was sitting on it. The cross section was re-rounded again after excavator left it and finally it was re-rounded to the maximum with the removal of overburden.

As presented in Table 3.9, the maximum vertical deformation was -0.46 mm and horizontal deformation was +0.48 mm when the excavator was at Section 4. The corresponding maximum ovalization was 0.10%. When this section was exposed, the maximum vertical deformation was +0.71 mm and the maximum horizontal deformation -0.42 mm. The corresponding maximum ovalization was -0.12% in opposite direction. The maximum deformation in diagonal direction was +0.26 mm and -0.13 mm, which were less than the maximum deformation in vertical and horizontal directions.

3.2.3.3 Longitudinal strains

The summary results of the maximum longitudinal strains in summer pressurized test are presented in Table 3.10.

The maximum longitudinal strains happened under critical condition 1 and 2. The maximum longitudinal strains under critical condition 1 are shown in Figure 3.36. The maximum longitudinal strains were +66με at bottom and -58με at top. The maximum longitudinal strains under critical condition 2 are shown in Figure 3.37. The maximum longitudinal strains were +52με at top and -45με at bottom. The maximum longitudinal strains measured in the whole excavation process were +66με and -58με.

3.2.4 Comparison of Summer Un-Pressurized and Pressurized Tests

3.2.4.1 Hoop strains

In Table 3.11 is presented the maximum hoop strain measured at a specific instrumented section under two critical conditions: (1) when the excavator was just sitting on this section, and (2) when the excavator was at the final position, i.e. Section 7. Under both critical conditions, the maximum hoop strains in pressurized test are all less than the strains in un-pressurized test. The maximum hoop strains under these two conditions are

summarized in Figure 3.38. Under critical condition 1, the maximum hoop strains were +195με and −144με in un-pressurized test while they were +32με and −28με in pressurized test. The ratio of maximum hoop strain of un-pressurized test to pressurized test was about 5.6. Under critical condition 2, the maximum hoop strains were +144με and −128με in un-pressurized test while they were +77με and −76με in pressurized test. The ratio of maximum hoop strain of un-pressurized test to pressurized test was about 1.8.

3.2.4.2 Ovalization

The comparison of deformation is shown in Tables 3.12 and 3.13 for un-pressurized and pressurized tests. The maximum ovalizations are summarized in Table 3.14. All the ovalizations in un-pressurized tests are greater than the ovalization in pressurized test either in critical condition 1 or 2. Under critical condition 1, the maximum ovalization was 0.59% in un-pressurized test and 0.10% in pressurized test. The ratio of maximum ovalization of un-pressurized test to pressurized test was about 5.9. Under critical condition 2, the maximum ovalization was 0.24% in un-pressurized test and 0.12% in pressurized test. The ratio of maximum ovalization of un-pressurized test to pressurized test was about 2.0. The maximum ovalizations under these two critical conditions are summarized in Figure 3.39.

For both the un-pressurized and pressurized tests, the maximum ovalization was produced due to the maximum deformation in vertical and horizontal directions.

3.2.4.3 Longitudinal strains

The comparison of longitudinal strains in un-pressurized and pressurized tests is showed in Table 3.15.

By comparing the strains of pressurized and un-pressurized test in the table, it was found:

1. The magnitude of maximum negative longitudinal strains in pressurized test was smaller than those in un-pressurized test under critical condition 1.
2. The magnitude of maximum positive longitudinal strain at bottom was less than the magnitude of maximum negative strain at top in un-pressurized test under critical condition 1. However, they are closer in pressurized test.
3. The maximum longitudinal strains of un-pressurized and pressurized tests have not significant difference under critical condition 2. Moreover, the magnitude of maximum negative strain at bottom and maximum positive strain at top were also close.

The maximum longitudinal strains under the two conditions are summarized in Figure 3.40. Under critical condition 1, the maximum longitudinal strains were +72με at bottom and –126με at top for un-pressurized test while they were +66με at bottom and –58με at top for pressurized test. Under critical condition 2, the maximum hoop strains were +52με at top and –59με at bottom in un-pressurized test while they were +52με at top and –45με at bottom in pressurized test.

3.3 Impact Factor

The impact factor was investigated by comparing the peak strain and static strain under critical condition 1. The peak strain is caused by the weight, rocking and digging of excavator. The static strain results from the weight of excavator.

The result of impact factor of hoop strain in summer un-pressurized tests is shown in Figure 3.41. The impact factors vary from 1.14 to 2.00 with the average of 1.38.

The result of impact factor of longitudinal strain in summer un-pressurized tests is shown in Figure 3.42. The impact factors vary from 1.07 to 1.42 with the average of 1.27.

The impact factors of deformation in summer un-pressurized tests vary from 1.16 to 1.27 with the average of 1.22.

For pressurized tests, the impact factors of hoop strain vary from 1.33 to 2.55 with the average of 1.74. For longitudinal strain, they vary from 1.11 to 1.85 with the average of 1.44.

Table 3.1 Summary result of hoop strain in summer un-pressurized test 1

Excavator Position	Strain	Section 1			Section 3				Section 5				Section 7		
		Top	Side(R)	Btm	Top(o)	Side(R)	Btm	Side(L)	Top	Side(R)	Btm	Side(L)	Top	Side(R)	Btm(o)
2	Max	80	55	59		118	116	79	62	69	87	54	14	18	
	Min	-81	-49	-60	-120	-134	-134	-106	-54	-82	-90	-54	-13	-17	-38
2~4	Max	Start to re-round				98	115	111	132	90	110	91	28	29	
	Min				-118	-116	-132	-118	-111	-108	-136	-108	-18	-33	-65
4	Max				Start to re-round				176	116	114	110	54	45	
	Min								-142	-143	-144	-134	-26	-44	-77
4~7	Max								78	57	56	64	115	89	
	Min								-70	-68	-79	-66	-62	-88	-128
7	Max	45	84	123	43	81	144	76	23	37	83	40	195	118	
	Min	-48	-49	-119		-78	-120	-70	-32	-40	-84	-39	-132	-130	-140

Note:
Side(R): Right side (90°) Top: (0°)
Side(L): Left side (270°) Btm: Bottom(180°)

Table 3.2 Summary results of ovalization measured at Section 6 in summer un-pressurized test 1

Excavator Position		Section 6 Displacement(mm)		Additional Ovalization(%)
		Vertical	Horizontal	
2R	Avg	-0.82	0.83	0.18
	Max	-0.70	1.57	0.34
	Min	-1.58	0.60	
2~4R	Avg	-1.16	1.16	0.25
	Max	-0.81	1.71	0.38
	Min	-1.73	0.81	
2~4L	Avg	-1.58	1.56	0.34
	Max	-0.90	2.27	0.49
	Min	-2.20	0.91	
4L	Avg	-2.18	2.11	0.47
	Max	-1.43	2.60	0.59
	Min	-2.77	1.43	
4R	Avg	-1.54	1.57	0.34
	Max	-1.25	1.82	0.41
	Min	-1.89	1.07	
4~7L	Avg	-1.02	1.11	0.23
	Max	-0.68	1.67	0.36
	Min	-1.65	0.85	
7R	Avg	1.21	-0.88	0.23
	Max	1.24	-0.81	0.24
	Min	1.20	-0.97	

Table 3.3 Maximum deformation measured in summer un-pressurized tests

Section		Section 6			
Position & Direction		Vertical	45-225	Horizontal	135-315
Test #1	Max	1.24	0.91	2.60	1.27
	Min	-2.77	-0.64	-0.97	-0.87
Test #2	Max	1.18	0.52	1.58	1.21
	Min	-1.26	-0.93	-0.77	-0.57

Table 3.4 Summary result of longitudinal strain in summer un-pressurized test 1

Excavator Position	Strain	Section 1			Section 2				S3	Section 4				S5	Section 7		
		Top(o)	BTM(i)	BTM(o)	Top(o)	Top(i)	BTM(i)	BTM(o)	Top(o)	Top(o)	Top(i)	BTM(i)	BTM(o)	Top(o)	Top(o)	BTM(i)	BTM(o)
2	Avg	-8	3	-10	-71	-72	50	33	-67	P.M. Increasing ↓					N.M. Increasing ↓		
	Max	3	13	1	-17	-23	61	40	-13								
	Min	-37	-3	-20	-92	-93	22	9	-85								
2~4	Avg	Transition from P.M. to N.M.													11	-15	-29
	Max														16	13	-2
	Min														-8	-18	-33
4	Avg	30	-28	-32	Transition from P.M. to N.M.					-76	-78	44	37	-96	Transition from N.M. to P.M.		
	Max	36	-22	-28						-31	-36	56	47	-38			
	Min	23	-34	-37						-108	-106	19	16	-126			
4~7	Avg	N.M.Decreasing ↓								P.M. Decreasing ↓					P.M. Increasing ↓		
	Max																
	Min																
7	Avg	14	-14	-12	45	37	-35	-55	43	Transition from P.M. to N.M.				Transition	103	66	50
	Max	21	-10	-9	52	44	-30	-50	48						-46	72	56
	Min	11	-20	-18	39	30	-40	-59	35						-124	45	29

Note: **P.M.—Positive Moment Strain**

N.M.—Negative Moment Strain

Table 3.5 Comparison of hoop strain between summer un-pressurized tests 1 and 2

Section	Excavator Position		Top (με)		Side (με)		Bottom (με)	
			Test 1	Test 2	Test 1	Test 2	Test 1	Test 2
Section 1	Section 2	Max.	80	82	55	24	59	20
		Min.	-81	-64	-49	-32	-60	-31
	Section 7	Max.	45	48	84	92	123	127
		Min.	-48	-47	-49	-50	-119	-128
Section 3	Section 2	Max.	---	---	118	65	116	34
		Min.	-120	-122	-134	-90	-134	-51
	Section 7	Max.	43	44	81	83	144	144
		Min.	---	---	-78	-79	-120	-122
Section 5	Section 4	Max.	176	155	116	65	114	14
		Min.	-142	-127	-143	-95	-144	-38
	Section 7	Max.	23	27	40	37	83	84
		Min.	-32	-28	-40	-44	-84	-93
Section 7	Section 7	Max.	195	195	118	99	---	---
		Min.	-132	-96	-130	-124	-140	-115

Table 3.6 Comparison of ovalization between summer un-pressurized tests 1 and 2

Excavator Position	Deflection measured (mm)				Ovalization	
	Vertical		Horizontal			
	Test 1	Test 2	Test 1	Test 2	Test 1	Test 2
Section 4	-2.77	-1.26	2.6	1.58	0.59	0.31
Section 7	1.24	1.18	-0.97	-0.77	0.24	0.21

Table 3.7 Comparison of longitudinal strain between summer un-pressurized tests 1 and 2

Excavator Position		Section 1		Section 2		Section 3	
		Test 1	Test 2	Test 1	Test 2	Test 1	Test 2
Section 2	Top	-37	-36	-93	-106	-85	-89
	Bottom	13	22	61	69		
Section 4	Top	36	20				
	Bottom	-37	-22				
Section 7	Top			52	34	48	36
	Bottom			-59	-52		

Excavator Position		Section 4		Section 5		Section 7	
		Test 1	Test 2	Test 1	Test 2	Test 1	Test 2
Section 2	Top						
	Bottom						
Section 4	Top	-108	-97	-126	-109		
	Bottom	56	43				
Section 7	Top					-124	-117
	Bottom					72	72

Table 3.8 Summary of the hoop strain in summer pressurized test

Excavator Position	Strain	Section 1 Top	Section 1 Side(R)	Section 1 Btm	Section 3 Top(o)	Section 3 Side(R)	Section 3 Btm	Section 3 Side(L)	Section 5 Top	Section 5 Side(R)	Section 5 Btm	Section 5 Side(L)	Section 7 Top	Section 7 Side(R)	Section 7 Btm(o)
2	Max	4 o	7 i	9 i	4	2 o	4 i	19 o	5 o	6 i	3 o	6 i	10 o	10 i	10
	Min	-5 i	0 o	-6 o	-3	-12 i	-13 o	-24 i	-10 i	-10 o	-6 i	-6 o	-24 i	-7 o	
2~4L(1)	Max	Getting exposed			11	-1 i	7 i	27 o	5 o	6 i	4 o	5 i			
	Min	and re-rounded			-4	-20 i	-27 o	-25 i	-10 i	-11 o	-9 i	-7 o			
2~4L(2)	Max				10	7 o	2 i	12 o	7 o	6 i	5 o	6 i			
	Min				-21	-23 i	-20 o	-19 i	-14 i	-14 o	-14 i	-8 o			Buried
2~4R(3)	Max				17	11 i	13 o	9 i	3 o	5 i	8 o	5 i			
	Min				7	-13 o	-28 i	-13 o	-12 i	-17 o	-20 i	-8 o			
4	Max				25				34 i	9 o	12 o	7 o			
	Min				Getting exposed				-26 o	-28 i	-34 i	-20 i			
4~7	Max				and re-rounded				21 i	9 i	23 o	7 i	6 o	8 i	6
	Min								-21 o	-18 o	-41 i	-14 i	-27 i	-19 o	
7	Max	21 o	55 i	73 o	15	46 i	77 o	41 i	12 o	36 i	65 o	35 i	31 i	5 i	0
	Min	-33 i	-27 o	-76 i		-42 o	-66 i	-35 o	-23 i	-43 o	-60 i	-34 o	-27 o	-18 o	-14
													32 i	12 i	10
													-27 i	-23 o	-13

7R

7L

i---Inside
o---Outside

Table 3.9 Summary of the deformation measured at Section 6 in summer pressurized test

Excavator Position	Average			Maximum			Minimum		
	Vertical	Horizontal	Diagonal	Vertical	Horizontal	Diagonal	Vertical	Horizontal	Diagonal
[illegible]	0.17	-0.10	0.06	0.20	-0.08	0.08	0.16	-0.12	0.03
[illegible]	0.18	-0.08	0.08	0.21	-0.06	0.12	0.15	-0.11	0.04
[illegible]	0.20	-0.07	0.09	0.27	0.02	0.17	0.12	-0.14	0.07
[illegible]	0.22	-0.06	0.05	0.29	-0.02	0.08	0.16	-0.12	0.03
[illegible]	-0.10	0.22	0.07	0.30	0.30	0.12	-0.29	0.05	0.03
[illegible]	-0.08	0.21	0.12	0.09	0.48	0.18	-0.46	0.09	0.08
[illegible]	0.23	-0.06	0.07	0.41	0.13	0.14	-0.03	-0.23	0.01
[illegible]	0.13	0.05	-0.07	0.27	0.17	-0.01	0.00	-0.08	-0.13
[illegible]	0.45	-0.22	0.13	0.66	-0.03	0.26	0.24	-0.40	-0.01
[illegible]	0.63	-0.37	0.08	0.71	-0.20	0.25	0.44	-0.42	0.00

Table 3.10 Summary of the longitudinal strain in summer pressurized test

Excavator Position		Section 1			Section 2			Section 3	Section 4		Section 5	Section 7		
		Top	BTM(i)	BTM(o)	Top	BTM(i)	BTM(o)	Top	Top	BTM	Top	Top	BTM(i)	BTM(o)
[redacted]	Avg	6	-5	-4	-18	21	20	-21	12	3	19	6	3	3
	Max	9	1	-3	-10	24	22	-17	17	5	26	6	6	5
	Min	4	-8	-6	-25	19	19	-25	9	1	7	5	3	2
[redacted]	Avg	Increasing			-16	32	30	-22	Transition			Increasing		
	Max	↓			3	39	37	-5	↓			↓		
	Min				-39	23	23	-41						
[redacted]	Avg	35	-31	-24	Transition				-26	45	-29	17	6	4
	Max	39	-29	-22	↓				-2	56	-5	18	9	8
	Min	31	-33	-27					-47	38	-51	12	4	1
[redacted]	Avg	19	-15	-8	49	-43	-41	49	41	-17	37	-34	57	54
	Max	22	-12	-6	52	-39	-37	51	46	-1	43	-20	66	62
	Min	17	-18	-11	46	-45	-44	45	25	-21	21	-58	46	45

Table 3.11 Comparison of maximum hoop strain between summer un-pressurized test and pressurized test

Section	Excavator Position		Top			Side			Bottom		
			Test 1	Test 2	Test 3	Test 1	Test 2	Test 3	Test 1	Test 2	Test 3
Section 1	Section 2	Max.	80	82	4	55	24	7	59	20	9
		Min.	-81	-64	-5	-49		0	-60	-31	-6
	Section 7	Max.	45	48	21	84	92	55	123	127	73
		Min.	-48	-47	-33	-49	-50	-27	-119	-128	-76
Section 3	Section 2	Max.				118	65	19	116	34	4
		Min.	-120	-122	-3	-134	-90	-24	-134	-51	-13
	Section 7	Max.	43	44	15	81	83	46	144	144	77
		Min.				-78	-79	-42	-120	-122	-66
Section 5	Section 4	Max.	176	155	34	116	65	9	114	14	12
		Min.	-142	-127	-26	-143	-95	-28	-144	-38	-34
	Section 7	Max.	23	27	12	40	37	36	83	84	65
		Min.	-32	-28	-23	-40	-44	-43	-84	-93	-60
Section 7	Section 7	Max.	195	195	32	118	99	12			
		Min.	-132	-96	-27	-130	-124	-23	-140	-115	-14

Table 3.12 Comparison of maximum vertical and horizontal deformation between summer un-pressurized test and pressurized test (unit: mm)

Excavator Position	Vertical direction			Horizontal direction		
	Test 1	Test 2	Test 3	Test 1	Test 2	Test 3
Section 4	-2.77	-1.26	-0.46	2.60	1.58	0.48
Section 7	1.24	1.18	0.71	-0.97	-0.77	-0.42

Table 3.13 Comparison of maximum diagonal deformation between summer un-pressurized test and pressurized test

	Test 1		Test 2		Test 3	
	Deformation (mm)	Excavator Position	Deformation (mm)	Excavator Position	Deformation (mm)	Excavator Position
Max.	1.27	Between. Section 2 and 4	1.21	Between. Section 4 and 7	0.26	Section 7
Min.	-0.87	Between. Section 4 and 7	-0.93	Between. Section 4 and 7	-0.13	Between. Section 4 and 7

Table 3.14 Comparison of maximum ovalization between summer un-pressurized test and pressurized test

Test No.	Critical Condition 1	Critical Condition 2
	Buried	Exposed
Test 1	0.59%	-0.24% *
Test 2	0.31%	-0.21% *
Test 3	0.10%	-0.12% *

*: "-" means the deformation is in opposite direction.

Table 3.15 Comparison of maximum longitudinal strain between summer un-pressurized test and pressurized test

Excavator Position	Test #	Section 1			Section 2			Section 3			Section 4			Section 5			Section 7		
		1	2	3	1	2	3	1	2	3	1	2	3	1	2	3	1	2	3
Section 2	Top	-37	-36	9	-93	-106	-25	-85	-89	-25									
	Bottom	13	22	-8	61	69	24												
Section 2~4 *	Top			36			-39			-41									
	Bottom			-28			39												
Section 4	Top	36	20	39							-108	-97	-47	-126	-109	-51			
	Bottom	-37	-22	-33							56	43	56						
Section 7	Top				52	34	52	48	36	51							-124	-117	-58
	Bottom				-59	-52	-45										72	72	66

Note: * Excavator was between Section 2 and 4

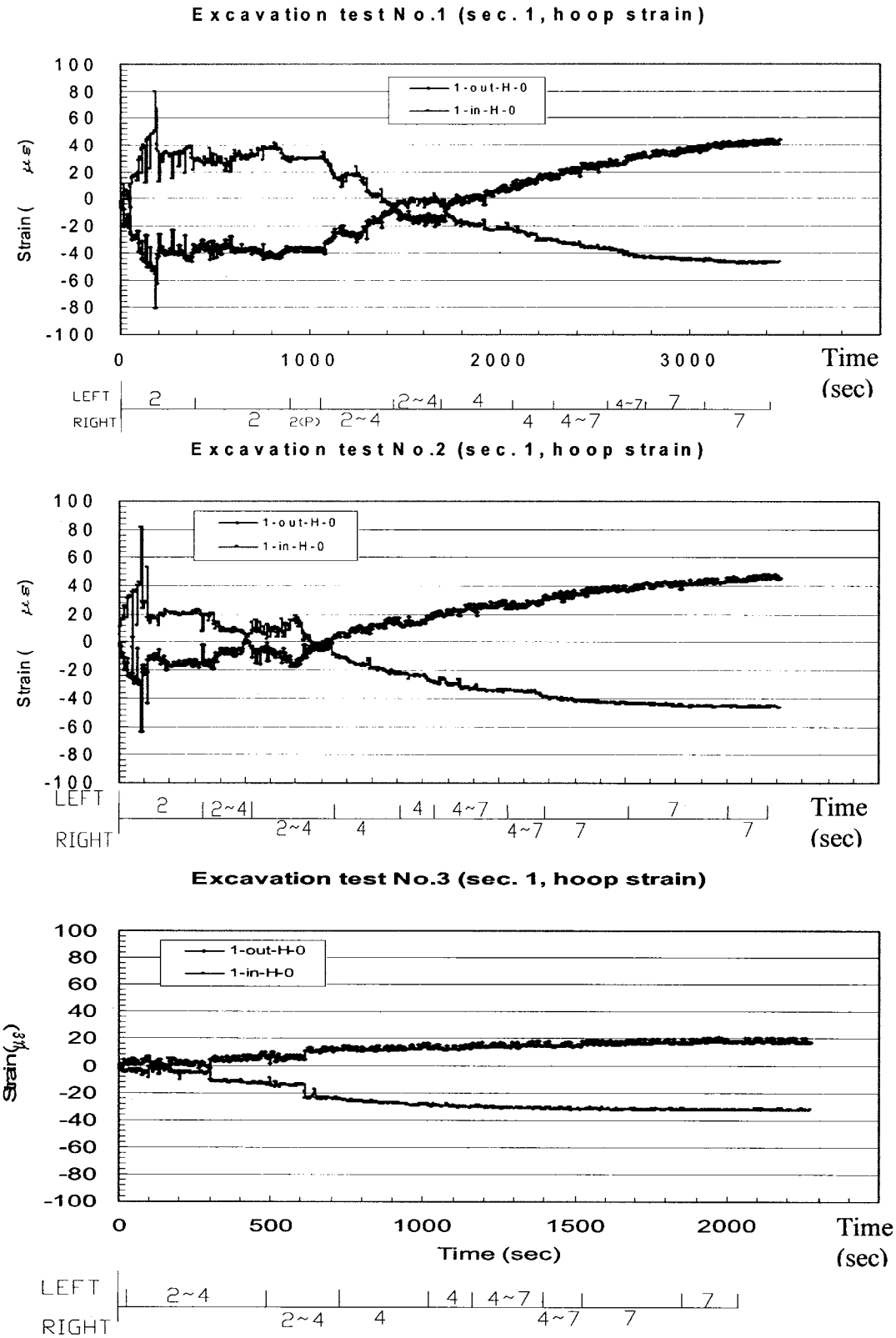

Figure 3.1 Results of hoop strain at the top (0°) of Section 1 in summer tests 1, 2, & 3 (low speed data)

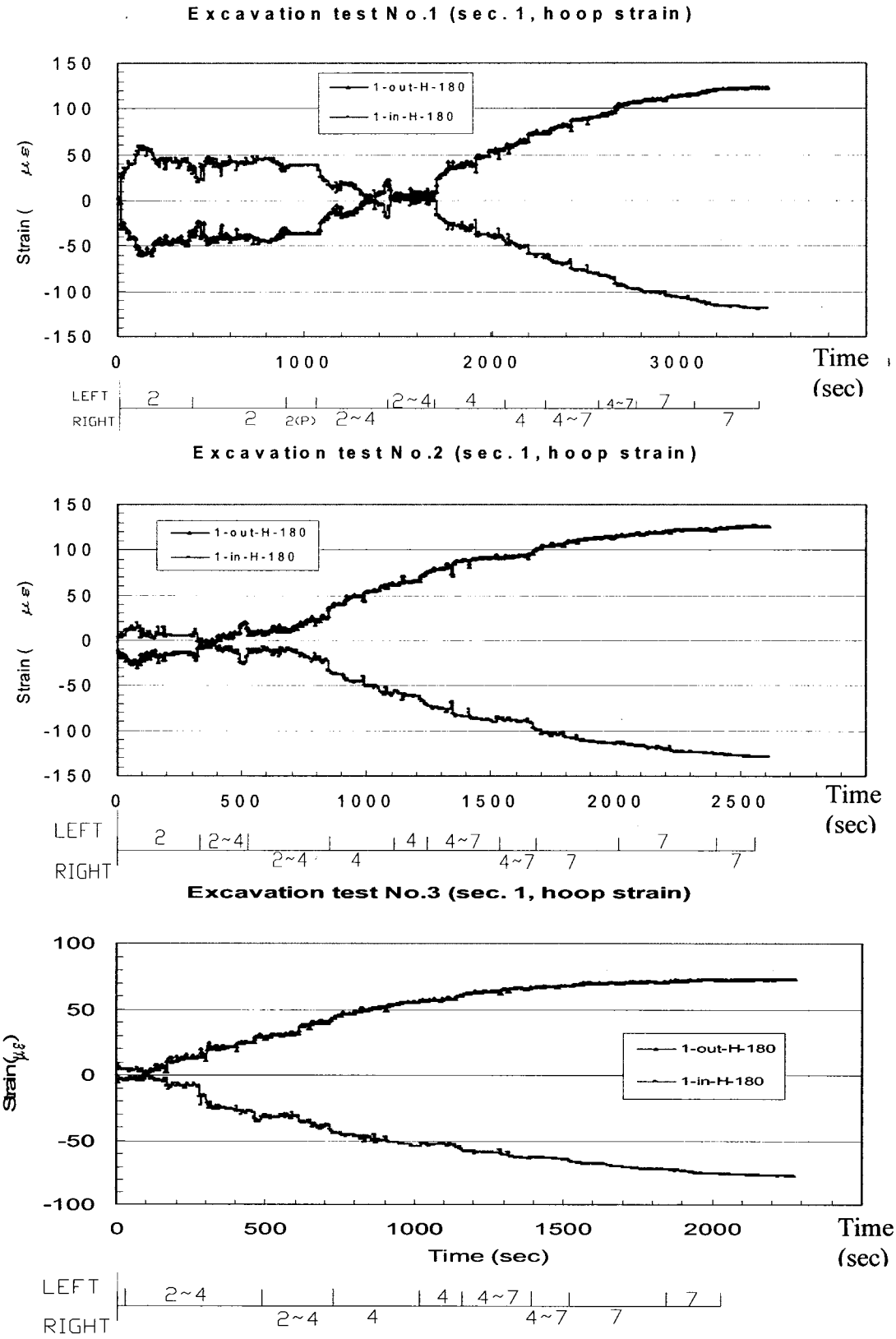

Figure 3.2 Results of hoop strain at the bottom (180°) of Section 1 in summer tests 1, 2, & 3 (low speed data)

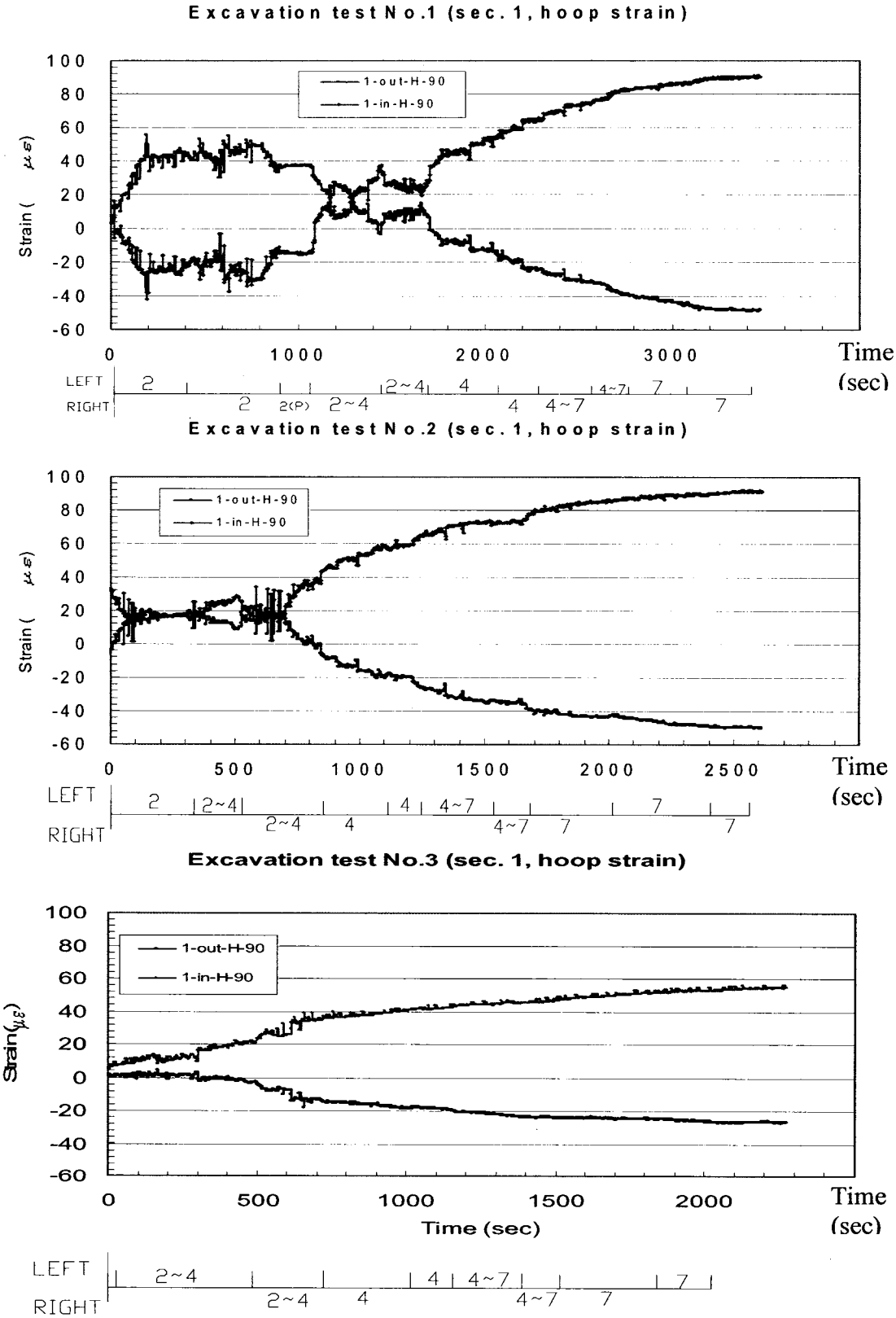

Figure 3.3 Results of hoop strain at the side (90°) of Section 1 in summer tests 1, 2, & 3 (low speed data)

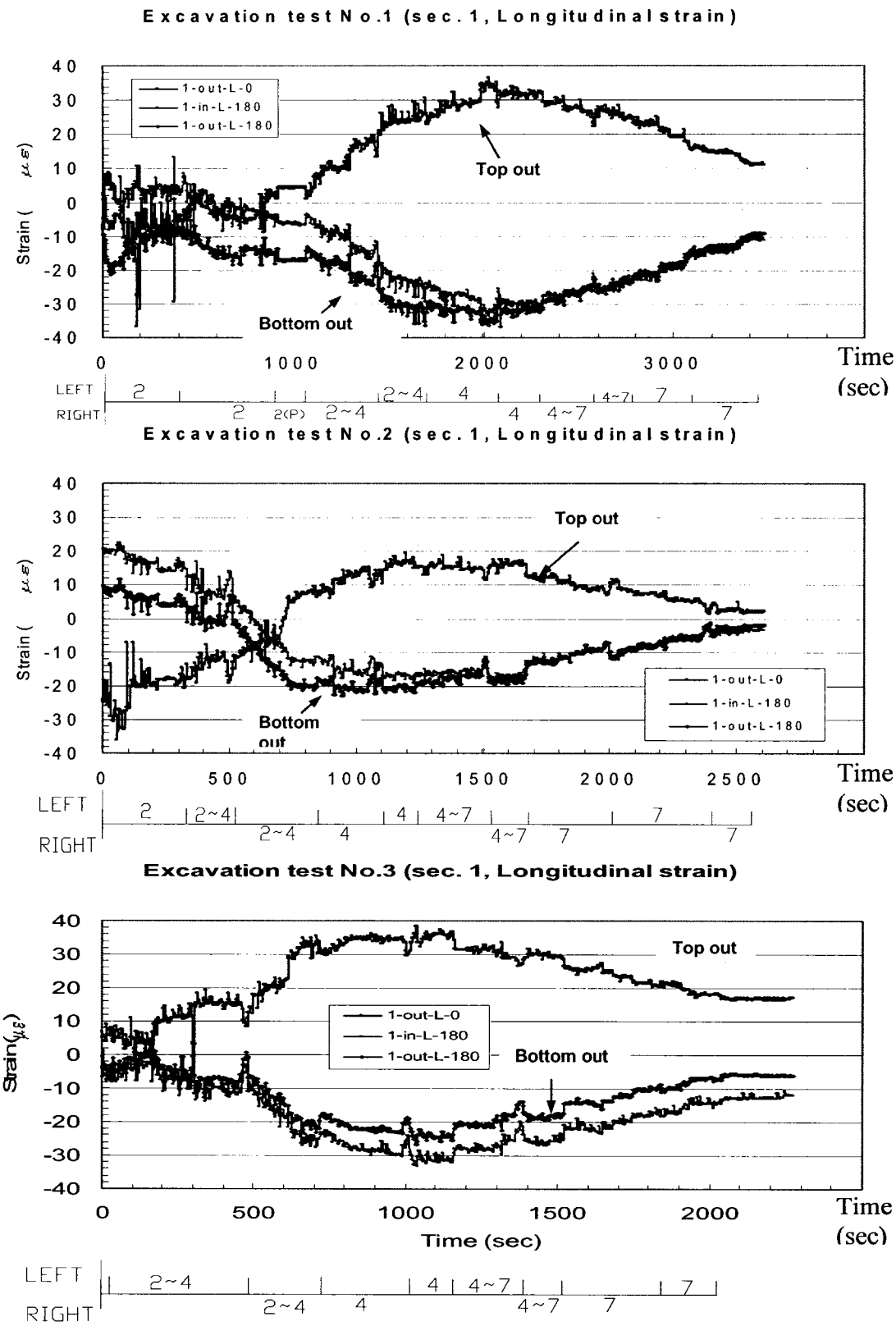

Figure 3.4 Results of longitudinal strain at the top (0°) and bottom (180°) of Section 1 in summer tests 1, 2, & 3 (low speed data)

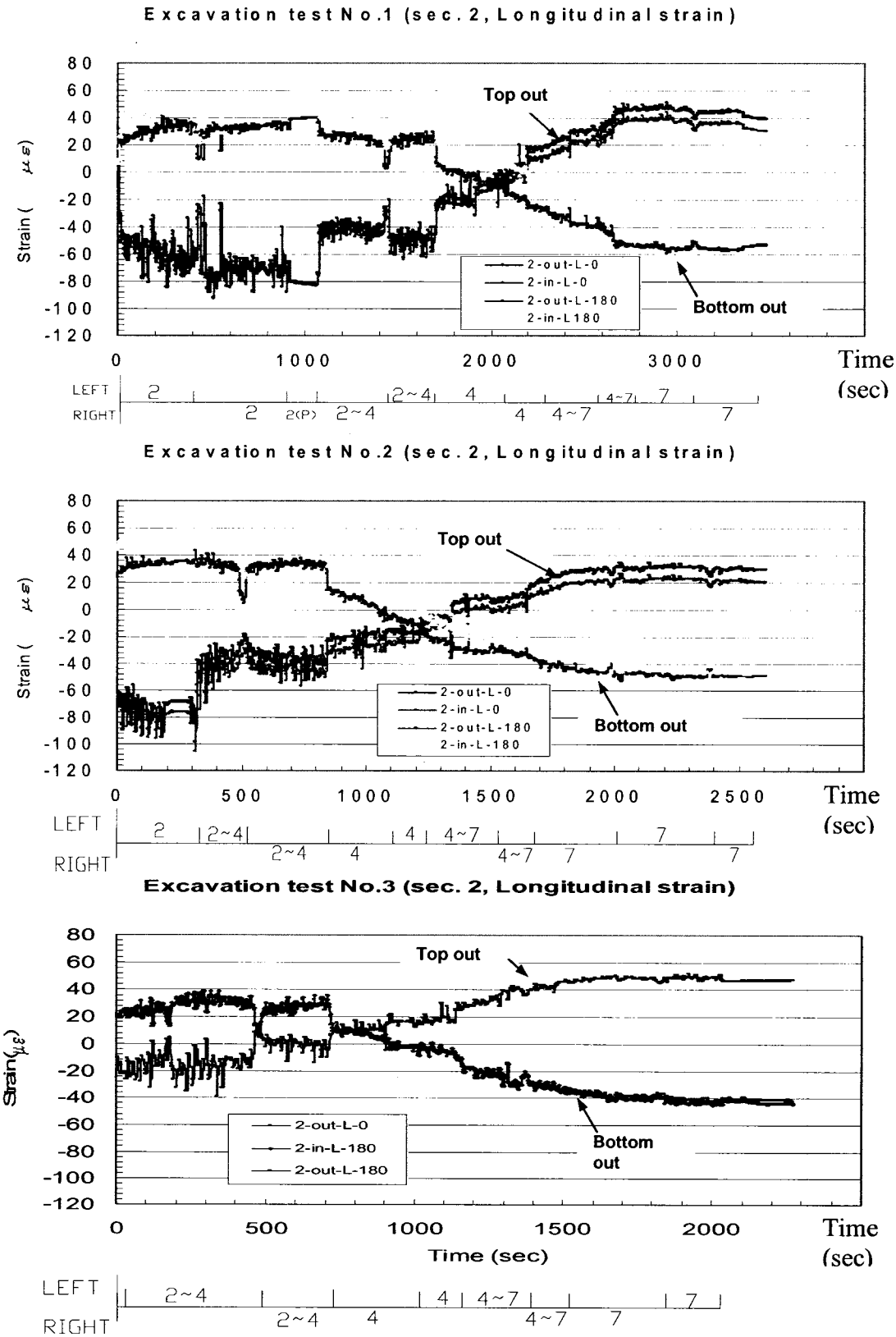

Figure 3.5 Results longitudinal strain at the top (0°) and bottom (180°) of Section 2 in summer tests 1, 2, & 3 (low speed data)

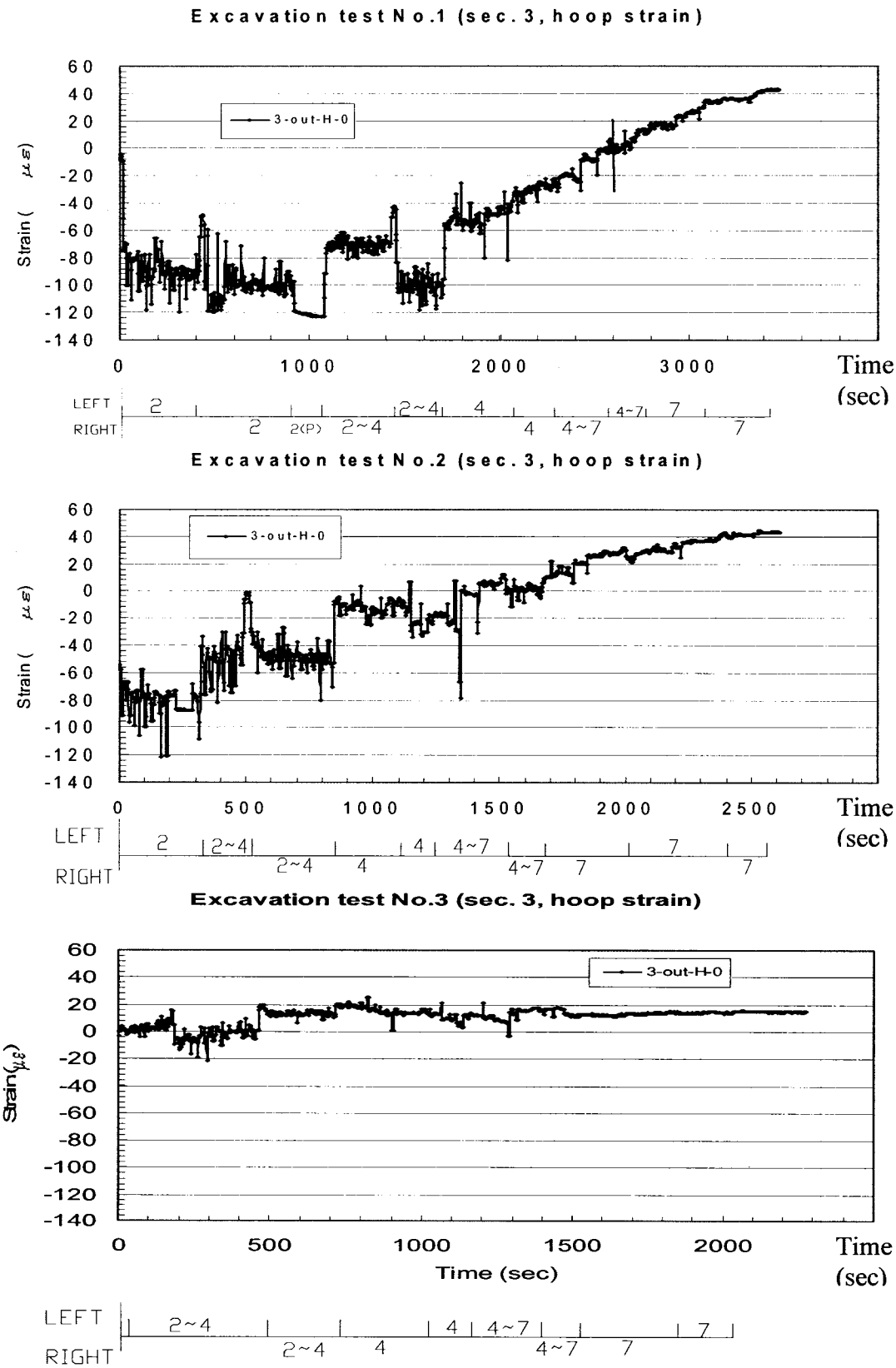

Figure 3.6 Results of hoop strain at the top (0°) of Section 3 in summer tests 1, 2, & 3 (low speed data)

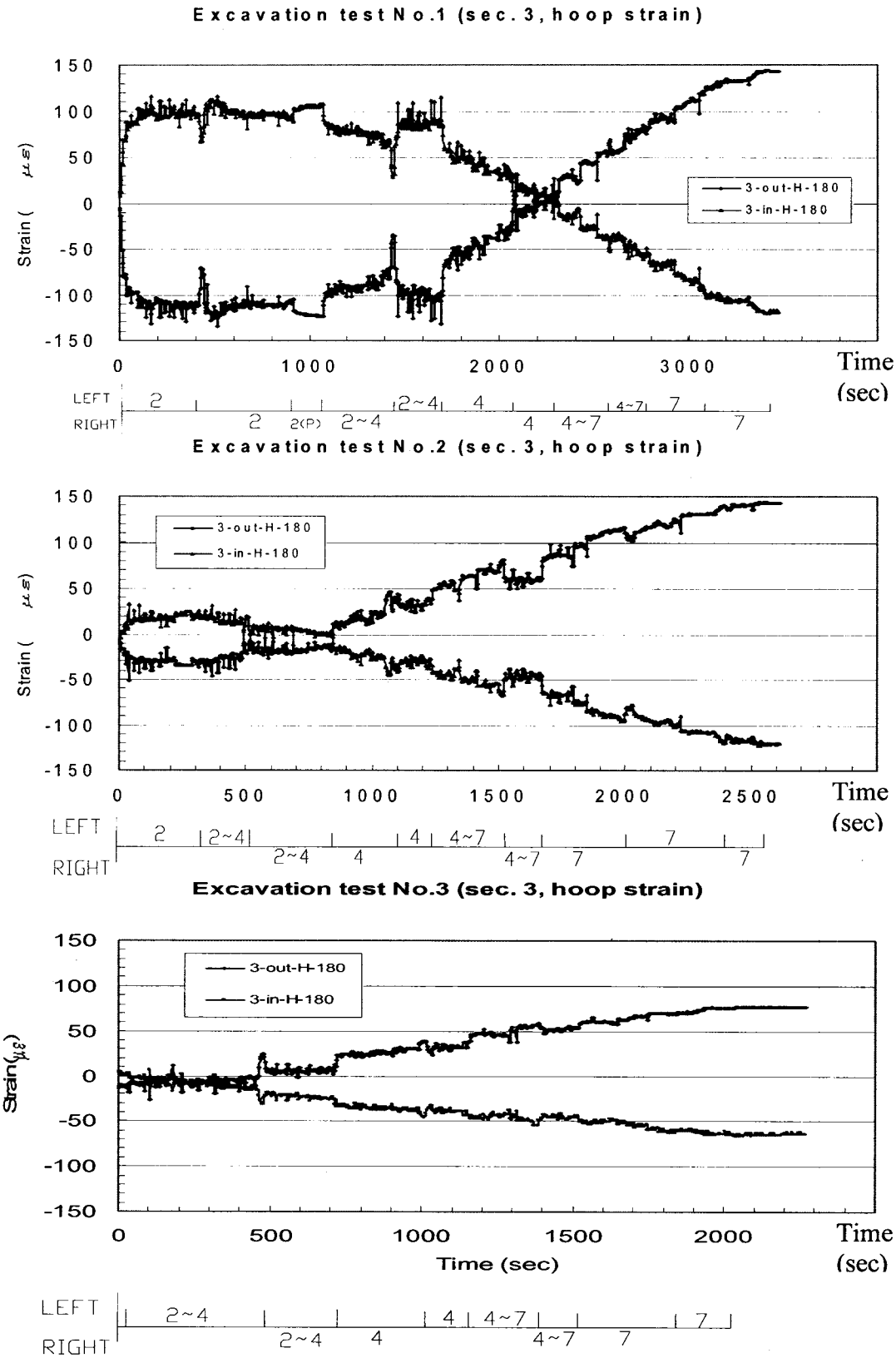

Figure 3.7 Results of hoop strain at the bottom (180°) of Section 3 in summer tests 1, 2, & 3 (low speed data)

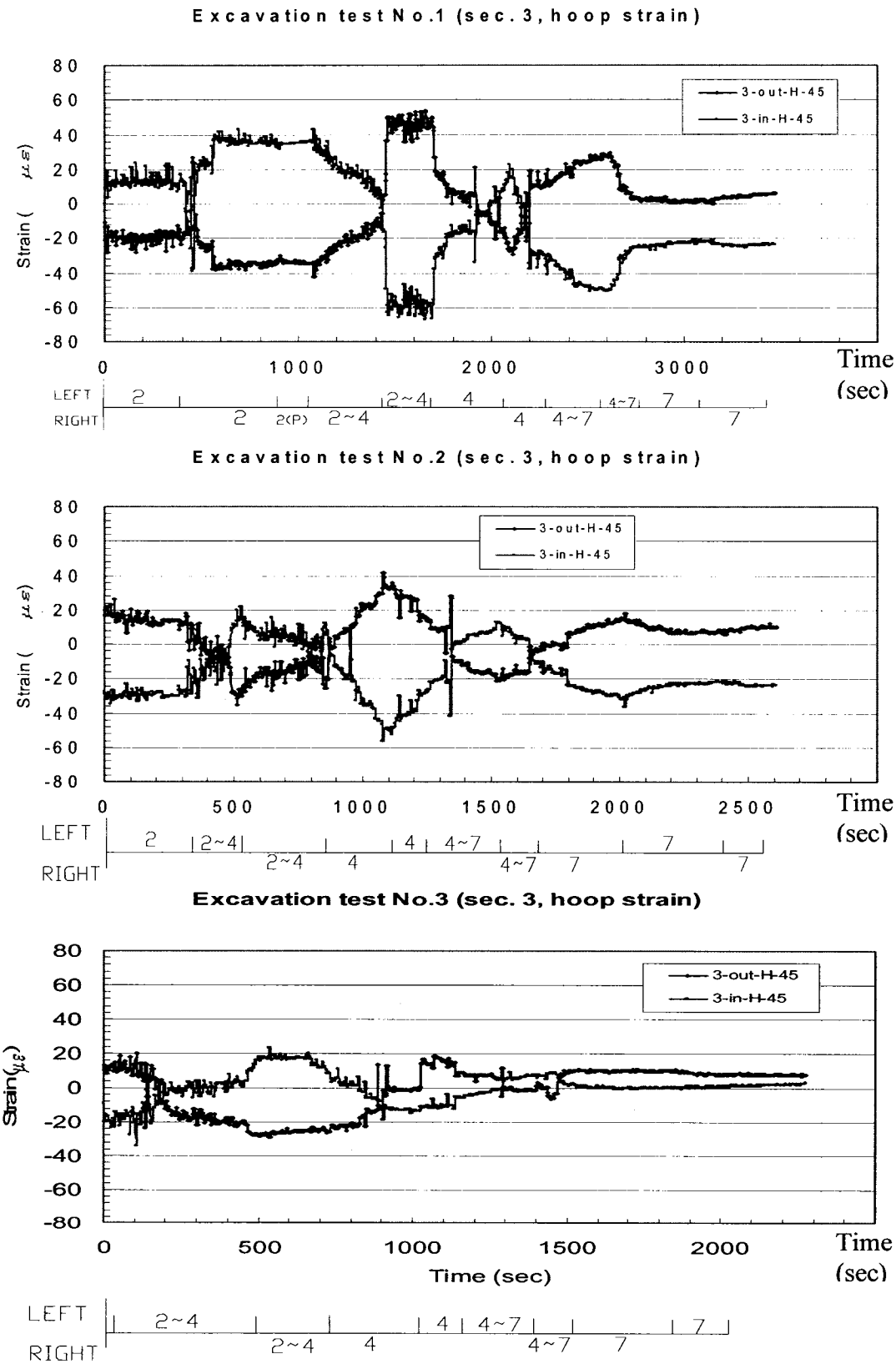

Figure 3.8 Results of hoop strain (45°) of Section 3 in summer tests 1, 2, & 3 (low speed data)

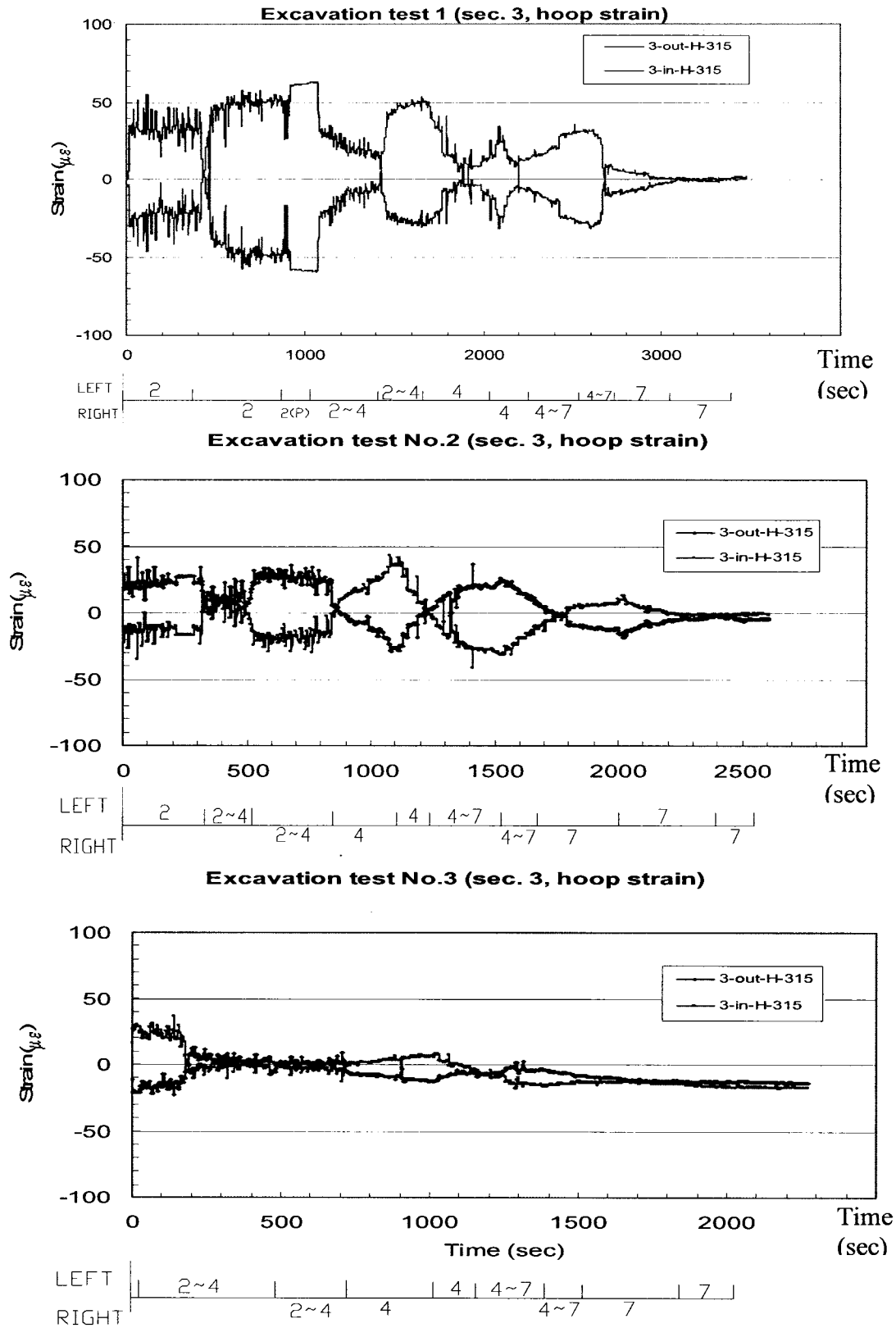

Figure 3.9 Results of hoop strain (315°) of Section 3 in summer tests 1, 2, & 3 (low speed data)

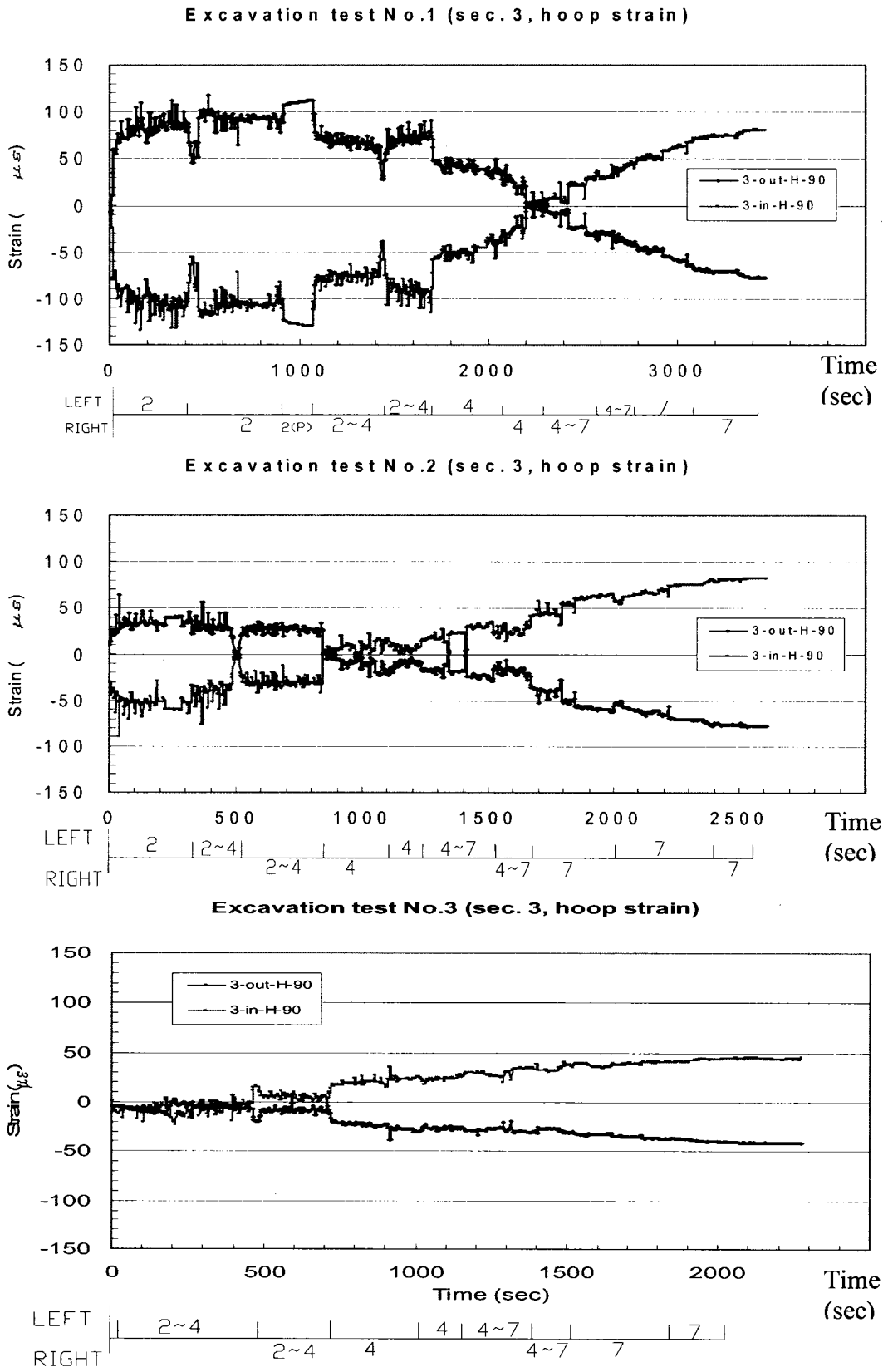

Figure 3.10 Results of hoop strain at the side (90°) of Section 3 in summer tests 1, 2, & 3 (low speed data)

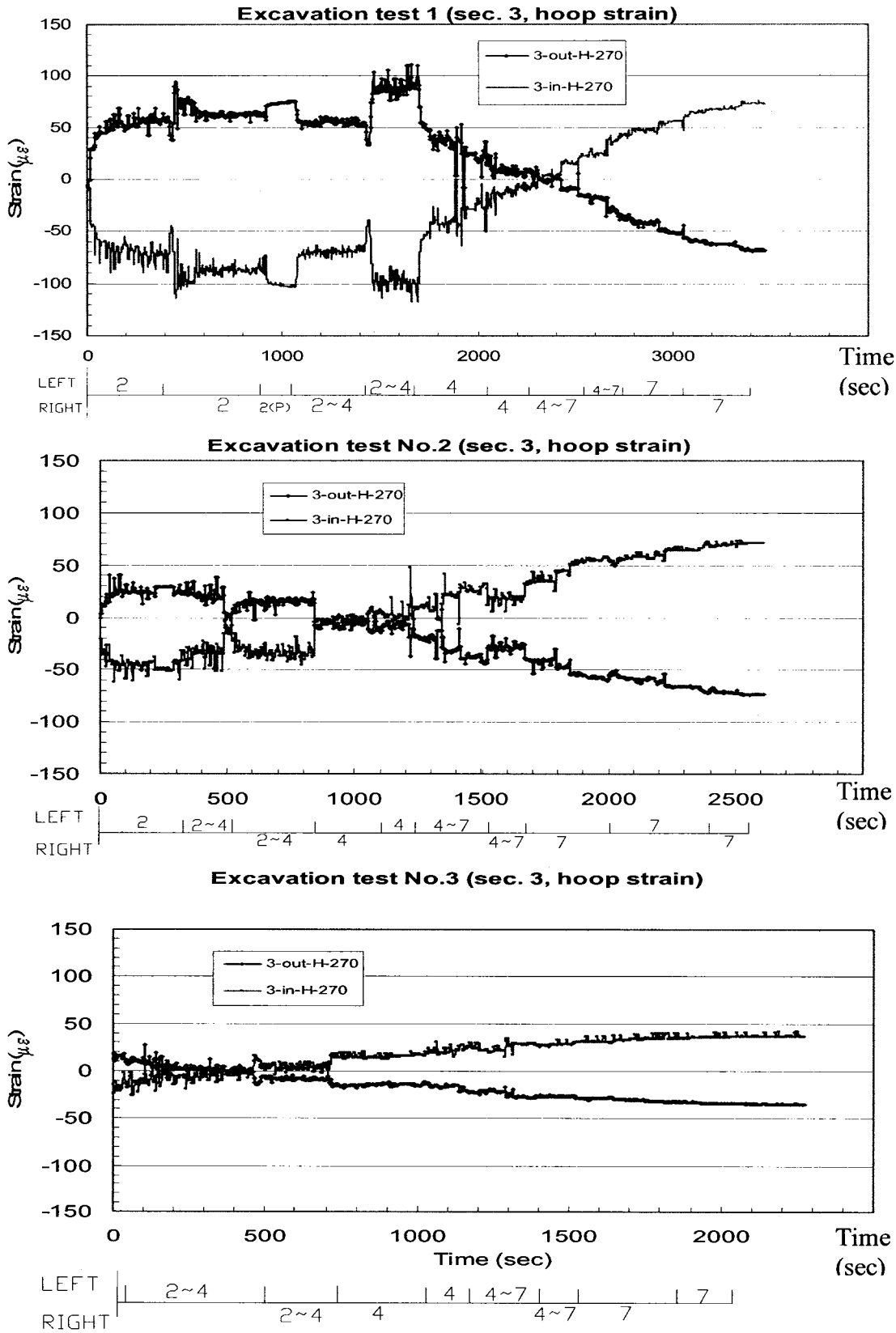

Figure 3.11 Results of hoop strain at the side (270°) of Section 3 in summer tests 1, 2, & 3 (low speed data)

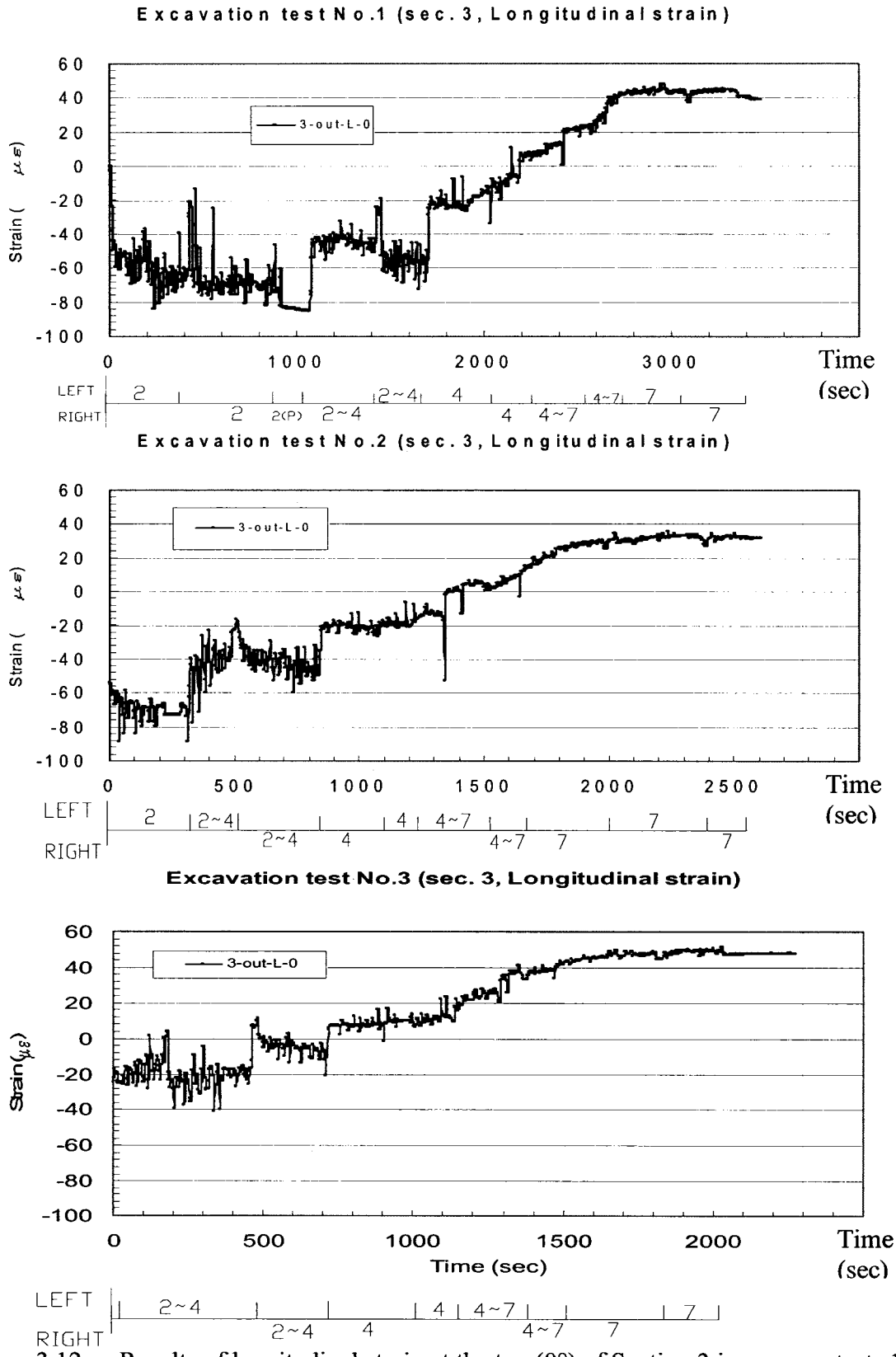

Figure 3.12 Results of longitudinal strain at the top (0°) of Section 3 in summer tests 1, 2, & 3 (low speed data)

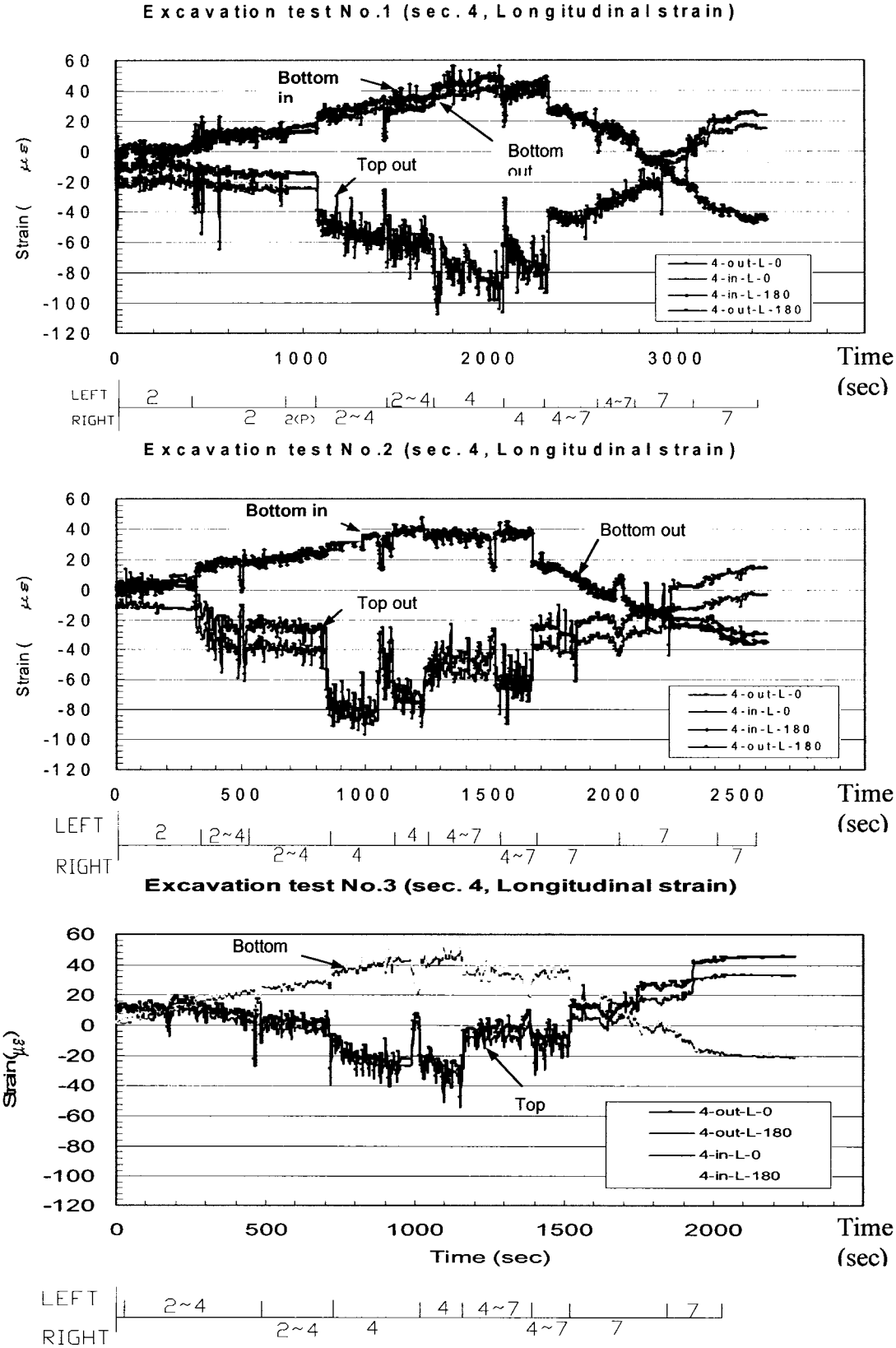

Figure 3.13 Results of longitudinal strain at the top (0°) and bottom (180°) of Section 4 in summer tests 1, 2, & 3 (low speed data)

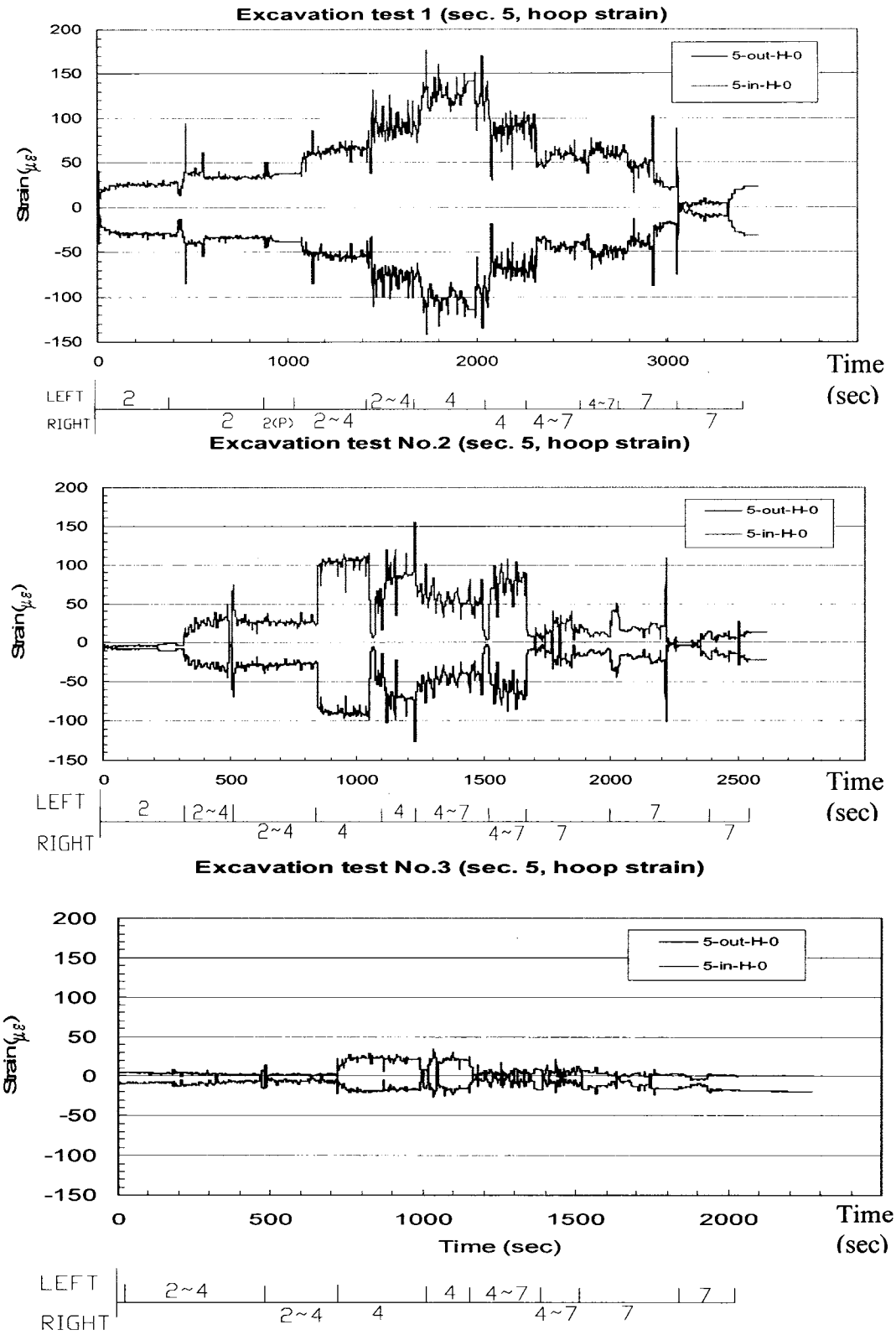

Figure 3.14 Results of hoop strain at the top (0°) of Section 5 in summer tests 1, 2, & 3 (low speed data)

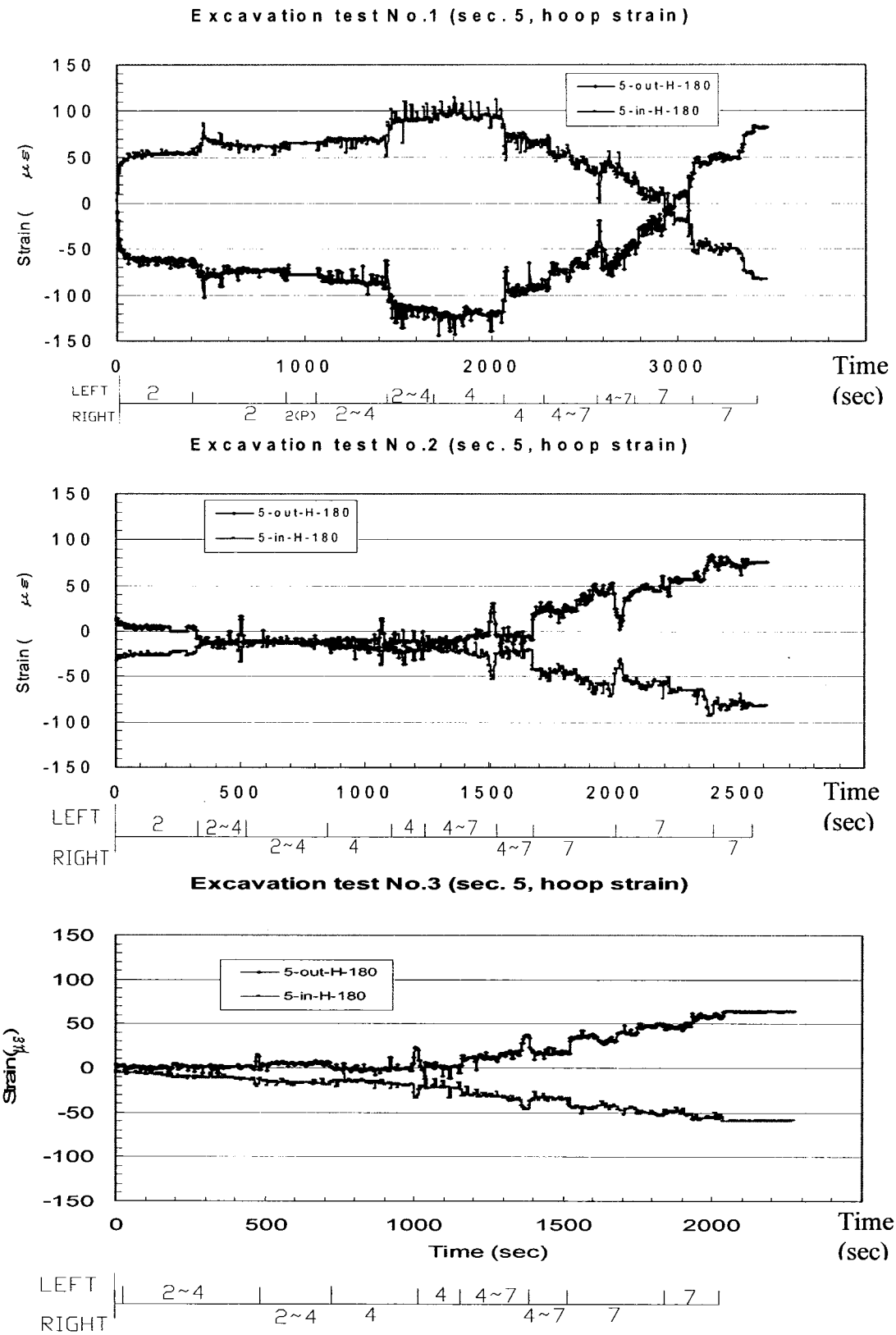

Figure 3.15 Results of hoop strain at the bottom (180°) of Section 5 in summer tests 1, 2, & 3 (low speed data)

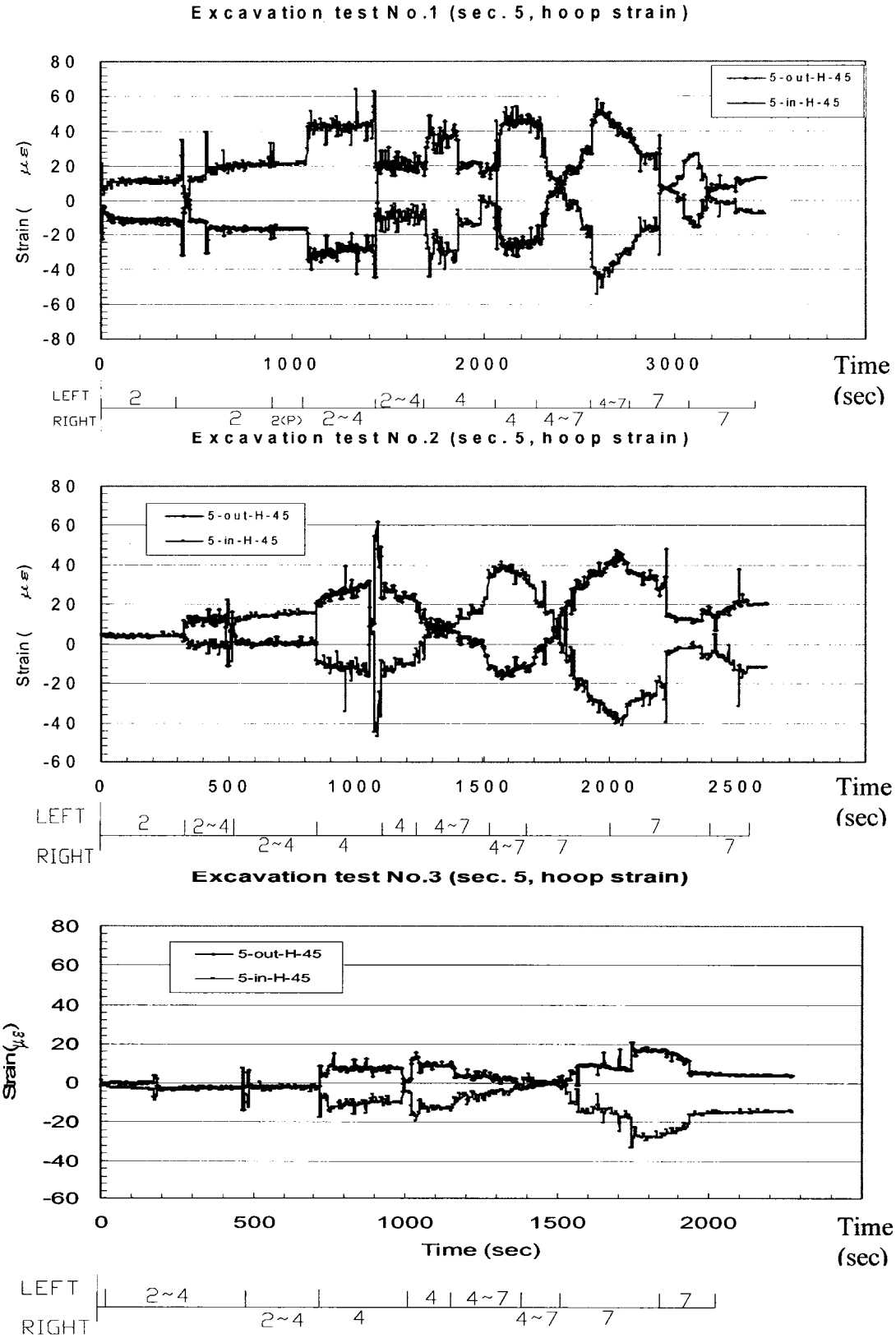

Figure 3.16 Results of hoop strain (45°) of Section 5 in summer tests 1, 2, & 3 (low speed data)

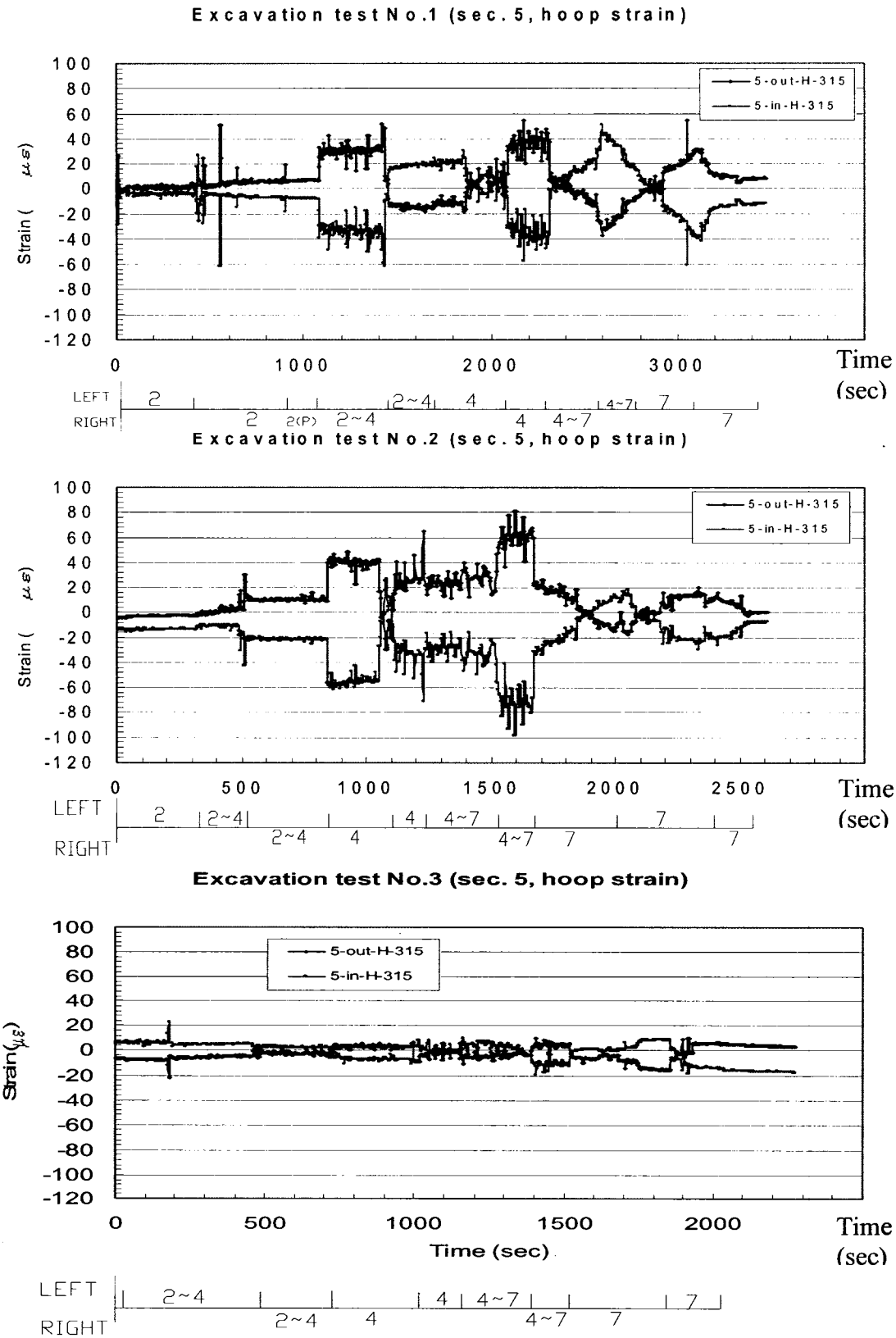

Figure 3.17 Results of hoop strain (315°) of Section 5 in summer tests 1, 2, & 3 (low speed data)

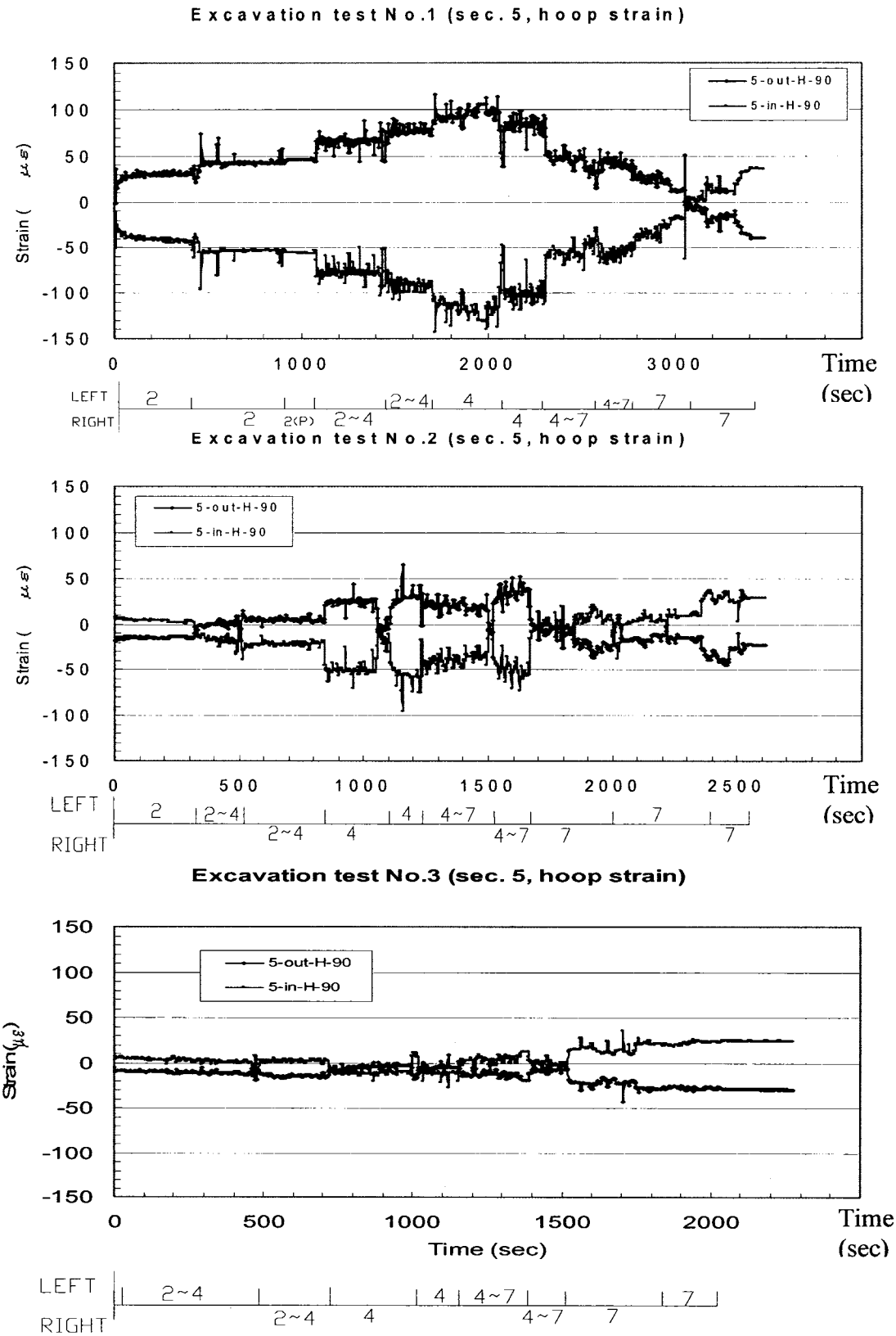

Figure 3.18 Results of hoop strain at the side (90°) of Section 5 in summer tests 1, 2, & 3 (low speed data)

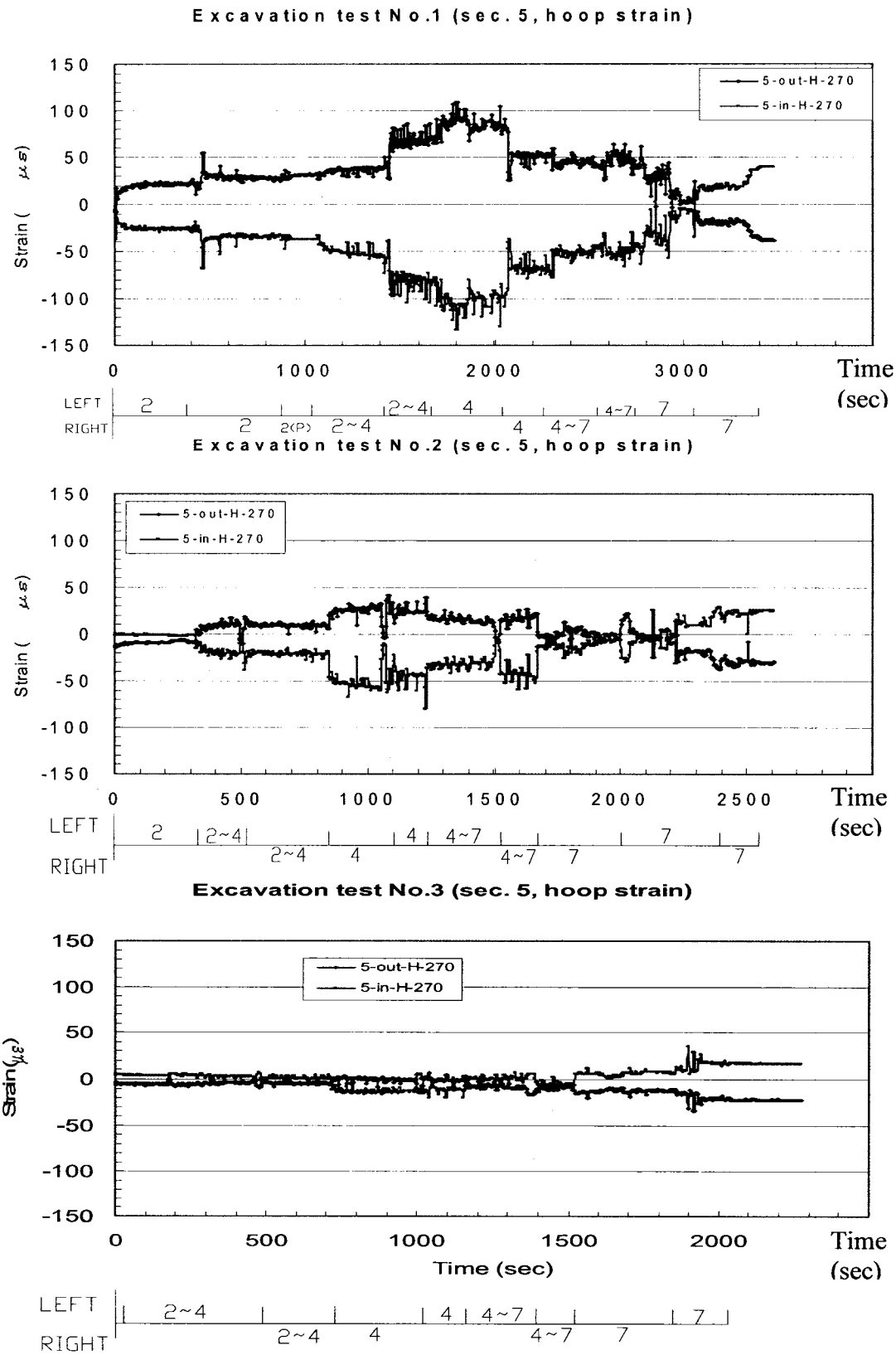

Figure 3.19 Results of hoop strain at the side (270°) of Section 5 in summer tests 1, 2, & 3 (low speed data)

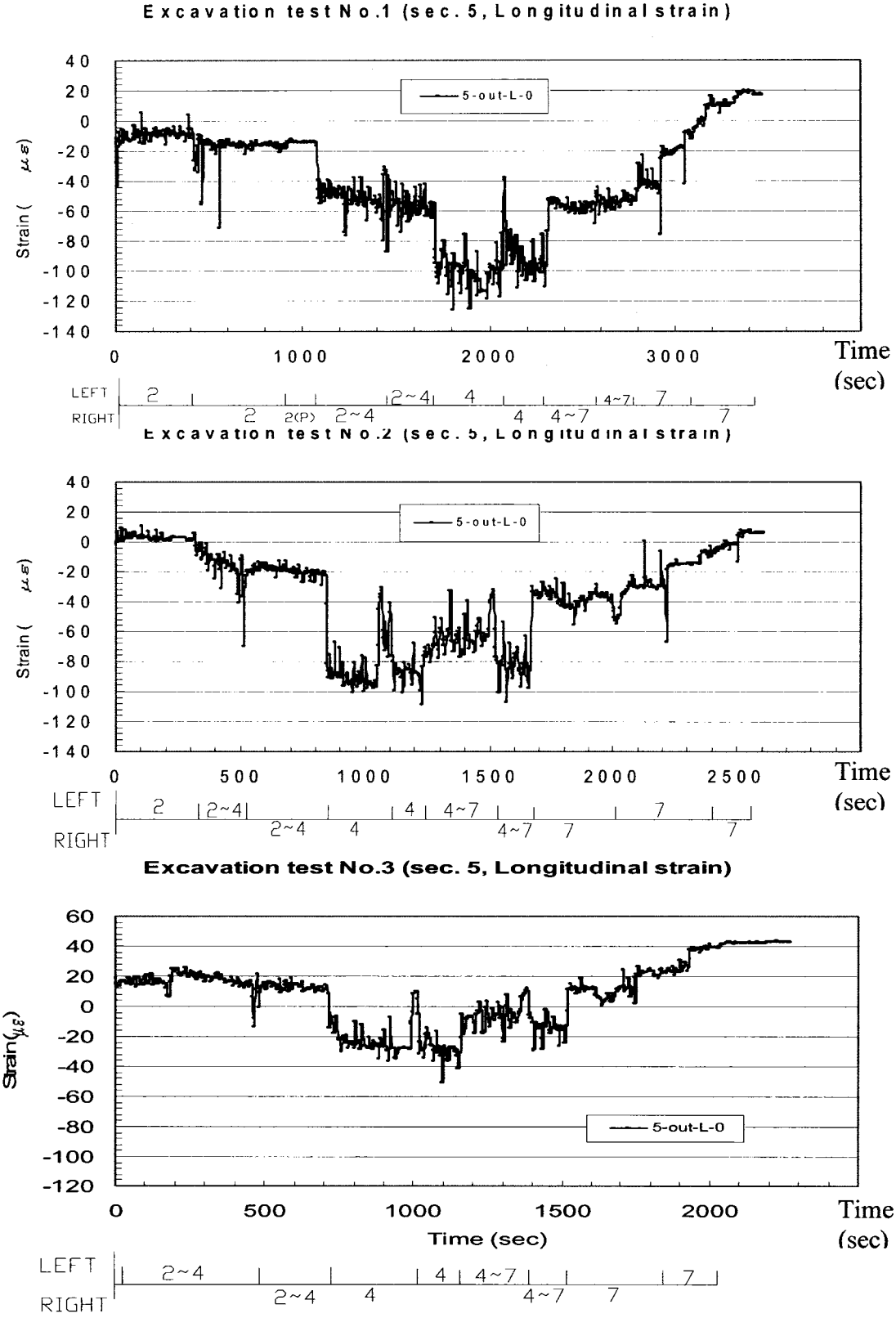

Figure 3.20 Results of longitudinal strain at the top (0°) of Section 5 in summer tests 1, 2, & 3 (low speed data)

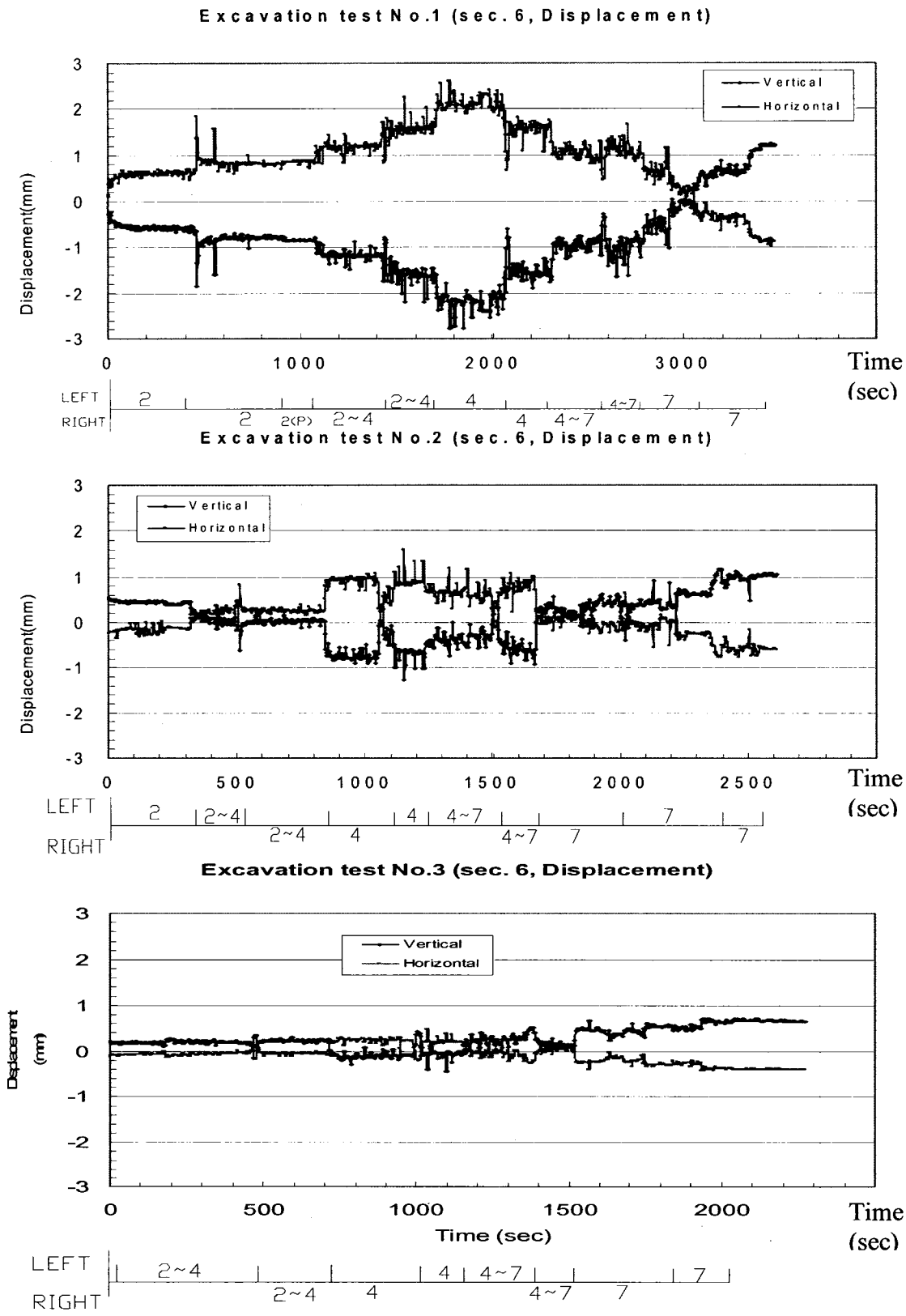

Figure 3.21 Results of deformation (vertical and horizontal) of Section 6 in summer tests 1, 2, & 3 (low speed data)

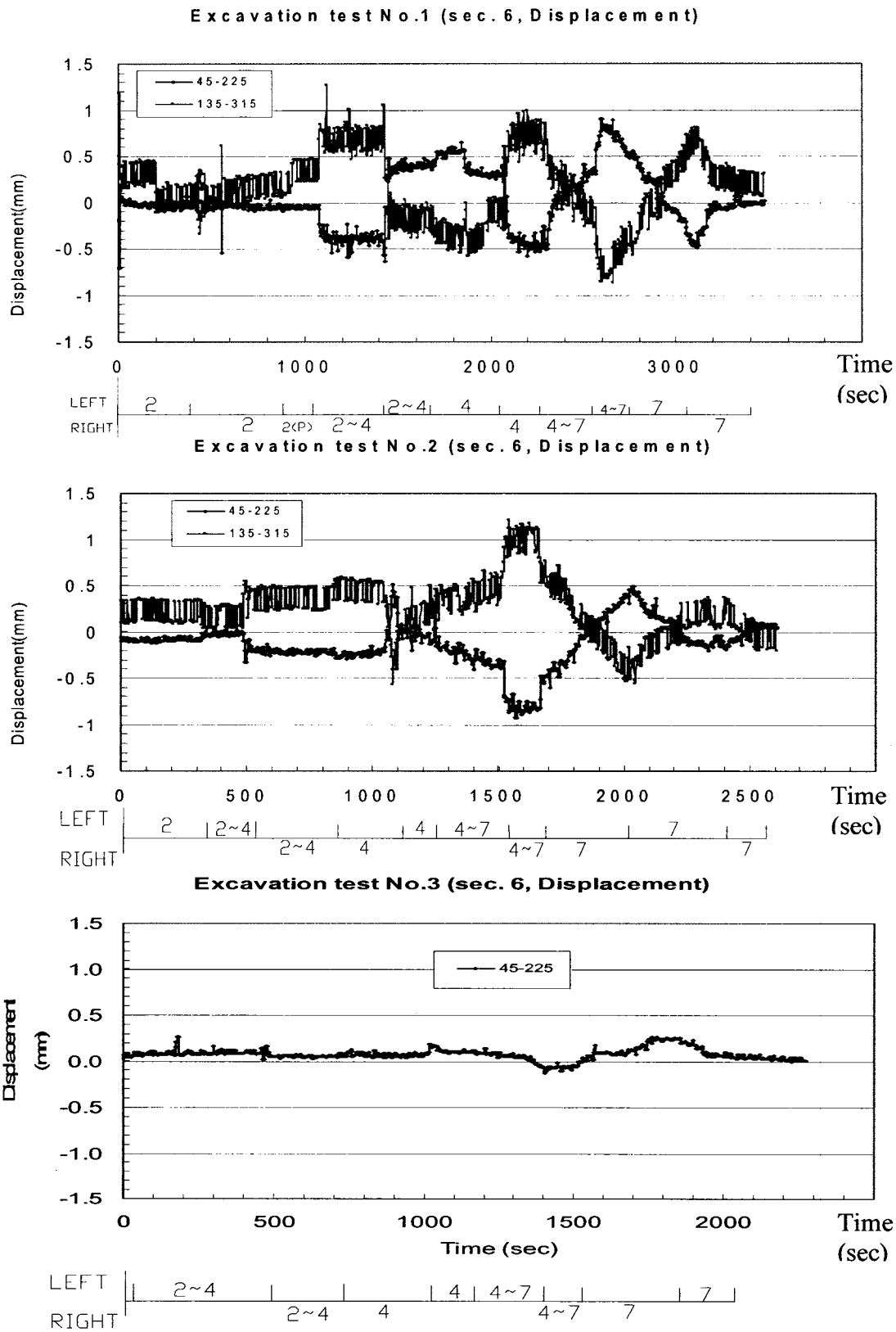

Figure 3.22 Results of deformation (diagonal) of Section 6 in summer tests 1, 2, & 3 (low speed data)

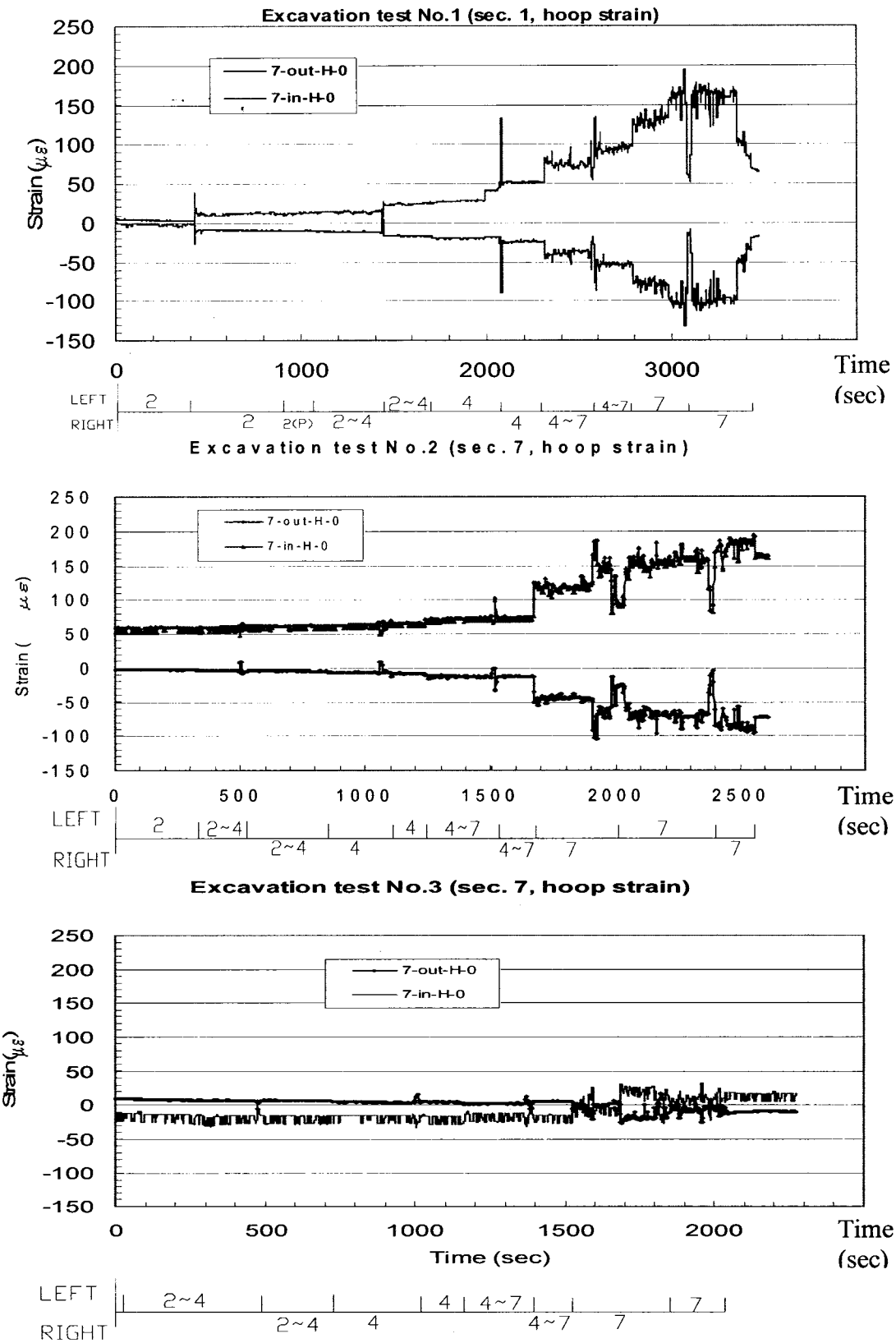

Figure 3.23 Results of hoop strain at the top (0°) of Section 7 in summer tests 1, 2, & 3 (low speed data)

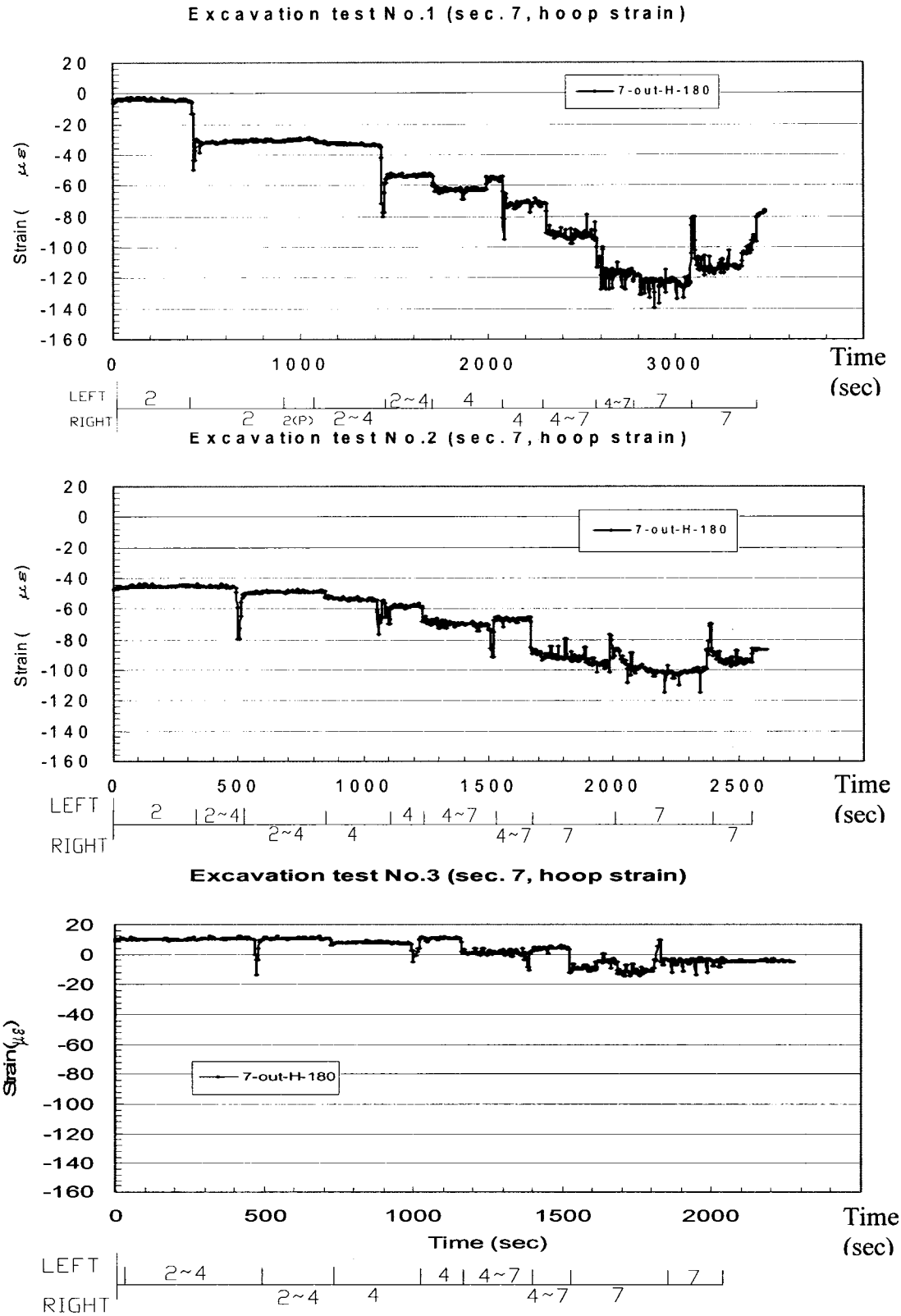

Figure 3.24 Results of hoop strain at the bottom (180°) of Section 7 in summer tests 1, 2, & 3 (low speed data)

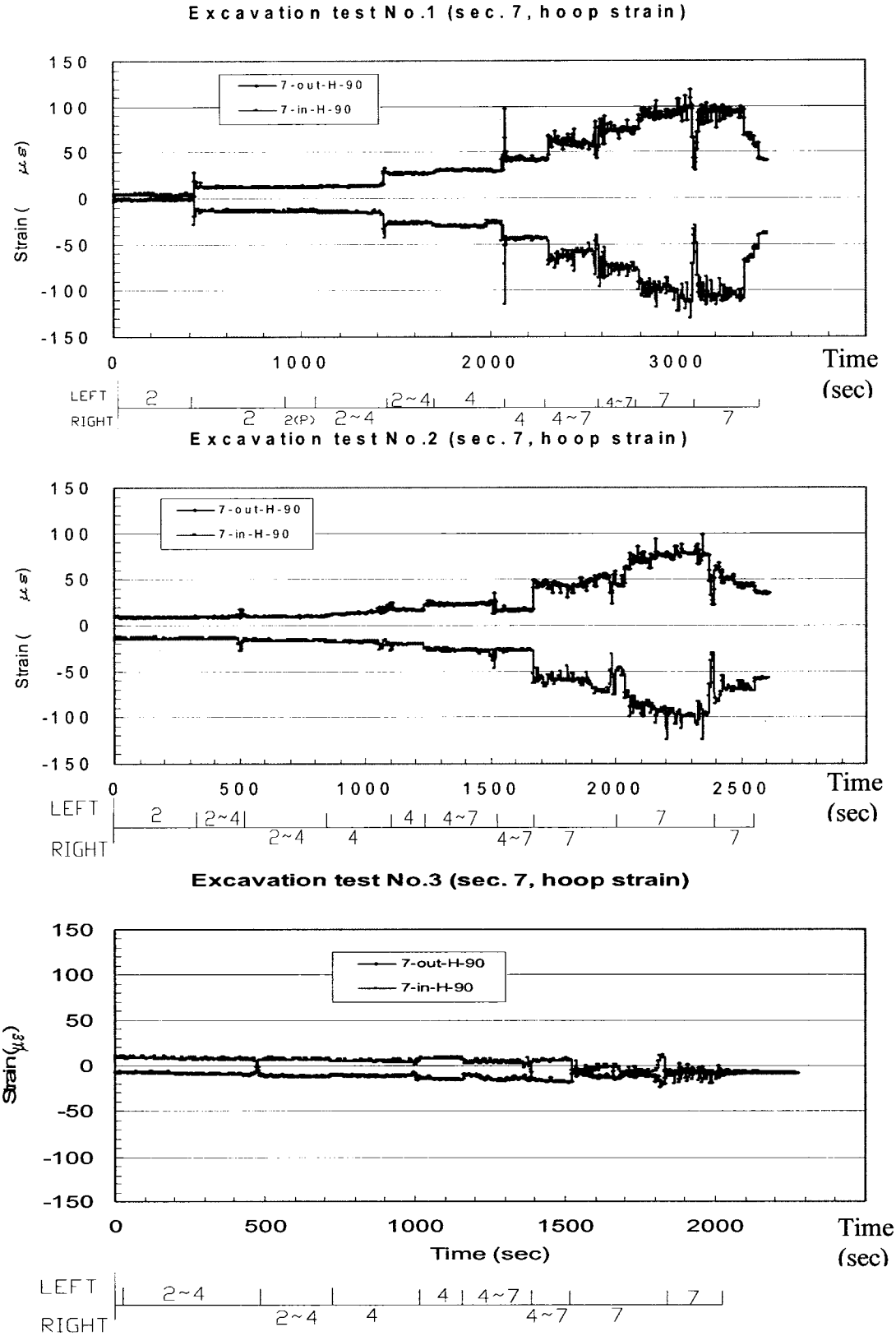

Figure 3.25 Results of hoop strain at the side (90°) of Section 7 in summer tests 1, 2, & 3 (low speed data)

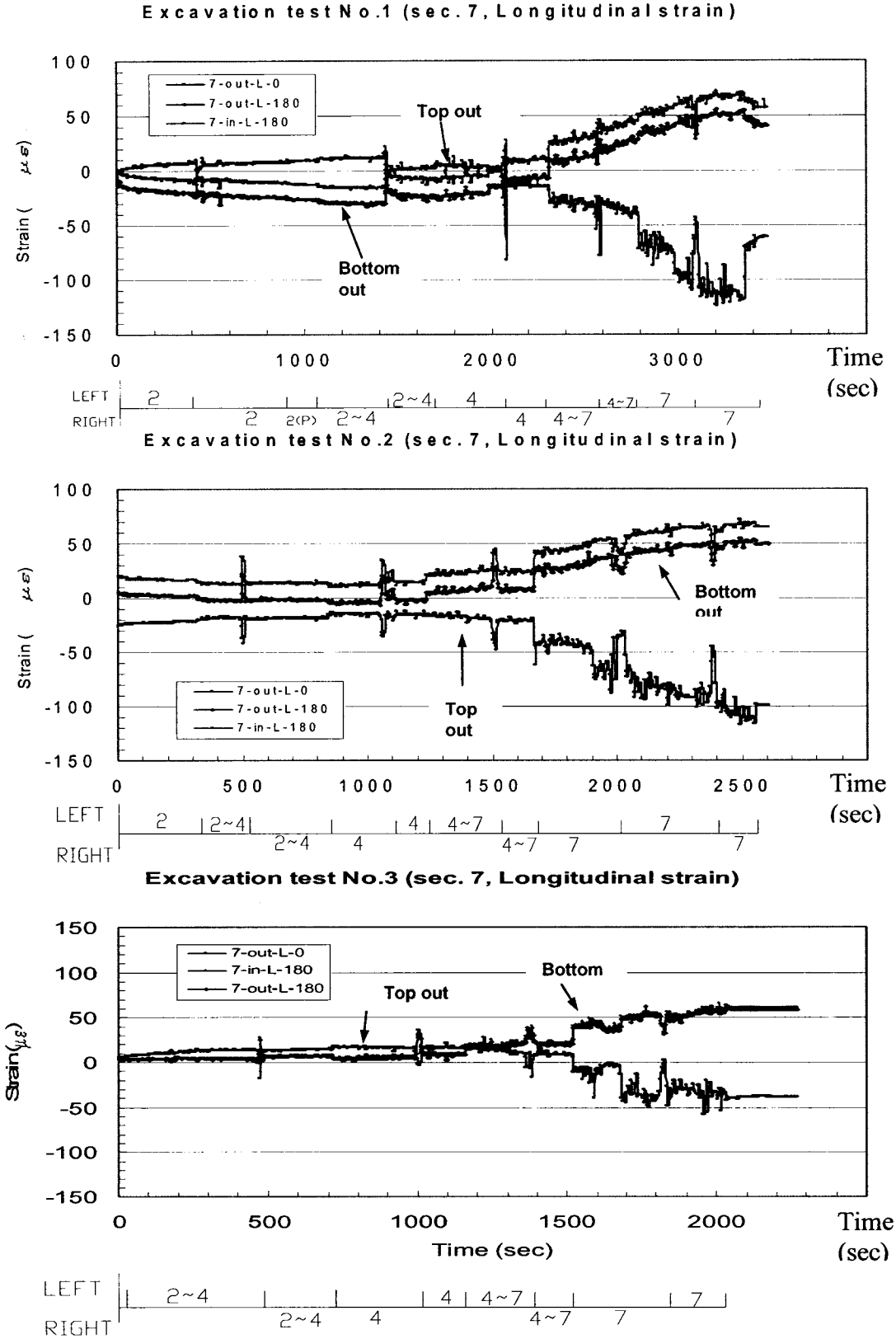

Figure 3.26 Results of longitudinal strain at the top (0°) and the bottom (180°) of Section 7 in summer tests 1, 2, & 3 (low speed data)

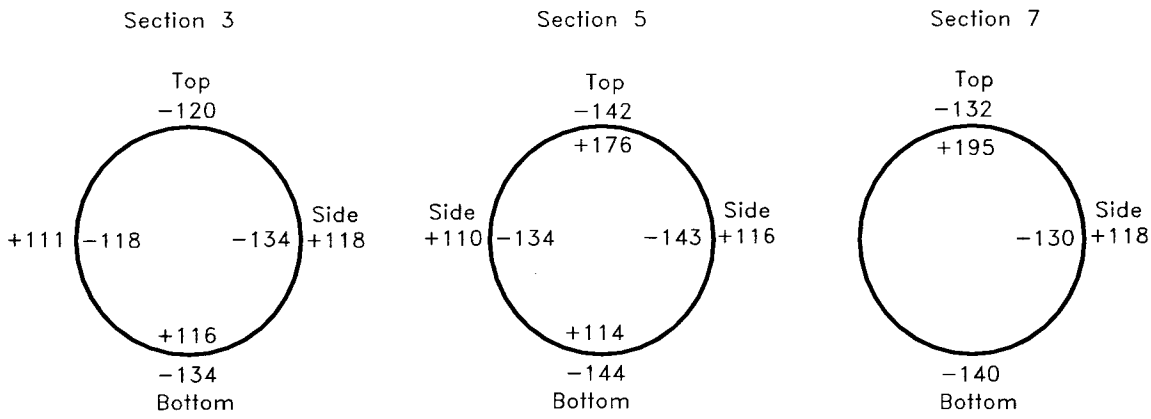

Figure 3.27 Maximum hoop strain in summer un-pressurized test 1 at buried state

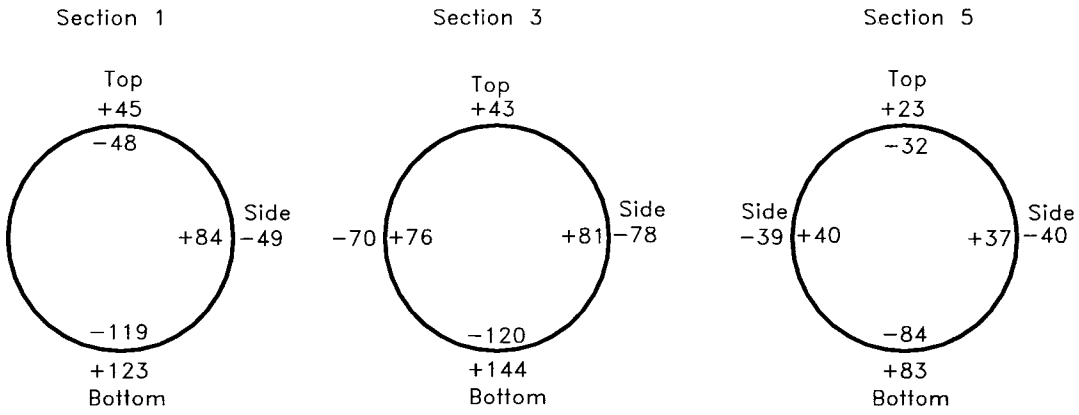

Figure 3.28 Maximum hoop strain in summer un-pressurized test at exposed state

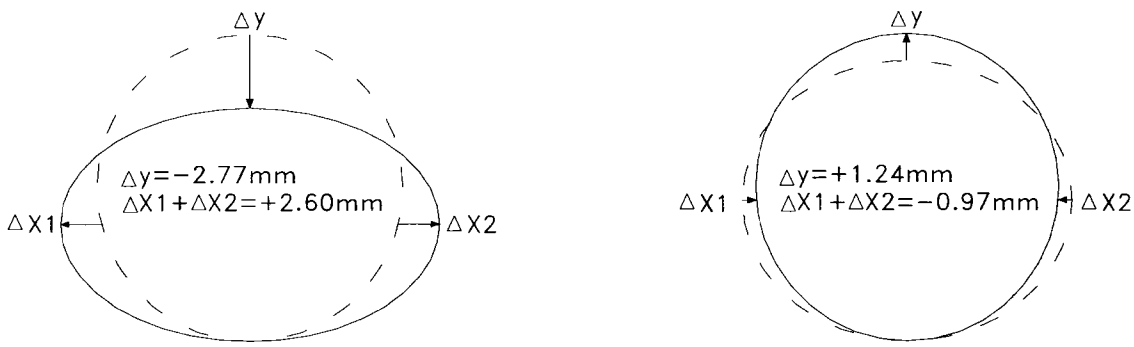

Excavator at Section 4

Maximum ovalization = 0.59%

Excavator at Section 7

Maximum ovalization = 0.24%

Maximum Vertical and Horizontal Displacement at Section 6

Outward Movement Positive

Figure 3.29 Maximum deformation and ovalization in summer un-pressurized test 1

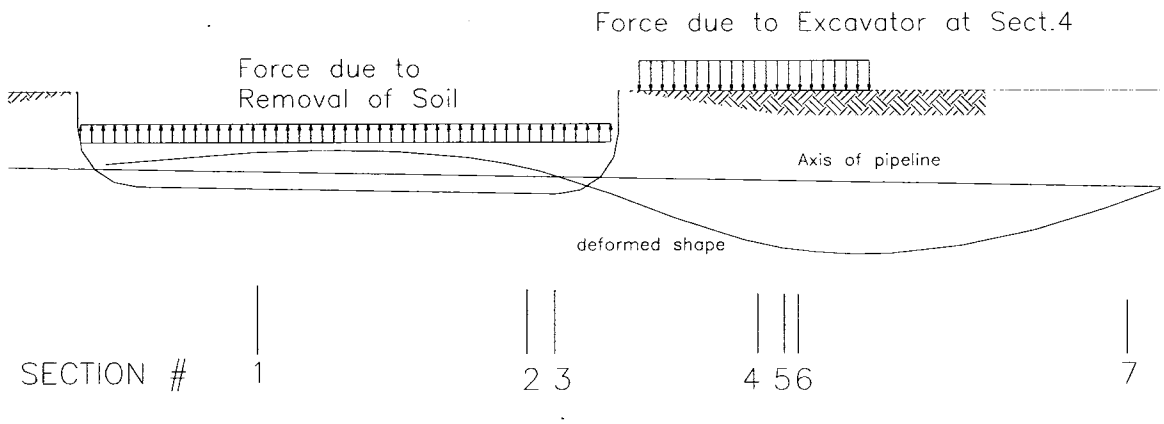

Figure 3.30 Schematic diagram of longitudinal deformation in excavation process

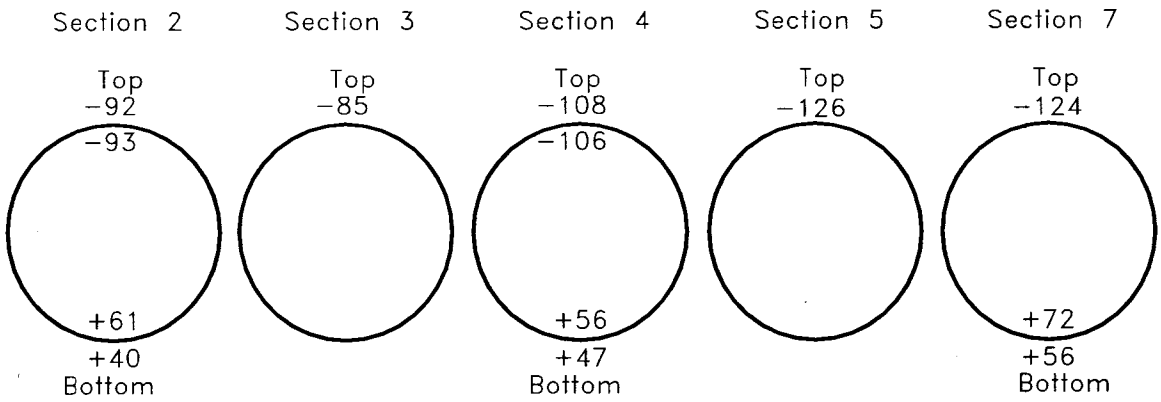

Figure 3.31 Maximum longitudinal strain in summer un-pressurized test 1 at buried state

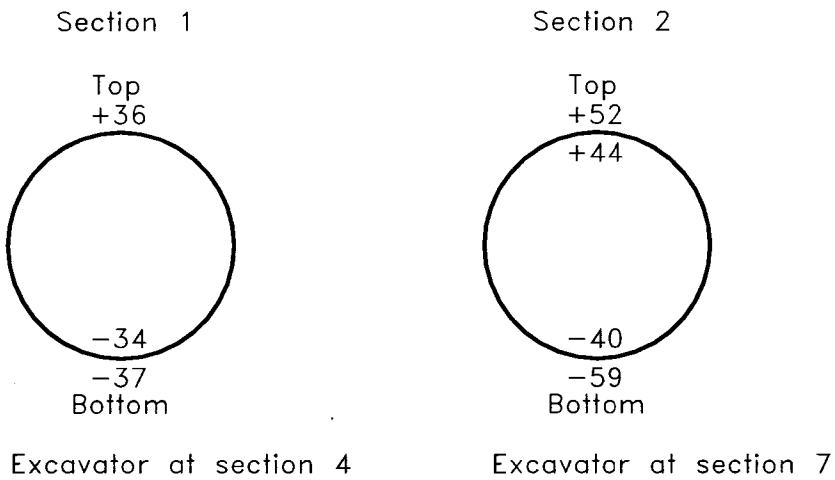

Figure 3 32 Maximum longitudinal strain in summer un-pressurized test 1 at exposed state

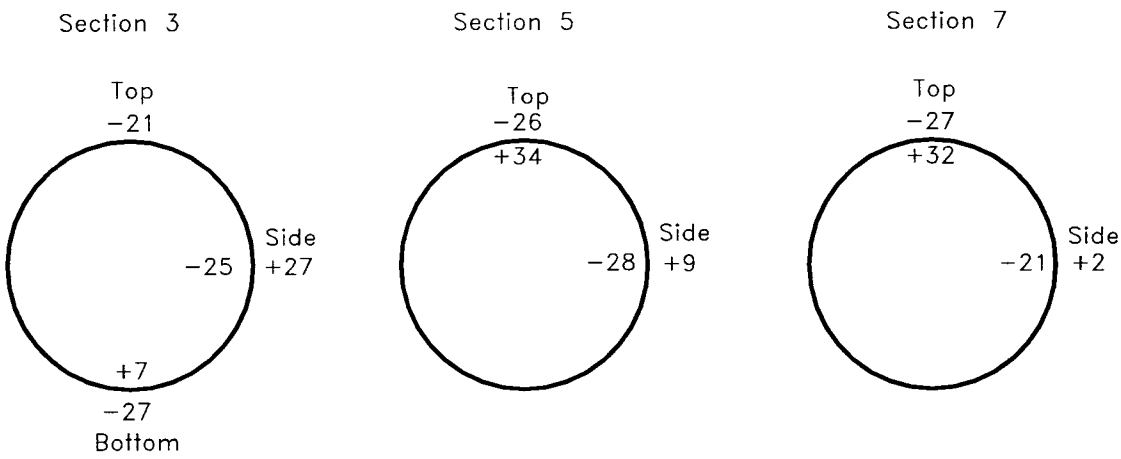

Figure 3.33 Maximum hoop strain in summer pressurized test---Situation 1

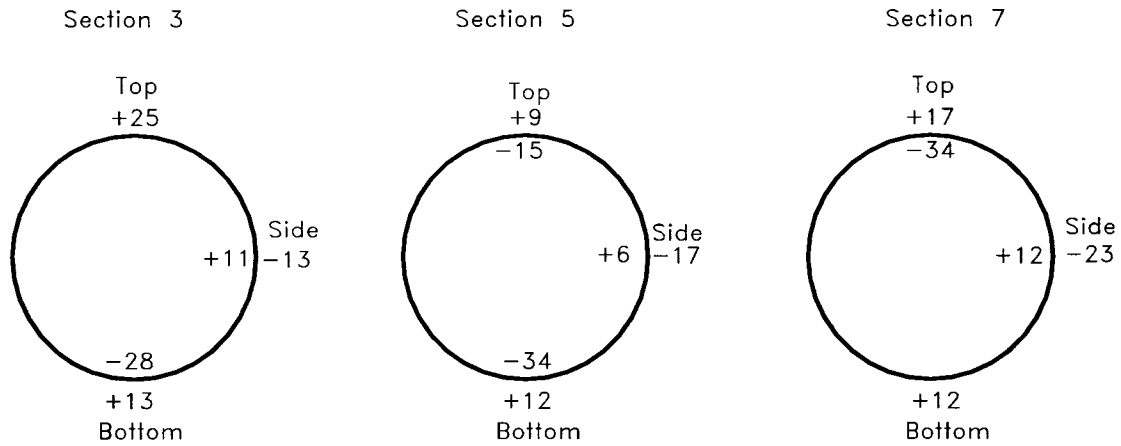

Figure 3.34 Maximum hoop strain in summer pressurized test---Situation 2

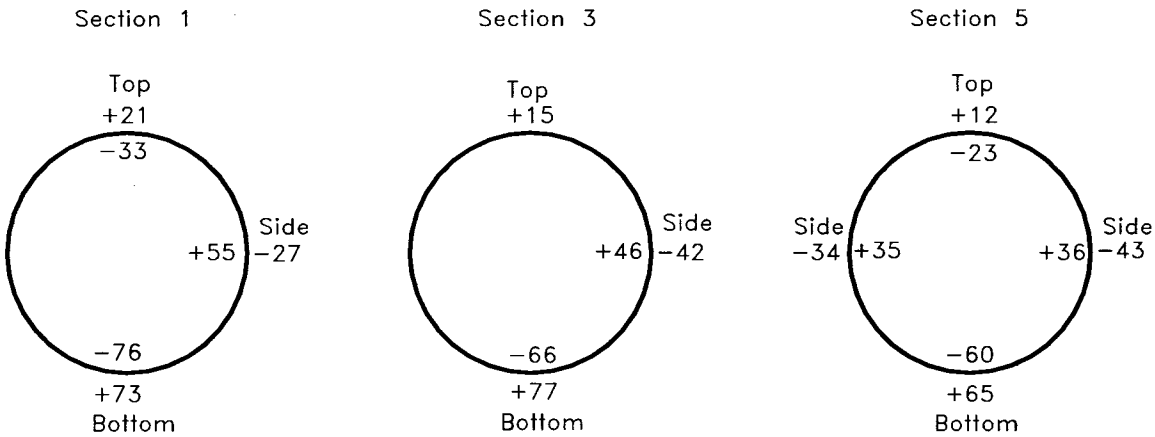

Figure 3.35 Maximum hoop strain in summer pressurized test---Situation 3

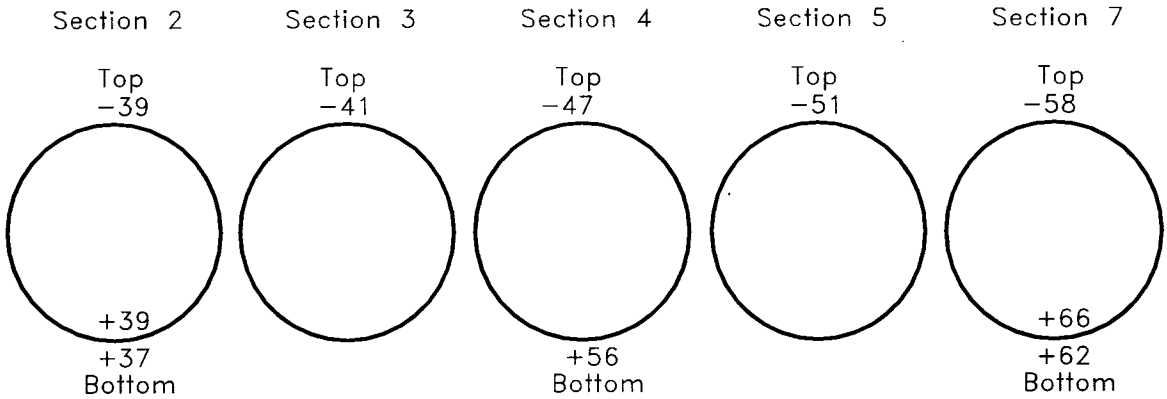

Figure 3.36 Maximum longitudinal strain in summer pressurized test at buried state

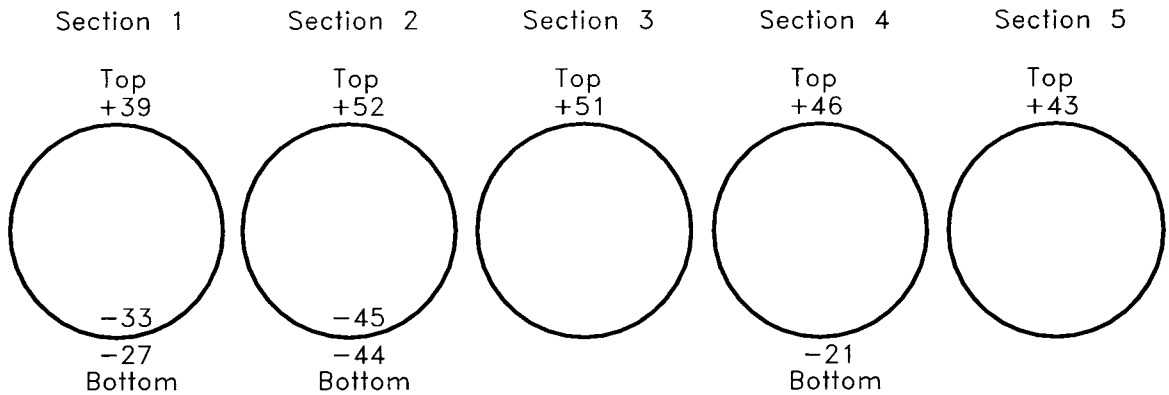

Figure 3.37 Maximum longitudinal strain in summer pressurized test at exposed state

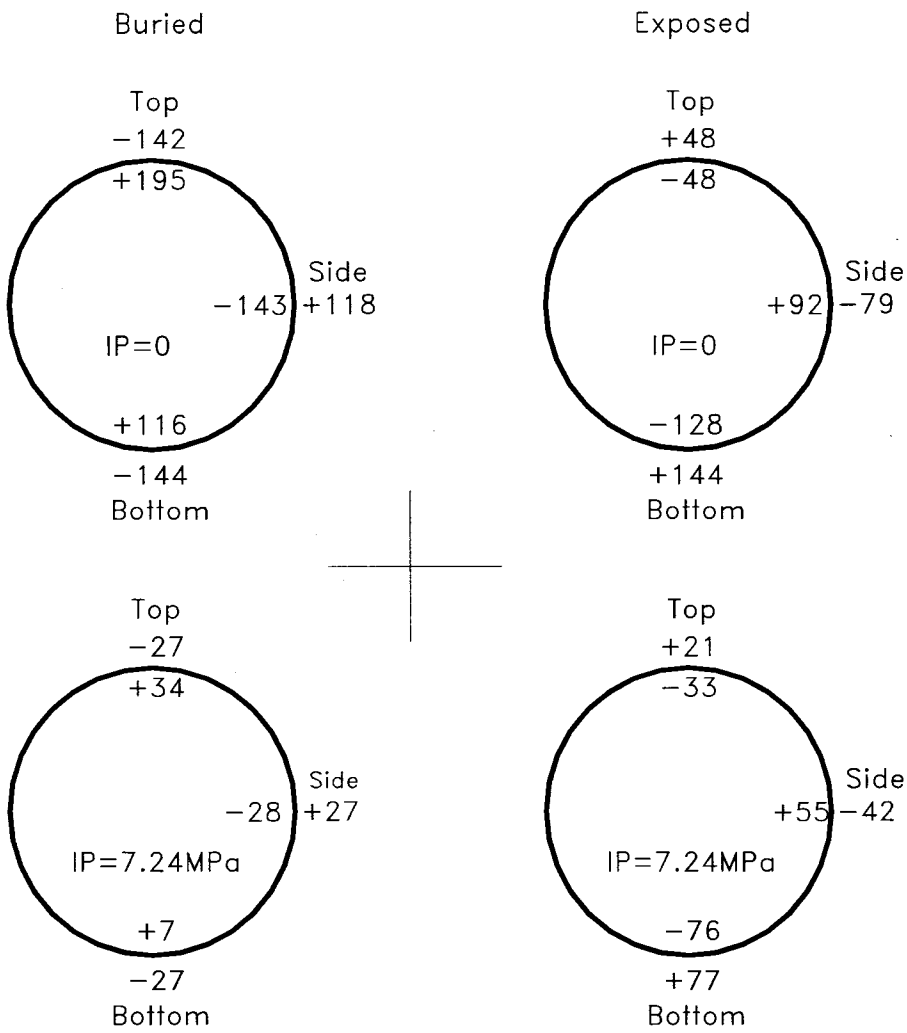

Figure 3.38 Comparison of maximum hoop strains between summer un-pressurized and pressurized tests

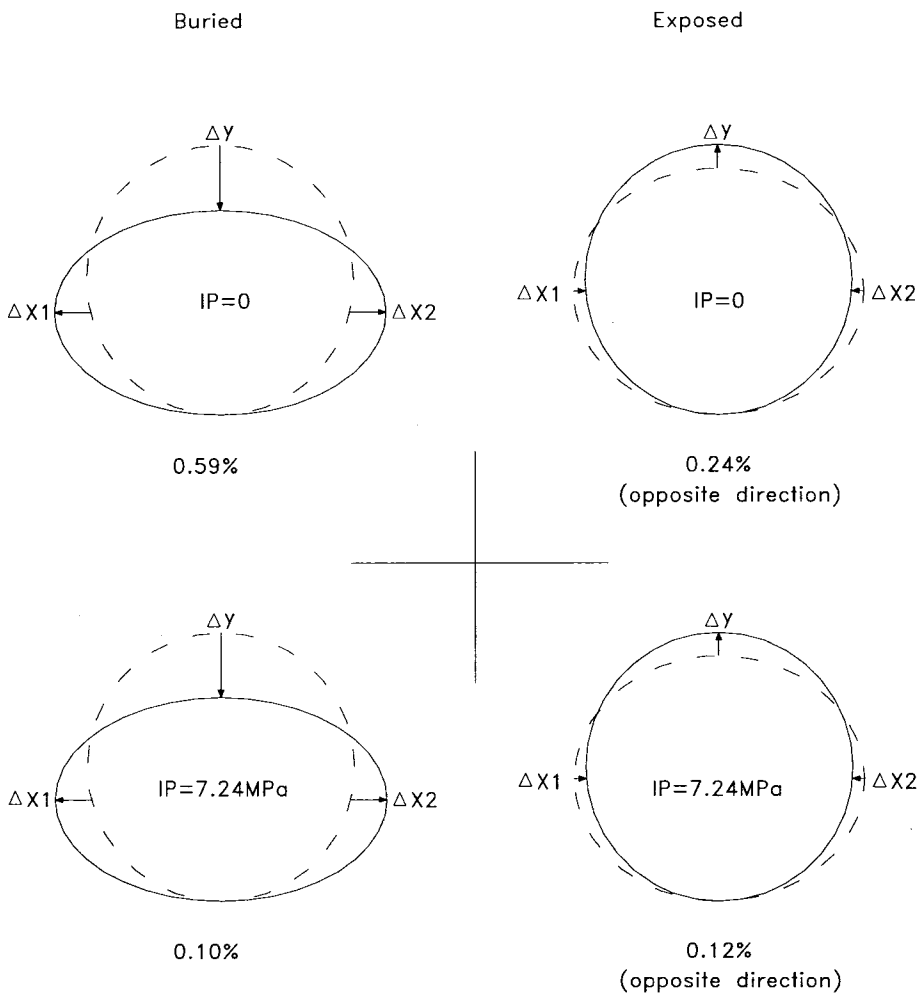

Figure 3.39 Comparison of maximum ovalization between summer un-pressurized and pressurized tests

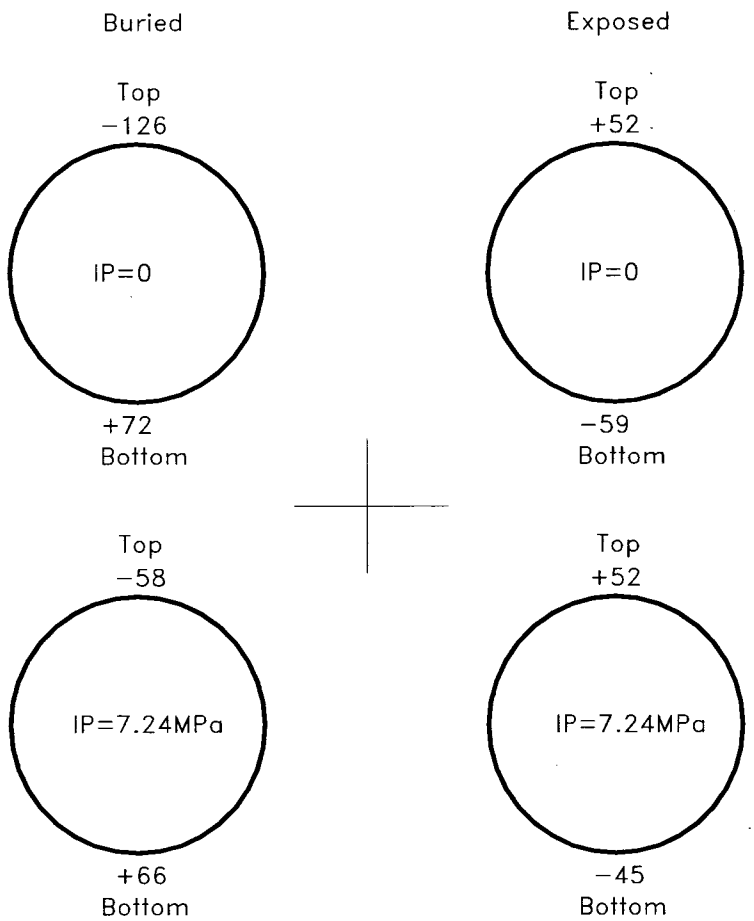

Figure 3.40 Comparison of maximum longitudinal strains between summer un-pressurized and pressurized tests

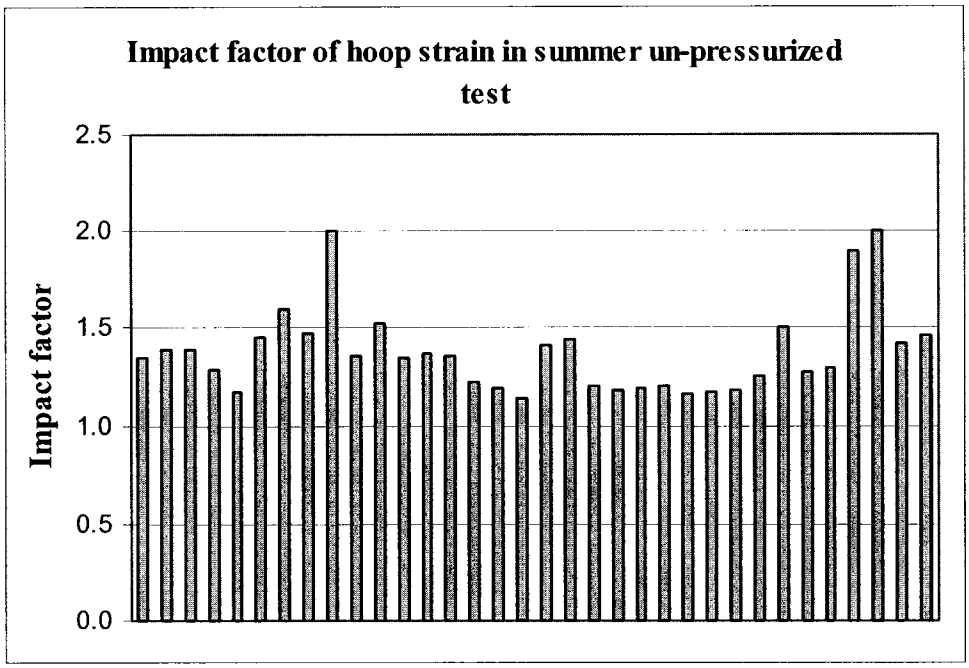

Figure 3.41 Impact factors of hoop strain in summer un-pressurized tests

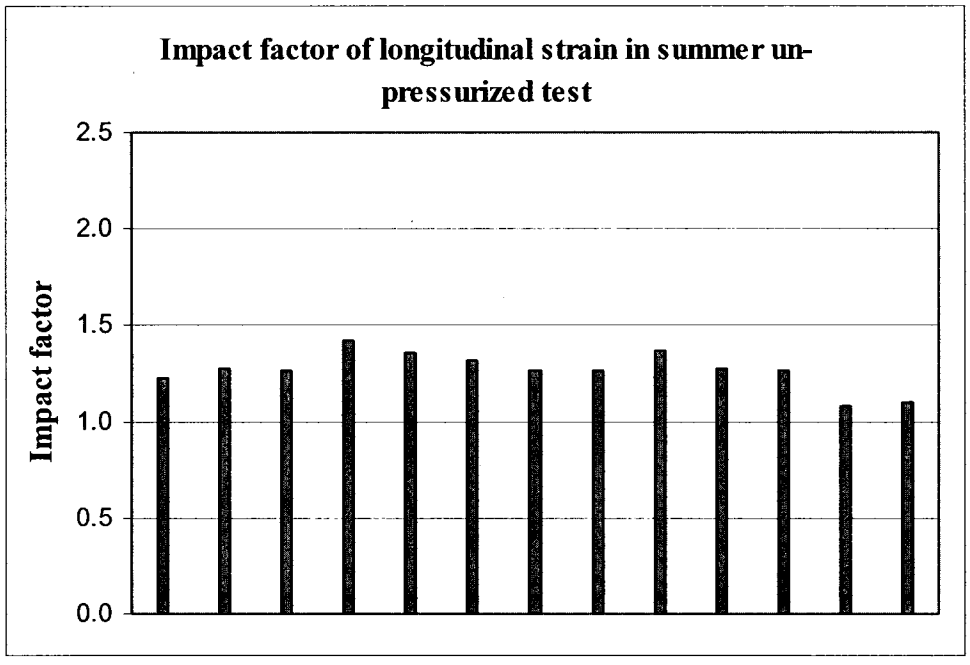

Figure 3.42 Impact factors of longitudinal strain in summer un-pressurized tests

4 TEST RESULTS AND DATA ANALYSIS OF WINTER EXCAVATION TESTS

The histories of the hoop and longitudinal strains and deformation of winter pressurized test are shown in from Figure 4.1 to Figure 4.14. The strain (hoop and longitudinal) and deformation histories of winter un-pressurized test are shown in from Figure 4.16 to Figure 4.40. The horizontal axis is time in second. The vertical axis is strain (unit: micro-strain) for Sections 1, 2, 3, 4, 5 and 7 and deformation (unit: millimeter) for Section 6. The positions of excavator are indicated by the number of instrumented section. At each position, the excavator may be at left or right side. For winter pressurized test, the excavator position was only at Section 2 due to premature failure of the pipe caused by excavation.

4.1 Winter Pressurized Test

4.1.1 Test Results of Pressurized Test

4.1.1.1 Strains from low-speed data acquisition system

History of hoop strain at the top (0°) of Section 1 in low-speed during winter pressurized test is shown in Figure 4.1. The maximum hoop strain was +4με (inside) and -14με (outside) when the excavator was at Section 2.

History of hoop strain at the right side (90°) of Section 1 in low-speed during test is shown in Figure 4.2. The maximum hoop strain was +5με at outside when the excavator was at Section 2.

History of hoop strain at the bottom (180°) of Section 1 in low-speed during winter pressurized test is shown in Figure 4.3. The maximum hoop strain was +12με (outside) and -10με (inside) when the excavator was at Section 2.

History of longitudinal strain at the top (0°) and bottom (180°) of Section 1 in low-speed during winter pressurized test is shown in Figure 4.4. The longitudinal strain at the top was positive and the maximum was +22με. The longitudinal strain at the bottom was negative and the maximum was -33με.

History of longitudinal strain at the top (0°) and bottom (180°) of Section 2 in low-speed during winter pressurized test is shown in Figure 4.5. The longitudinal strain at the top was negative and the maximum was -60με when the excavator was at Section 2. The longitudinal strain at the bottom was positive and the maximum was +51με when the excavator was at Section 2.

History of longitudinal strain at the top (0°) of Section 3 in low-speed during winter pressurized test is shown in Figure 4.6. The longitudinal strain at the top was negative and the maximum was -40με when the excavator was at Section 2.

4.1.1.2 Comparison of strains obtained from high-speed and low-speed data acquisition system

History of hoop strain at the top (0°) of Section 2 in high speed and the top (0°) of Section 3 in low speed during winter pressurized test is shown in Figure 4.7. The maximum hoop strain in high speed was +37με (inside) and -42με (outside) when the excavator was at Section 2. The maximum hoop strain in low speed was +19με (inside) and -27με (outside) when the excavator was at Section 2. The strains of high-speed and low-speed agreed well in the test.

History of hoop strain at the position of 30° of Section 2 in high speed and at the position of 45° of Section 3 in low speed during winter pressurized test is shown in Figure 4.8. History of hoop strain at the position of 60° of Section 2 in high speed and at the position of 45° of Section 3 in low speed during winter test 1 is shown in Figure 4.9. The maximum hoop strain in high speed was +16με (outside) and -25με (inside) when the excavator was at Section 2. The maximum hoop strain in low speed was +19με (outside) and -31με (inside) when the excavator was at Section 2. The strains of high-speed and low-speed agreed well in the test.

History of hoop strain at the right side (90°) of Section 2 in high speed and at the right side (90°) of Section 3 in low speed during winter pressurized test is shown in Figure 4.10. The maximum hoop strain in high speed was +9με (outside) and -32με (inside) when the excavator was at Section 2. The maximum hoop strain in low speed was +5με (outside) and -27με (inside) when the excavator was at Section 2. The strains of high-speed and low-speed agreed well in the test.

History of hoop strain at the bottom (180°) of Section 2 in high speed and at the bottom (180°) of Section 3 in low speed during winter pressurized test is shown in Figure 4.11. The maximum hoop strain in high speed was +6με (inside) and -32με (outside) when the excavator was at Section 2. The maximum hoop strain in low speed was +7με (inside) and -27με (outside) when the excavator was at Section 2. The strains of high-speed and low-speed agreed well in the test.

History of hoop strain at the left side (270°) of Section 2 in high speed and at the left side (270°) of Section 3 in low speed during winter pressurized test is shown in Figure 4.12. The maximum hoop strain in high speed was +19με (outside) and -35με

(inside) when the excavator was at Section 2. The maximum hoop strain in low speed was +14με (outside) and -27με (inside) when the excavator was at Section 2. The strains of high-speed and low-speed agreed well in the test.

History of hoop strain at the position of 315° of Section 2 in high speed and at the position of 315° of Section 3 in low speed during winter pressurized test is shown in Figure 4.13. The maximum hoop strain in high speed was +16με (inside) and -14με (outside) when the excavator was at Section 2. The maximum hoop strain in low speed was +16με (inside) and -15με (outside) when the excavator was at Section 2. The strains of high-speed and low-speed agreed well in the test.

By comparing the strain history in winter pressurized test, it can be found the strains in high speed change in the same trends as in low speed. The maximum hoop strains in high-speed at Section 2 and in low-speed at Section 3 are compared in Figure 4.14. The maximum strains were at the top of Section 2 measured in high-speed, which were +37με inside and -42με outside. The maximum hoop strains of the high speed and low speed are presented in Table 4.1.

4.1.1.3 Ovalization

History of deformation in vertical and horizontal direction at Section 6 during winter pressurized test is shown in Figure 4.15. The maximum vertical deformation was -0.20 mm and maximum horizontal deformation was +0.21 mm when the excavator was at Section 2.

History of deformation in diagonal direction at Section 6 during winter pressurized test is shown in Figure 4.16. The maximum deformation was +0.17 mm when the excavator was at Section 2.

The winter pressurized test was not finished due to the failure of a fitting caused by the excavator. The excavator stayed only at Section 2 and test stopped. Compared with the strains in Sections 2 and 3 as presented above, the strains in Sections 4, 5 and 7 were even smaller and were not presented.

In summary, based on the analysis of the strain and deformation history in the process of winter pressurized excavation test, it can be concluded that the pipe cross-section is under a through-wall or localized bending as evidenced by the inside and outside hoop strains. By comparing the top and bottom longitudinal strains, it is apparent that the specimen is under a longitudinal bending. There is a good agreement of the hoop strain between high-speed at Section 2 and low-speed at Section 3.

4.2 Winter Un-pressurized Test

4.2.1 Test Results of Un-pressurized Test

4.2.1.1 Section 1

History of hoop strain at the bottom (180°) of Section 1 in low-speed during winter un-pressurized test is shown in Figure 4.17. The maximum hoop strain was +138με (outside) and -137με (inside) when the excavator was at Section 7. The sign of the inside hoop strain changed from positive to negative while the sign of the outside hoop strain changed from negative to positive when the excavator was at Section 2. By comparing the inside and outside hoop strains, it can be concluded that the pipe cross-section was under a through-wall or localized bending.

History of longitudinal strain at the bottom (180°) of Section 1 during winter un-pressurized test is shown in Figure 4.18. The maximum longitudinal strain was -67με at

the bottom when the excavator was at Section 7.

4.2.1.2 Section 2 and Section 3

History of longitudinal strain at the top (0°) and bottom (180°) of Section 2 during winter un-pressurized test is shown in Figure 4.19. The maximum longitudinal strain was -93με at the top and +53με at the bottom when the excavator was sitting above this section. When the excavator moved to Section 7, the maximum longitudinal strain was +22με at the top and -58με at the bottom. The sign of the bottom longitudinal strain changed from positive to negative while the sign of the top longitudinal strain changed from negative to positive when the excavator moved to Section 4.

History of longitudinal strain at the top (0°) of Section 3 during winter un-pressurized test is shown in Figure 4.20. The maximum longitudinal strain was -80με at the top when the excavator was sitting above this section. When the excavator moved to Section 7, the maximum longitudinal strain was +47με at the top. The sign of the top longitudinal strain changed from negative to positive when the excavator moved to the middle of Sections 4 and 7.

History of hoop strain at the top (0°) of Section 2 in high-speed and Section 3 in low-speed during winter un-pressurized test is shown in Figure 4.21. The maximum hoop strain in high speed at section 2 was +129με (inside) and -180με (outside) when the excavator was sitting above this section. The maximum hoop strain in low speed at section 3 was +61με (inside) and -76με (outside) when the excavator was at Section 2. When the excavator moved to Section 7, the maximum hoop strain in high speed at Section 2 was -68με (inside) and +76με (outside) while the maximum hoop strain in low speed at Section 3 was -35με (inside) and +53με (outside). The sign of the inside hoop

strain changed from positive to negative while the sign of the outside hoop strain changed from negative to positive when the excavator was at the middle of Sections 4 and 7. By comparing the inside and outside hoop strains, it can be concluded that the pipe cross-section is under a through-wall or localized bending. The strains of high-speed and low-speed agreed well in the test.

History of hoop strain at the 30° position of Section 2 in high-speed and at the 45° position of Section 3 in low-speed during winter un-pressurized test is shown in Figure 4.22. The maximum hoop strain in high speed at the 30° position of Section 2 was +133με (inside) and -133με (outside) at the second of 4976 when the excavator was at the middle of Sections 4 and 7. At the same time, the maximum hoop strain in low speed at the 45° position of Section 3 was +118με (inside) and -119με (outside). By comparing the inside and outside hoop strains, it can be concluded that the pipe cross-section is under a through-wall or localized bending. The strains of high-speed and low-speed agreed well in the test.

History of hoop strain at the 60° position of Section 2 in high-speed and at the 45° position of Section 3 in low-speed during winter un-pressurized test 2 is shown in Figure 4.23. The maximum hoop strain in high speed at the 60° position of Section 2 was +45με (outside) and -79με (inside) at the second of 6066 when the excavator was at the middle of Sections 4 and 7. At the second of 4976, the maximum hoop strain in low speed at the 45° position of Section 3 was +118με (inside) and -119με (outside). By comparing the inside and outside hoop strains, it can be concluded that the pipe cross-section is under a through-wall or localized bending. The strains of high-speed and low-speed agreed well in the test.

History of hoop strain at the right side (90°) of Section 2 in high-speed and Section 3 in low-speed during winter un-pressurized test is shown in Figure 4.24. The maximum hoop strain in high speed at Section 2 was +27με (outside) and -56με (outside) when the excavator was sitting above this section. The maximum hoop strain in low speed at Section 3 was +17με (inside) and -40με (outside) when the excavator was at Section 2. When the excavator moved back to Section 4 and Section 7, the maximum hoop strain in high speed at Section 2 was -79με (outside) and +53με (inside) while the maximum hoop strain in low speed at Section 3 was -59με (outside) and 50με (inside). The sign of the outside hoop strain changed from positive to negative while the sign of the inside hoop strain changed from negative to positive when the excavator was at Section 4. The maximum hoop strain in high speed at Section 2 was +63με (outside) and -108με (inside) at the second of 4976 when the excavator was at the middle of Sections 4 and 7. At the same time, the maximum hoop strain in low speed at Section 3 was +70με (outside) and -93με (outside). By comparing the inside and outside hoop strains, it can be concluded that the pipe cross-section is under a through-wall or localized bending. The strains of high-speed and low-speed agreed well in the test.

History of hoop strain at the bottom (180°) of Section 2 in high-speed and Section 3 in low-speed during winter un-pressurized test is shown in Figure 4.25. The maximum hoop strain in high speed at Section 2 was +28με (inside) and -47με (outside) when the excavator was sitting above this section. The maximum hoop strain in low speed at Section 3 was +26με (inside) and -45με (outside) when the excavator was at Section 2. When the excavator moved to Section 7, the maximum hoop strain in high speed at Section 2 was -95με (inside) and +98με (outside) while the maximum hoop strain in low

speed at Section 3 was -78με (inside) and +80με (outside). The sign of the inside hoop strain changed from positive to negative while the sign of the outside hoop strain changed from negative to positive when the excavator was at Section 4. By comparing the inside and outside hoop strains, it can be concluded that the pipe cross-section is under a through-wall or localized bending. The strains of high-speed and low-speed agreed well in the test.

History of hoop strain at the left side (270°) of Section 2 in high-speed and Section 3 in low-speed during winter un-pressurized test is shown in Figure 4.26. The maximum hoop strain in high speed at Section 2 was +36με (outside) and -58με (inside) when the excavator was sitting above this section. The maximum hoop strain in low speed at Section 3 was +28με (outside) and -38με (inside) when the excavator was at Section 2. When the excavator moved back to Section 7, the maximum hoop strain in high speed at Section 2 was -56με (outside) and +35με (inside) while the maximum hoop strain in low speed at Section 3 was -56με (outside) and 45με (inside). The sign of the outside hoop strain changed from positive to negative while the sign of the inside hoop strain changed from negative to positive when the excavator was at Section 4. The maximum hoop strain in high speed at Section 2 was +40με (outside) and -84με (inside) at the second of 6067 when the excavator was at Section 7. At the same time, the maximum hoop strain in low speed at Section 3 was +38με (outside) and -71με (outside). By comparing the inside and outside hoop strains, it can be concluded that the pipe cross-section is under a through-wall or localized bending. The strains of high-speed and low-speed agreed well in the test.

History of hoop strain at the 315° position of Section 2 in high-speed and of Section 3 in low-speed during winter un-pressurized test is shown in Figure 4.27. The maximum hoop strain in high speed at Section 2 was +77με (outside) and -59με (inside). The maximum hoop strain in low speed at section 3 was +63με (inside) and -72με (outside). By comparing the inside and outside hoop strains, it can be concluded that the pipe cross-section is under a through-wall or localized bending. The strains of high-speed and low-speed agreed well in the test.

4.2.1.3 Section 4 and Section 5

History of longitudinal strain at the top (0°) and bottom (180°) of Section 4 during winter un-pressurized test is shown in Figure 4.28. The maximum longitudinal strain was -82με at the top and +70με at the bottom when the excavator was sitting above this section. The sign of the top longitudinal strain changed from positive to negative while the sign of the bottom longitudinal strain changed from negative to positive when the excavator moved on this section.

History of longitudinal strain at the top (0°) of Section 5 during winter un-pressurized test is shown in Figure 4.29. The maximum longitudinal strain was +20με when the excavator was at Section 2. The maximum longitudinal strain was -63με when the excavator was at Section 4. The sign of the top longitudinal strain changed from positive to negative when the excavator moved on this section.

History of hoop strain at the top (0°) of Section 4 in high-speed and Section 5 in low-speed during winter un-pressurized test is shown in Figure 4.30. The maximum hoop strain in high speed at Section 4 was +68με (inside) and -73με (outside) at the second of 6770. The maximum hoop strain in low speed at Section 5 was +48με (inside) and -76με

(outside). By comparing the inside and outside hoop strains, it can be concluded that the pipe cross-section is under a through-wall or localized bending. The strains of high-speed and low-speed agreed well in the test.

History of hoop strain at the 45° position of Section 4 in high-speed and Section 5 in low-speed during winter un-pressurized test is shown in Figure 4.31. The maximum hoop strain in high speed at Section 4 was +220με (inside) and -211με (outside) at the second of 5638. These were the transient strains captured by high speed DAS only. The maximum hoop strain in low speed at Section 5 was +49με (inside) and -79με (outside) at the second of 6745. By comparing the inside and outside hoop strains, it can be concluded that the pipe cross-section is under a through-wall or localized bending. The strains of high-speed and low-speed agreed well in the test.

History of hoop strain at the 45° position of Section 4 in high-speed and the 315° position of Section 5 in low-speed during winter un-pressurized test is shown in Figure 4.32. The maximum hoop strain in low speed at 315° position of Section 5 was +89με (inside) and -112με (outside) at the second of 6860. By comparing the inside and outside hoop strains, it can be concluded that the pipe cross-section is under a through-wall or localized bending. The strains of high-speed and low-speed agreed well in the test.

History of hoop strain at the right side (90°) of Section 4 in high-speed and Section 5 in low-speed during winter un-pressurized test is shown in Figure 4.33. The maximum hoop strain in high speed at Section 4 was +152με (outside) and -133με (inside) at the second of 5633. These were the transient strains captured by high speed DAS only. The maximum hoop strain in low speed at Section 5 was +89με (outside) and -130με (inside) when the excavator was at Section 7. By comparing the inside and

outside hoop strains, it can be concluded that the pipe cross-section was under a through-wall or localized bending. The strains of high-speed and low-speed agreed well in the test.

History of hoop strain at the bottom (180°) of Section 4 in high-speed and Section 5 in low-speed during winter un-pressurized test is shown in Figure 4.34. The maximum hoop strain in high speed at Section 4 was +94με (inside). The maximum hoop strain in low speed at Section 5 was +93με (inside) and -85με (outside). By comparing the inside and outside hoop strains, it can be concluded that the pipe cross-section was under a through-wall or localized bending. The strains of high-speed and low-speed agreed well in the test.

History of hoop strain at the left side (270°) of Section 4 in high-speed and Section 5 in low-speed during winter un-pressurized test is shown in Figure 4.35. The maximum hoop strain in high speed at Section 4 was +101με (outside) and -140με (inside) at the second of 6816. These were the transient strains captured by high speed DAS only. The maximum hoop strain in low speed at Section 5 was +101με (outside) and -113με (inside) when the excavator was at Section 7. By comparing the inside and outside hoop strains, it can be concluded that the pipe cross-section was under a through-wall or localized bending. The strains of high-speed and low-speed agreed well in the test.

4.2.1.4 Section 6

History of deformation in the vertical and horizontal directions of Section 6 during winter un-pressurized test is shown in Figure 4.36. The maximum deformation was -1.41 mm (vertical) and +1.61 mm (horizontal) when the excavator was at Section 7. By comparing the vertical and horizontal displacement, it can be concluded that the pipe cross-section was flattened in the process of excavation.

History of diagonal deformation of Section 6 during winter un-pressurized test is shown in Figure 4.37. The maximum deformation was +0.19 mm and -0.42 mm.

4.2.1.5 Section 7

History of hoop strain at the top (0°) of Section 7 in low-speed during winter un-pressurized test is shown in Figure 4.38. The maximum hoop strain was +92με (inside) and -60με (outside) when the excavator was sitting at this section. By comparing the inside and outside hoop strains, it can be concluded that the pipe cross-section was under a through-wall or localized bending.

History of hoop strain at the right side (90°) of Section 7 in low-speed during winter un-pressurized test is shown in Figure 4.39. The maximum hoop strain was +43με (outside) and -75με (inside) when the excavator was sitting at this section. By comparing the inside and outside hoop strains, it can be concluded that the pipe cross-section was under a through-wall or localized bending.

History of hoop strain at the bottom (180°) of Section 7 in low-speed during winter un-pressurized test is shown in Figure 4.40. The maximum hoop strain was -72με (outside) when the excavator was sitting at this section.

History of longitudinal strain at the top (0°) and bottom (180°) of Section 7 during winter un-pressurized test is shown in Figure 4.41. The maximum longitudinal strain was -78με at the top and +53με at the bottom when the excavator was sitting at this section.

In summary, based on analysis of the strain and deformation history in the process of winter excavation, it can be concluded that the pipe cross-section is under a through-wall or localized bending by comparing the inside and outside hoop strains. By comparing the top and bottom longitudinal strains, the pipeline was found to be under a

longitudinal bending. The signs of the strains changed at a specific position of excavator. There is a good agreement of the hoop strain in high-speed and low-speed.

4.2.2 Comparison of Hoop Strain in High-speed and Low-speed

Since the Sections 2 and 3 are close, comparison can be made between the high speed data at Section 2 and low speed data at Section 3. The same comparison can be made between Section 4 in high speed and Section 5 in low speed.

At buried state, the maximum hoop strains at Sections 2 and 4 in high speed and at Sections 3 and 5 in low speed were plotted in Figure 4.42. The maximum hoop strain in high speed is almost same as in low speed at the bottom of each section. At Section 2 and Section 3, the hoop strain at the top is the maximum of the section. The maximum hoop strains were-180με and +129με captured by high speed DAS.

At Section 4, the maximum hoop strains were -211με outside and +220με inside at the 45° position captured by high speed DAS at the seconds of 5638.35 when the excavator was at Section 7. At the same time and same position (45°) of Section 5, the maximum strains captured were only -32με and +18με in low speed. As shown in Figure 4.43, a dynamic transient hoop strain happened at this second and lasted only for 0.11 second. It reached the maximum and vanished in a very short time. The dynamic character was very significant. The other dynamic transient strains at the right side (90°) at the second of 5633.38 and left side (270°) at the second of 6816.00 of Section 4 were displayed in Figure 4.44 and Figure 4.45 respectively. They lasted only for 0.13 and 0.18 second. The dynamic transient strains at 45° position were positive inside and negative outside but opposite at 90° and 270° positions. This was caused by the transient downward digging force acting on the upper part of specimen in the excavation process.

At exposed state, the maximum hoop strains at Section 2 and Section 3 were plotted in Figure 4.46. Usually, the exposed pipe section experienced an opposite process of deformation indicated by the sigh change of inside and outside hoop strains from the buried state. As shown in the figure, the strains of the two sections in high speed and low speed are very comparable. At Section 2, the maximum hoop strains happened at the 30° position. They were -133με and +133με. At Section 3, the maximum hoop strains were -118με and +119με at the 45° position. The maximum strains of these two sections happened at the same second of 4976. The inside and outside hoop strain changed signs in a very short period at these two sections although the hoop strain has already indicated the section re-rounding. This phenomenon is called "strain reversal". They were observed at the positions of 30°, 45°, 90°, 270° and 315°. Their maximum values are shown in Figure 2.47. The short-time strain histories were plotted in Figure 2.48 to Figure 2.51 in detail. These reversals lasted for about 3.39 seconds to 11.06 seconds. The strain changed sign in this period and attained a maximum value and finally returned to original. Because of their longer duration, they can be captured well either by high speed or low speed DAS. The short time strain reversal resulted from the downward digging force acted on the top of the specimen around these sections. But comparing the force to cause transient strain, the force was applied very slowly and has not necessarily produced dynamic response.

Therefore, by comparing the maximum hoop strain captured by high speed and low speed DAS at buried state and exposed state, it is found that the strains in high speed has the same change trend as in low speed. The dynamic transient strains can be captured by high speed DAS only. The maximum dynamic transient hoop strains were -211με and

+220με. The short time strain reversal was captured well by high speed or low speed DAS due to their longer duration. The maximum hoop strain captured by high speed and low speed DAS was compared in Table 4.2.

4.3 Comparison of Winter Pressurized Test and Winter Un-pressurized Test

Because the winter pressurized test was finished only when the excavator stayed at section 2 and 3, the strains at Sections 2 and 3 in pressurized test can be compared with the strains at Sections 2, 3, 4, 5 and 7 in un-pressurized test when the excavator was sitting on them. Under this condition, the maximum hoop strain, ovalization and longitudinal strain of winter pressurized and un-pressurized test are presented in Table 4.3.

4.3.1 Hoop strains

The comparison of the maximum hoop strain of Section 2 (high speed) in the pressurized test and un-pressurized test are presented in Figure 4.52. The maximum hoop strain occurred at the top of the section. The maximum positive hoop strain in pressurized test was +37με, which was about 29% of the maximum positive hoop strain (+129με) in un-pressurized test. The maximum negative hoop strain in pressurized test was -42με, which was about 23% of the maximum negative hoop strain (-180με) of un-pressurized test.

The maximum hoop strain of Section 3 (low speed) in the winter pressurized test and un-pressurized test are presented in Figure 4.53. The maximum hoop strain occurred at the top of the section. The maximum positive hoop strain in pressurized test was +19με, which was about 31% of the maximum positive hoop strain (+61με) of un-

pressurized test. The maximum negative hoop strain in pressurized test was -27με, which was about 36% of the maximum negative hoop strain (-76με) of un-pressurized test.

Therefore, it can be concluded that the maximum hoop strain was significantly reduced in pressurized test.

As shown in Table 4.3, the maximum hoop strains in each section varied in un-pressurized test. The variation is caused by the location of excavator relative to the instrumented section. Besides, after the pressurized test, the exposed portion between Sections 1 and 2 was backfilled. Therefore, the soil structure was not original in this portion. The neighboring instrumented sections maybe were affected in the following un-pressurized test.

4.3.2 Ovalization

In pressurized test, the maximum ovalization measured at Section 6 was 0.04% when the excavator was at Section 2 and the test stopped. The maximum ovalization measured at Section 6 should occur when the excavator moved on this section. Assuming the linear relationship between ovalization to hoop strain (actually this is proved true by the test), the maximum ovalization under this condition was found to be 0.09% using the maximum hoop strain measured in Section 2. Under the same condition in un-pressurized test, the ovalization is 0.11% as shown in Table 4.3. However, in the whole process of un-pressured test, the maximum ovalization measured at Section 6 is 0.33% when the excavator was at Section 7. Because the soil at two sides of Section 6 was removed while the top soil remained to protect the sealing gland, the deformation got increased and the maximum ovalization happened. The maximum ovalization at the Section 6 in the winter pressurized test and un-pressurized test were presented in Figure 4.54.

4.3.3 Longitudinal Strains

The maximum longitudinal strain in the winter pressurized test and un-pressurized test were presented in Figure 4.55. The longitudinal stains of the instrumented section directly under the excavator were negative at the top and positive at the bottom.

The maximum negative longitudinal strain in pressurized test was -60με, which was about 65% of the maximum longitudinal strain (-93με) of un-pressurized test. The maximum positive longitudinal strain in pressurized test was +51με, which was about 73% of the maximum longitudinal strain (+70με) of un-pressurized test.

Therefore, in summary, the longitudinal strain in pressurized test is about 65% ~ 73% of that in un-pressurized test.

4.4 Impact Factor

The result of impact factor of hoop strain (high speed) in winter un-pressurized tests is shown in Figure 4.56. The impact factors vary from 1.13 to 2.96 with the average of 1.57.

The result of impact factor of hoop strain (low speed) in winter un-pressurized tests is shown in Figure 4.57. The impact factors vary from 1.06 to 2.86 with the average of 1.42.

The result of impact factor of longitudinal strain in winter un-pressurized tests is shown in Figure 4.48. The impact factors vary from 1.02 to 2.83 with the average of 1.48.

For pressurized tests, the impact factors of hoop strain in high speed vary from 1.43 to 3.00 with the average of 1.70. For hoop strain in low speed, they vary from 1.20 to

2.00 with the average of 1.60. For longitudinal strain, they vary from 1.27 to 1.58 with the average of 1.42.

Table 4.1 Comparison of maximum hoop strains captured by high-speed and low-speed DAS in winter pressurized test

Max. Hoop Strain (με)	High Speed	Low Speed
Positive	+37	+19
Negative	-42	-27

Table 4.2 Comparison of maximum hoop strains captured by high-speed and low-speed DAS in winter un-pressurized test

Maximum Hoop Strain		High Speed (με)	Low Speed (με)
Buried	Positive	+220	+101
	Negative	-211	-130
Exposed	Positive	+133	+118
	Negative	-133	-119

Table 4.3 Comparison of the maximum strain and ovalization between winter pressurized test and un-pressurized test

Type of Max. / Min. Strain or Deformation		Pressurized Test (7.24MPa)		Un-Pressurized Test (0.00MPa)				
Section Number		2	3	2	3	4	5	7
Hoop Strain(με)	Positive	+37	+19	+129	+61	+50	+48	+92
	Negative	-42	-27	-180	-76	-38	-39	-75
Longitudinal Strain(με)	Positive	+51	---	+53	---	+70	---	+53
	Negative	-60	-40	-93	-80	-82	-54	-78
Ovalization(%)		0.09*(Section 2)		0.11 (Section 6)				

Note:

- The maximum strain and deformation shown are under the condition the excavator was sitting above this section.
- *: Estimated based on the linear relation of hoop strain and deformation
- ---: No strain gauge mounted at this position

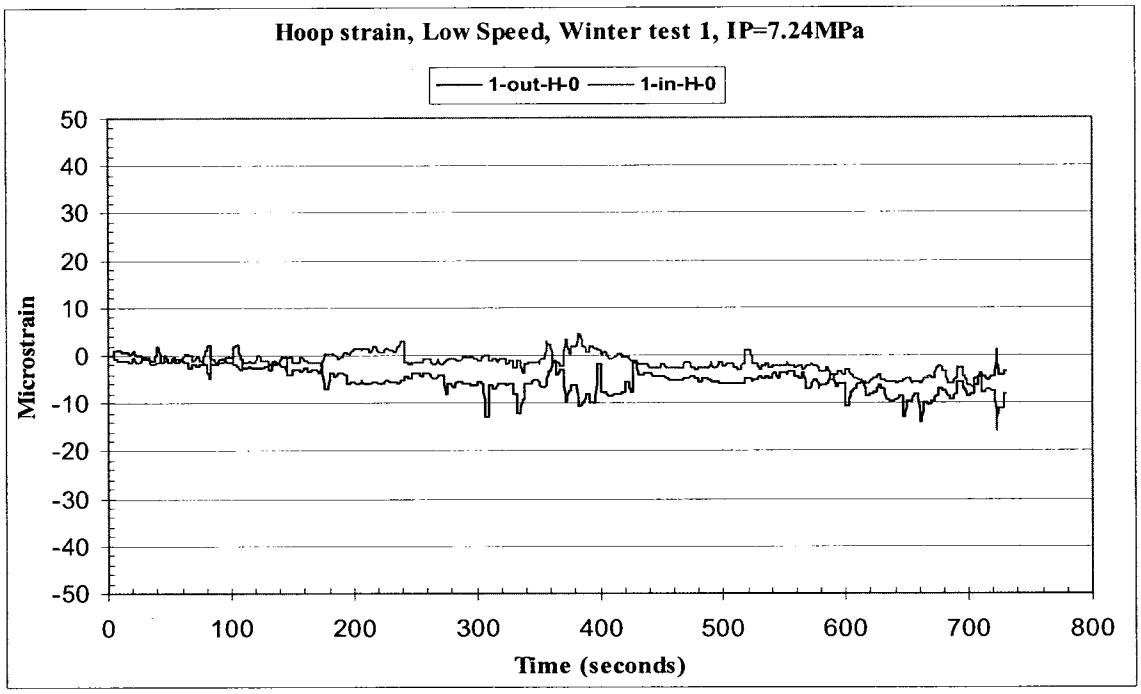

Figure 4.1 Hoop strain at the top (0°) of Section 1 in winter pressurized test, low speed

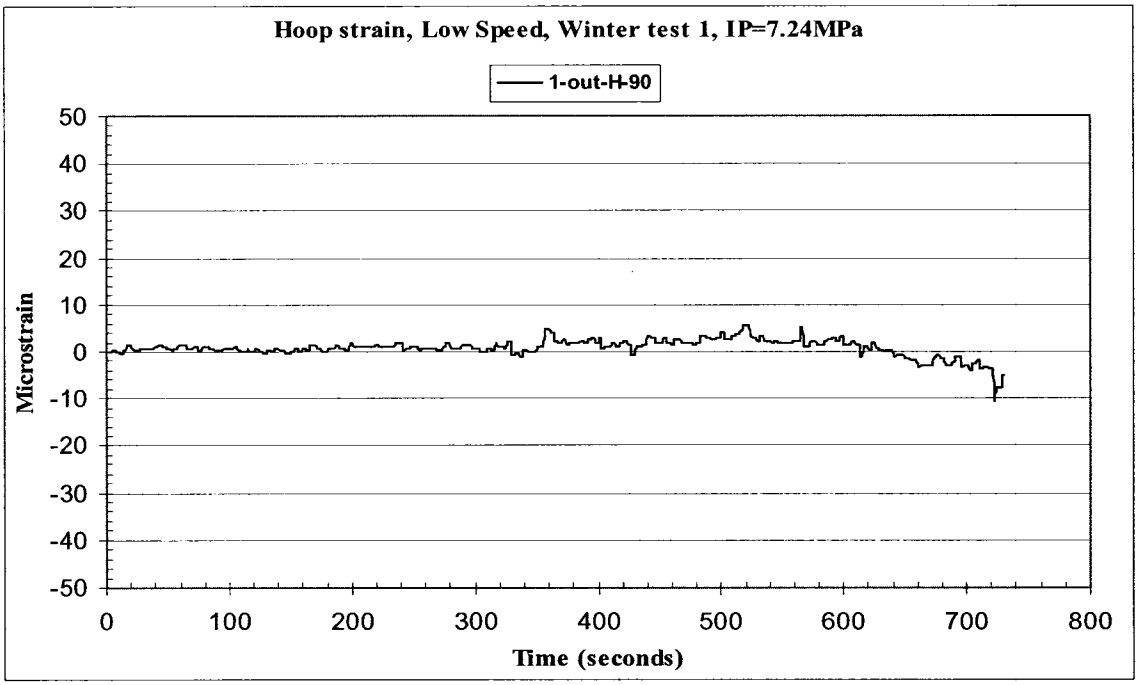

Figure 4.2 Hoop strain at the right side (90°) of Section 1 in winter pressurized test, low speed

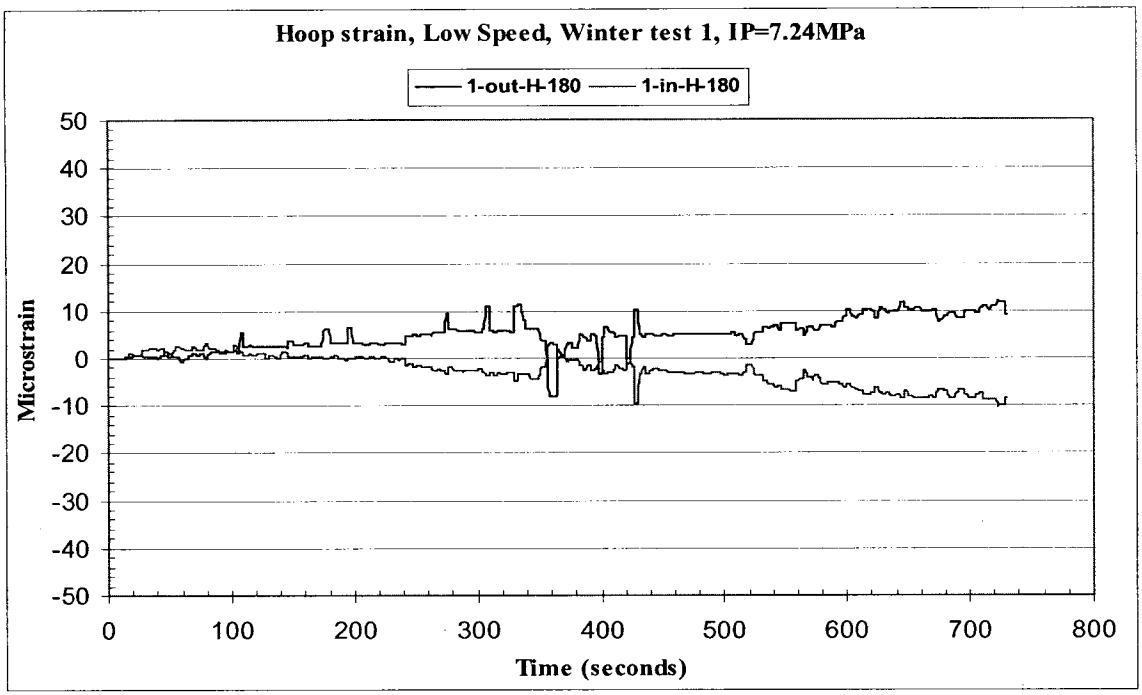

Figure 4.3 Hoop strain at the bottom (180°) of Section 1 in winter pressurized test, low speed

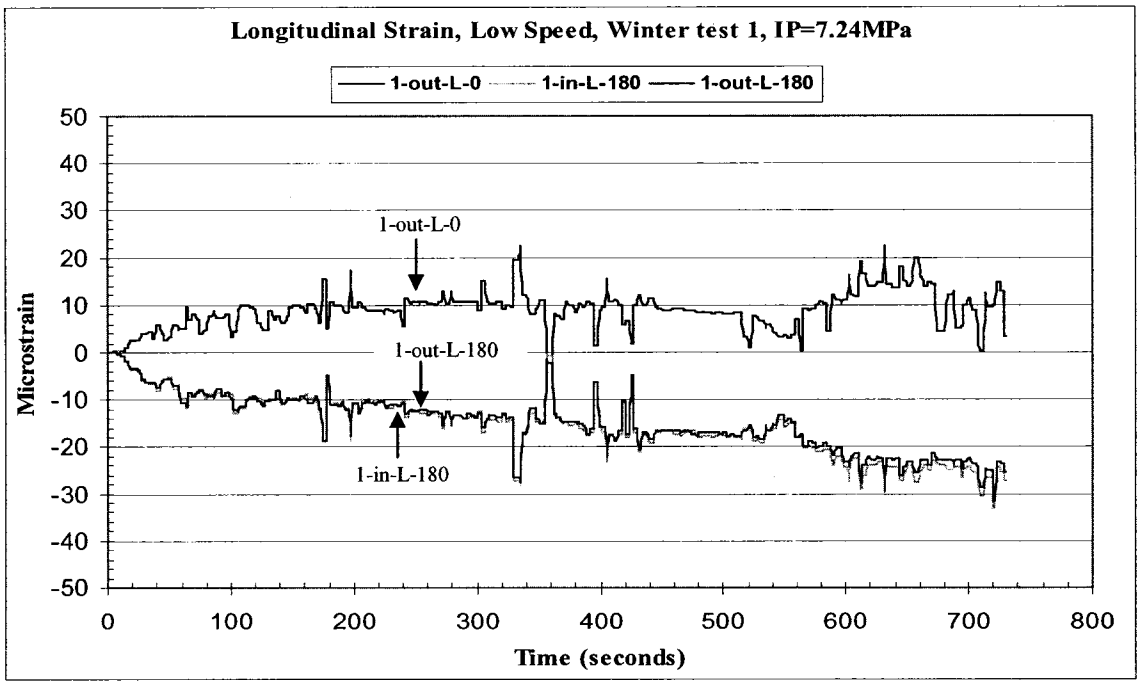

Figure 4.4 Longitudinal strain at the top (0°) and bottom (180°) of Section 1 in winter pressurized test, low speed

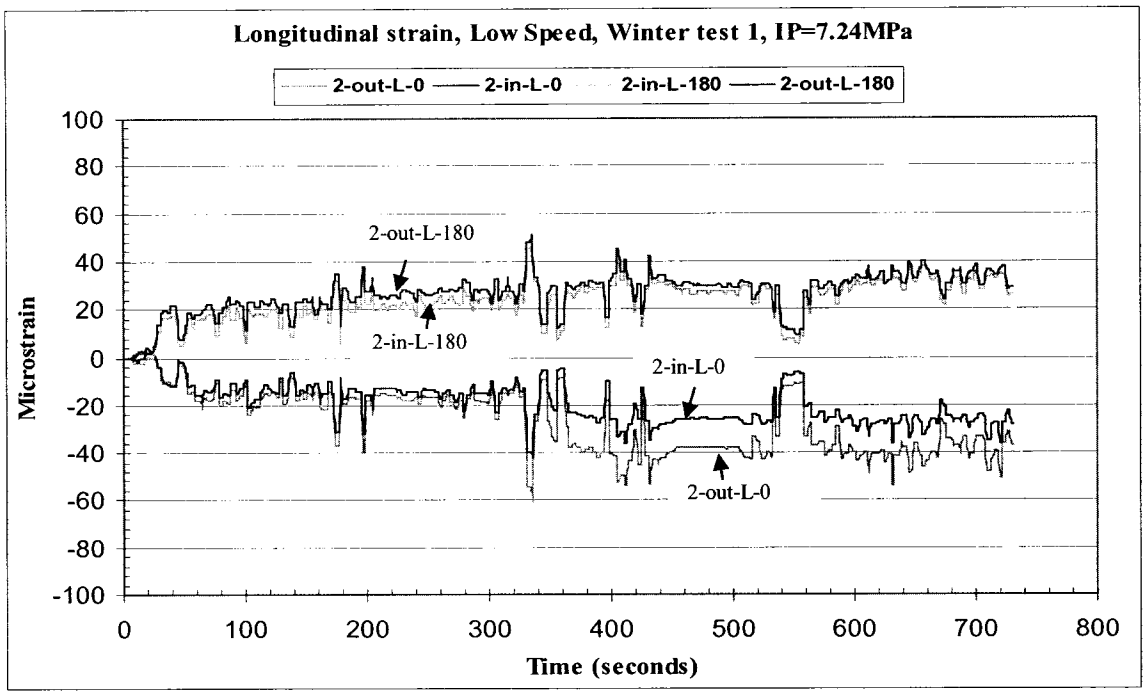

Figure 4.5 Longitudinal strain at the top (0°) and bottom (180°) of Section 2 in winter pressurized test, low speed

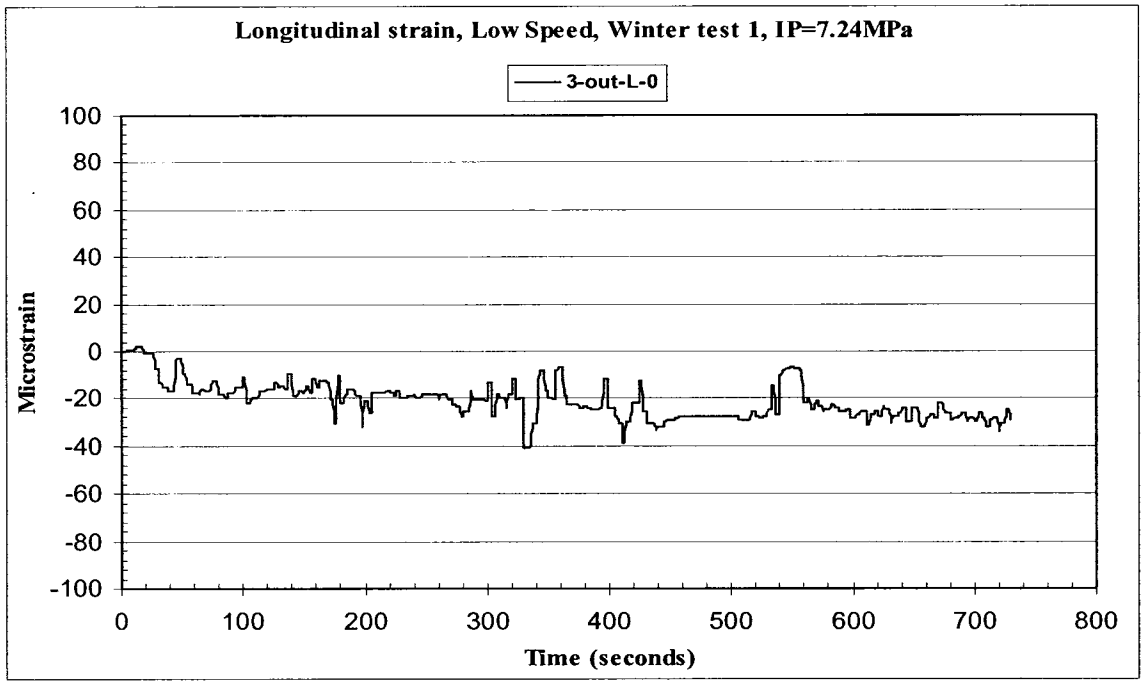

Figure 4.6 Longitudinal strain at the top (0°) of Section 3 in winter pressurized test, low speed

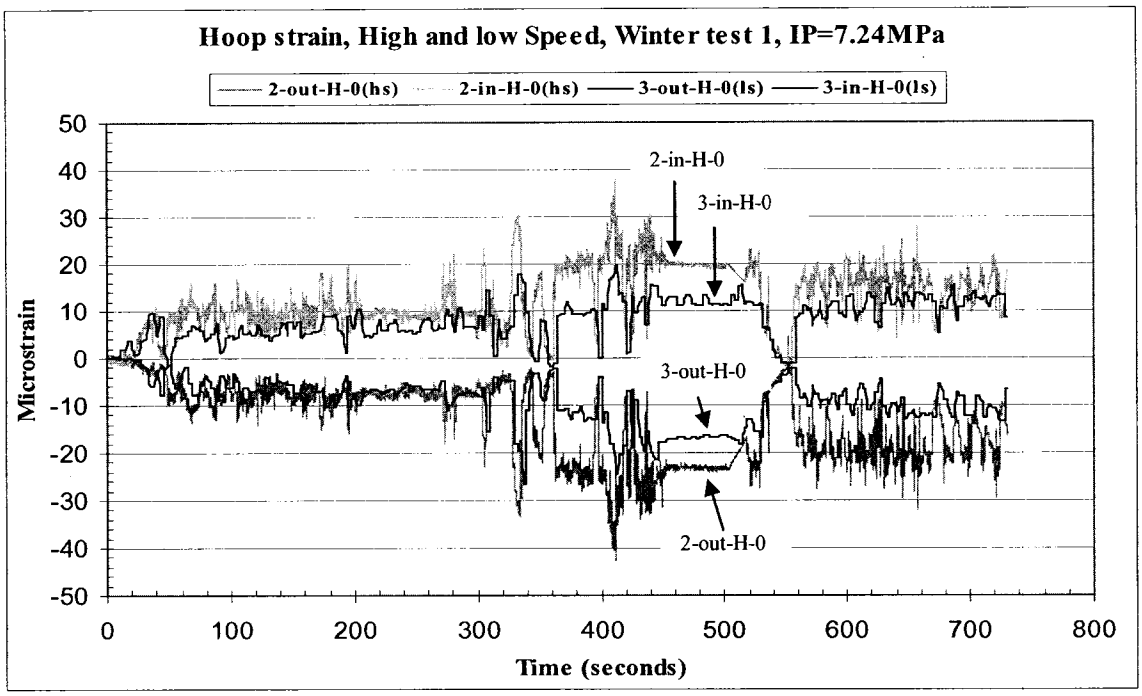

Figure 4.7 Hoop strain at the top (0°) of Section 2 (high speed) and Section 3 (low speed) in winter pressurized test

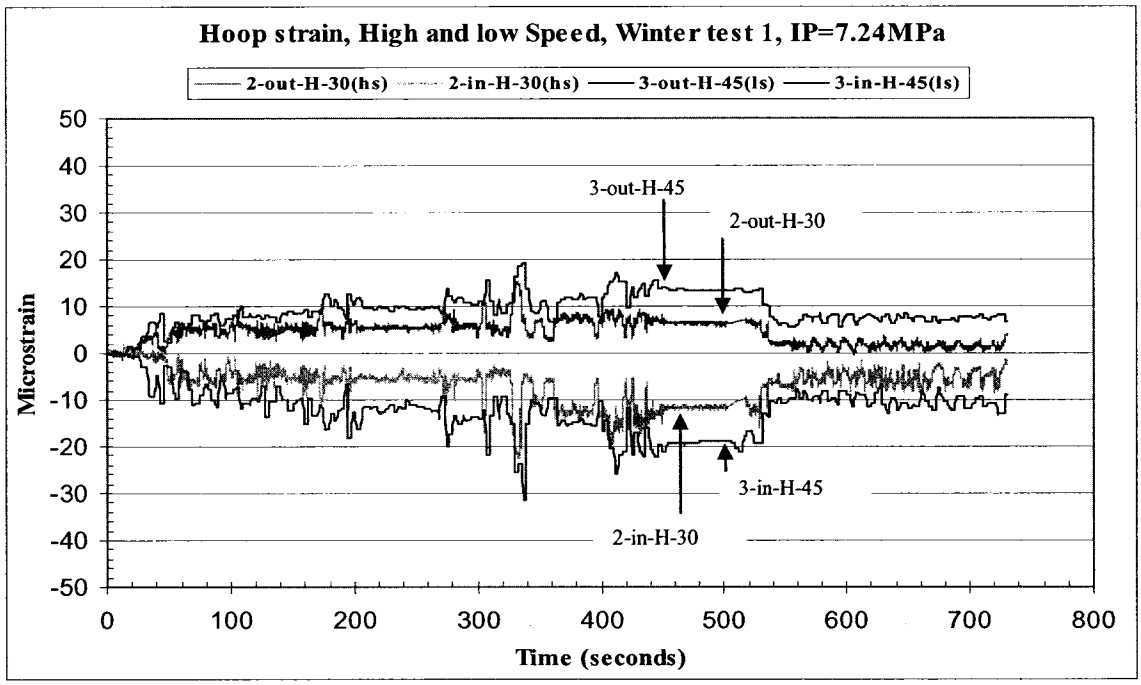

Figure 4.8 Hoop strain at the 30° of Section 2 (high speed) and the 45° of Section 3 (low speed) in winter pressurized test

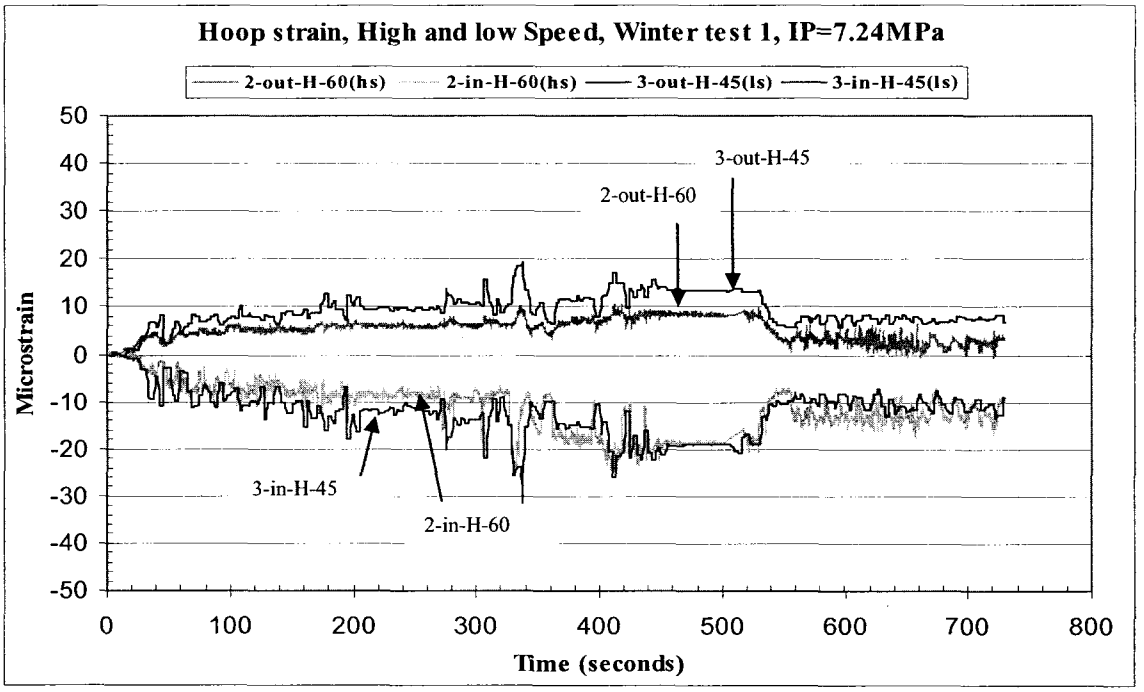

Figure 4.9 Hoop strain at the 60° of Section 2 (high speed) and the 45°of Section 3 (low speed) in winter pressurized test

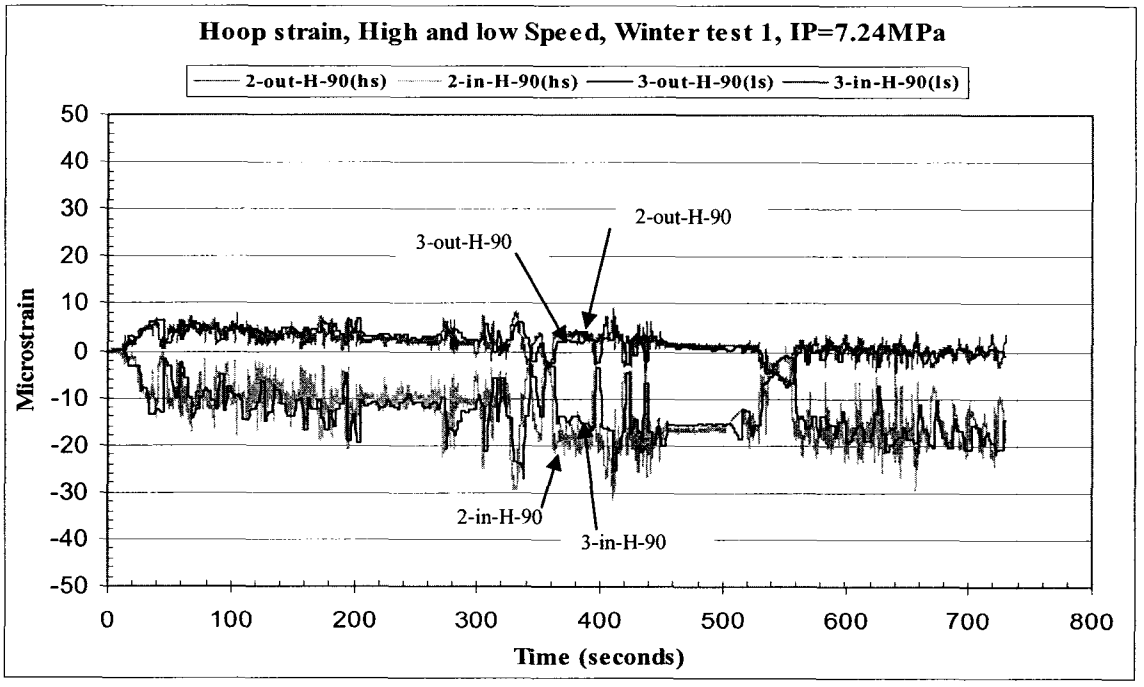

Figure 4.10 Hoop strain at the right side (90°) of Section 2 (high speed) and Section 3 (low speed) in winter pressurized test

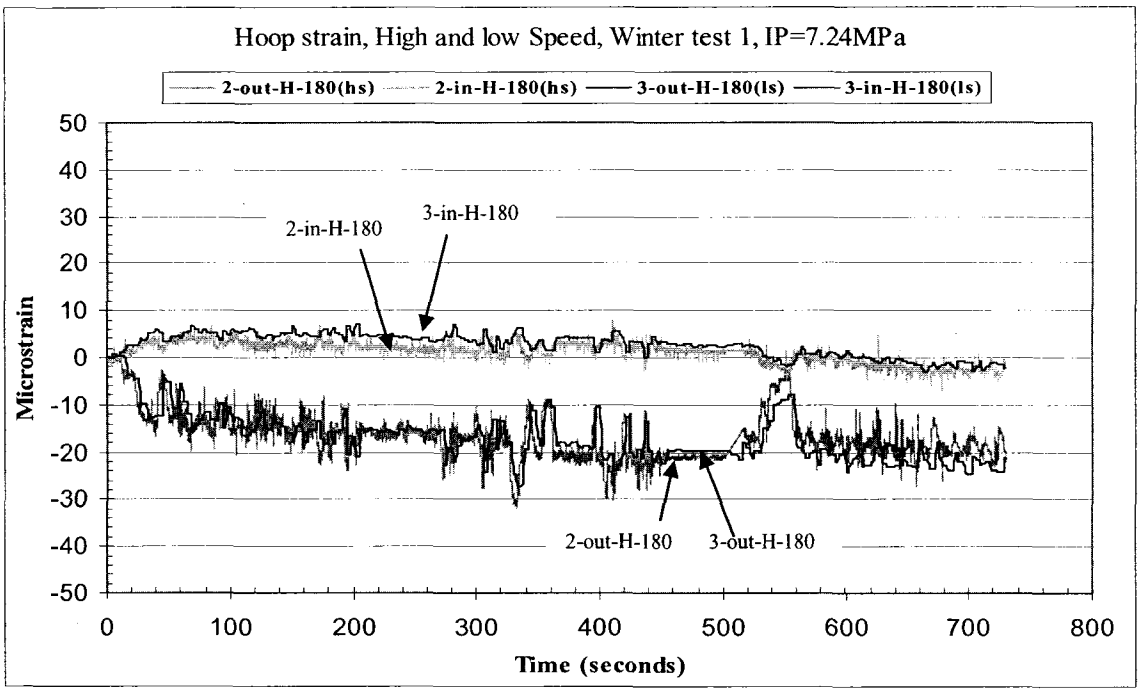

Figure 4.11 Hoop strain at the bottom (180°) of Section 2 (high speed) and Section 3 (low speed) in winter pressurized test

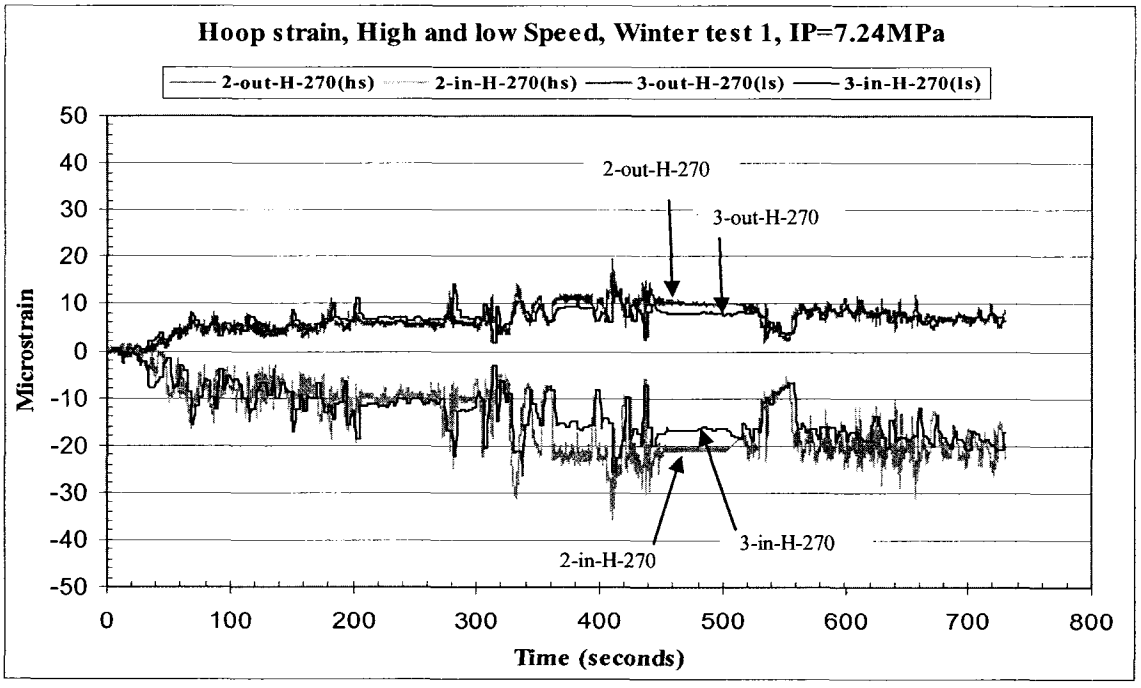

Figure 4.12 Hoop strain at the left side (270°) of Section 2 (high speed) and Section 3 (low speed) in winter pressurized test

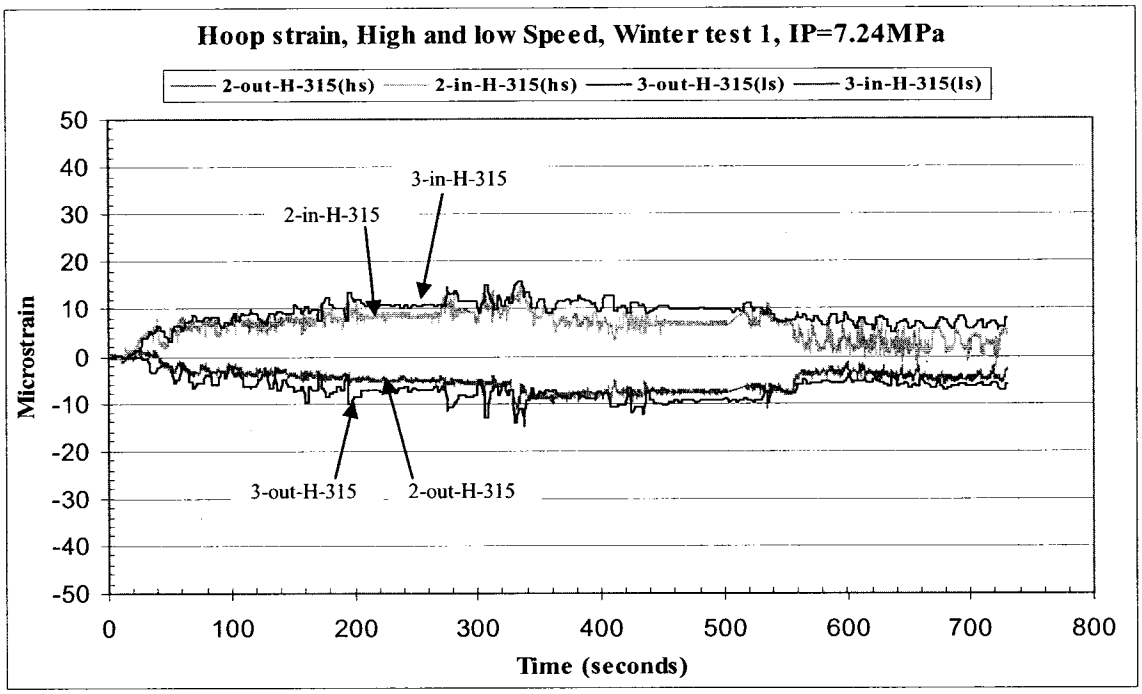

Figure 4.13 Hoop strain at the 315° of Section 2 (high speed) and Section 3 (low speed) in winter pressurized test

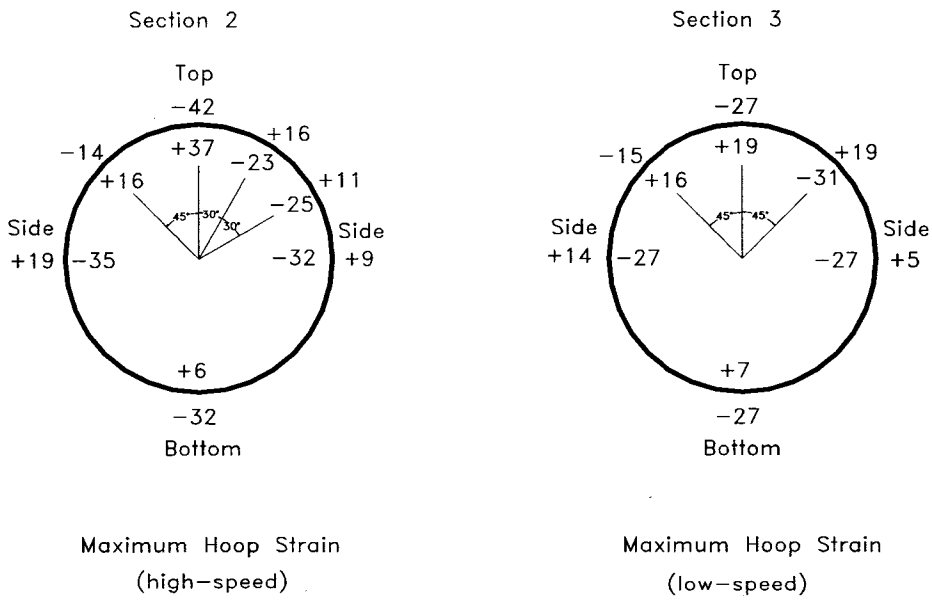

Figure 4.14 Comparison of maximum hoop strains in high-speed and low-speed in winter pressurized test

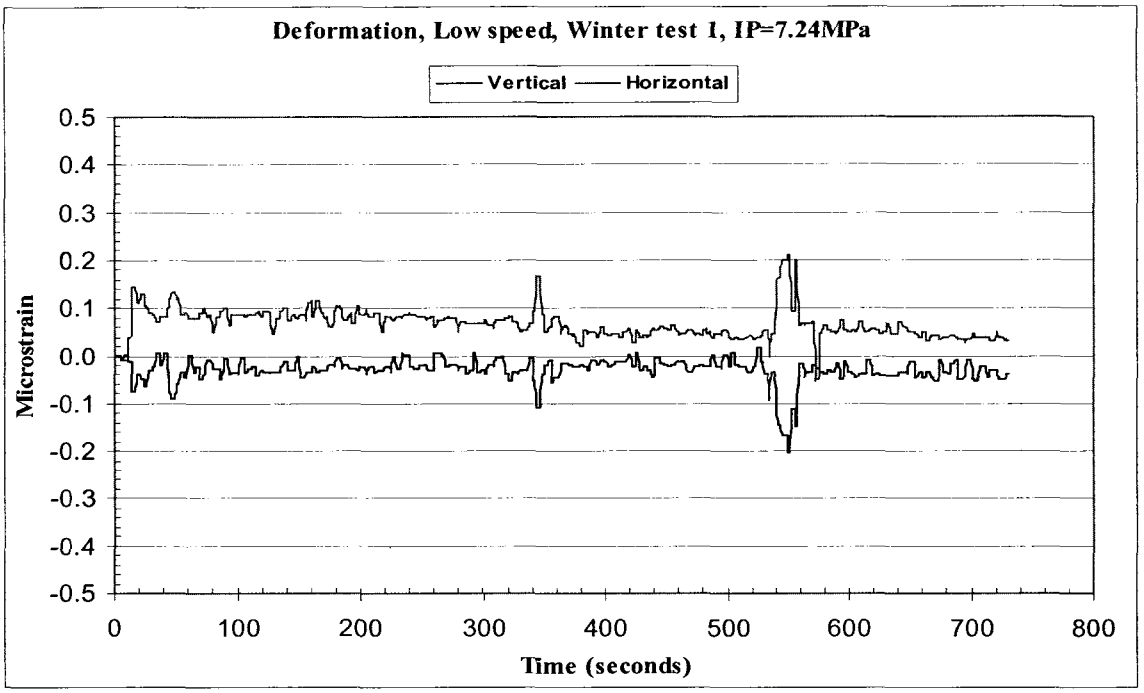

Figure 4.15 Deformation in vertical and horizontal direction at Section 6 (low speed) in winter pressurized test

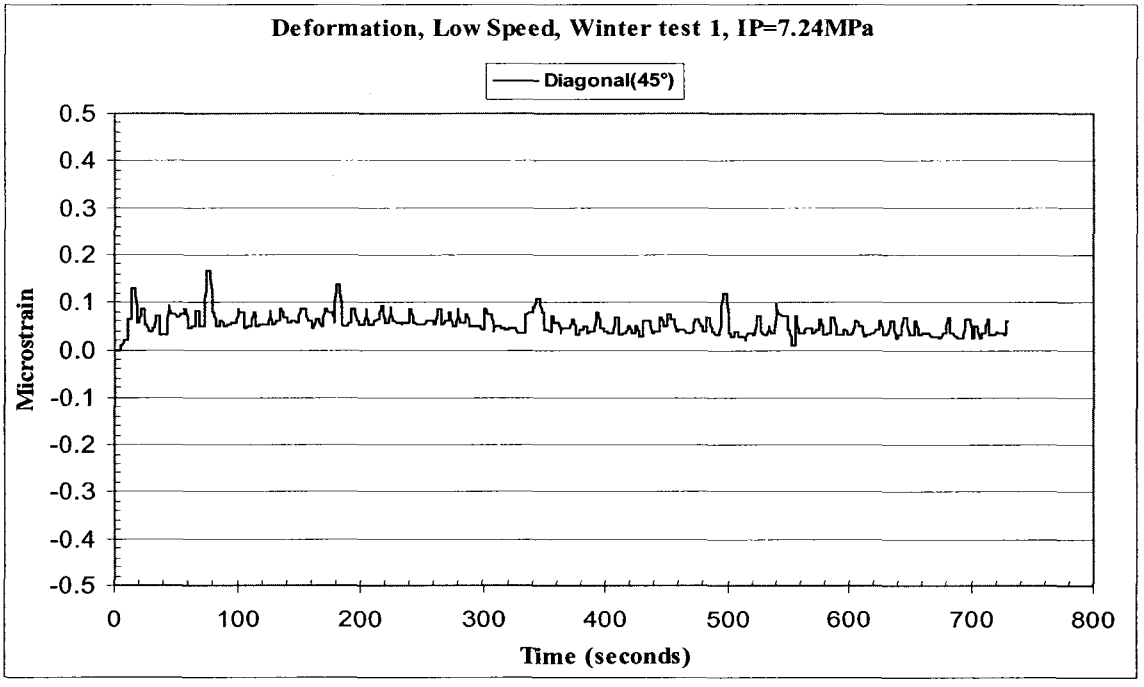

Figure 4.16 Deformation in diagonal direction at Section 6 (low speed) in winter pressurized test

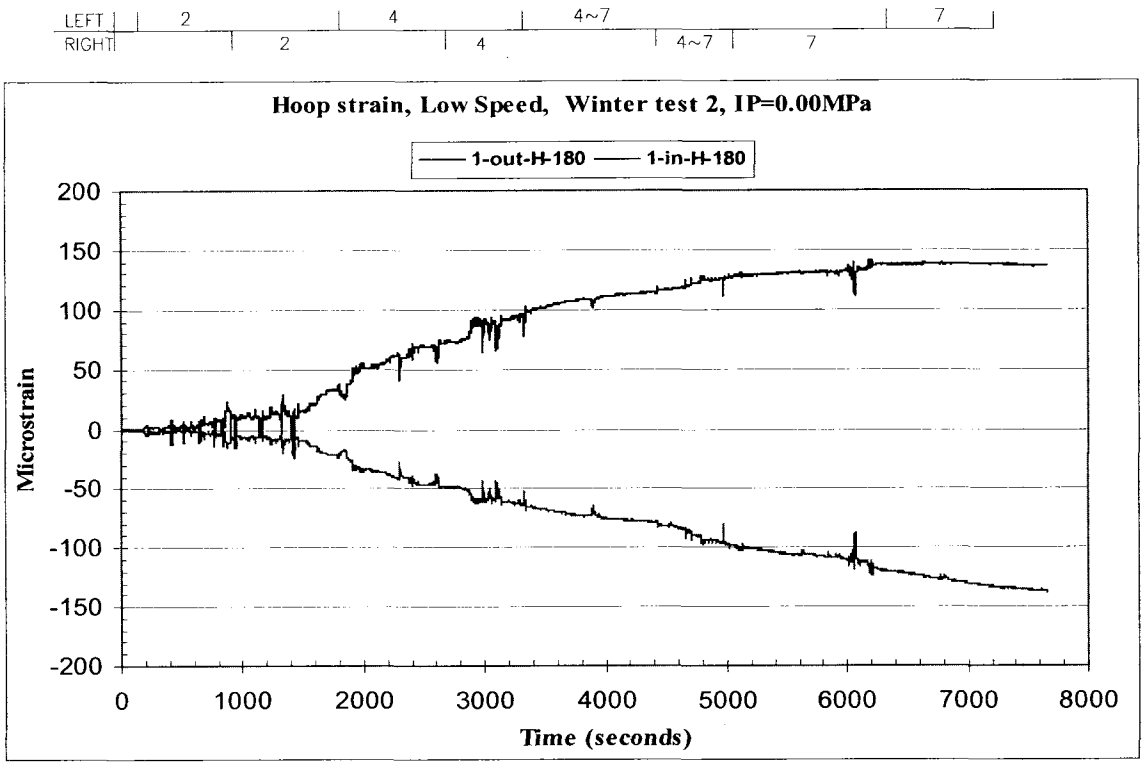

Figure 4.17 Hoop strain at the bottom (180°) of Section 1 in winter un-pressurized test, low speed

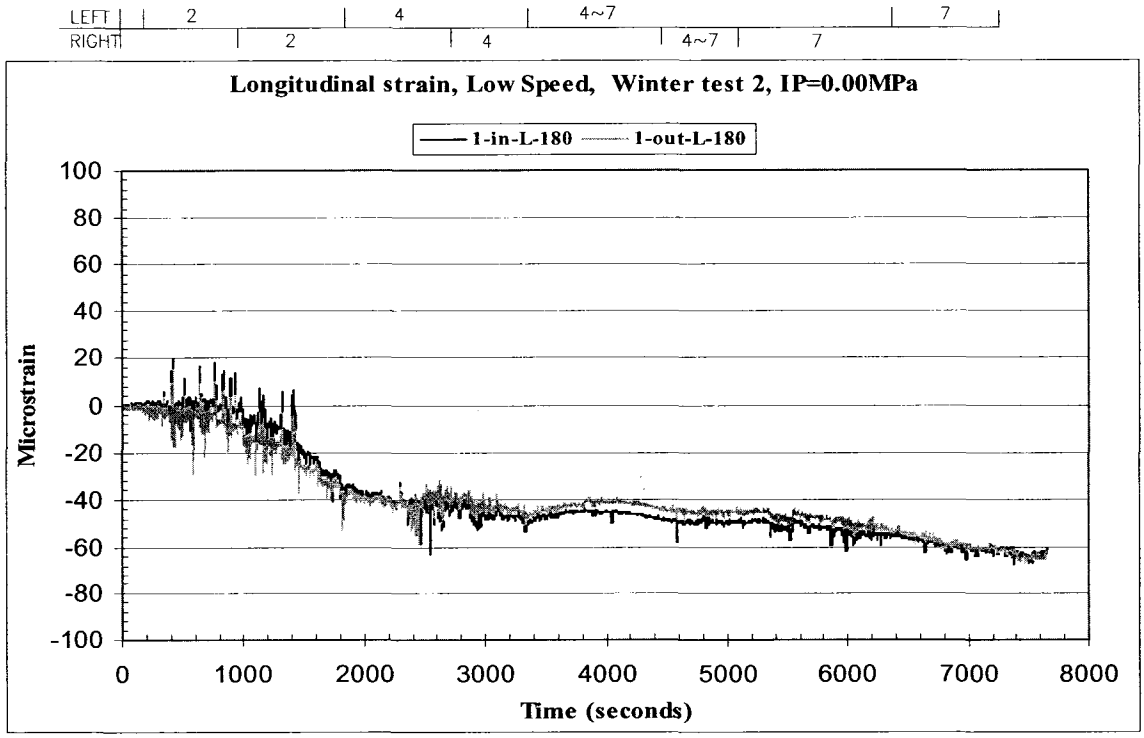

Figure 4.18 Longitudinal strain at bottom (180°) of Section 1 in winter un-pressurized test, low speed

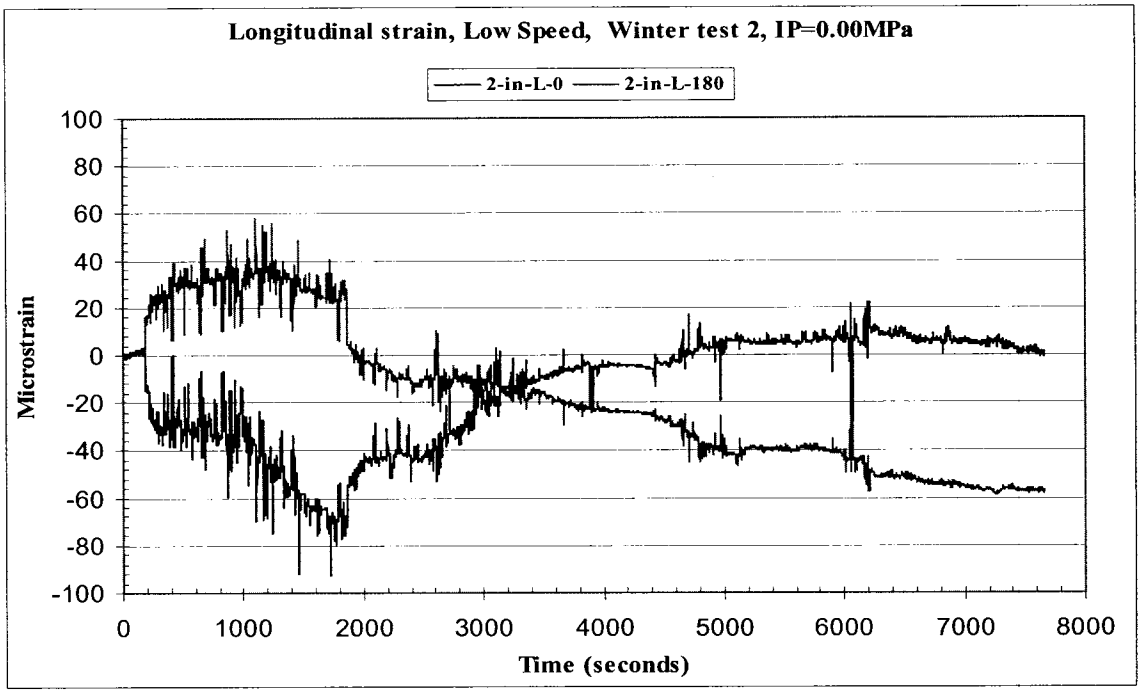

Figure 4.19 Longitudinal strain at the top (0°) and bottom (180°) of Section 2 in winter un-pressurized test, low speed

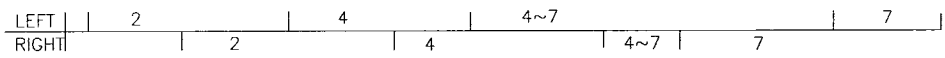

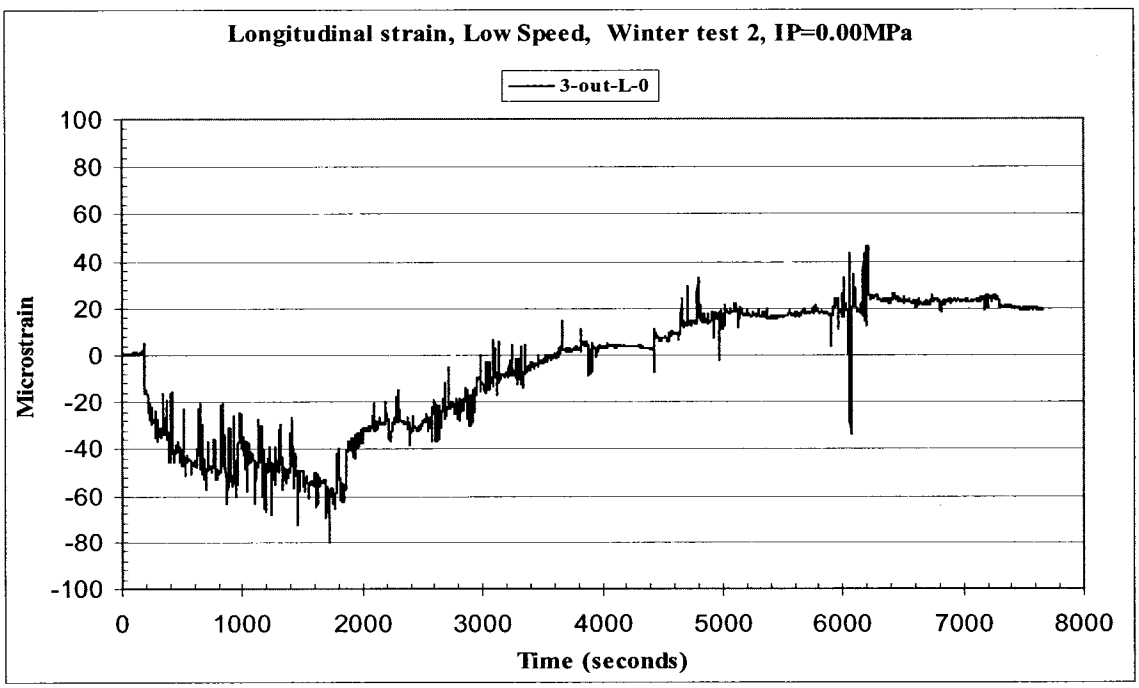

Figure 4.20 Longitudinal strain at bottom (180°) of Section 3 in winter un-pressurized test, low speed

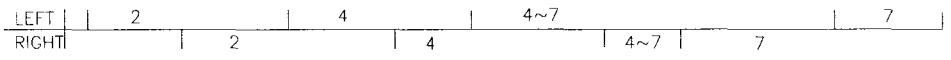

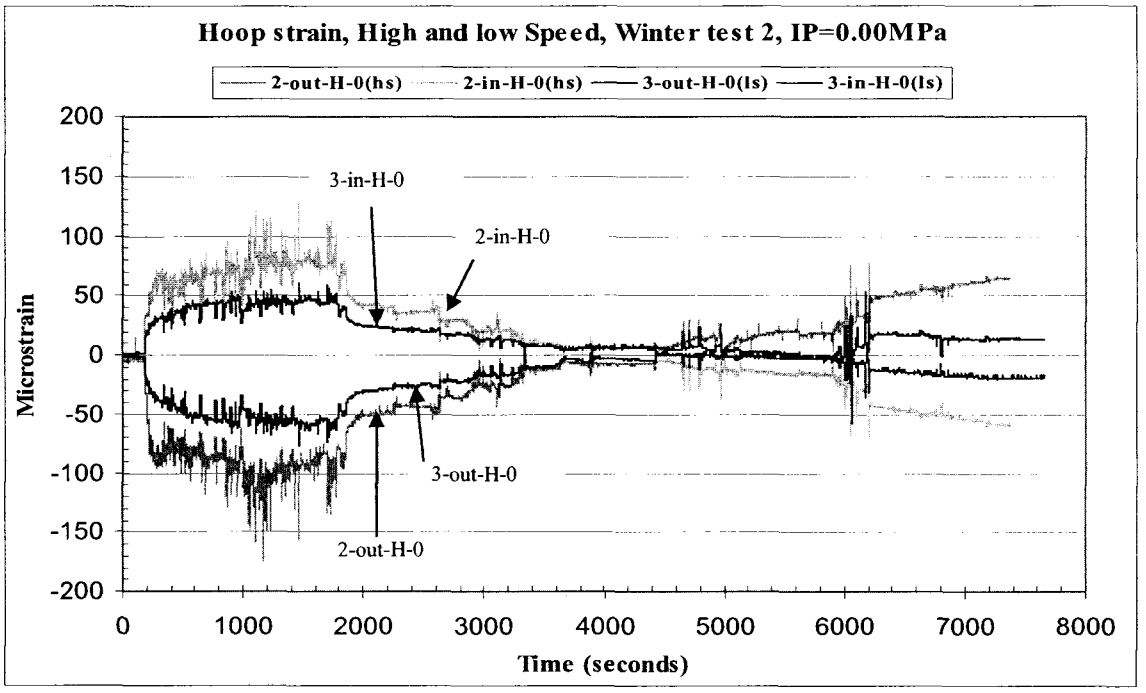

Figure 4.21 Hoop strain at the top (0°) of Section 2 (high speed) and Section 3 (low speed) in winter un-pressurized test

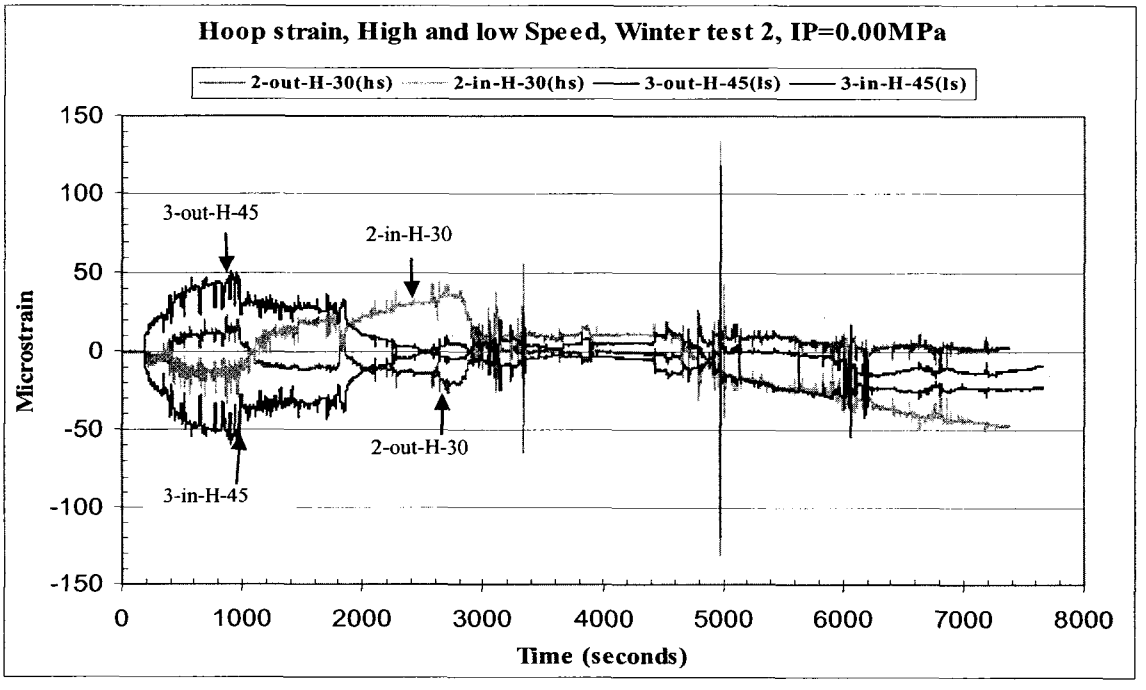

Figure 4.22 Hoop strain at the 30° of Section 2 (high speed) and the 45° of Section 3 (low speed) in winter un-pressurized test

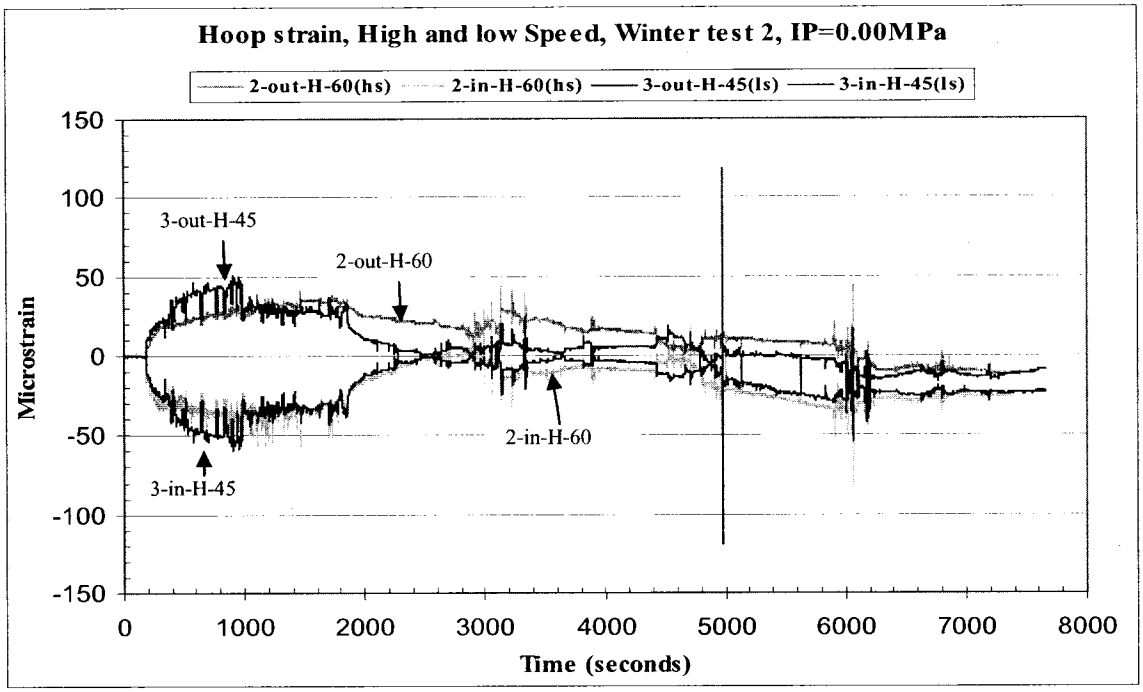

Figure 4.23 Hoop strain at the 60° of Section 2 (high speed) and the 45° of Section 3 (low speed) in winter un-pressurized test

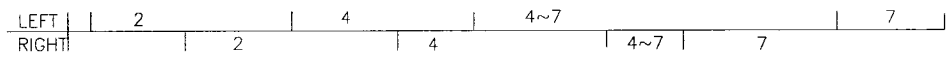

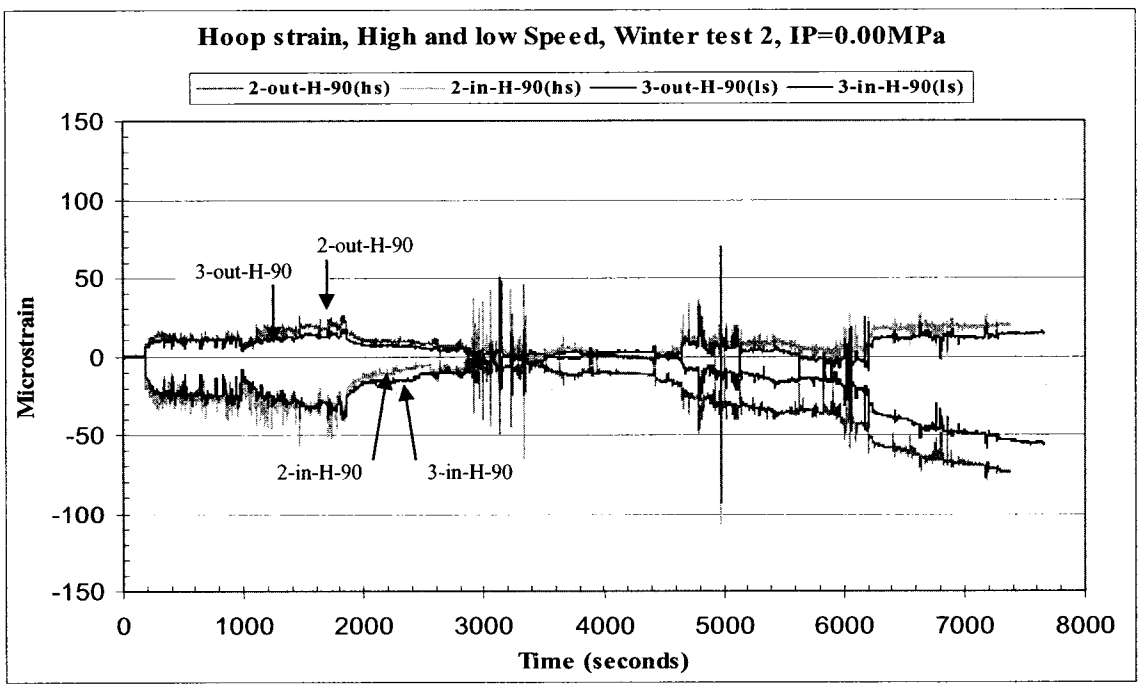

Figure 4.24 Hoop strain at the right side (90°) of Section 2 (high speed) and Section 3 (low speed) in winter un-pressurized test

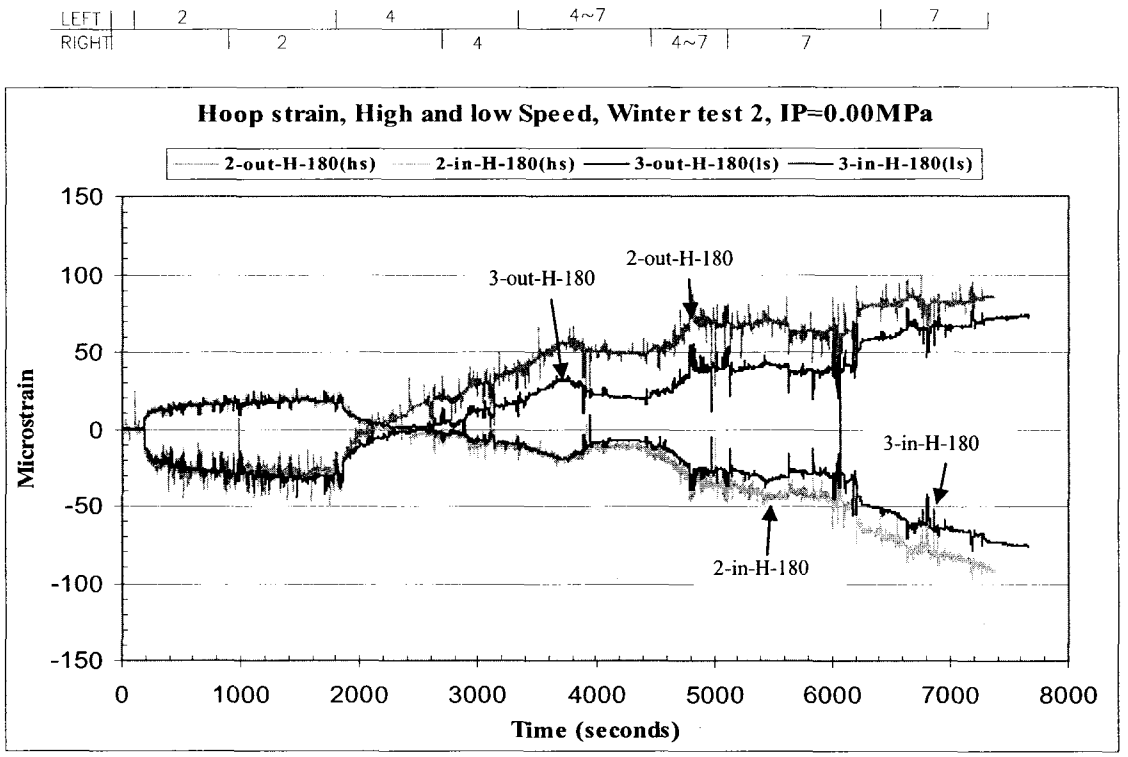

Figure 4.25 Hoop strain at the bottom (180°) of Section 2 (high speed) and Section 3 (low speed) in winter un-pressurized test

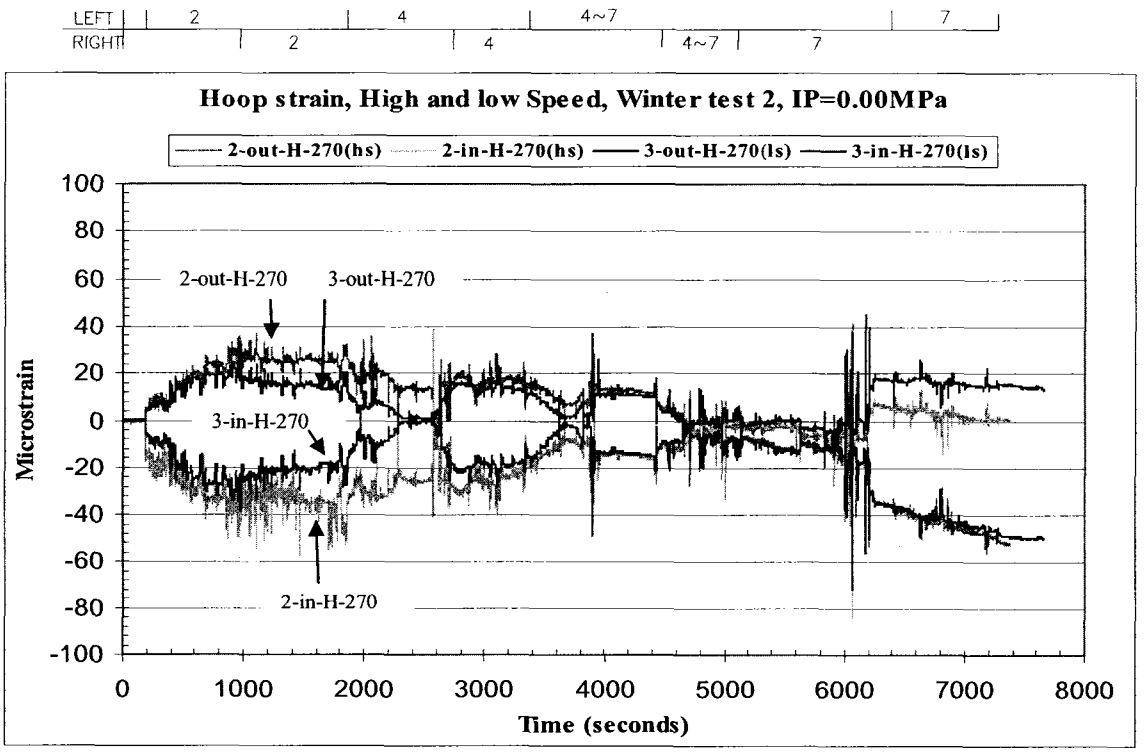

Figure 4.26 Hoop strain at the left side (270°) of Section 2 (high speed) and Section 3 (low speed) in winter un-pressurized test

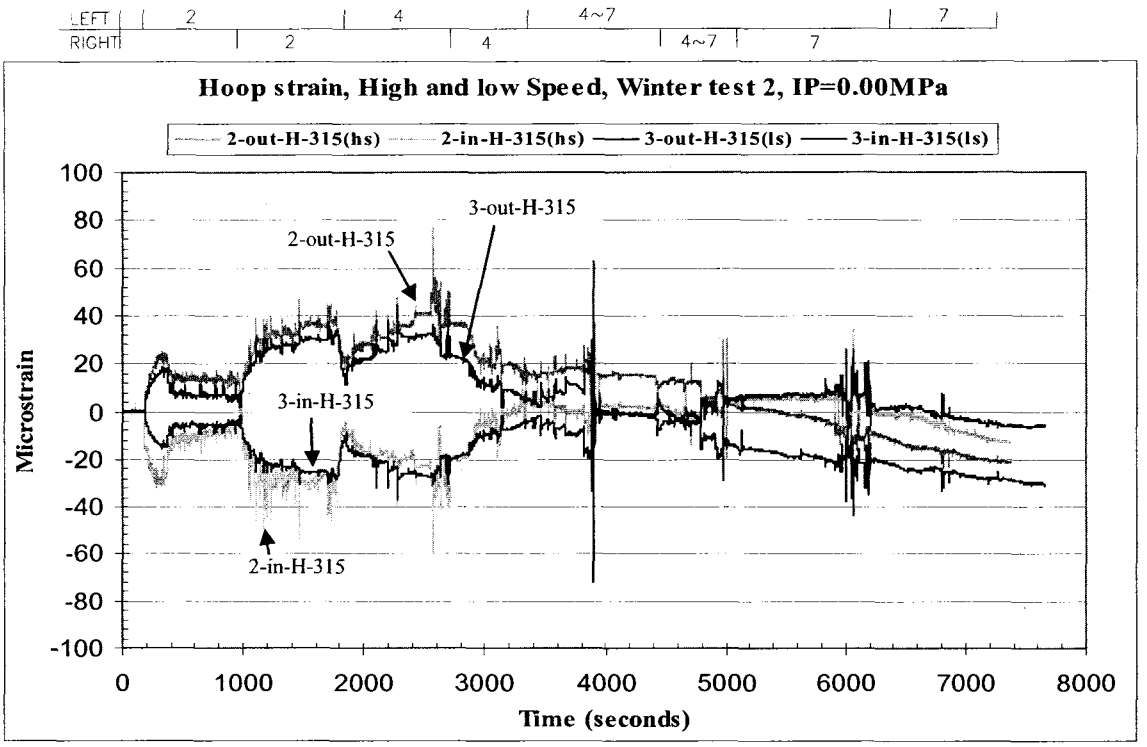

Figure 4.27 Hoop strain at the 315° of Section 2 (high speed) and Section 3 (low speed) in winter un-pressurized test

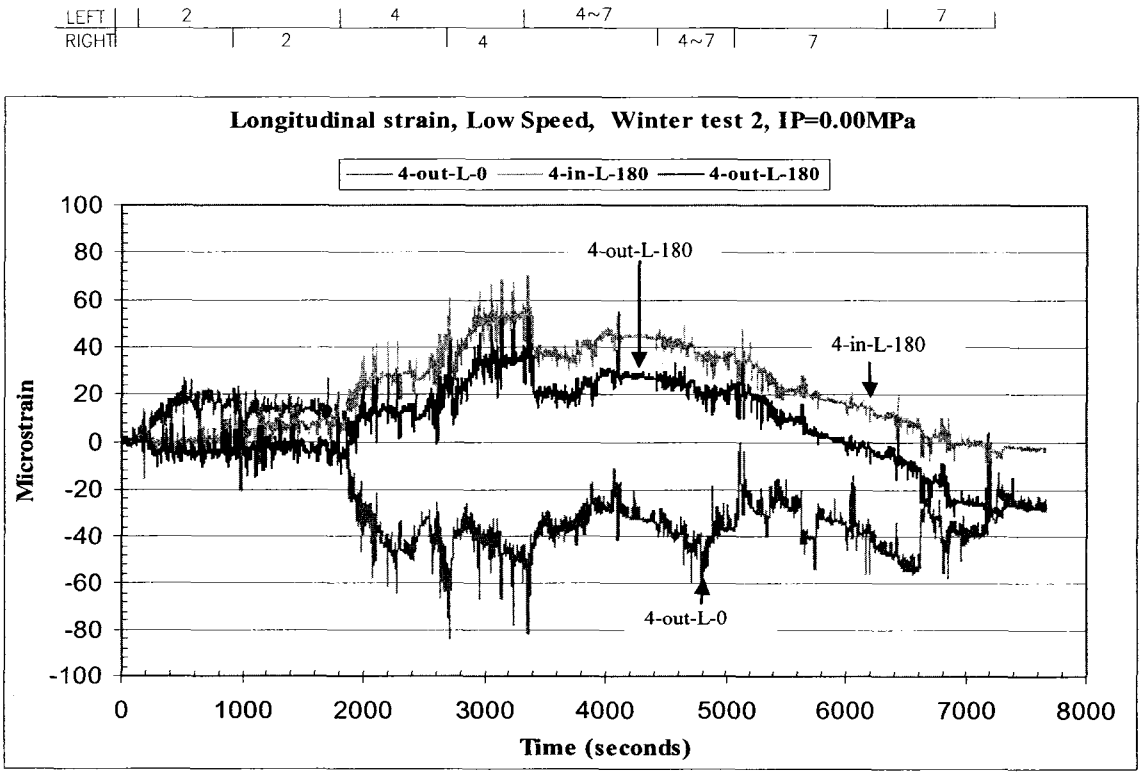

Figure 4.28 Longitudinal strain at the top (0°) and bottom (180°) of Section 4 in winter un-pressurized test, low speed

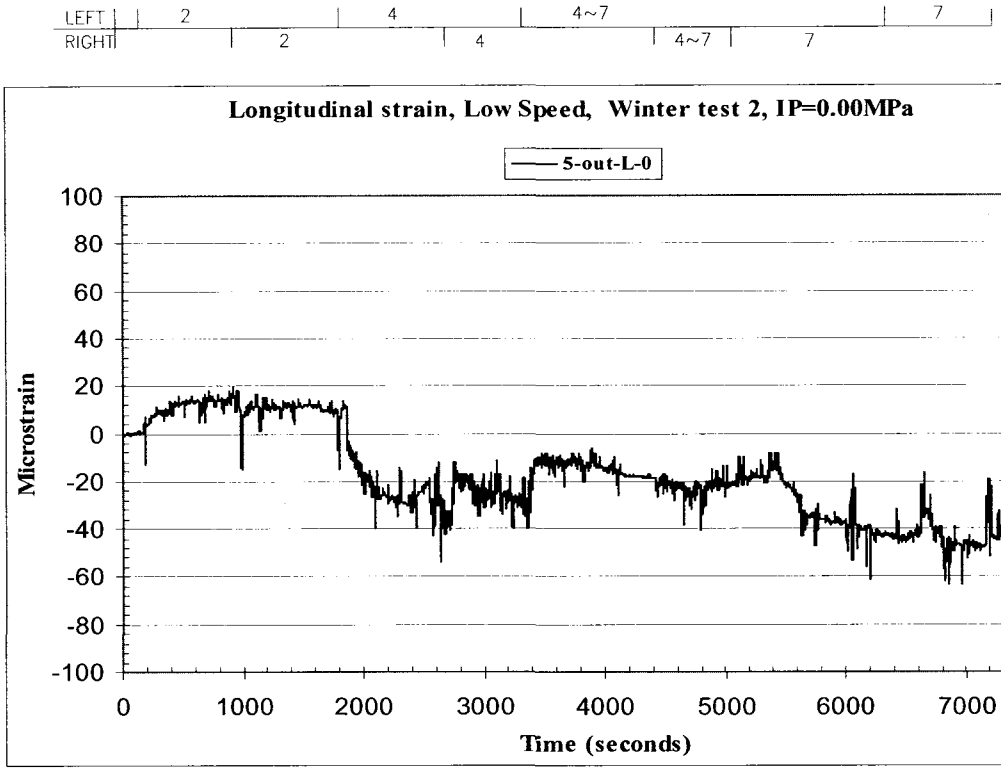

Figure 4.29 Longitudinal strain at the top (0°) of Section 5 in winter un-pressurized test, low speed

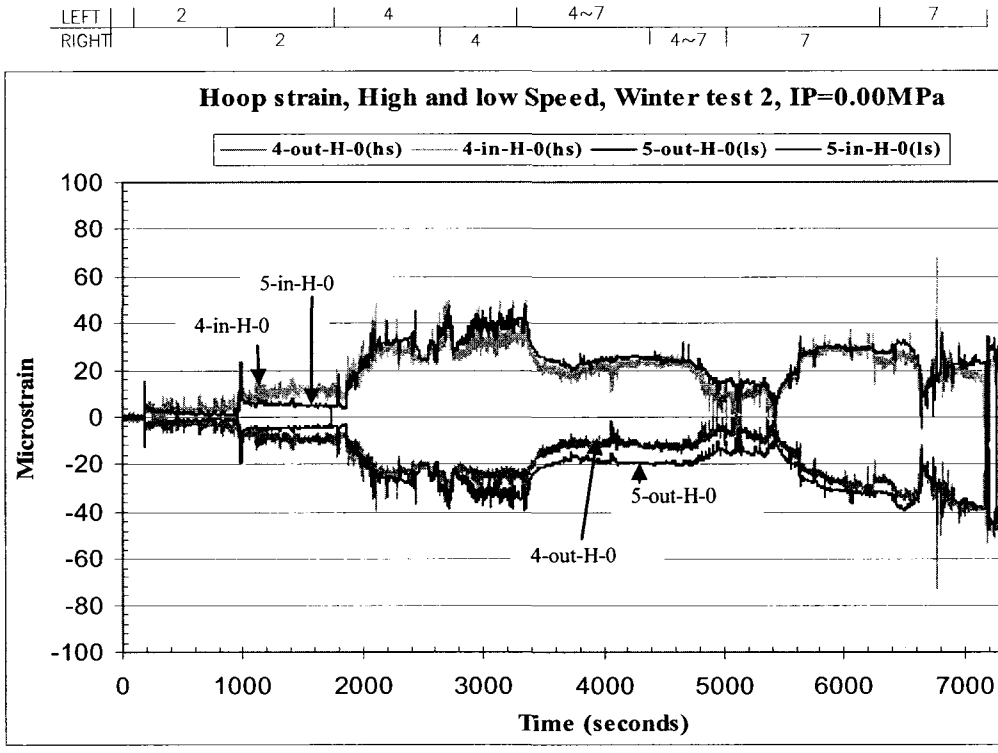

Figure 4.30 Hoop strain at the top (0°) of Section 4 (high speed) and Section 5 (low speed) in winter un-pressurized test

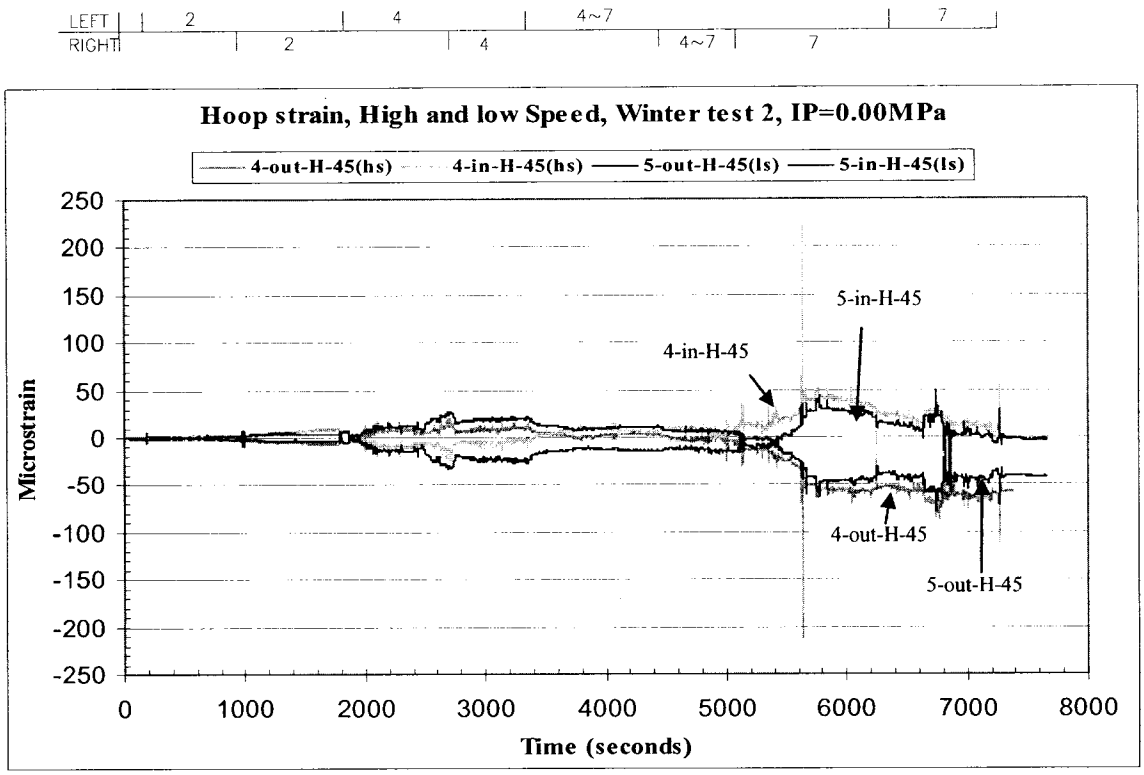

Figure 4.31 Hoop strain at the 45° of Section 4 (high speed) and Section 5 (low speed) in winter un-pressurized test

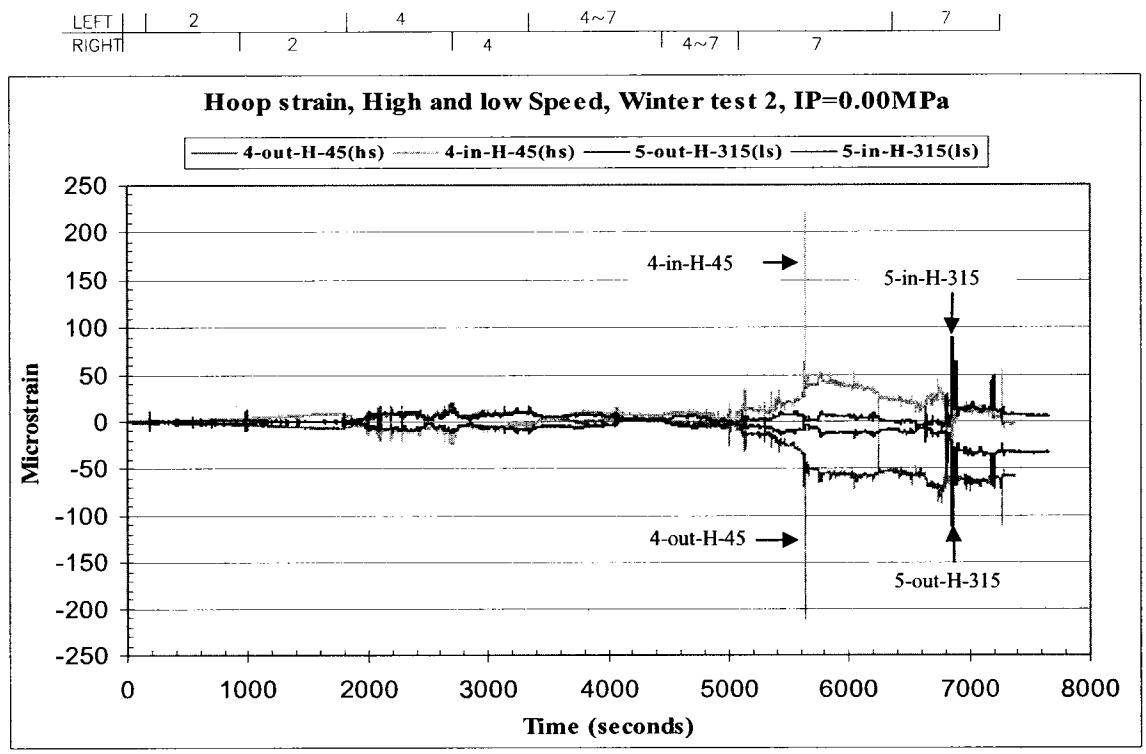

Figure 4.32 Hoop strain at the 45° of Section 4 (high speed) and the 315° of Section 5 (low speed) in winter un-pressurized test

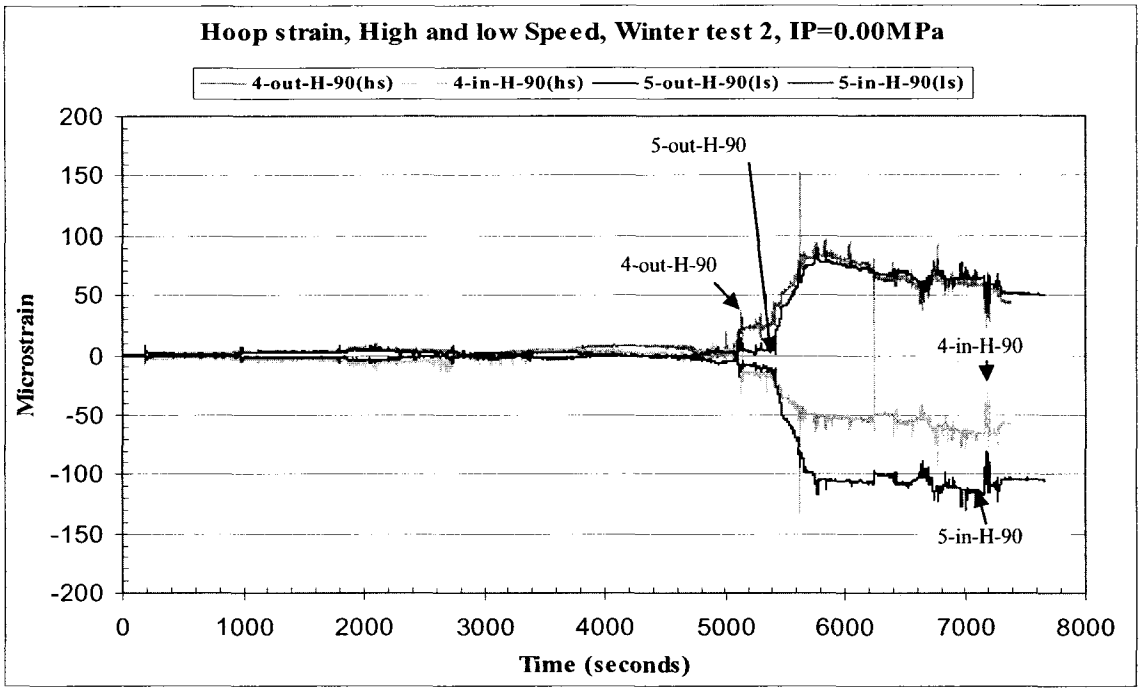

Figure 4.33 Hoop strain at the right side (90°) of Section 4 (high speed) and Section 5 (low speed) in winter un-pressurized test

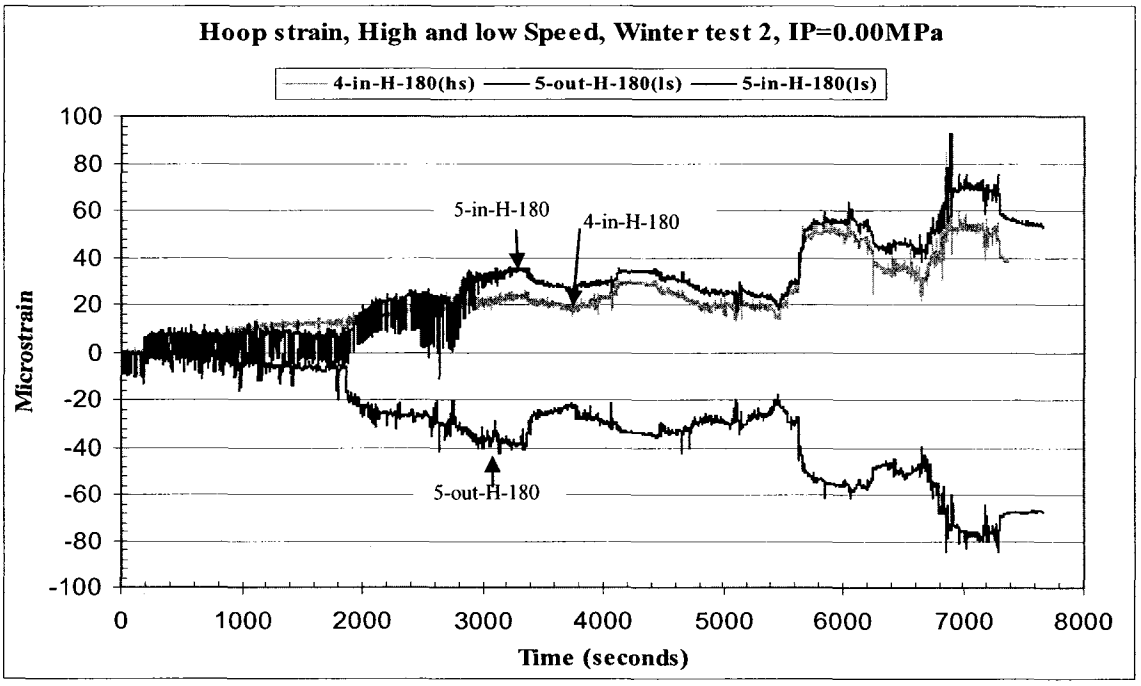

Figure 4.34 Hoop strain at the bottom (180°) of Section 4 (high speed) and Section 5 (low speed) in winter un-pressurized test

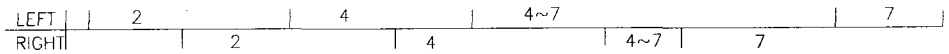

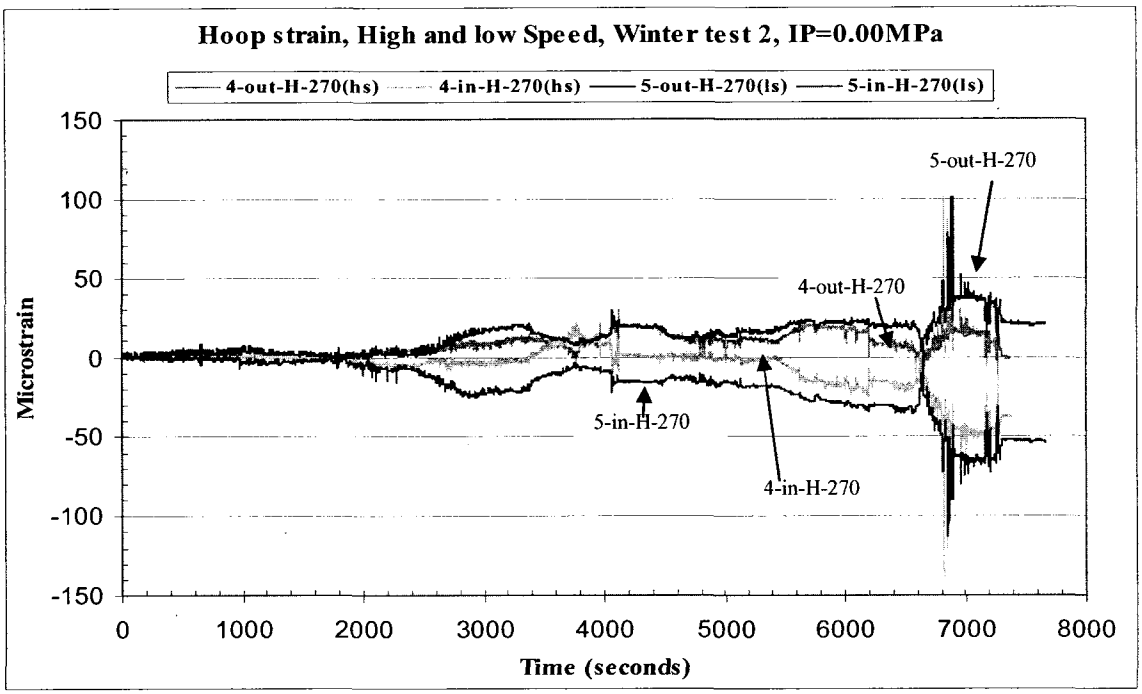

Figure 4.35 Hoop strain at the left side (270°) of Section 4 (high speed) and Section 5 (low speed) in winter un-pressurized test

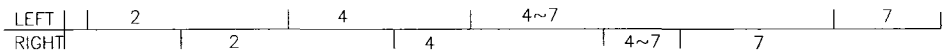

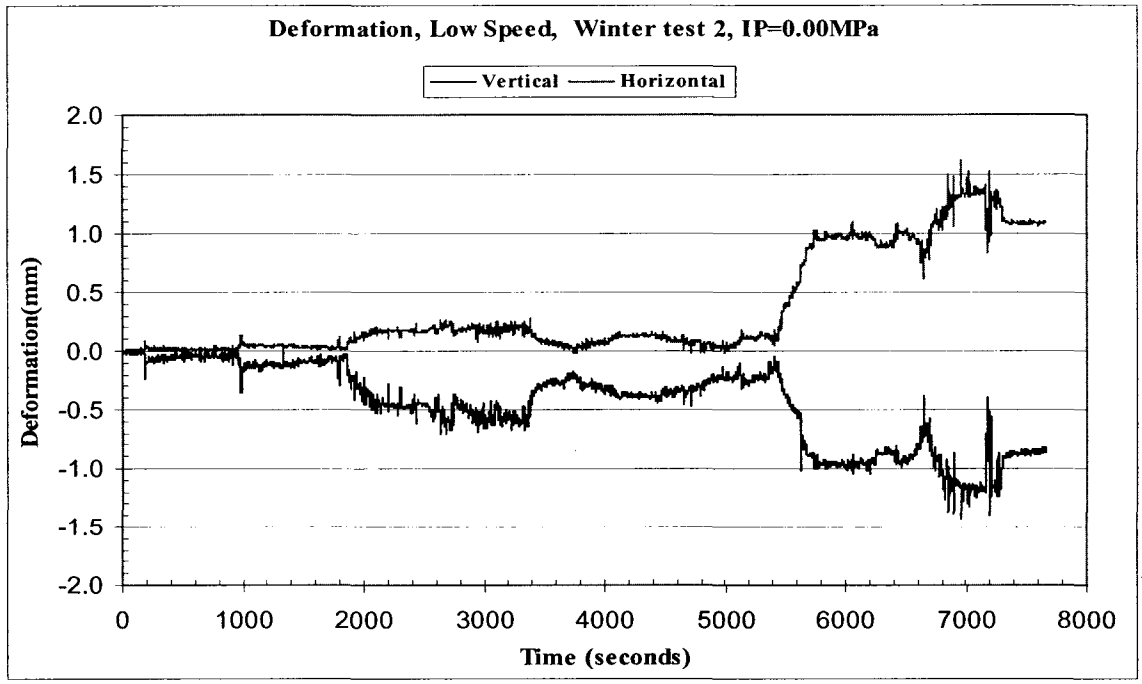

Figure 4.36 Deformation in vertical and horizontal direction at Section 6 (low speed) in winter un-pressurized test

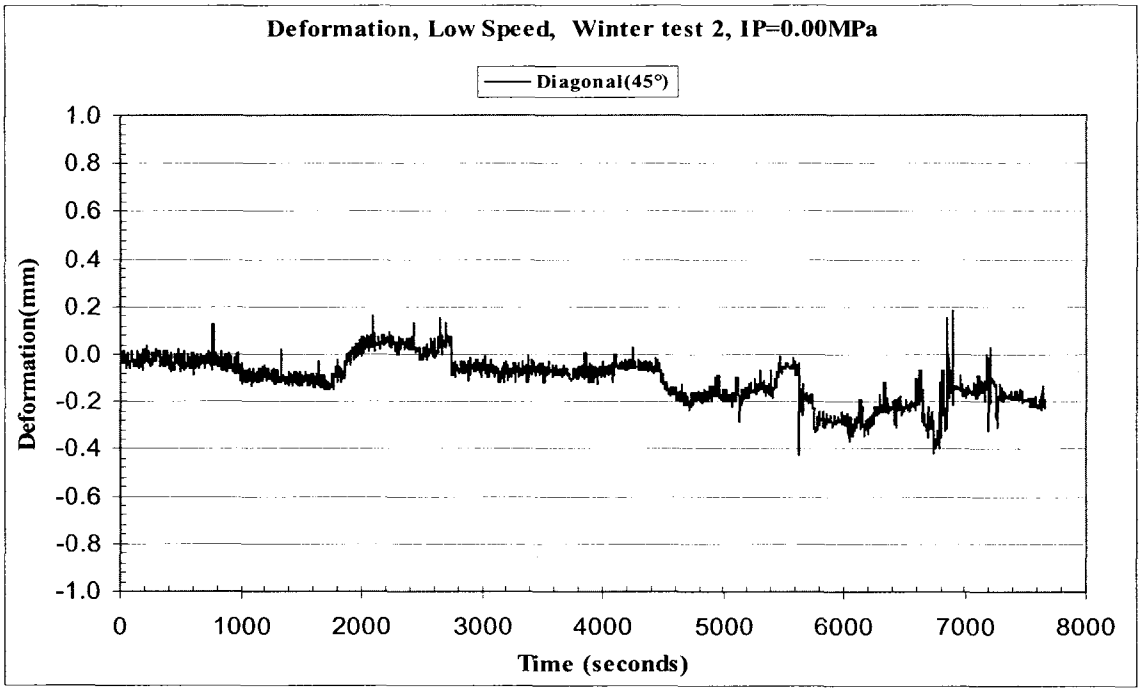

Figure 4.37 Deformation in diagonal direction at Section 6 (low speed) in winter un-pressurized test

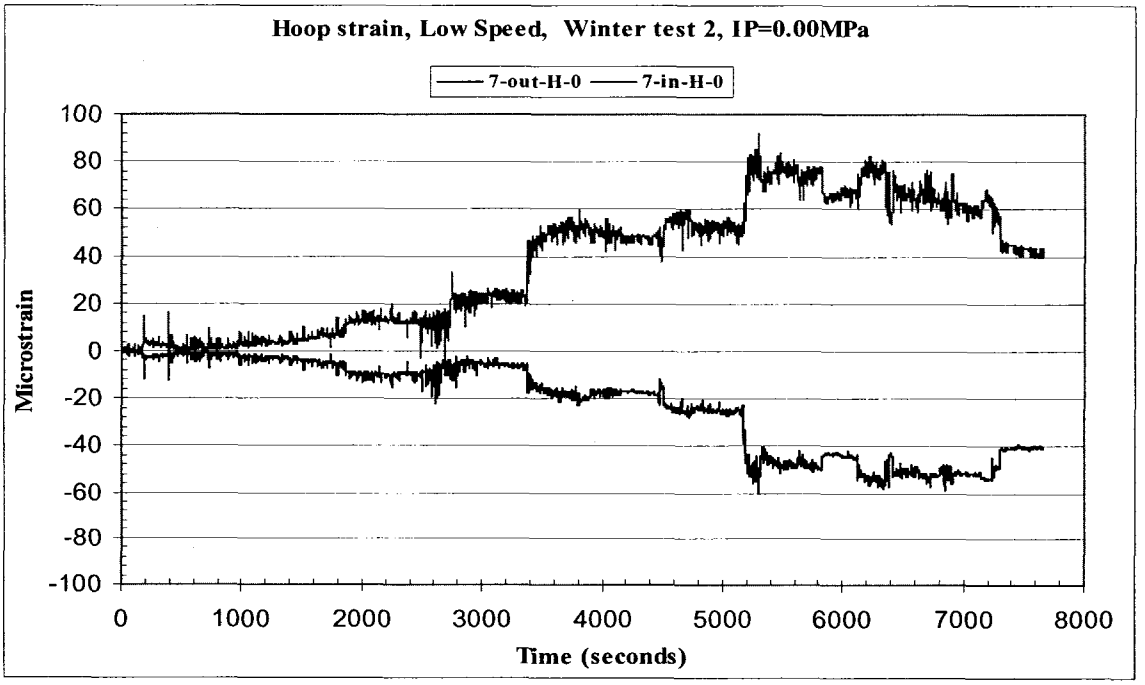

Figure 4.38 Hoop strain at the top (0°) of Section 7 in winter un-pressurized test, low speed

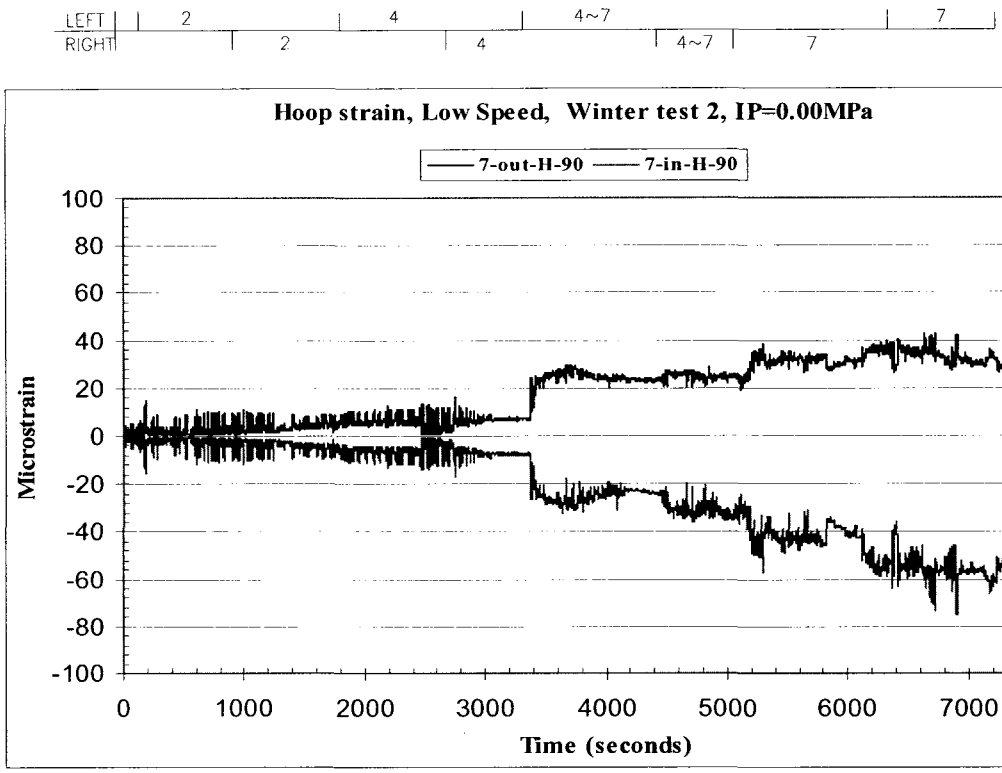

Figure 4.39 Hoop strain at the right side (90°) of Section 7 in winter un-pressurized test, low speed

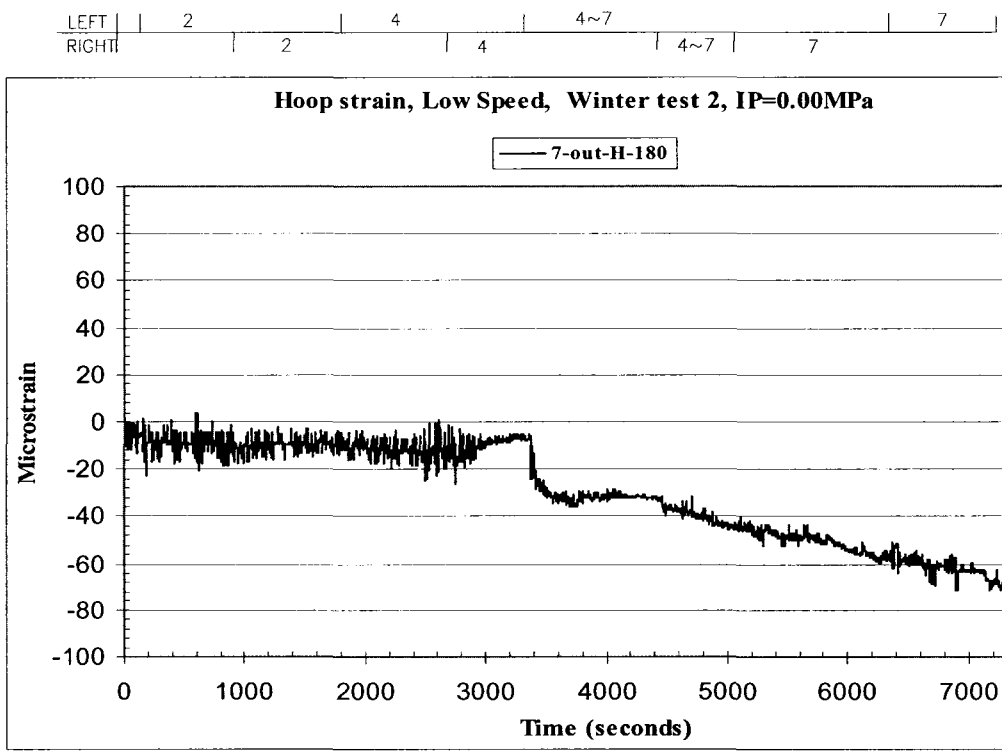

Figure 4.40 Hoop strain at the bottom (180°) of Section 7 in winter un-pressurized test, low speed

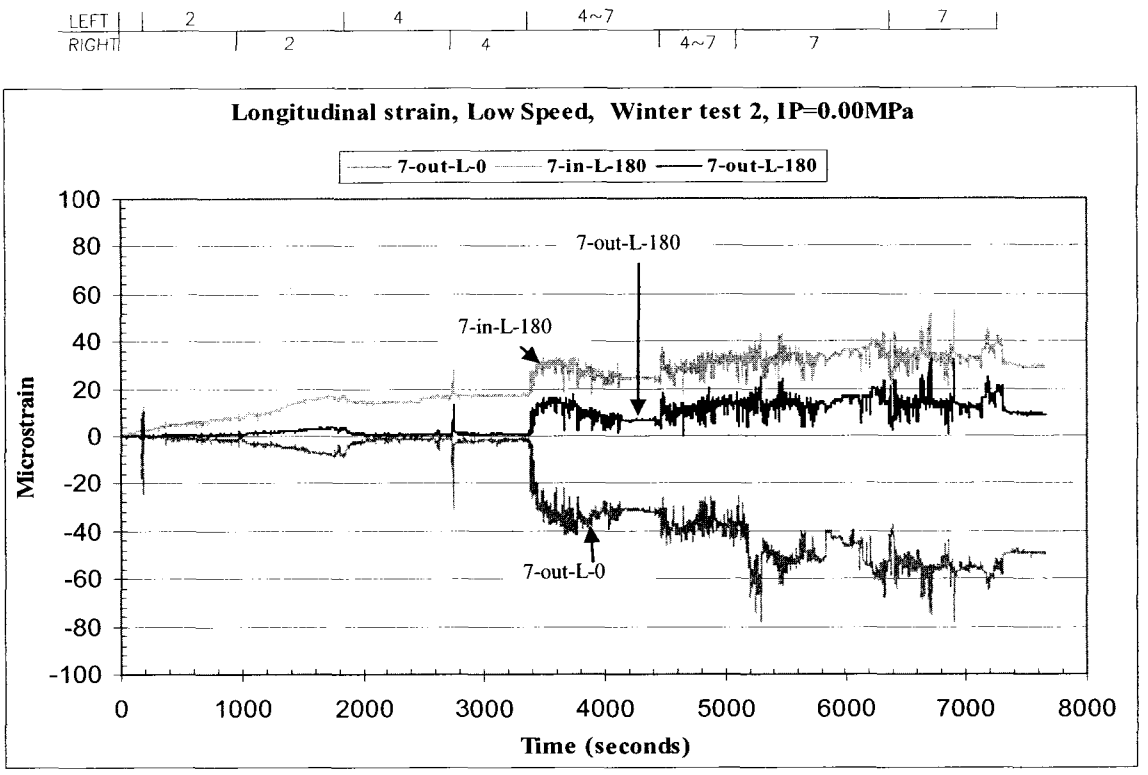

Figure 4.41 Longitudinal strain at the top (0°) and bottom (180°) of Section 7 in winter un-pressurized test, low speed

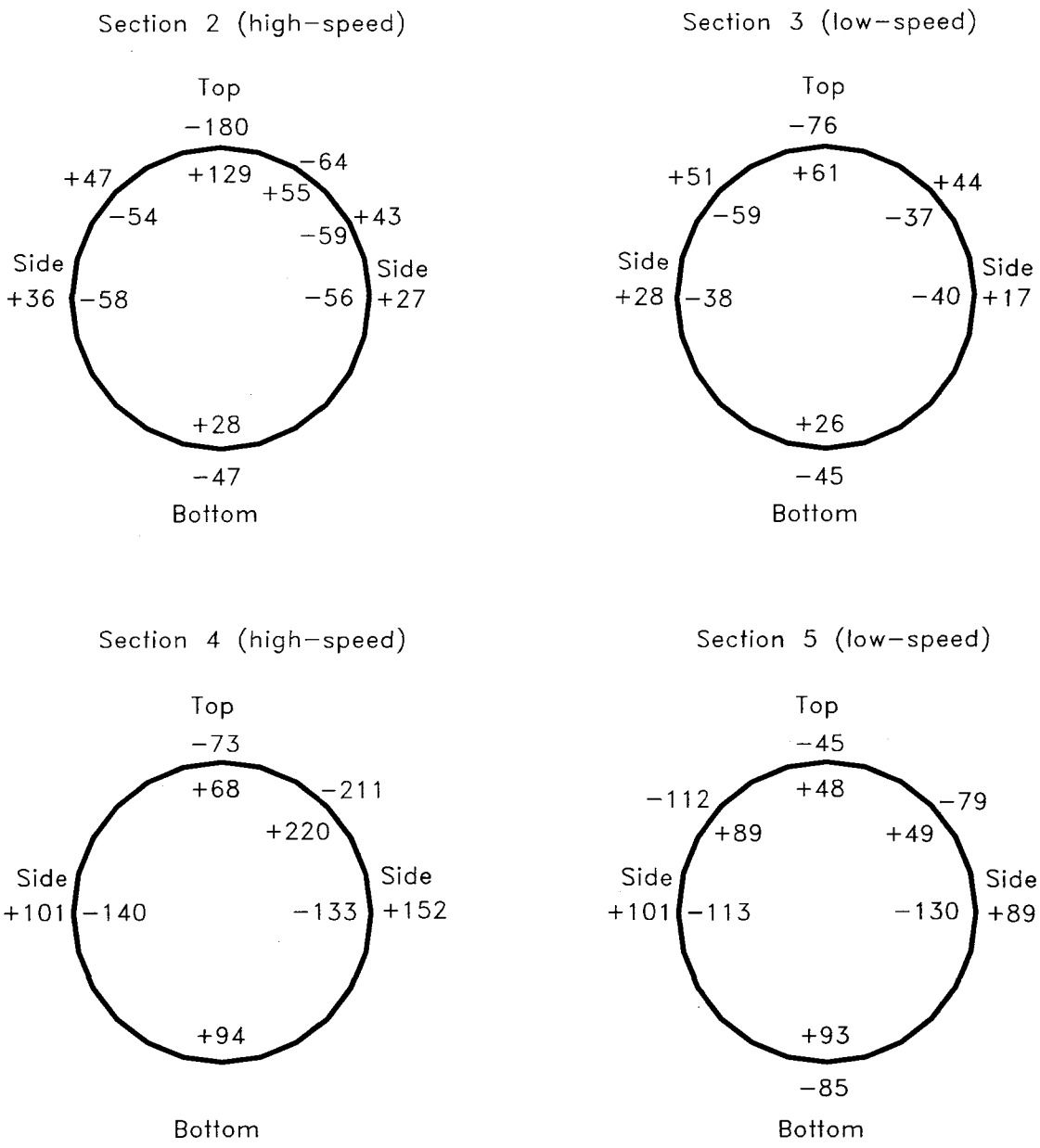

Figure 4.42 Comparison of maximum hoop strain in high speed and low speed in winter un-pressurized test at buried state

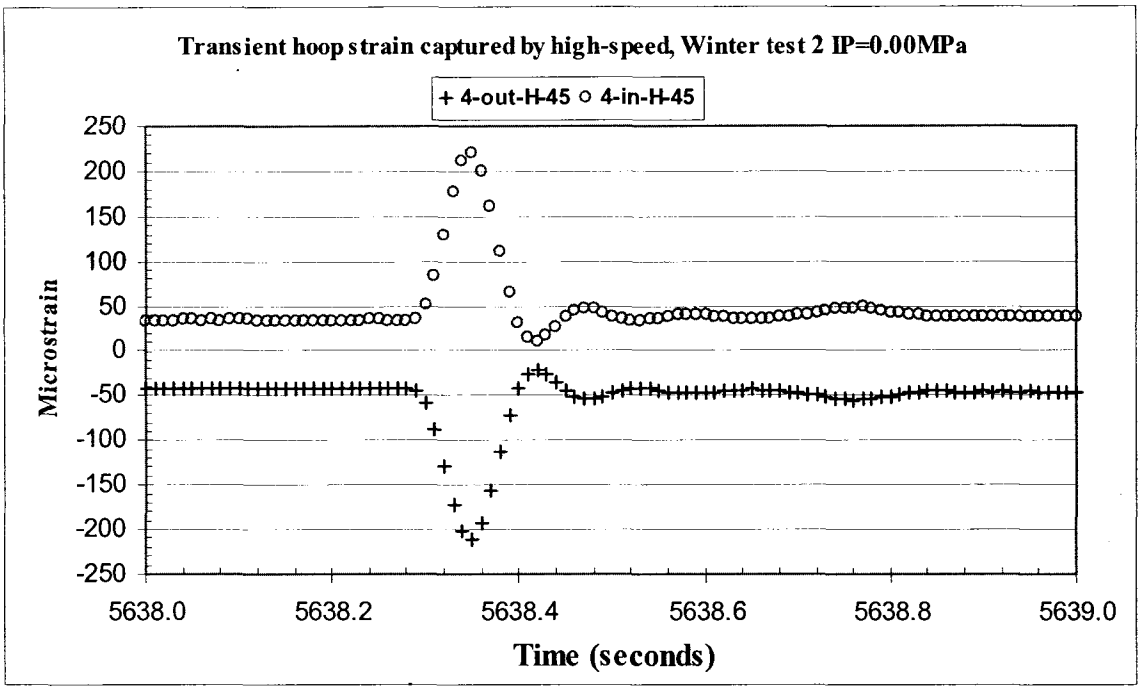

Figure 4.43 Transient hoop strain at 45° position of Section 4 at second of 5638 captured by high speed DAS in winter un-pressurized test

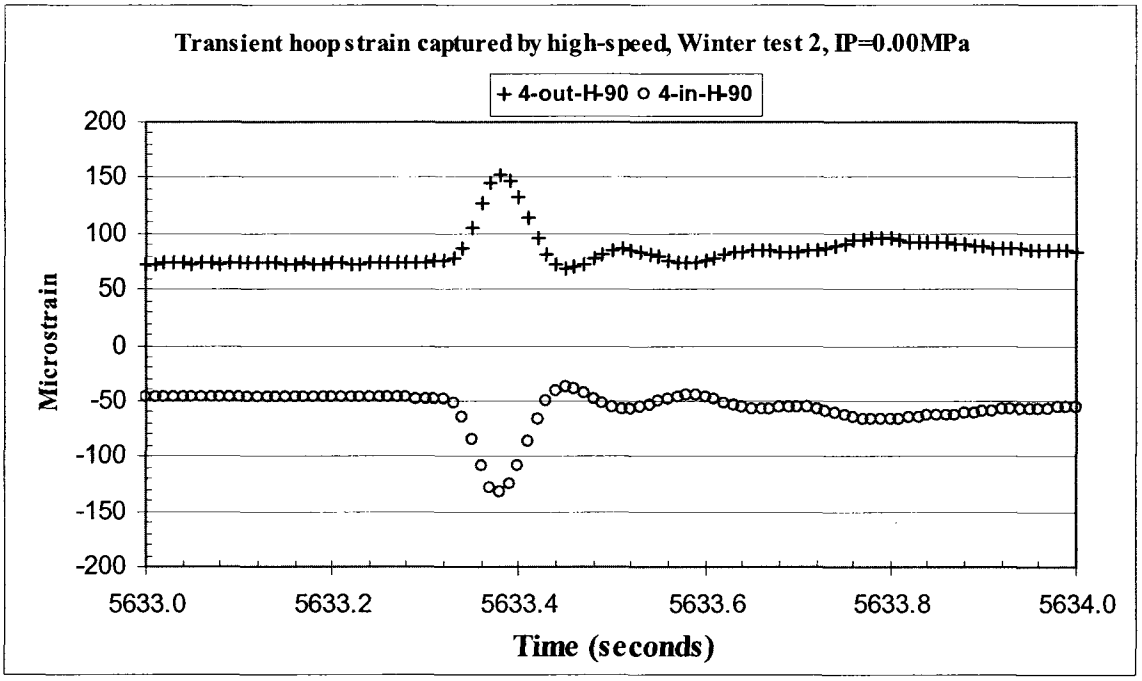

Figure 4.44 Transient hoop strain at right side of Section 4 (90°) at second of 5633 captured by high speed DAS in winter un-pressurized test

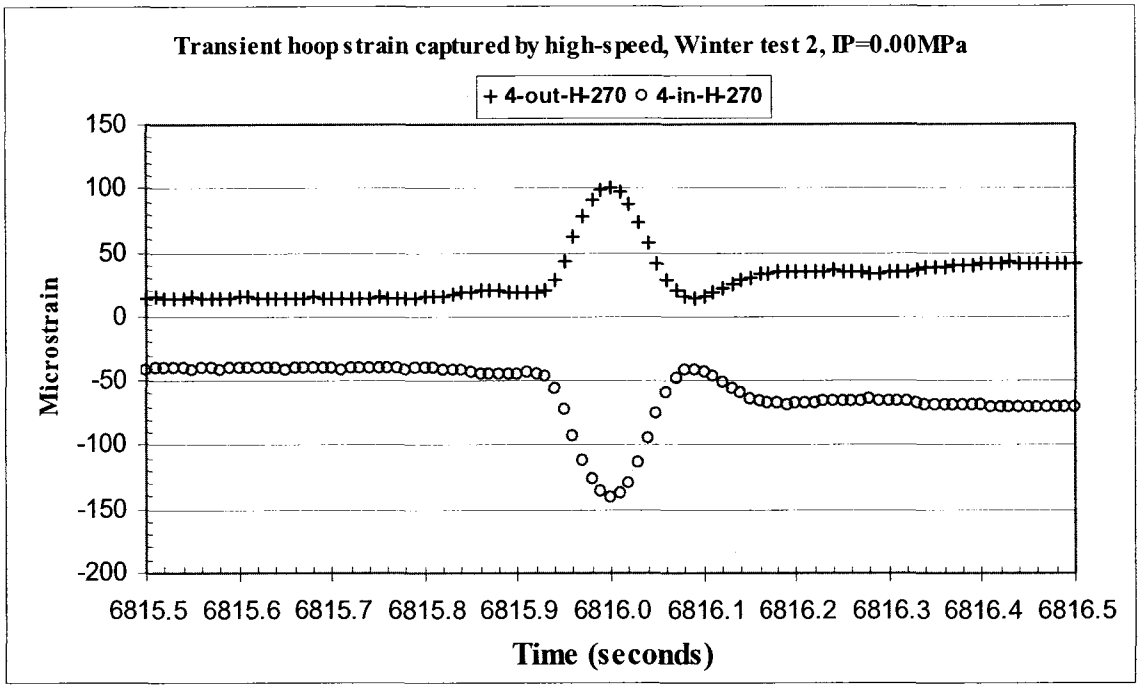

Figure 4.45 Transient hoop strain at left side of Section 4 (270°) at second of 6816 captured by high speed DAS in winter un-pressurized test

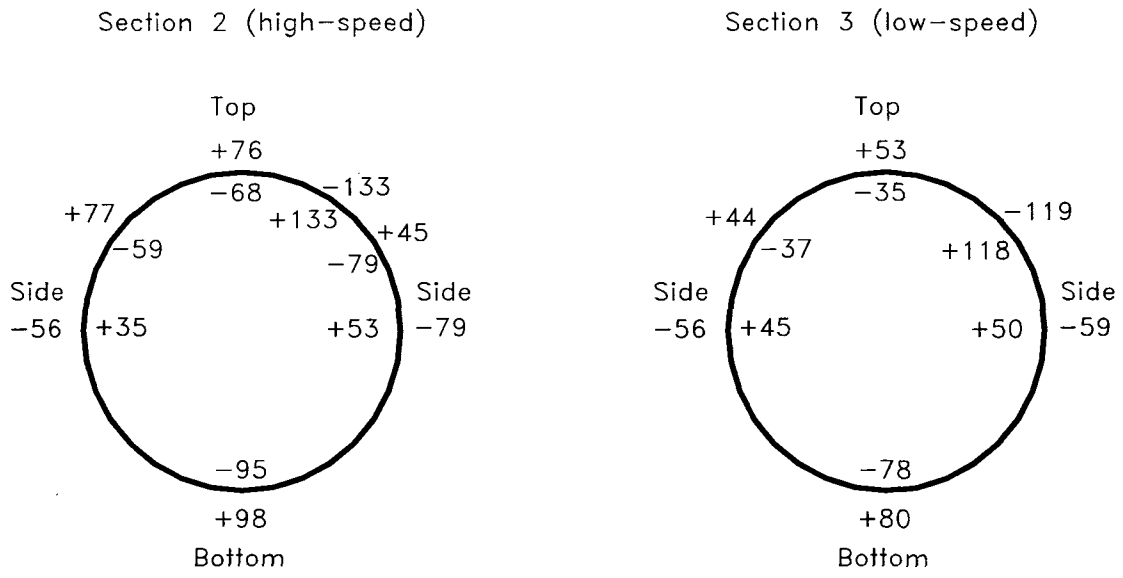

Comparison of high-speed and low-speed maximum hoop strain

(exposed state)

Figure 4.46 Comparison of maximum hoop strain in high speed and low speed in winter un-pressurized test at exposed state

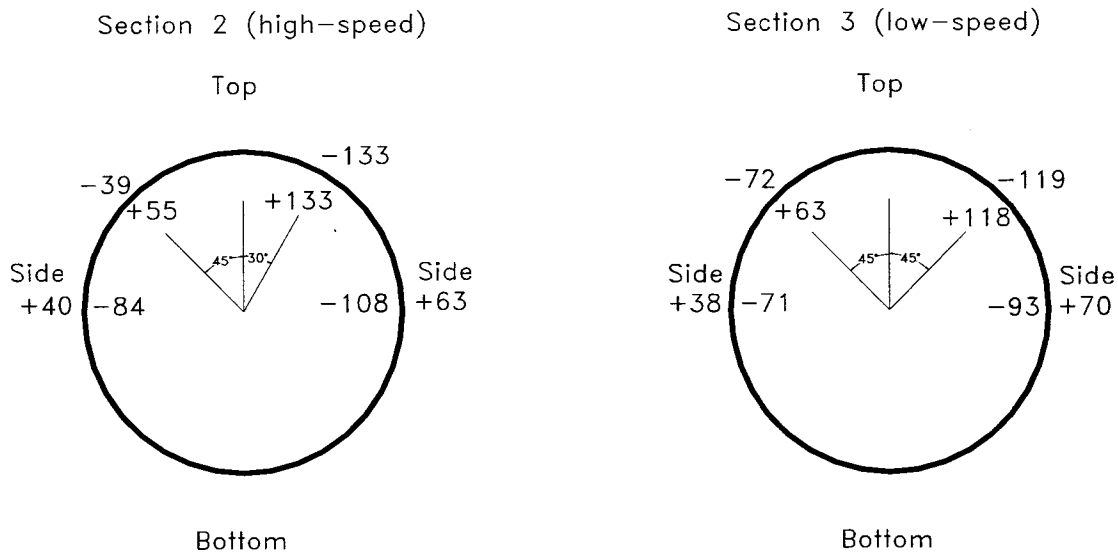

Figure 4.47 Comparison of hoop strain reversal captured by high speed and low speed DAS in winter un-pressurized test

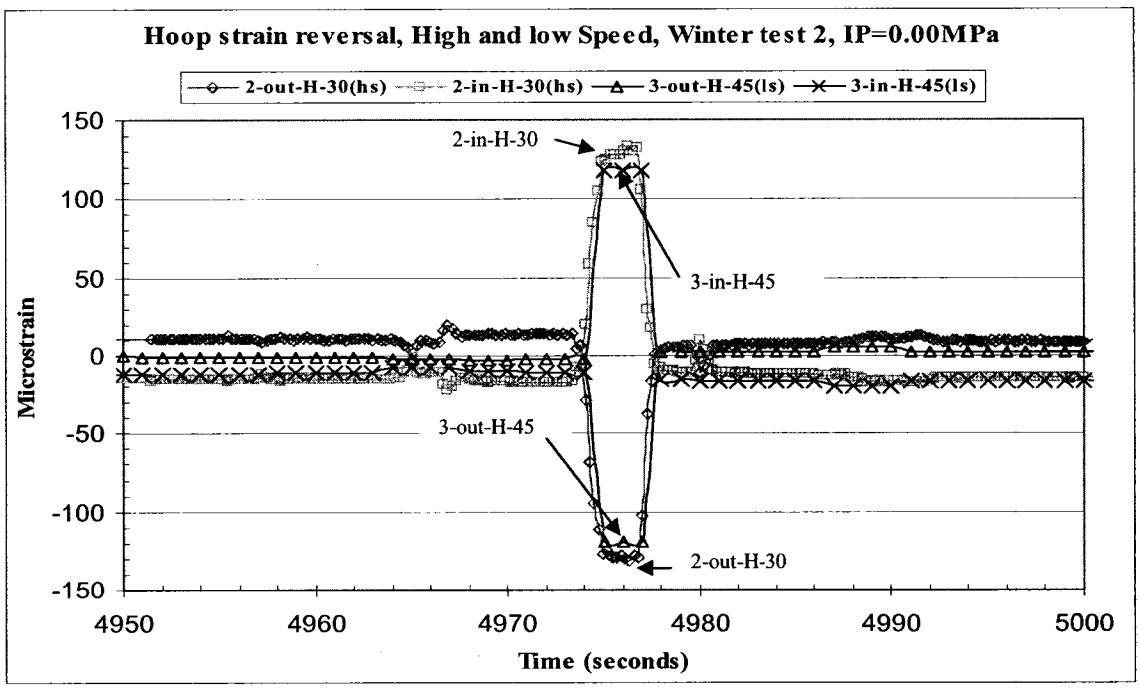

Figure 4.48 Hoop strain reversal at 30° of Section 2 and 45° of Section 3 at second of 4976 in high speed and low speed in winter un-pressurized test

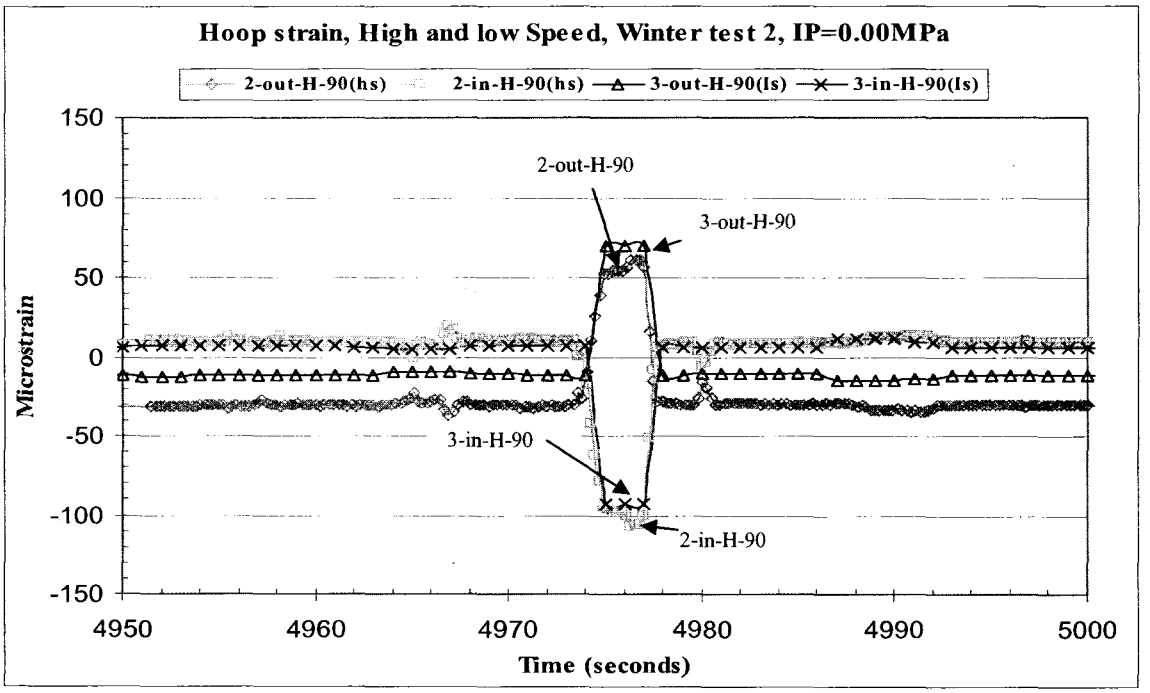

Figure 4.49 Hoop strain reversal at right side (90°) of Section 2 and Section 3 at second of 4976in high speed and low speed in winter un-pressurized test

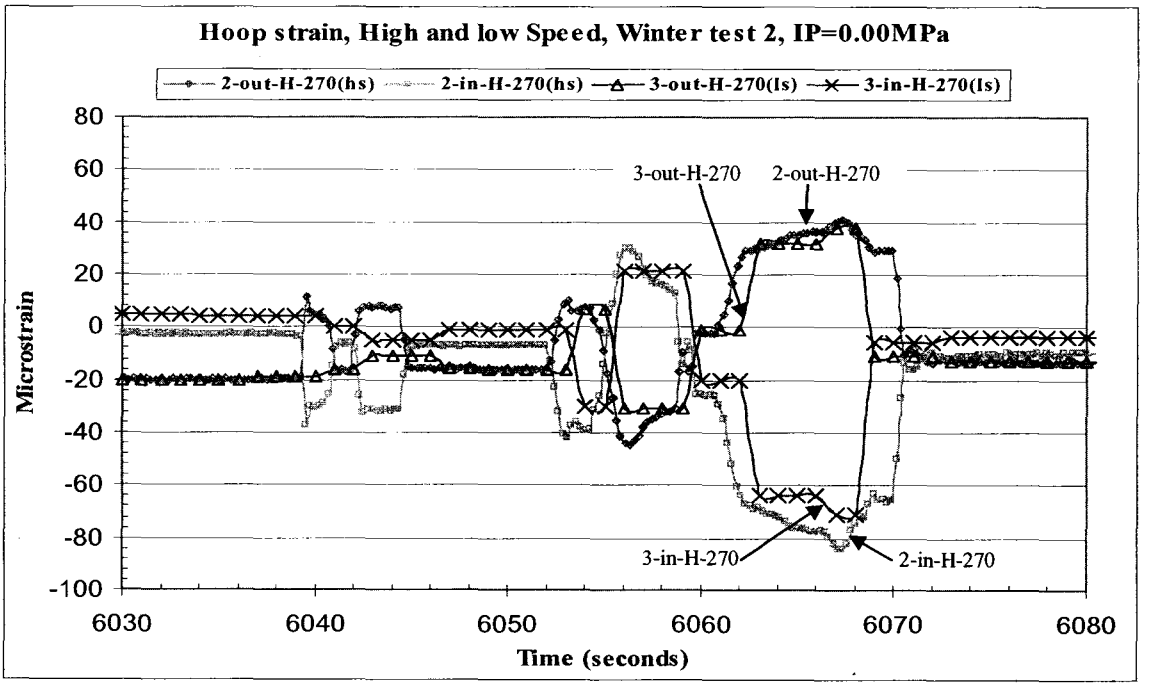

Figure 4.50 Hoop strain reversal at left side (270°) of Section 2 and Section 3 at second of 6067 in high speed and low speed in winter un-pressurized test

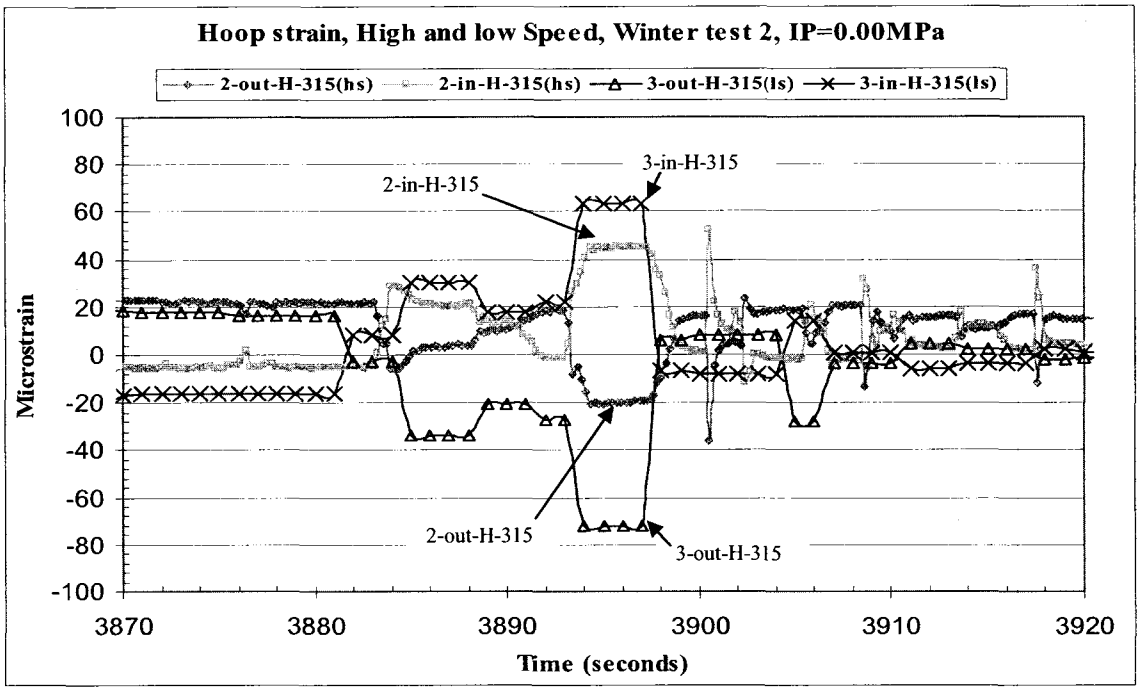

Figure 4.51 Hoop strain reversal at the 315° position of Section 2 and Section 3 at second of 3896 in high speed and low speed in winter un-pressurized test

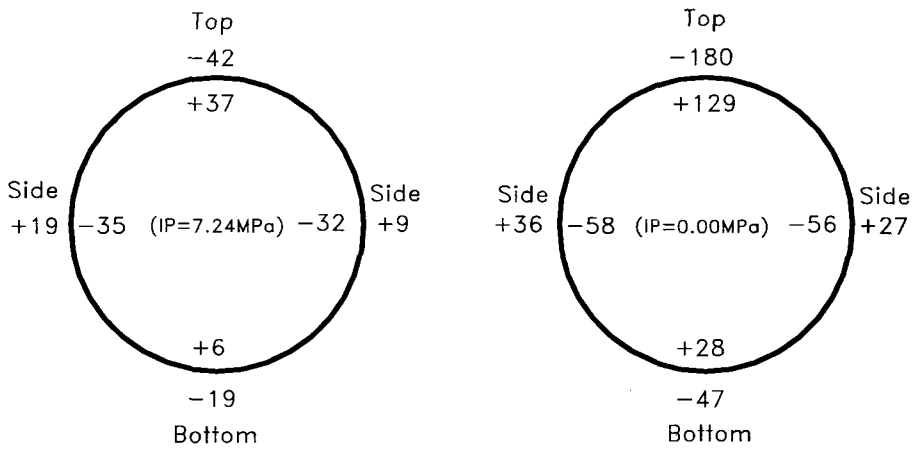

Figure 4.52 Comparison of maximum hoop strain of winter pressurized test and un-pressurized test (high speed)

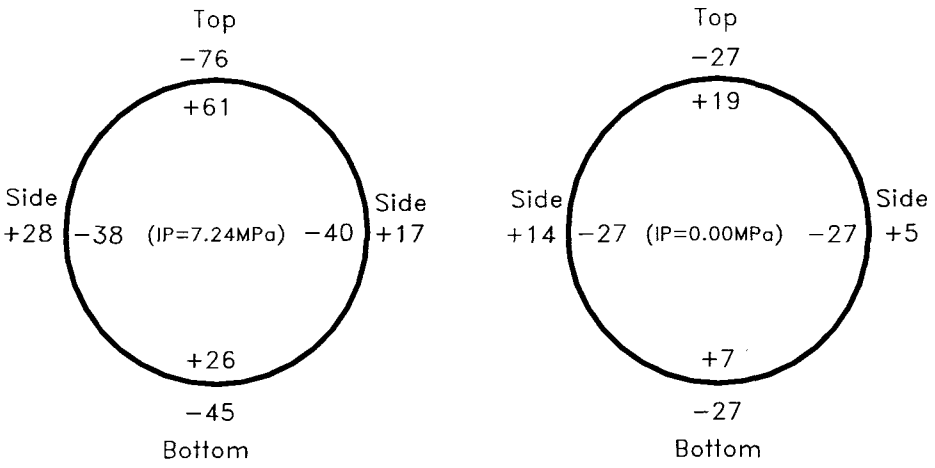

Figure 4.53 Comparison of maximum hoop strain of winter pressurized test and un-pressurized test (low speed)

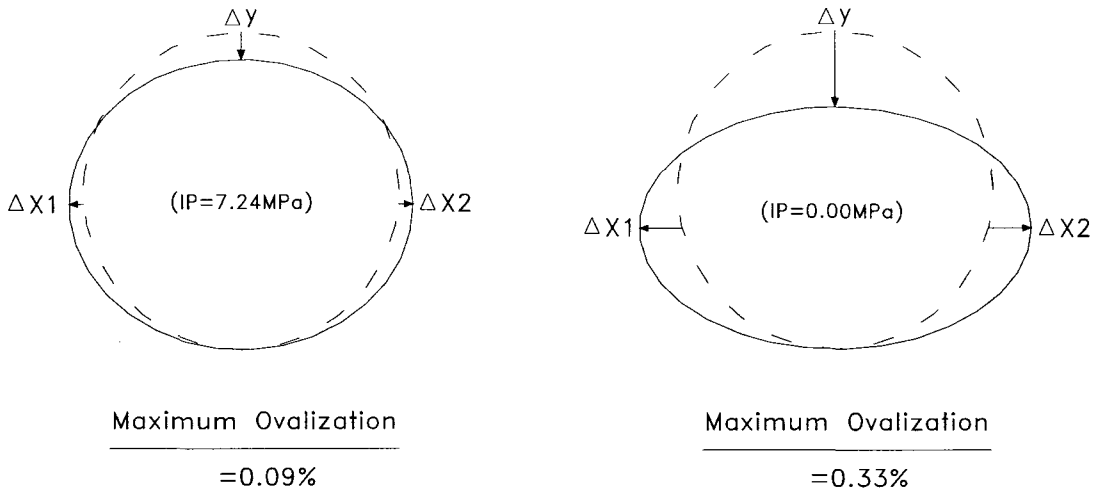

Figure 4.54 Comparison of maximum ovalization of winter pressurized test and un-pressurized test at buried state

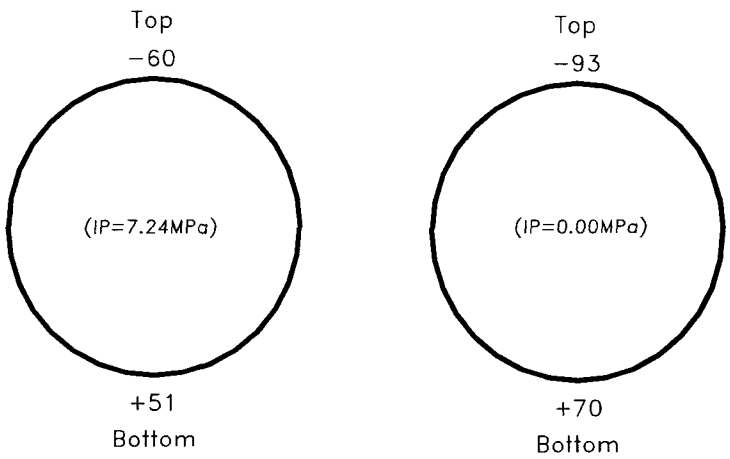

Figure 4.55 Comparison of maximum longitudinal strain of winter pressurized test and un-pressurized test in the instrumented section that the excavator is directly sitting on

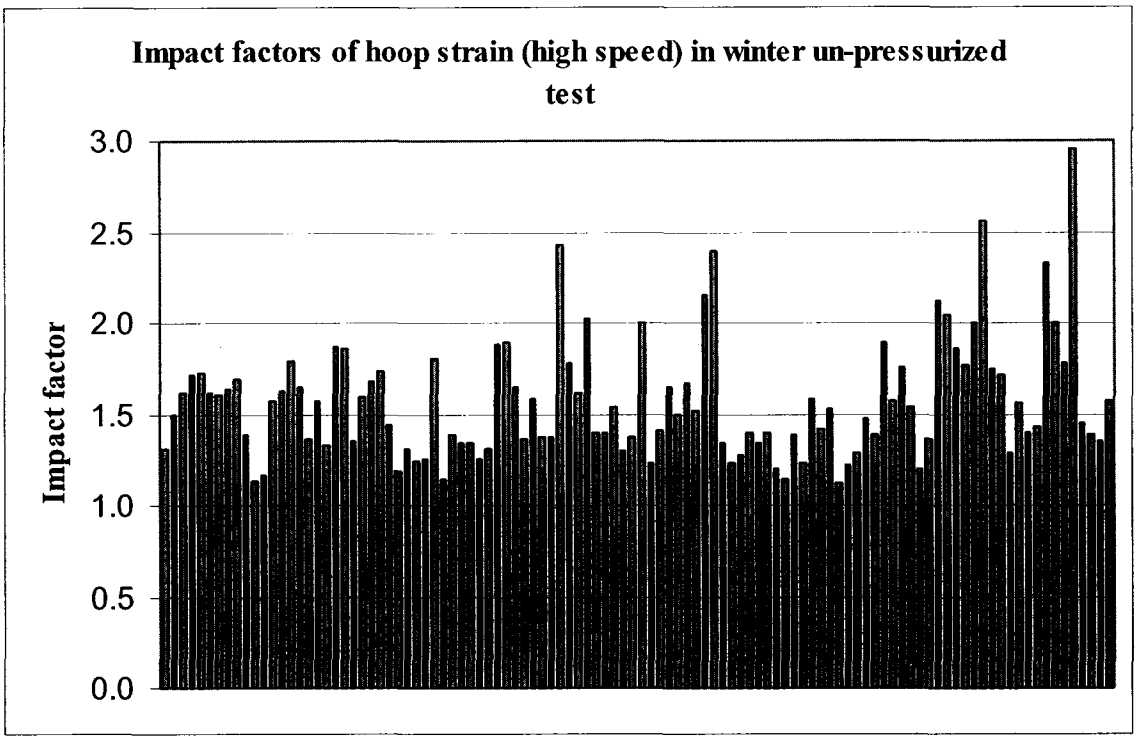

Figure 4.56 Impact factors of hoop strain (high speed) in winter un-pressurized test

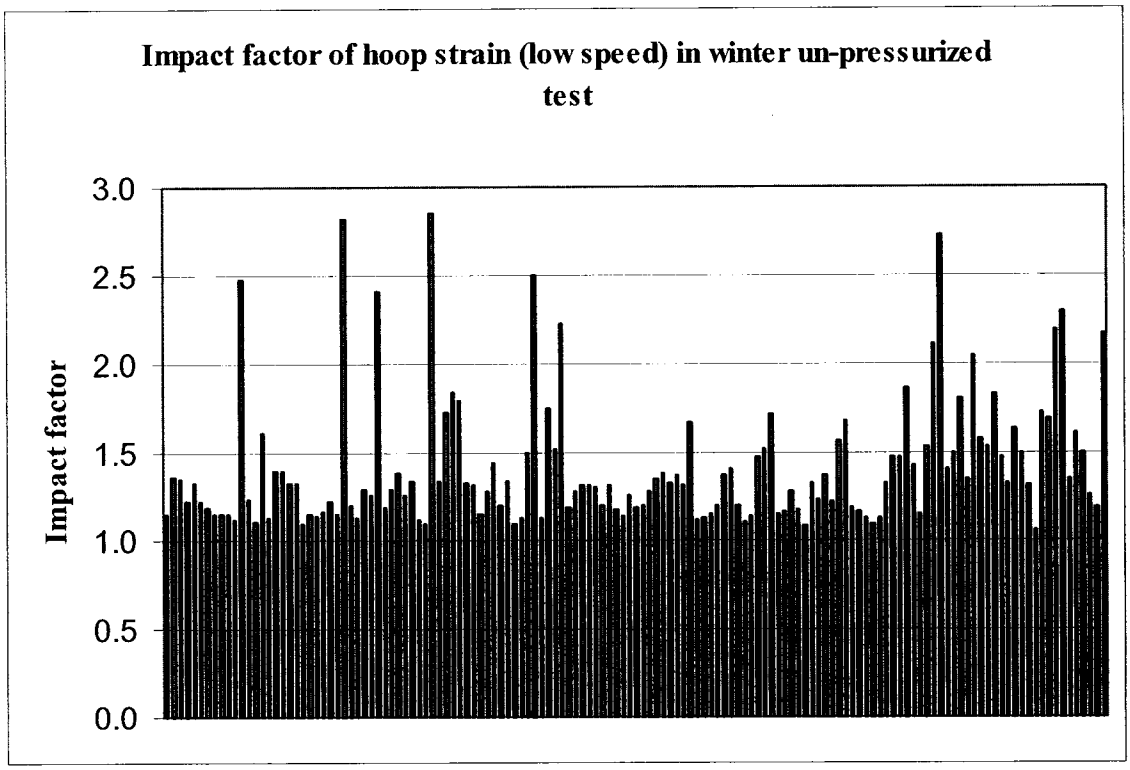

Figure 4.57 Impact factors of hoop strain (low speed) in winter un-pressurized test

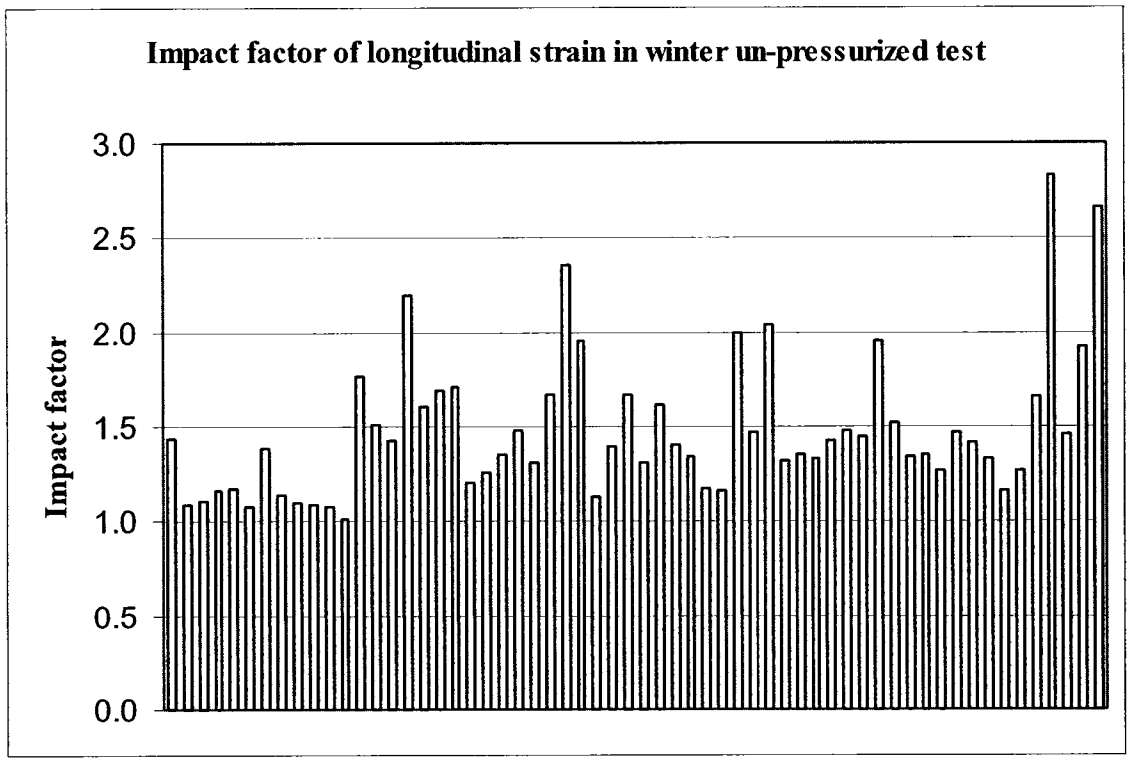

Figure 4.58 Impact factors of longitudinal strain in winter un-pressurized test

5 COMPARISONS OF SUMMER AND WINTER TESTS

5.1 Comparisons of Summer Tests and Winter Tests

5.1.1 Hoop Strain

For the un-pressurized tests, as shown in Figure 5.1, the maximum hoop strains in summer were +195με and -144με. They happened in the instrumented section under track shoes as a result of the weight and rocking of excavator during excavation. The maximum hoop strains in winter test were +220με and -211με at the 45° position of Section 4 (see Figure 4.43) which was being excavated by the excavator sitting at Section 7. They are caused by the digging force of excavator bucket. They are dynamic and transient in nature. In fact, they are the maximum hoop strains captured in both summer and winter excavation tests.

Comparing the history of hoop strain, it can be found that the pipeline section experienced the process of deformation from flattening by excavator to re-rounding by removal of soil in both summer and winter tests. After the instrumented section was exposed, the maximum hoop strains all happened at the bottom of the pipe, as shown in Figure 5.1. For summer test, the maximum hoop strains were +144με and -128με. For winter test, they were +138με and -137με. Hence, the maximum hoop strains in summer test are very close to those in winter test. In winter test, the short time hoop strain reversal was observed. However, the reversal was not observed in summer test. The maximum reversing hoop strains in winter were +133με and -133με captured at the 30° position of Section 2. The reversal resulted from that the part of top soil around Section 2 was removed. A downward force through the excavator bucket was produced, which changed the signs of hoop strain in Section 2.

For pressurized tests, comparison can be made between summer and winter test under the same condition that the excavator was just sitting on the instrumented section. As showed in Figure 5.1, the maximum hoop strains were +34με and -28με in summer. In winter, they were +37με and -42με. The maximum hoop strains in winter were close to those in summer.

Compared the maximum hoop strain of pressurized and un-pressurized test either in summer or winter, it can be found the maximum hoop strains were significantly reduced in pressurized test. The maximum ratios of the maximum hoop strain of un-pressurized over pressurized were 5.7 in summer and 4.3 in winter.

5.1.2 Ovalization

The maximum ovalization in summer and winter excavation tests was presented in Figure 5.2.

For the un-pressurized test, the maximum ovalization was 0.59% in summer test. This happened as a result of the weight and rocking of excavator when the instrumented Section 6 was under track shoes. The maximum ovalization is 0.33% in winter test which resulted from the loss of lateral support soil removed by the excavator sitting on Section 7. In winter, when the excavator was sitting on Section 6, the measured ovalization is only 0.11%.

For the pressurized test, the maximum ovalization was 0.10% in summer test and 0.09% in winter test under the same condition that the excavator was just sitting on the instrumented section.

In summer tests, the maximum ovalization was significantly reduced in pressurized tests. The ratio of the maximum ovalization in un-pressurized over that in

pressurized was 5.9. Because the winter pressurized test was not finished, the maximum ovalization can only be estimated based on the measured maximum hoop strain. The effects of internal pressure on ovalization can be evaluated by comparing the maximum hoop strain.

In winter test, the re-rounding of pipeline at Section 6 due to the removal of overburden was not observed. This may result from the fact that the top soil on the section 6 was not removed to protect the sealing gland near Sections 4 and 5.

5.1.3 Longitudinal Strain

The comparison of the maximum longitudinal strain of summer and winter is shown in Figure 5.3. The maximum longitudinal strain of the specimen was caused either by the weight and rocking of excavator at the instrumented section directly under the excavator or by the removal of soil at the exposed instrumented section.

For the un-pressurized test, the maximum longitudinal strains are +72με and -126με in summer. In winter they are +70με and -93με. At exposed state, they changed to +52με and -59με in summer and +47με and -67με in winter.

For pressurized tests, the maximum longitudinal strains were +66με and -58με in summer and +51με and -60με in winter under the same condition that the excavator was directly sitting above the instrumented section where the maximum strain was measured.

Therefore, the maximum longitudinal strains are similar in summer and winter.

5.2 Summary of Summer and Winter Excavation Tests

An experimental program was designed in order to investigate the effect of excavation on buried pipelines under different excavation conditions, mainly soil

condition (frozen vs. unfrozen soil) and internal pressure. In the first phase of the program, three summer excavation tests were conducted on October 14 and 15, 2004 when soil was unfrozen. In the second phase of the program, two winter excavation tests were done on March 22 and 24, 2005 when the soil was frozen.

The specimen was 27.5 meter long with nominal diameter of 914 mm (36") and thickness of 13.7 mm. The specified yield strength of the pipe material was 483 MPa. The specimen was buried underground. The depth of cover was from 0.8 m at high end to 1.3 m at low end of the pipe. The average depth of cover was 1.05 m. The average depth of ditch was about 2.0 m.

A total of eighty strain gauges and four thermistors were mounted on seven different cross sections along the specimen. Both inside and outside of the pipe were instrumented in order to capture any localized bending as a result of excavation. Four custom-made devices for measuring ovalization were made and installed in vertical, horizontal and two diagonal directions. Two sealing glands were fitted in the specimen to take out the wires from inside of the pipe. Twenty four strain gauges were connected to high-speed data acquisition (DAQ) system and the rest of strain gauges to low-speed data acquisition system. The low speed DAQ system was collecting 1 reading per second while the high speed DAQ was collecting data at a rate of about 100 readings per second.

The specimen was filled with water in the test. In summer excavation tests, test 1 and 2 were conducted under zero internal pressure while test 3 was conducted at internal pressure of 7.24 MPa, which developed the hoop stress equal to 50% specified minimum yield strength (SMYS) in the pipe. In winter excavation tests, test 1 was conducted at internal pressure of 7.24 MPa while test 2 was conducted at zero internal pressure.

The excavator used in summer was the Komatsu Avance PC 220LC. In winter excavation test, it was DEERE 270C LC. The excavation procedure was similar in the tests. The excavation zone was from about 2 m before Section 1 to about 2 m after Section 4. The total excavation length was about 13 m. On average, the excavator could excavate a length of about 2.6 m at each position.

(1) The maximum hoop strain, ovalization and longitudinal strain in summer excavation tests are summarized in Table 5.1.

In summer un-pressurized test, the maximum hoop strain was +195με and minimum -144με. This happened at the instrumented section the excavator was sitting directly on. In summer pressurized test, the maximum hoop strain was +77με and the minimum -76με. This occurred at the instrumented section which was exposed due to the removal of soil while the excavator moved backwards on the last position (Section 7).

In summer un-pressurized test, the maximum ovalization measured at Section 6 was 0.59% when the excavator was sitting on this section. When the excavator moved backwards on the last position of test, Section 7, another maximum ovalization was measured as -0.24%. The negative sign indicates that the cross section was re-rounded due to the removal of soil. Similarly, the maximum ovalizations measured at Section 6 in summer pressurized test were 0.10% and -0.12% respectively.

In summer un-pressurized test, the maximum longitudinal strain was +72με and the minimum -126με. This happened in the instrumented section which the excavator was sitting directly on. In summer pressurized test, the maximum longitudinal strain was +66με and the minimum -58με under the same condition.

(2) Critical conditions (critical conditions 1 and 2) in summer tests are shown in Figure 5.4.

Investigation of the results shows that for a specific instrumented section of the pipe, two kinds of the maximum hoop and longitudinal strains and deformation observed in two different critical conditions. The sign of the strain and deformation was opposite in these two conditions. Under critical condition 1 the maximum strains was observed with positive hoop strain at the inside of top and bottom and outside of two sides, and positive longitudinal strain at the bottom and with negative hoop stain at the opposite side of the wall and negative longitudinal strain at the top. The deformation was negative in vertical direction and positive in horizontal direction. They were measured in the instrumented sections directly under the track shoes and resulted from the weight and rocking action of excavator. On the contrary, under critical condition 2 the maximum values were observed in the instrumented section exposed due to excavation with the excavator moving backwards to Section 7. The strain and deformation changed to opposite sign. This indicates the section releasing the effects of overburden as a result of the removal of soil.

(3) The maximum hoop strains, ovalization and longitudinal strain in winter excavation tests are summarized in Table 5.2.

In winter un-pressurized test, the maximum hoop strain was +220με and the minimum -211με. This happened in the instrumented section (Section 4) which was being excavated by the excavator sitting at Section 7. In winter pressurized test, the maximum hoop strain measured was +37με and the minimum -42με measured at Section 2 when the excavator was sitting above this section.

In winter un-pressurized test, the maximum ovalization measured at Section 6 was 0.33%. This happened when this section was being excavated by the excavator sitting at Section 7. The maximum ovalization measured at Section 6 was 0.04% when the excavator was at Section 2. However, since the winter pressurized test was not finished, the maximum ovalization is expected when the excavator moved on Section 6. Assuming linear relationship of hoop strain and deformation (actually this was true in the tests), the maximum ovalization is estimated as 0.09%.

In winter un-pressurized test, the maximum longitudinal strain was +70με and the minimum -93με. This happened in the instrumented section which the excavator was sitting on. Under the same condition the maximum longitudinal strain measured in winter pressurized test was +51με and the minimum -60με at Section 2.

(4) Critical conditions in winter test (critical conditions 3 and 4) are illustrated in Figure 5.4 and Figure 5.5.

As shown in Figure 5.5, the critical condition happened in the portion or the instrumented section being excavated. The maximum hoop strain was caused by the digging force under critical condition 3. The digging had the impact to cause either transient strain or hoop strain reversal. The maximum ovalization occurred under critical condition 4. Under this condition, the soil at the top of pipeline remained because of the need of protecting sealing glands and difficulty of removing hard frozen soil and the two side soil got removed. As a result, the loss of lateral soil support increased the hoop strain and deformation as shown in the strain history at section 4 and deformation history at Section 6.

(5) Effects of internal pressure in summer tests are summarized in Table 5.3

The internal pressure applied in the pressurized excavation test was 7.24 MPa, which can produce a hoop stress of 241.5 MPa corresponding to 50% of Specified Minimum Yield Stress (SMYS). In this table, the maximum hoop strain, ovalization and longitudinal strain of the summer pressurized and un-pressurized tests were compared under critical conditions 1 and 2.

The internal pressure has significant effect to reduce the maximum hoop strain and ovalization under critical condition 1. The ratio of maximum hoop strain of pressurized over un-pressurized was 0.174. For ovalization, this ratio was 0.169.

(6) Effects of internal pressure in winter tests are summarized in Table 5.4

Because the winter pressurized excavation test was not finished due to the fitting failure, the comparison with winter un-pressurized test can be made only between the instrumented sections under critical condition 1. In pressurized test, these sections were Sections 2 and 3 while for winter un-pressurized test they are Sections 2, 3, 4, 5, 6 and 7. The effect of internal pressure in winter test was already shown in Table 4.3. The maximum values are demonstrated in Table 5.4.

The internal pressure has significant effect in reducing the maximum hoop strain under critical condition 1. The ratio of maximum hoop strain of pressurized over un-pressurized was 0.233.

(7) Summary of the maximum hoop strain, ovalization and longitudinal strain in summer and winter tests is presented in Table 5.5. For pressurized tests the data is under critical condition 1.

The effects of frozen soil can be demonstrated in Table 5.6 by comparing the summer and winter un-pressurized tests under critical condition 1. As shown in this

table, basically, the maximum strain and deformation decreased in winter test. Because the soil was frozen, the excavator weight and rocking has less effect on the instrumented section under the track shoes.

However, because the soil was frozen in winter, the excavator had to break the soil at the top of pipeline using the bucket, which caused greater downward force or impact on the section being excavated before the excavator. Under this condition (critical condition 3), the transient hoop strain (lasting 0.11 to 0.18 second) or short-time hoop strain reversal (lasting 3.39 to 11.06 seconds) was measured. The maximum hoop strain captured was +220με and minimum was -211με in winter un-pressurized test, which were the greatest in the whole excavation tests. Under this condition (critical condition 4), the maximum ovalization can also occur in the section being excavated because of the loss of lateral soil support. However, in summer test, the soil at the top of the pipeline can be removed without significant digging impact on the section being excavated since the soil was very loose.

(8) Summary of impact factors is presented in Table 5.7. Because of the soil condition, the maximum impact factor can be 3 in winter. On average, the impact factor is between 1.22 and 1.74.

5.3 Conclusions of Summer and Winter Excavation Tests

Following conclusions can be drawn from the analysis of the summer and winter excavation program. (It is worth nothing that all values of strains were measured relative to beginning of the excavation when the pipe was buried. In other words, all strains were initialized at the start of excavation):

(1) The maximum strain and deformation captured in each test are obtained in Table 5.8

(2) In summer tests, maximum strain and deformation measured in two critical conditions Table 5.9.

(3) In winter tests, maximum strain and deformation measured in four critical conditions Table 5.10.

(4) Effects of internal pressure

Internal pressure has the most significant effect on the reduction of hoop strain under critical condition 1. The minimum reduction ratio (pressurized over un-pressurized) was about 17% in summer and 23% in winter test respectively. For longitudinal strain, the ratio was 46% in summer and 65% for the top negative strain in winter. Under critical condition 2, as shown in the Table 5.3, the internal pressure also had the greatest effect on the reduction of hoop strain and ovalization, the ratio was about 50%. For longitudinal strain, the ratio was 76%.

(5) Effects of frozen soil

In winter test, the excavation became harder because the soil was frozen. Frozen soil influenced critical condition of the hoop strain. The impact of the bucket digging was proved to be the most critical condition. However, in summer, the most critical condition was caused by the rocking of excavator track shoes. Frozen soil also

influenced the critical condition of ovalization. In winter the maximum ovalization happened at the instrumented section being excavated by the excavator before the section (critical condition 4). In summer, this occurred under the track shoes of excavator (critical condition 1).

(6) During excavation process, the temperature hardly changed and its effect on the pipeline was negligible.

(7) The pipeline is basically experienced through-wall or localized bending in the cross section by observing the inside and outside hoop strains and longitudinal or global bending in the axial direction by observing the top and bottom longitudinal strains.

(8) In the whole test, a comparative study of the tests under same condition was performed in summer un-pressurized tests 1 and test 2. The strains history of test 1 and test 2 agreed well during the whole excavation process as shown in Figure 3.1 to 3.26. The maximum positive and negative hoop strains are +195με and -144με in test 1. In test 2 they are +195με and -128με. Under buried state, the maximum ovalization observed in test 1 was 0.59% while in test 2 this was 0.31%. The slight difference in the results between test 1 and 2 was because of the variation of soil compaction and probably different excavation procedure in two tests.

(9) Impact due to the rocking of excavator in the excavation process is significant under critical condition 1 and the impact factor can be obtained by the analysis of test data. The digging impact can cause the hoop strain to increase by 190με in winter un-pressurized test under critical condition 3.

Table 5.1 Summaries of maximum hoop strain, ovalization and longitudinal strain in summer excavation tests

Strain or Ovalization	Un-pressurized (0.00 MPa)				Pressurized (7.24 MPa)			
	Buried State		Exposed State		Buried State		Exposed State	
Hoop Strain (με)	+195	-144	+144	-128	+34	-28	+77	-76
Longitudinal Strain (με)	+72	-126	+52	-59	+66	-58	+52	-45
Ovalization (%)	0.59		-0.24		0.10		-0.12	

Table 5.2 Summaries of maximum hoop strain, ovalization and longitudinal strain in winter excavation tests

Strain or Ovalization	Un-pressurized (0.00 MPa)				Pressurized (7.24 MPa)	
	Buried State		Exposed State		Buried State	
Hoop Strain (με)	+220	-211	+138	-137	+37	-42
Longitudinal Strain (με)	+70	-93	+47	-67	+51	-60
Ovalization (%)	0.33		---		0.09	

Table 5.3 Effects of internal pressure in summer tests

Critical Condition	Type of Max. / Min. Strain or Deformation		7.24 MPa (1)	0.00 MPa (2)	Ratio (1) / (2)
1	Hoop Strain (με)	Positive	+34	+195	0.174
		Negative	-34	-144	0.236
	Ovalization(%)	---	0.10	0.59	0.169
	Longitudinal Strain (με)	Positive	+66	+72	0.917
		Negative	-58	-126	0.460
2	Hoop Strain (με)	Positive	+77	+144	0.535
		Negative	-76	-128	0.594
	Ovalization(%)	---	0.12	0.24	0.500
	Longitudinal Strain(με)	Positive	+52	+52	1.000
		Negative	-45	-59	0.763

Table 5.4 Effects of internal pressure in winter tests

Type of Max. / Min. Strain or Deformation		Pressurized Test (7.24 MPa) (1)	Un-Pressurized Test (0.00 MPa) (2)	Ratio (1) / (2)
Hoop Strain(με)	Positive	+37	+129	0.287
	Negative	-42	-180	0.233
Longitudinal Strain(με)	Positive	+51	+70	0.729
	Negative	-60	-93	0.645
Ovalization(%)		0.09*	0.11	0.818

Note: 1: The pressurized and un-pressurized results are compared under critical condition 1.

2: * estimated by measured maximum hoop strain.

Table 5.5 Summary of the maximum hoop strain, ovalization and longitudinal strain in summer and winter tests

			Summer	Winter
Un-pressurized Test	Hoop Strain (με)	Max.	+195	+220
		Min.	-144	-211
	Ovalization (%)	Max.	0.59	0.33
	Longitudinal Strain (με)	Max.	+72	+70
		Min.	-126	-93
Pressurized Test *	Hoop Strain (με)	Max.	+34	+37
		Min.	-28	-42
	Ovalization (%)	Max.	0.10	0.09
	Longitudinal Strain (με)	Max.	+66	+51
		Min.	-58	-60

*Note: under critical condition 1.

Table 5.6 Comparison of maximum strain and ovalization in summer and winter test under critical condition 1

Section Number	Type of Strain	Hoop Strain(με)		Longitudinal Strain(με)		Ovalization(%)	
		Summer	Winter	Summer	Winter	Summer	Winter
2	Max.	---	+129	+69	+53	0.59	0.11
	Min.	---	-180	-106	-93		
3	Max.	+118	+61	---	---		
	Min.	-134	-76	-89	-80		
4	Max.	---	+50	+56	+70		
	Min.	---	-38	-108	-82		
5	Max.	+176	+48	---	---		
	Min.	-144	-43	-126	-54		
7	Max.	+195	+92	+72	+53		
	Min.	-140	-75	-124	-78		

Note: 1.The maximum strain and deformation shown are under critical condition 1.

2. "---": Not available.

Table 5.7 Summary of impact factors

Season	Strain or deformation	Un-pressurized Test			Pressurized Test		
		Min.	Max.	Avg.	Min	Max	Avg
Summer	Hoop Strain(low speed)	1.14	2.00	1.38	1.33	2.55	1.74
	Longitudinal Strain	1.07	1.42	1.27	1.11	1.85	1.44
	Deformation	1.16	1.27	1.22	---	---	---
Winter	Hoop Strain(high speed)	1.13	2.96	1.57	1.43	3.00	1.70
	Hoop Strain(low speed)	1.06	2.86	1.42	1.20	2.00	1.60
	Longitudinal Strain	1.02	2.83	1.48	1.27	1.58	1.42

Table 5.8 Summaries of maximum hoop strains, ovalization and longitudinal strain in summer and winter excavation tests

Strain or Ovalization		Un-pressurized (0.00 MPa)		Pressurized (7.24 MPa)	
		Summer	Winter	Summer	Winter*
Hoop Strain (με)	max	+195	+220	+77	+37
	min	-144	-211	-76	-42
Ovalization (%)	max	0.59	0.33	0.10	0.09
Longitudinal Strain (με)	max	+72	+70	+66	+51
	min	-126	-93	-58	-60

*Note: only under critical condition 1

Table 5.9 Critical conditions in summer tests

Critical Condition	Reasons	Position	Max. and Min. Strain or Deformation		
			Hoop	Ovalization	Longitudinal
1	Excavator weight and rocking	Under the track shoes of excavator	+195με -144με	0.59%	+72με -126με
2	Soil removal	Exposed part	+144με -128με	-0.24%	+52με -59με

Table 5.10 Critical conditions in winter tests

Critical Condition	Reasons	Position	Max. and Min. Strain or Deformation		
			Hoop	Ovalization	Longitudinal
1	Excavator weight and rocking	Under the track shoes of excavator	+129με -180με	0.11%	+70με -93με
2	Soil removal	Exposed part	+138με -137με	---	+47με -67με
3	Digging impact of bucket	Under the bucket	+220με -211με	---	---
4	Loss of lateral soil support	Part before the excavator	+92με -130με	0.33%	---

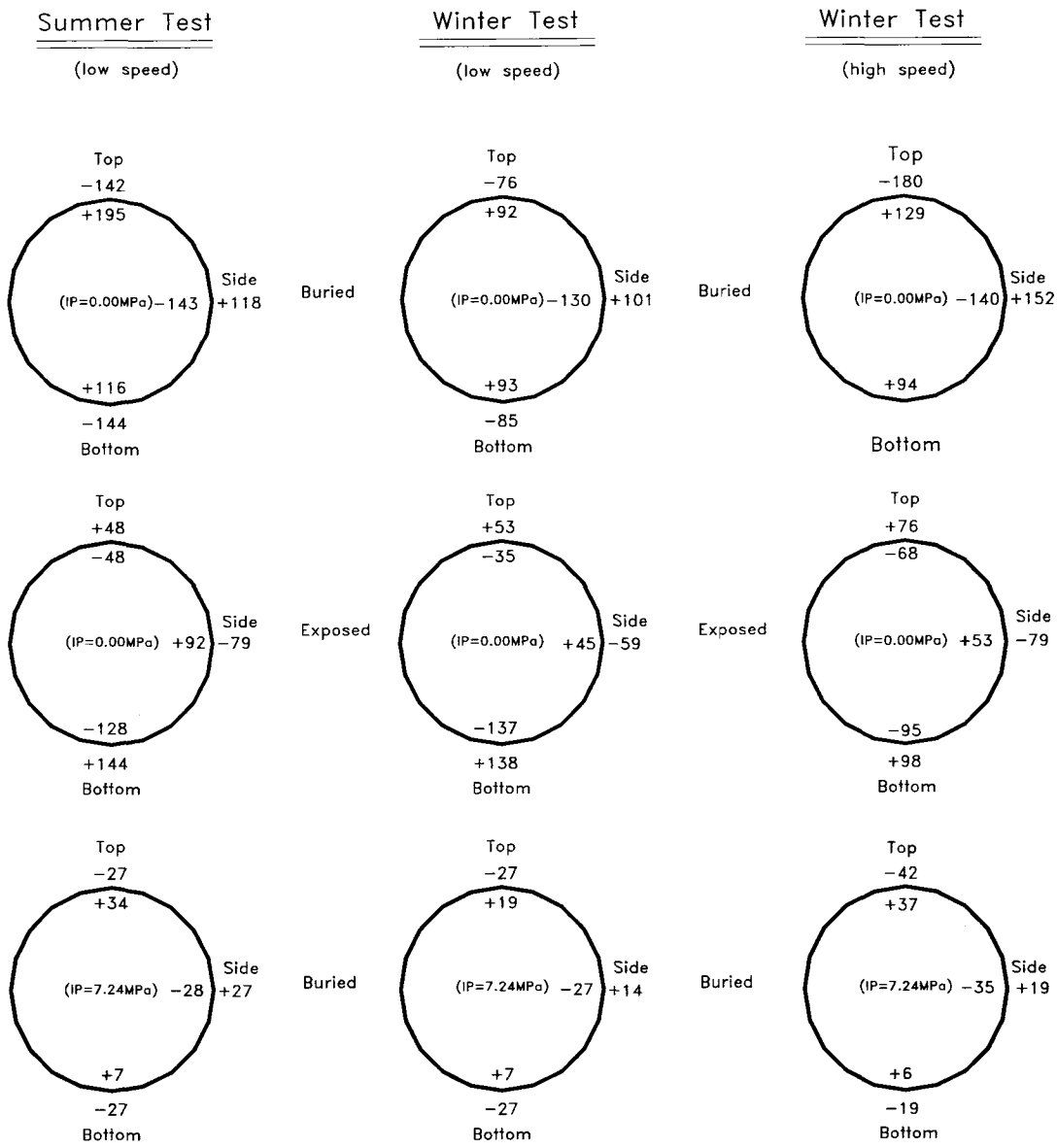

Figure 5.1 Comparison of the maximum hoop strain in summer test (low speed) and winter test (low speed and high speed)

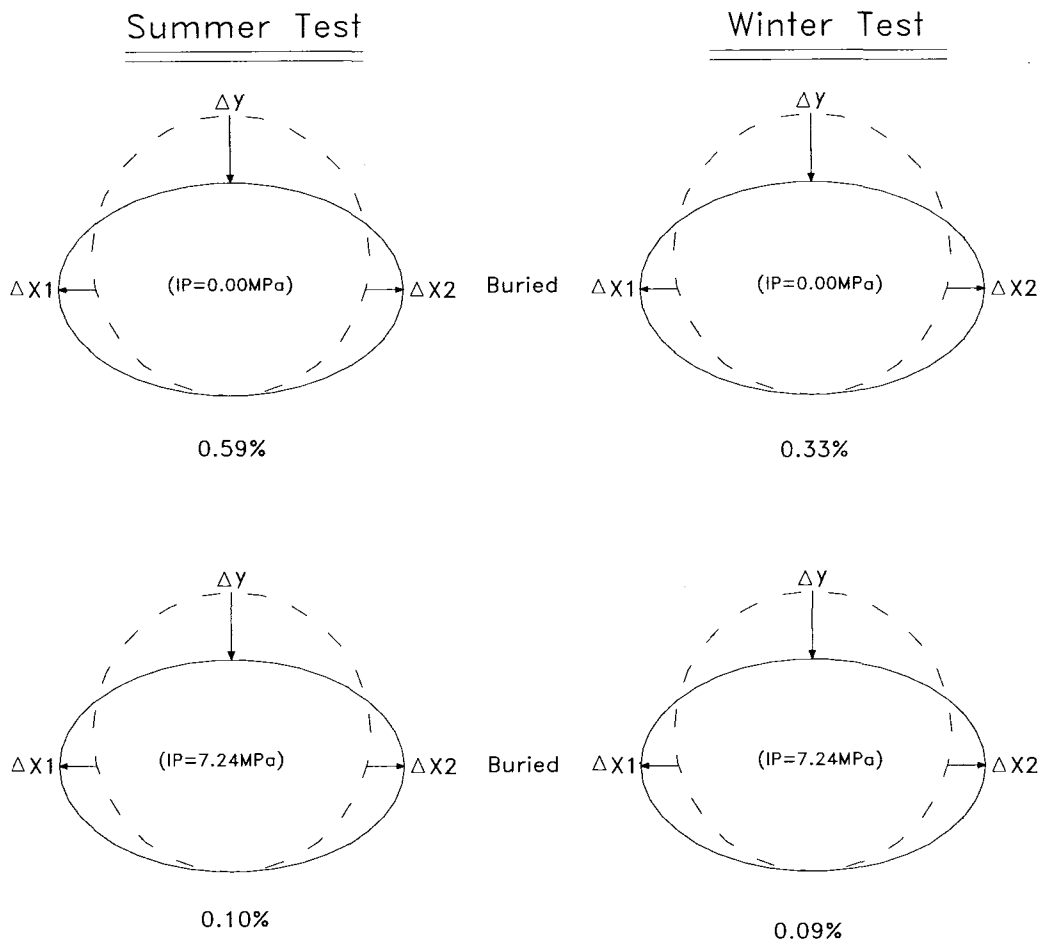

Figure 5.2 Comparison of the maximum ovalization in summer test and winter test

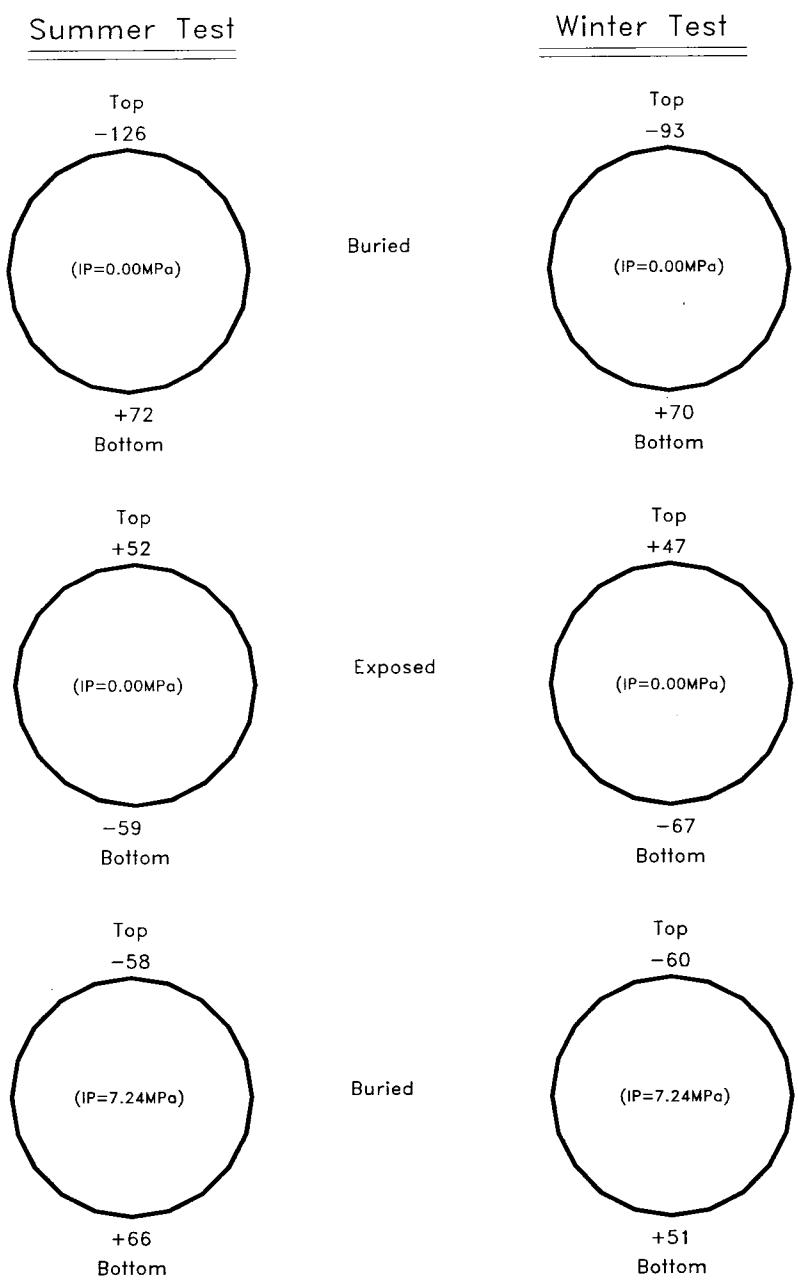

Figure 5.3 Comparison of the maximum longitudinal strain in summer test and winter test

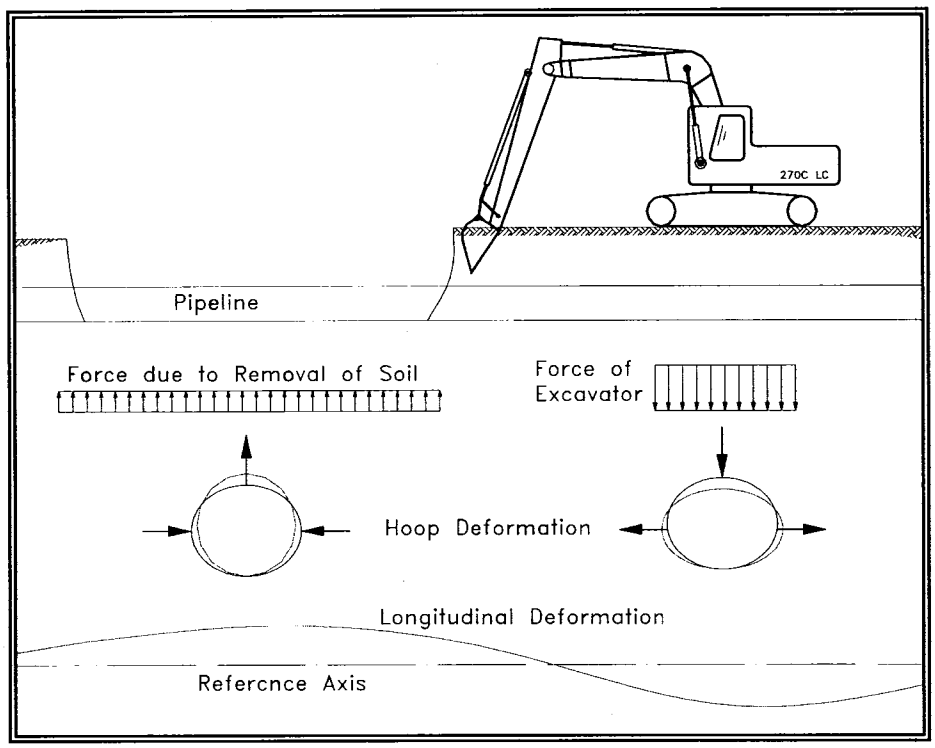

Figure 5.4 Critical conditions (summer or winter)

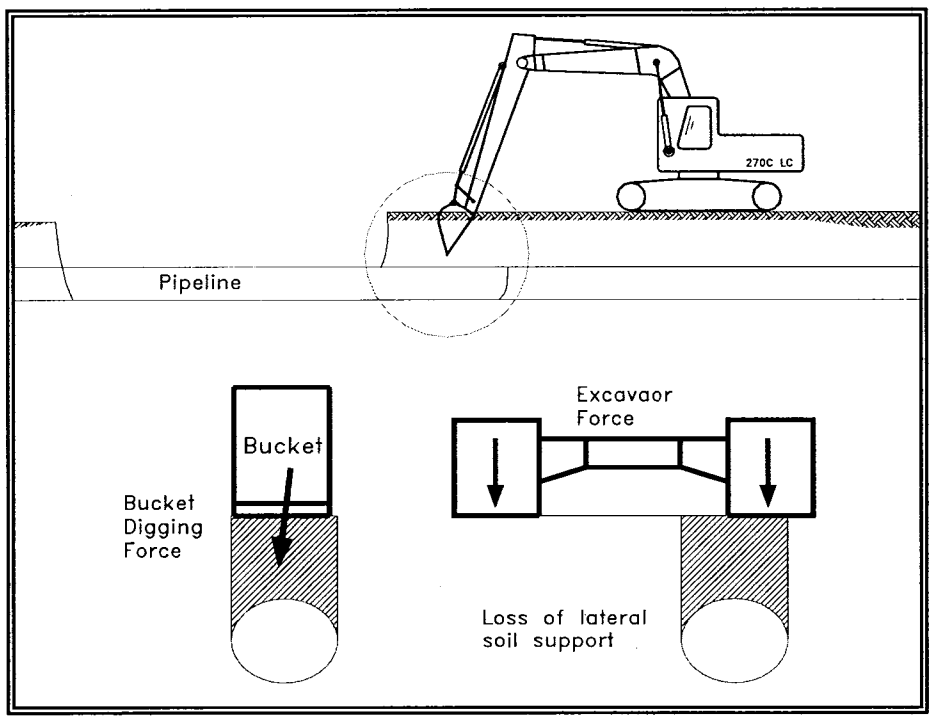

Figure 5.5 Critical conditions (winter)

6 SOIL TESTS

6.1 Introduction

To develop a finite element model to simulate the structural behaviour of buried pipeline during excavation, the in-situ soil properties must be obtained through soil testing. The tests should give a general description and usage characteristics of the soil. The accurate determination of stress-strain relationship of soil is necessary for the simulation of the interaction of soil and pipeline. Other soil properties, for example, the shear strength, are also used by utilizing the soil material models in the finite element program ABAQUS.

The following soil tests were conducted:

(1) Soil Classification Tests;

(2) Triaxial Tests.

6.2 Soil Tests

The soil tests were conducted at Soil Mechanics Laboratory, Department of Civil and Environmental Engineering, University of Alberta.

6.2.1 Soil Classification Tests

Soil classification tests consist of the tests to determine the grain size distribution and Atterberg limits.

The grain size distribution was determined by the sieve analysis and hydrometer test. The grain size curve is shown in Figure 6.1. The discontinuity occurred in the range where the two analysis overlap. This is because that soil particles are generally irregular in shape (Das, 2000). The percent of soil passing the No. 200 sieve is 74% based on sieve

analysis and 54% on hydrometer test. Taking average, the percent of soil passing the No. 200 sieve is 64%.

Atterberg limit test can give the liquid limit and plastic limit of the soil. Plastic limit is defined as the moisture content at the point of transition from semisolid to plastic state, at which the soil, when rolled into threads of 3.2 mm in diameter, crumbles. The moisture content at the point of transition from plastic to liquid state is the liquid limit. The specific gravity and water content were also obtained in the tests.

6.2.2 Triaxial Tests

Soil sample were taken from the field using steel tubes provided by the Soil Mechanics Laboratory. The size of sample was 100 mm in diameter and 200 mm in height (see Figure 6.2).

Consolidated undrained test (CU test) was conducted according to the procedure from Geotechnical Graduate Laboratory. Back pressure was 400 kPa and cell pressures were 410 and 440 kPa respectively. The effective confining pressures were 10, 20 and 40 kPa. The technique of applying a constant back pressure to the pore water is commonly used in the soil testing. The purpose of a back pressure is to saturate the sample by dissolving any air or gas presented in the pore water. Provided that the results are expressed in terms of effective stress, the magnitude of the back pressure will have no influence on the tests (Atkins, 1978). Other soil properties, such as the water content, density, void ratio, saturation and B-value, were all measured in the test. The CU triaxial test setup and soil sample at the end of test are shown in Figures 6.3 and 6.4.

6.3 Test Data Analysis

6.3.1 Soil Classification

Based on the grain size curve, 64% soil passing through the No. 200 sieve, using the unified system of soil classification, the soil was classified as fine-grained soil. The Atterberg limit and other soil properties were obtained as follows:

- Liquid limit: 33.3
- Plastic limit: 21.5
- Plasticity index: 11.8
- Specific gravity: 2.66
- Water content: 20.3%-21.0%

According to the Atterberg limit, the soil was classified as inorganic clays with group symbol, CL, in the unified system of soil classification as shown in Figure 6.5. Such kind of soil has low to medium plasticity. The A-line separate the inorganic clays from the inorganic silts. Plots of plasticity indexes against liquid limits for inorganic clays lie above the A-line, which is for our case. The empirical A-line is given by equation $PI = 0.73(LL\text{-}20)$. The U-line is approximately the upper limit of the relationship of the plasticity index to the liquid limit for any soil found so far $PI = 0.9(LL\text{-}8)$ (Das, 2000).

6.3.2 Determination of Modulus of Elasticity

The initial modulus of elasticity can be determined at different confining stress (Bowles, 1992) and the results are summarized in Table 6.1.

6.3.3 Determination of Shear Strength

The effective principal stresses at failure for tests of 10 kPa and 40 kPa were obtained in the CU triaxial tests, and the Mohr's circle can be drawn and the failure

envelope can be determined, as shown in Figure 6.7. The cohesion was almost zero and effective friction angle was 32.3°.

6.3.4 Other Soil Parameters from CU Triaxial Test

Other soil properties obtained from CU triaxial test are summarized in Table 6.2. The average wet density is found to be 1941 kg/m^3 and the average void ratio is 0.677.

Table 6.1 Modulus of elasticity determined in CU triaxial tests

Effective Confining Pressure (kPa)	Modulus of Elasticity (MPa)
10	5.714
40	37.000

Table 6.2 Other soil parameters determined from CU triaxial test

Sample ID	Depth	Cell Pressure	Dia.	H	Area	Area after Consolidation	Volume	Mass
	m	kPa	mm	mm	mm 2	mm 2	cm 3	g
#1	~1.0	10	96.570	195.50	7324.44	7192.60	1431.928	2808.3
#8	~2.0	20	96.835	201.75	7364.69	7232.13	1485.827	2858.2
#3	~1.0	40	95.610	208.08	7179.54	7050.31	1493.918	2813.7
#9	~1.0	40	96.550	199.90	7321.41	7299.44	1463.549	2923.3

Sample ID	Initial W. C.	Final W.C .	Wet Density	Dry Density	Void Ratio	Initial Saturation	B- values before Consolidation	B- values after
	%	%	g/ cm 3	g/ cm 3		%		
#1	19.1		1.961	1.647	0.615	83	0.963	0.980
#8	23.0	25.7	1.924	1.564	0.701	87	0.990	1.000
#3	23.0	25.7	1.883	1.531	0.737	83	0.990	1.000
#9	24.3		1.997	1.607	0.655	98.6	0.969	1.000

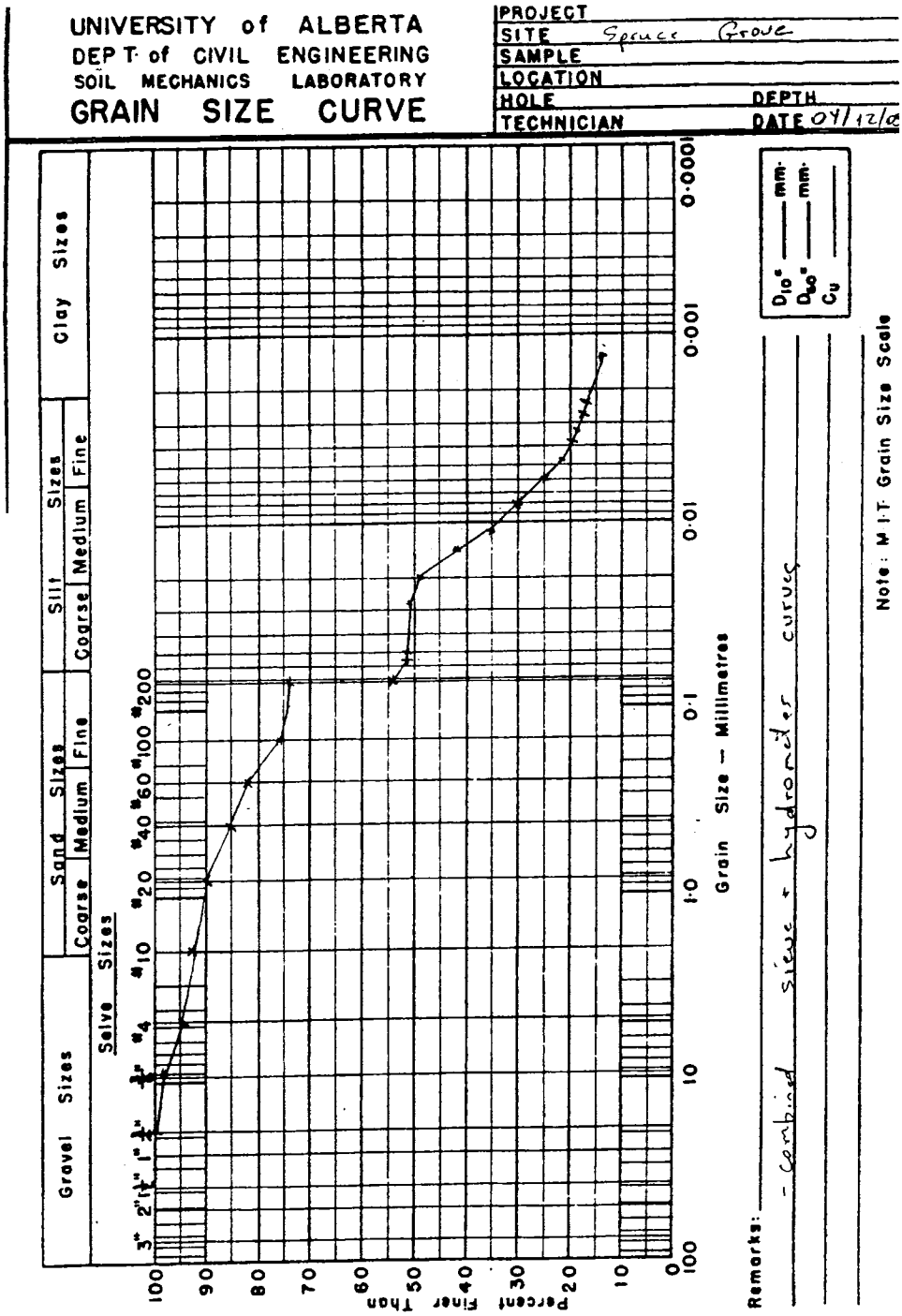

Figure 6.1 Grain size curve

Figure 6.2 Soil sample taken from excavation field for CU triaxial test

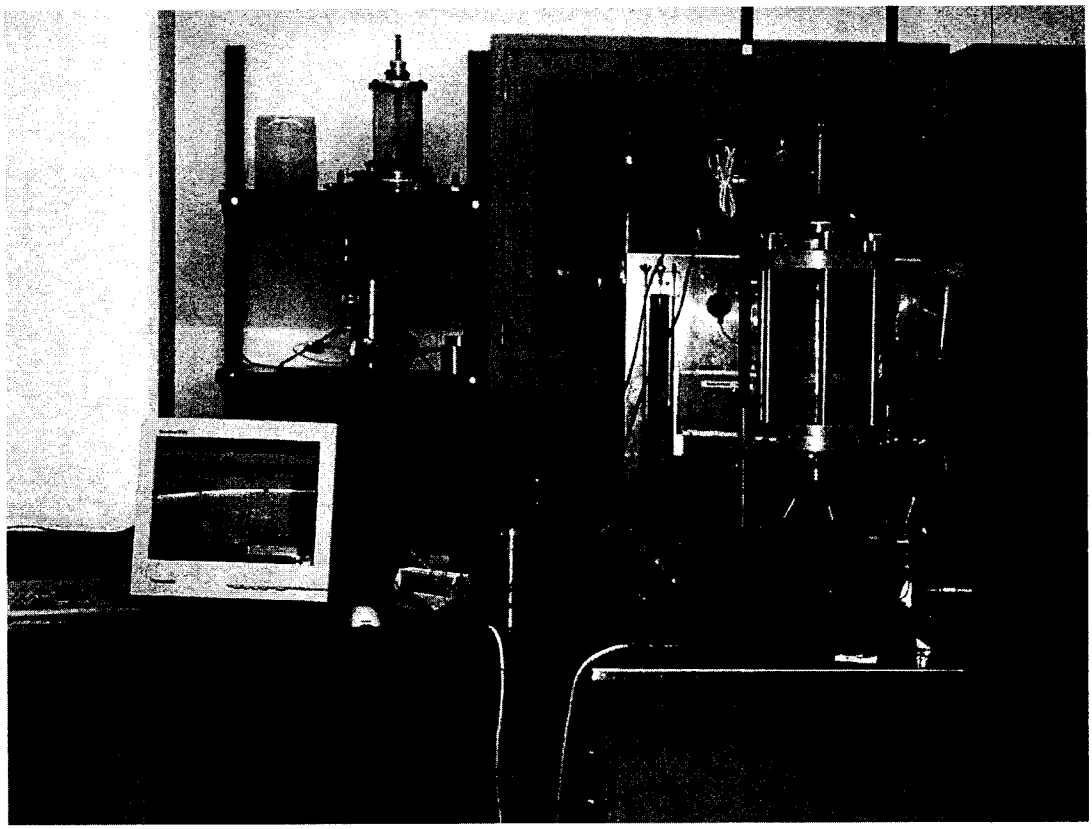

Figure 6.3 CU triaxial test setup

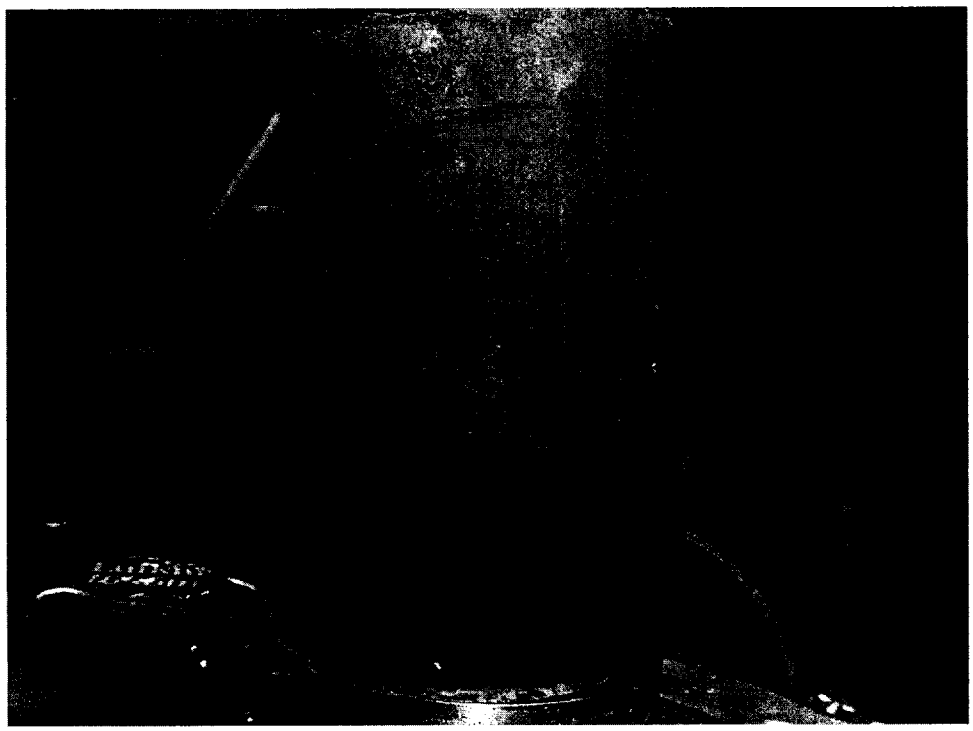

Figure 6.4 Soil sample after CU triaxial test

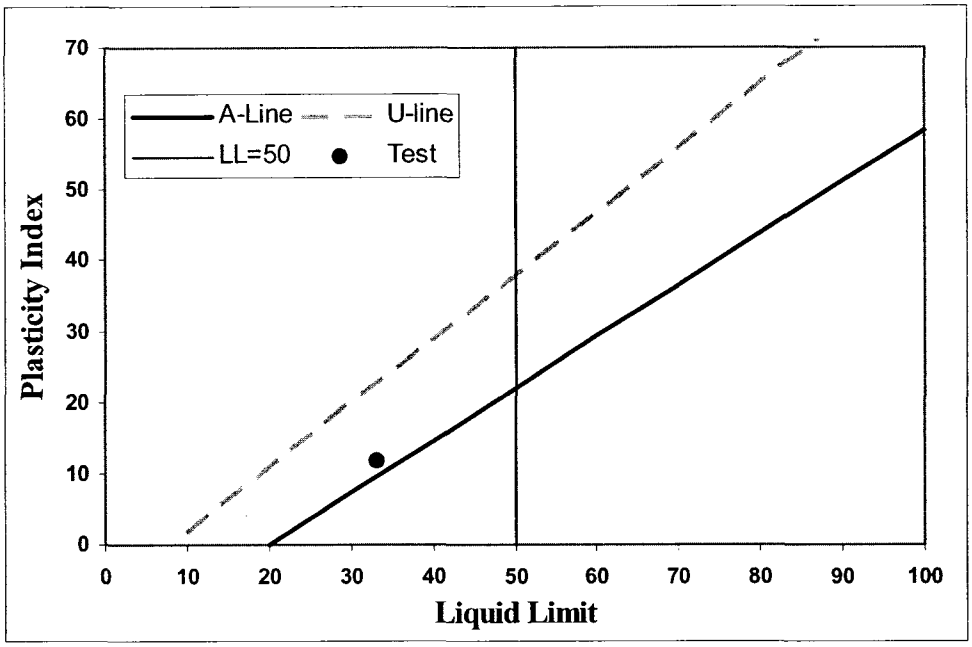

Figure 6.5 Soil classification

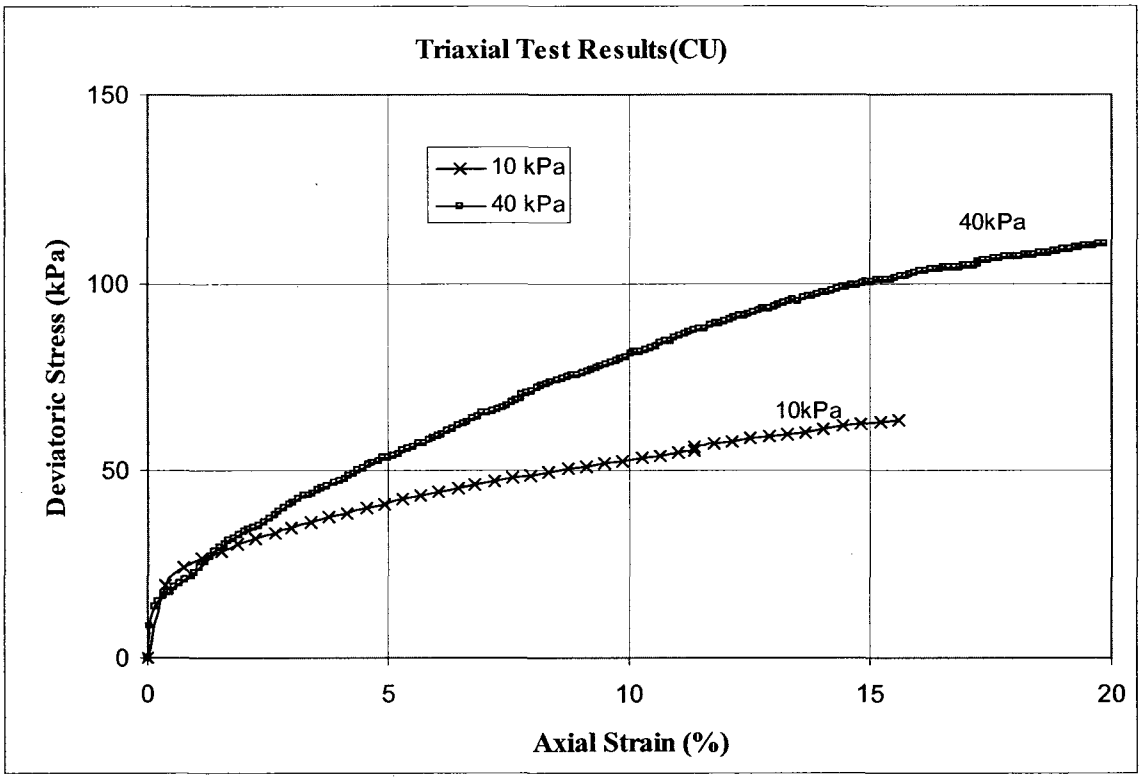

Figure 6.6 Results of CU triaxial tests

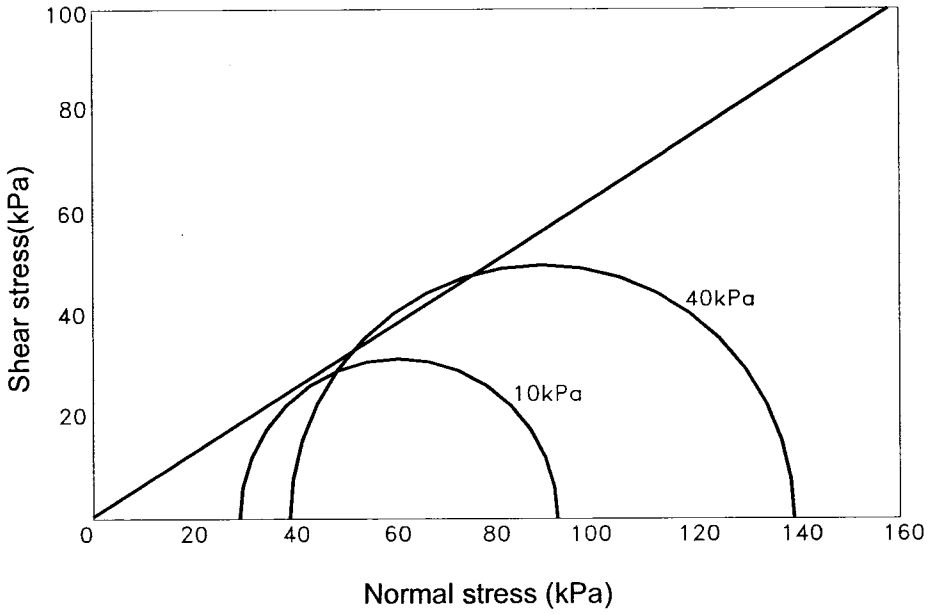

Figure 6.7 Effective stress failure envelops for CU triaxial tests

7 FINITE ELEMENT ANALYSIS

7.1 Introduction

Field excavation tests had been done with a specimen that was 914 mm (36") in diameter and about 27.5 m in length. The average depth of cover was about 1.0 m.

The goal of the finite element analysis is to build a model to analyse the additional strain produced in the specimen during the excavation test. To simulate this process, the selection of mesh, type of element, material model of soil and steel pipeline, the interactive interface between soil and pipeline, boundary conditions, action or loading of excavator, and process of excavation (removal of soil) should be decided in the model.

7.2 Description of Models

7.2.1 Mesh Selection

The boundaries of the simulated soil body should exceed the excavation affected area so that the boundaries condition can be applied appropriately. On the boundaries, the additional stress or strain in the soil shall be negligible, i.e. the soil stress or strain shall be close to the original, un-disturbed state. Since the importance of pipeline strain and deformation produced under the excavator track shoes, the mesh should be finer around the pipe and under the excavator track shoes.

Boussinesq's equation was used to decide the boundaries of the soil to be simulated. The excavator applied pressure on the ground surface through the track shoes in a rectangular shape. This surface pressure is transmitted in a semi-infinite medium, assumed as an ideally elastic, homogeneous, isotropic mass of material in Boussinesq's Equation. Figure 7.1 shows the contours of equal vertical stress under a loaded area of

width B (infinitely long foundation and square foundation) according to Boussinesq analysis (Spangler, 1982). The track shoe of the excavator used in the test has an underground length of 3.845 m and width of 0.8 m. The detail calculation can be done through the Newmark's equation. Although the real soil is not like what is assumed in Boussinesq's equation, extensive experiments showed that the transmitted loads never exceeded the theoretical value (Spangler, 1982).

Around the circumferential direction of the pipeline, there were 24 nodes with average interval about 0.120 m. Along the longitudinal direction the pipeline was divided into 57 segments with average interval about 0.482 m. There were two additional nodes at the center of caps (welded-neck flange) at ends of the specimen. Hence, there are 1394 nodes in all to form the mesh of specimen. The mesh of soil was refined around the pipeline and under the track shoes, and gradually getting coarse approaching to the boundaries. There were 277 nodes at every cross section and totally, 16,066 nodes makes up the mesh of soil body.

The dimension of the mesh in X-Z plane is shown in Figure 7.2 (only left part was shown and the right part is symmetry). The whole mesh in this plane is shown in Figure 7.3. Figure 7.4 shows the mesh after excavation. The mesh in Y-Z plane at X = 0 was displayed in Figure 7.5. At the X-Z plane, the boundary is 5 m away from the center of pipe either to left or to right. The total width is 10 m. The depth is 5 m below the ground surface. The length in longitudinal direction is the same as the specimen, 27.573 m. Through calculation using Newmark equation, the addition vertical stress produced by excavator was less than 5% of the ground pressure of excavator at the boundaries.

The followings are the dimensions used in the model:

- Track shoe: 3.845 m x 0.8 m, 2pcs with center distance about 2.6 m;
- The pipe diameter, D, is 914 mm;
- Two side: 5D (3B, B: width of excavator track shoe) to each side boundary;
- Top: 1D to ground surface;
- Bottom: 3D to bottom boundary.

7.2.2 Elements

The pipeline specimen is discretized using the shell element – S4R (in ABAQUS element library) in the pipe body and STRI3 (in ABAQUS element library) at the two end caps in the finite element model. The soil is represented by the solid (continuum) element, C3D8R (in ABAQUS element library).

7.2.3 Material Models

The field excavation tests showed the measured strain of the specimen was far below the yielding strain. The pipeline response was in an elastic range, therefore the linear elasticity material model was chosen for the steel pipeline. The modulus of elasticity of steel E was assumed as 205,000 MPa and Poisson ratio v was 0.3.

The selection of soil material model is complicated. The soil model should be an "interaction" model. The two parts in the model, elastic part and plastic part shall be defined. The additional stress produced by the excavator at the buried pipeline is about 20% of the ground pressure of the track shoes based on the Boussinesq's equation. The excavation will not cause the failure of soil and most of the deformation is small. The soil is not failed but progressively yielding. Therefore, the plastic part of the soil model will combine with elastic material model.

The critical state (clay) plasticity model was decided to be used for the material model of soil. The elastic part of the deformation was required to be defined by using the *POROUS ELASTIC option (elastic behaviour of porous materials) within the same material definition block. The porous elastic material model is valid for small elastic strains (normally less than 5%). It is a nonlinear, isotropic elasticity model in which the pressure stress varies as an exponential function of volumetric strain and allows a zero or nonzero elastic tensile stress limit. It can be used by itself, or combined with the critical state (clay) plasticity model (ABAQUS User's Manual, 2004).

Defining the volumetric behaviour

Often, the elastic part of the volumetric behaviour of porous materials is modeled accurately by assuming that the elastic part of the change in volume of the material is proportional to the logarithm of the pressure stress:

$$\frac{\kappa}{(1+e_o)}\ln\left(\frac{p_o+p_t^{el}}{p+p_t^{el}}\right)=J^{el}-1 \qquad [7\text{-}1]$$

where:

κ = the logarithmic bulk modulus;

e_0 = the initial void ratio;

p = the equivalent pressure stress, defined by

$$p=-\frac{1}{3}trace\sigma=-\frac{1}{3}(\sigma_{11}+\sigma_{22}+\sigma_{33}); \qquad [7\text{-}2]$$

p_0 = the initial value of the equivalent pressure stress;

J^{el} = the elastic part of the volume ratio between the current and reference configurations;

p_t^{el} = the "elastic tensile strength" of the material (in the sense that $J^{el} \to \infty$ as $p \to -p_t^{el}$).

Defining the shear behaviour

The deviatoric elastic behaviour of a porous material can be defined by defining the shear modulus. Give the shear modulus G, the deviatoric stress S, is then related to the deviatoric part of the total elastic strain, e^{el}, by

$$S = 2Ge^{el} \qquad [7.3]$$

Critical State Plasticity Model (Cam-clay Model)

The critical state (clay) plasticity model used in ABAQUS is a modified Cam-clay plasticity model which permits extensions of the original Roscoe model. The modified Cam-clay theory is a classical plasticity model. It uses a strain rate decomposition in which the rate of mechanical deformation of the soil is decomposed into elastic and plastic part; an elasticity theory; a yield surface; a flow rule; and a hardening rule (ABAQUS Theory Manual, 2004). The comparison of Cam-clay model with Cap Model (Modified Drucker-Prager Model) is described in the reference by Desai and Siriwardane (1984). Cap Model has two curves, two yield surfaces, two flow rule (non-associated in failure and transition regions and associated in cap regions) and two hardening rule (perfectly plastic yield surface, no hardening in Drucker-Prager segment, inelastic volume increase, dilation; and hardening in cap segment, compaction).

Yield surface

As shown in Figure 7.7 is the yielding surface in the p-t plane (t is a deviatoric stress measure), where M = material parameter defining the slope of the critical state lines; and β = "capping" parameter used to provide a different shaped yield ellipse on the

wet side of critical state; The "standard" Cam-clay yield function has β =1(ABAQUS Benchmarks Manual, 2004). The ratio of the flow stress in triaxial tension to the flow stress in triaxial compression, K, determines the shape of the yield surface in the plane of principal deviatoric stresses (the "Π -plane", Figure 7.8). ABAQUS requires that 0.778 < K < 1.0 to ensure that the yield surface remains convex.

Hardening law

The hardening law can have an exponential form. The exponential form of the hardening law is written in terms of some of the porous elasticity parameters and, therefore, can be used only in conjunction with the *POROUS ELASTIC option. The size of the yield surface at any time is determined by the initial value of the hardening parameter, a_0 , and the amount of inelastic volume change that occurs according to the equation

$$a = a_0 \exp[(1+e_0)\frac{1-J^{pl}}{\lambda - \kappa J^{pl}}] \qquad [7\text{-}4]$$

where:

J^{pl} = the inelastic volume change (that part of J, the ratio of current volume to initial volume, attributable to inelastic deformation);

κ = the logarithmic bulk modulus of the material defined in the *POROUS ELASTIC option;

λ = the logarithmic hardening constant defined in the *CLAY PLASTICITY option;

e_0 = the initial void ratio defined by the *INITIAL CONDITIONS;

a = the value of the equivalent pressure stress at critical state.

Parameter determination

The porous elastic material model has three soil parameters:

- logarithmic bulk modulus, κ
- shear modulus, G
- elastic tensile limit, p_t^{el}

The logarithmic bulk modulus κ can be determined based on the soil classification. There is a kind of relationship existed between swelling index (C_S), the commonly know quantity, and logarithmic bulk modulus (Atkins, 1978; Wood, 1990; Desai and Siriwardane, 1984).

$$C_s \approx 2.303\kappa \qquad [7.5]$$

The reason for the approximate relation is the usual assumption of a constant value of the coefficient of earth pressure at rest K_0

Swell index has a kind of correlation to liquid limit (LL) (Lambe and Whitman, 1969). LL is 33.3% in the soil test, and C_S is in a range of 0.05~0.1 from the correlation. Hence, κ is between 0.021 and 0.043. Swell Index (C_S) is appreciably smaller in magnitude than the compression index (C_C)and can generally be determined from laboratory tests. In most cases (Das, 1985),

$$C_s = \frac{1}{5} \sim \frac{1}{10} C_c \qquad [7.6]$$

The shear modulus G, is related to modulus of elasticity, E, by

$$G = \frac{E}{2(1+\nu)} \qquad [7.7]$$

E was determined by the triaxial test results.

It is very difficult to make an exact evaluation of the value of ν for use in any problem. Fortunately, the value of ν usually has a relatively small effect upon engineering predictions (Lambe and Whitman, 1969). Poisson's ratio for soil is closer to the upper limit of 0.5 than it is to the lower limit of zero. Therefore, the Poisson ratio ν, was taken as 0.4 (Spangler, 1982).

Usually, p_i^{el} is taken zero for soil.

The initial tangent modulus E_i has the following relationship with σ_3, the minor principal stress (Duncan and Chang, 1970),

$$E_i = Kp_a(\frac{\sigma_3}{p_a})^n \qquad [7.8]$$

where:

E_i = initial tangent modulus

σ_3 = the minor principal stress or minor effective principal stress

K = modulus number

n = exponent determining the rate of variation of E_i and σ_3

p_a = atmospheric pressure

In most practical problems, the stresses before loading are not isotropic as in the CU triaxial test. The effect of actual state of stress on modulus is not clear, but the best available rule is that modulus depends on the average of the initial principal stresses,

$$\sigma_v \frac{1+2K_0}{3} \qquad [7.9]$$

where σ_v is vertical normal stress and K_0 is the coefficient of lateral stress at rest (Lambe and Whitman, 1969).

For plastic part of the Cam-clay material model, compression index (C_c) can be calculated based on the soil classification (Spangler, 1982). Compression Index (C_c) is given by a correlation:

$$C_c = 0.009(LL - 10) \qquad [7.10]$$

The preceding relation has reliability in the range of ±30%.

Therefore, the λ can be determined by its relationship with compression index (Atkins, 1978; Wood, 1990; Desai and Siriwardane, 1984).

$$C_c = 2.303\lambda \qquad [7.11]$$

Usually, the compression index and swelling index are defined with respect to a one-dimensional consolidation test. However, the $e - \ln p$ curve for any constant stress ratio test, that is, for constant q/p ratio, is parallel to that obtained from a hydrostatic test, isotropic consolidation (Schofield and Worth, 1968). In fact, one-dimensional consolidation is a special case of a constant q/p test. The $e - \ln p$ curve obtained from hydrostatic test is parallel to that obtained under critical conditions (Desai and Siriwardane, 1984).

M (slope of critical state line) was determined by the triaxial tests (Figure 7.10) or by formula for triaxial compression (Wood, 1990)

$$M = \frac{6\sin\varphi'}{3 - \sin\varphi'} \qquad [7.12]$$

where φ' is Mohr-Coulomb friction angle.

The initial value of the hardening parameter a_0, defines the initial size of the yield surface which governed by the extent of initial overconsolidation. The overconsoildation ratio was defined as

$$R_p = \frac{p'_m}{p'} \qquad [7.13]$$

where the subscript p is a reminder that R_p is a ratio of the mean normal stresses. The value of R_p cannot be less than 1.0 and, if R_p=1.0, the soil is normally consolidated and its state lies on AC (Figure 7.11) (Atkinson, 1978). Based on our test as shown in Figure 6.6 and Figure 6.7, the soil was normally consolidated (Das, 2000).

At the start of a soils analysis with initial stresses, ABAQUS checks to see that the stress specified does not violate the initial yield surface. If it does, the hardening value (a, in the yield surface definition above) is modified to make the yield surface consistent with the stress state (ABAQUS Benchmarks, 2004).

7.2.4 Multi-point constraints (MPC)

Usually the interface between the pipeline and soil is simplified by nonlinear spring in different direction. When the force exceeds the breakaway limit, the soil is assumed yielded and deformation can develop with constant force. During the excavation process, the deformation is restricted in a non-linear zone and the soil was not failed yet. Therefore, the relative movement between the soil and specimen (pipeline) is very small, and simplification of the interface can be introduced in the model.

MPC (Multi-Point Constraint) in ABAQUS impose constraints between different degrees of freedom of the model. MPC type PIN provides a pinned joint between two nodes which makes the global displacements equal but leaves the rotations independent of each other. Taking into account the reality, the nodes of shell element (specimen or pipeline) are pinned together with the nodes of solid element (soil).

Although the PIN is practical to simulate the interface, some consideration should be given to the specific location around the whole circumference of the pipeline cross section. During the backfill, usually the space beneath the haunches was not compact well. It is better to release some pins at this position. According to the field tests, the hoop strain at the bottom was about 3 times of the hoop strain of the top. This demonstrated the unsymmetrical character of hoop strain about the horizontal centerline.

7.2.5 Boundary Condition

For the soil elements, the nodes at the east and west boundaries (the two lateral sides) were allowed to displace only in the vertical direction (Z) to simulate the settlement of soil due to gravity loads. The nodes at the south and north boundaries (the fore and back sides, except the nodes pinned with the nodes of pipeline elements) were allowed to move in the X and vertical direction (Z) to accommodate the deformation of pipeline cross-section. Displacements in other directions of these four sides were fixed. For bottom boundary, all the three degrees of freedom were fixed.

For the pipe element, the nodes at the south and north boundaries (including the nodes pinned with the nodes of soil elements), were allowed to displace in the vertical (Z) and X direction. However, spring elements were put to these nodes in the longitudinal direction (Y) to simulate the outside soil as springs.

Determination of the soil spring constant (k) was based on the kind of soil (Spangler, 1982). For medium strength clay, the horizontal direction, the modulus of subgrade reaction, k', is 20 MN/m^3. Therefore,

$$k = k'A = 524628 \text{ N/m}.$$

A is the average area of each node with axial spring, which is 0.02623 m^2.

7.2.6 Loading Condition – Excavator

Excavator usually needs to sit at either left or right of the pipe to excavate the soil at the left or right side of the pipe as shown in Figure 7.13.

Because the excavator may adjust its position during excavation process, critical position, which results in the maximum effect on the pipeline, is preferred to be used in the Finite Element Analysis. The first critical position is the excavator was sitting just in the center of the pipe and the distance of pipe center to either track shoe is identical. The second critical position is when one of the track shoes sitting directly on the pipe. These two critical conditions are displayed in Figure 7.14. The detail comparison of these two critical positions can be decided by making use of Boussinesq equation. The first position usually was not possible and convenient for the excavator to excavate the two side soil of the pipe. The second position is more practical in the excavation process.

In the process of excavation, the excavator will dig the soil, lift up the soil in the bucket, rotate the boom, unloading the soil in the bucket, rotate boom back and be ready for the next digging. This serial of actions will produce un-uniform pressure on the ground through the track shoes. Typically, there are four loading cases in the excavation process, which consists of a period of digging:

(1) Excavator was sitting and not working, which produces uniform pressure under the track shoes;

(2) Excavator is digging soil, which may produce a digging force and non-uniform pressure under the track shoes with higher pressure at the back part;

(3) Excavator is lifting up the soil in the bucket, which produces non-uniform pressure under the track shoes with higher pressure at the front part;

(4) Excavator unloads the soil in the bucket and the boom rotates about 90°, which produce different pressure under each track shoe with higher pressure at the right shoe (the ditch spoil was put at the right of pipeline).

The typical excavator operation was a periodical process of four cases mentioned above, (1) → (2) → (3) → (4) → (1).

The excavator position relative to the pipeline and loading cases in a period of digging are considered together to determine the most practical and critical excavator loading model in the FEA model.

7.2.7 Excavation – Removal of Soil

During the excavation process, the soil in the ditch before the excavator is removed gradually. The removal of soil is simulated by removing the soil elements which present the ditch soil. When the soil is removed, the load due to the gravity of the soil elements that is ever exerting on the remaining part of the model at the nodes on the boundary between them gradually ramped down to zero (ABAQUS User Manual, 2004). The effect of the removed region on the rest of the model is completely absent only at the end of the removal step. The forces are ramped down gradually to ensure that element removal has a smooth effect on the model.

7.2.8 Steps to Simulate Excavation Process

The excavation process is a process in which the excavator sits on the first position, removes the soil before it and moves backwards to the next new position. The effect of excavation is relative to the original buried state of the specimen, therefore, in the first step, the gravity load is applied to the soil elements.

The following sequence of steps is put in the FEA model:

(1) Apply Soil Gravity Loads ;(A geostatic stress field procedure is used to verify that the initial geostatic stress field is in equilibrium with applied loads and boundary conditions and to iterate, if necessary, to obtain equilibrium. The *GEOSTATIC procedure is normally used as the first step of a geotechnical analysis; in such cases gravity loads are applied during this step. Ideally, the loads and initial stresses should exactly equilibrate and produce zero deformations. However, in complex problems it may be difficult to specify initial stresses and loads that equilibrate exactly. ABAQUS will check for equilibrium during the *GEOSTATIC procedure and iterate, if needed, to obtain a stress state that equilibrates the prescribed boundary conditions and loads. This stress state, which is a modification of the stress field defined by the *INITIAL CONDITIONS option, will then be used as the initial stress field in a subsequent *SOILS or *STATIC analysis. ABAQUS standard user manual, 6.7.2, Geostatic stress state)

(2) Excavator Sitting at Section 3;

(3) Remove Soil Elements Before Section 3;

(4) Excavator Leave from Section 3;

(5) Excavator Sitting at the middle of Section 3 and 5;

(6) Remove Soil Elements Before the middle of Section 3 and 5;

(7) Excavator Leave from the middle of Section 3 and 5;

(8) Excavator Sitting at Section 5;

(9) Remove Soil Elements Before Section 5;

(10) Excavator Leave from Section 5;

(11) Excavator Sitting at the middle of Section 5 and 7;

(12) Remove Soil Elements Before the middle of Section 5 and 7;

(13) Excavator Leave from the middle of Section 5 and 7;

(14) Excavator Sitting at Section 7;

(15) Remove Soil Elements Before Section 7.

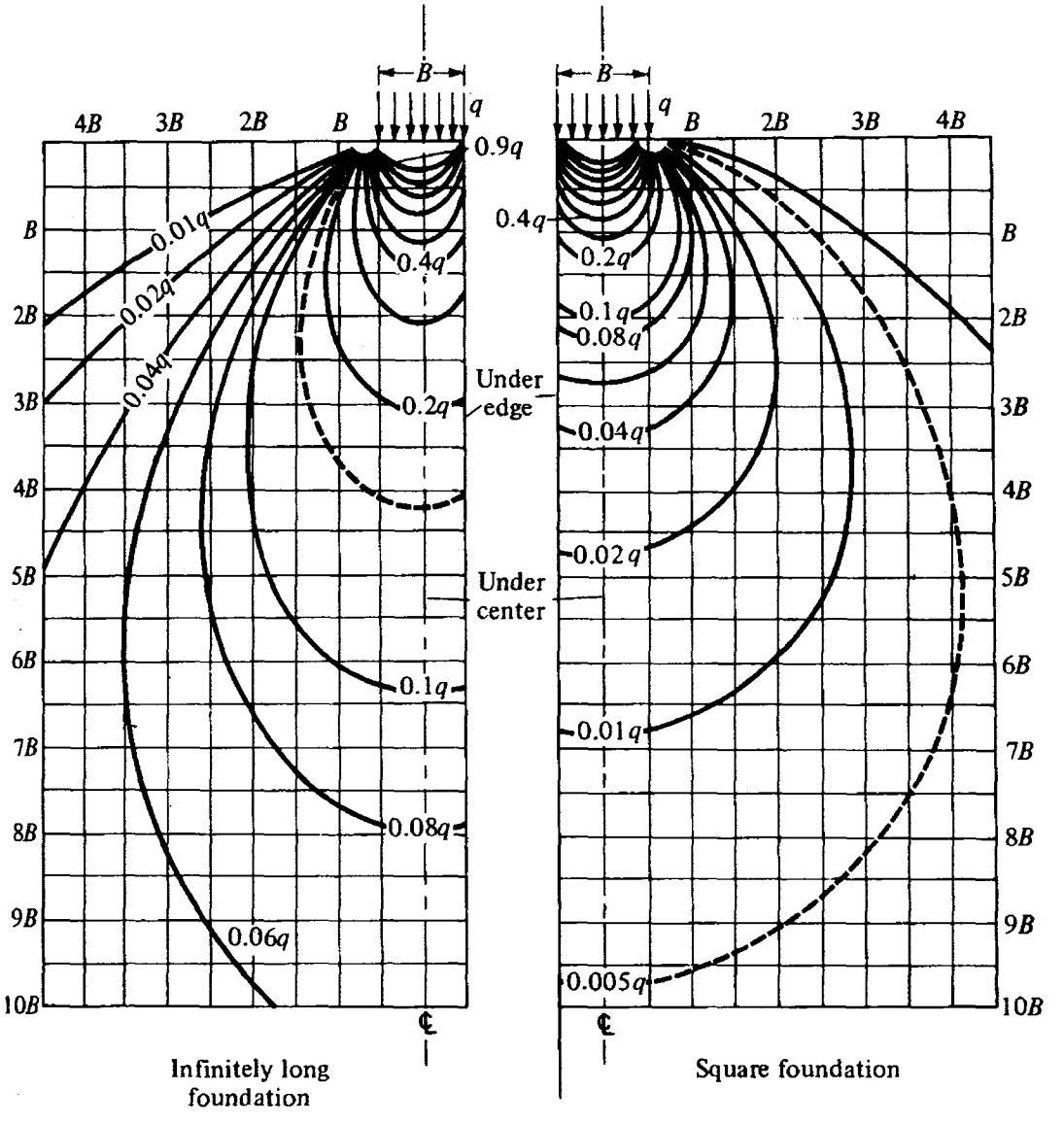

Figure 7.1 Contours of equal vertical stress under a loaded area of width B according to Boussinesq analysis (Spangler, 1982)

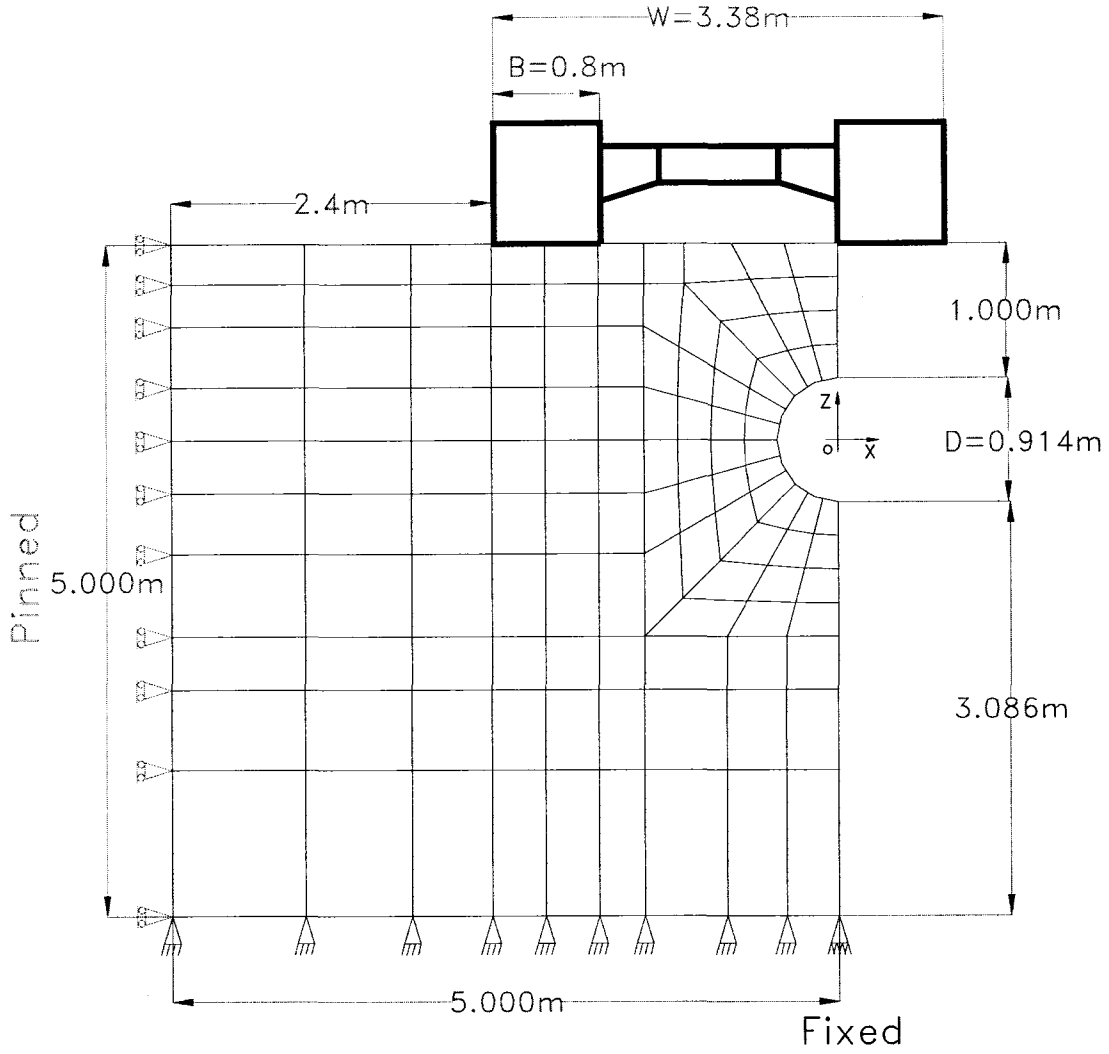

Figure 7.2 Dimension of the mesh in X-Z plane (only left part was shown and the right part is symmetry)

(X: horizontal, Z: vertical, Origin: center of pipe)

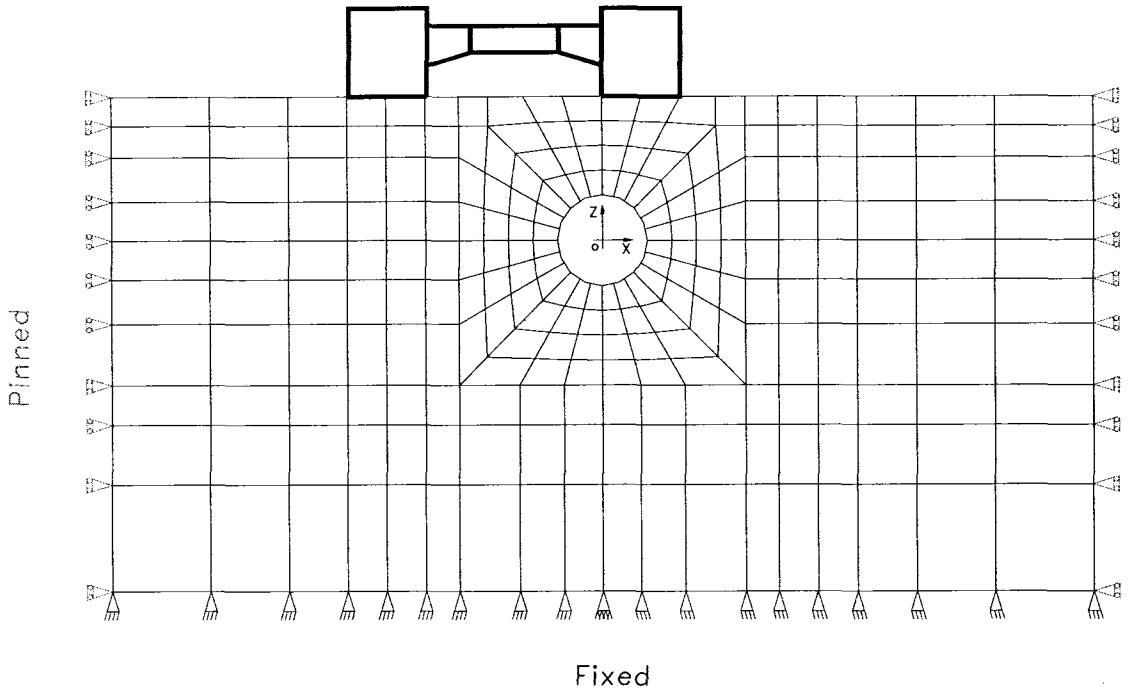

Figure 7.3 Whole meshes in X-Z plane

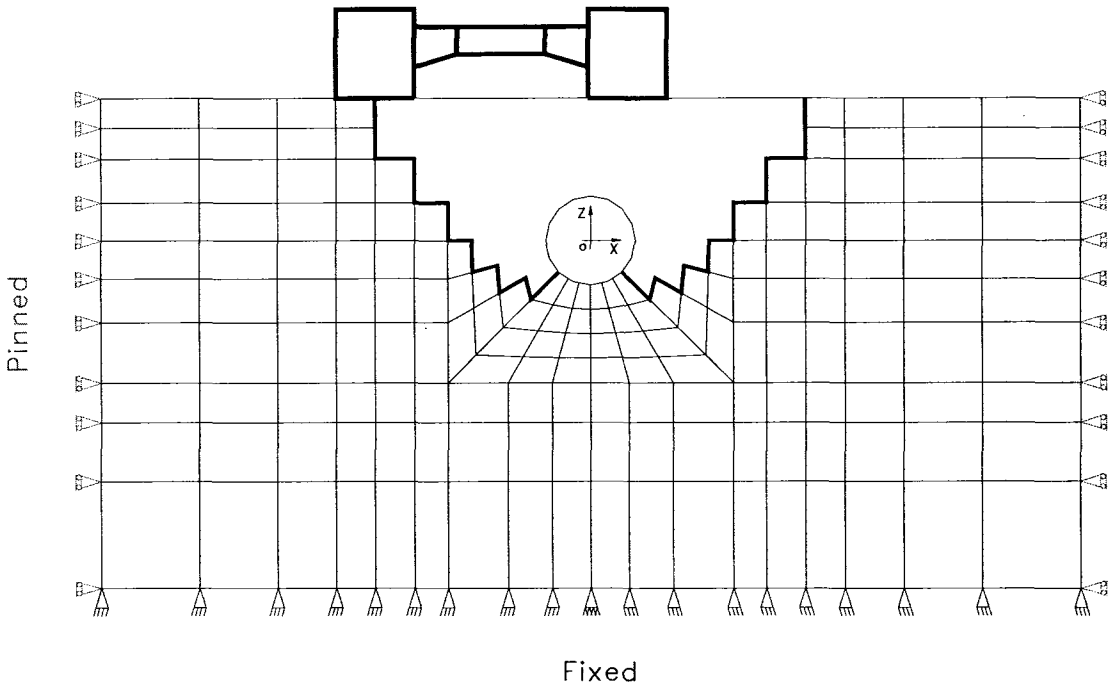

Figure 7.4 Whole meshes in X-Z plane after excavation

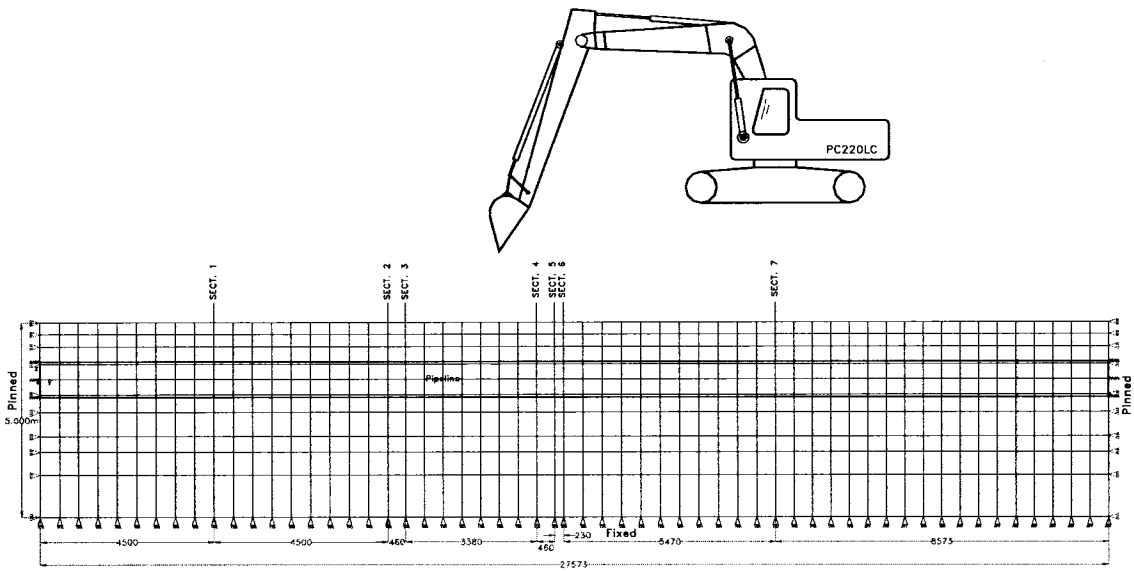

Figure 7.5 Mesh in Y-Z plane (X=0)

(Y: horizontal, Z: vertical, Origin: center pipe at the left end)

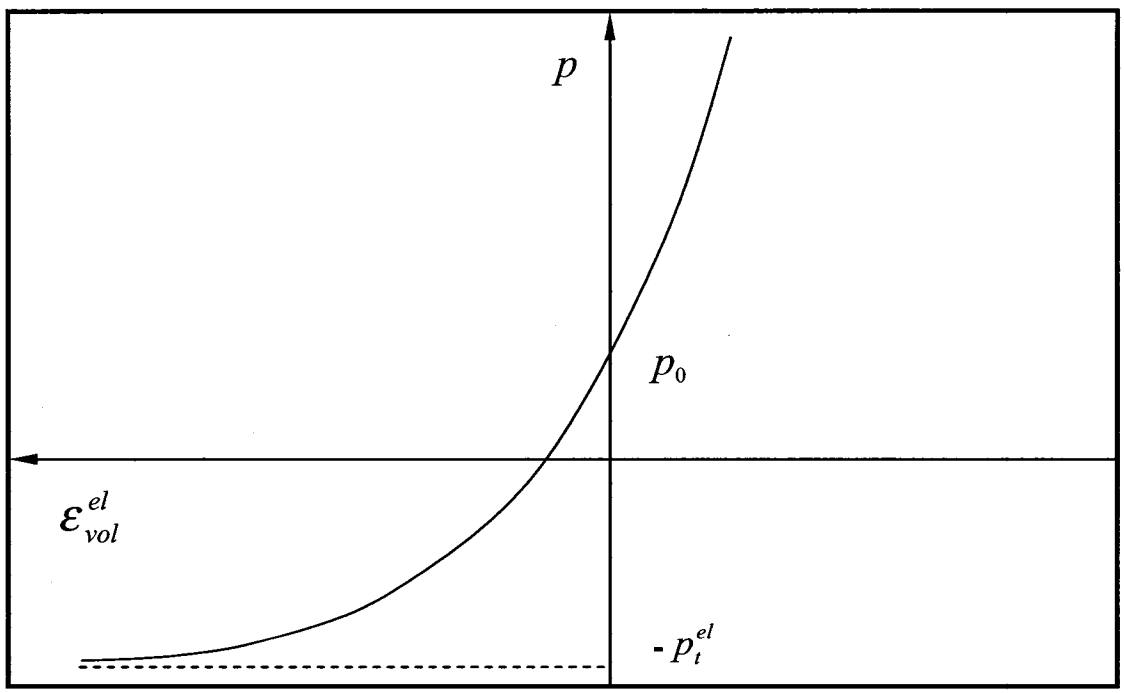

Figure 7.6 Porous elastic volumetric behaviour

(ε_{vol}^{el} = the elastic part of volume strain)

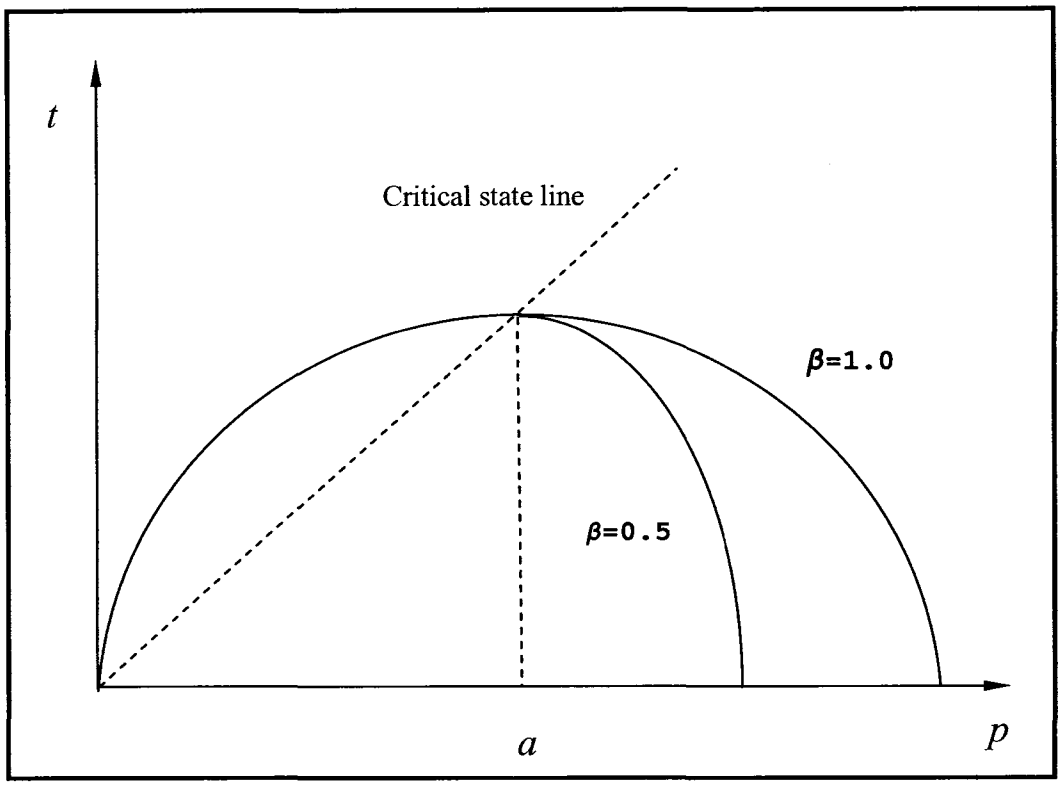

Figure 7.7 Clay yield surface in the p-t plane

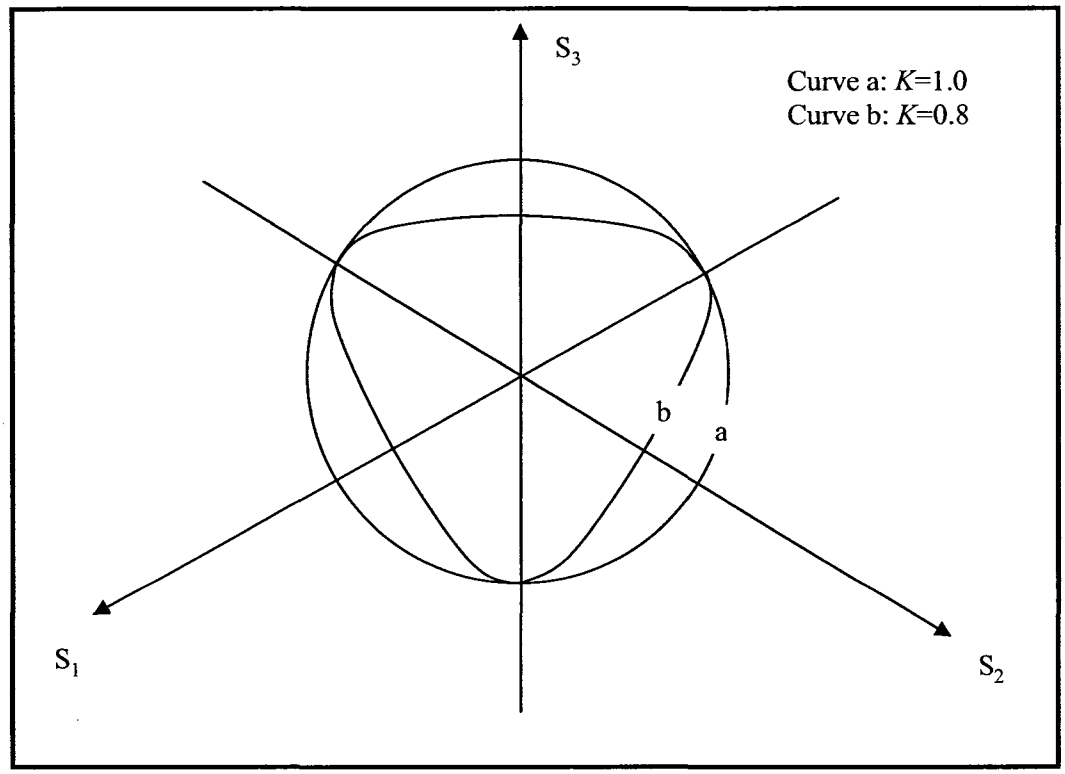

Figure 7.8 Clay yield surface sections in the Π-plane

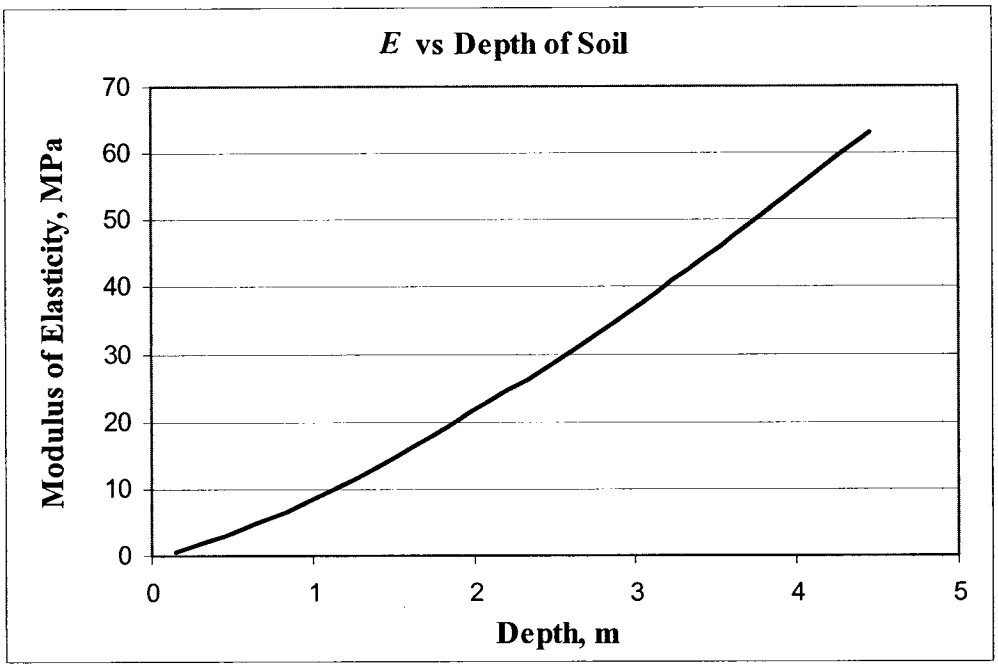

Figure 7.9 Modulus of elasticity E, varied with depth of soil (n=1.3475, K=1278)

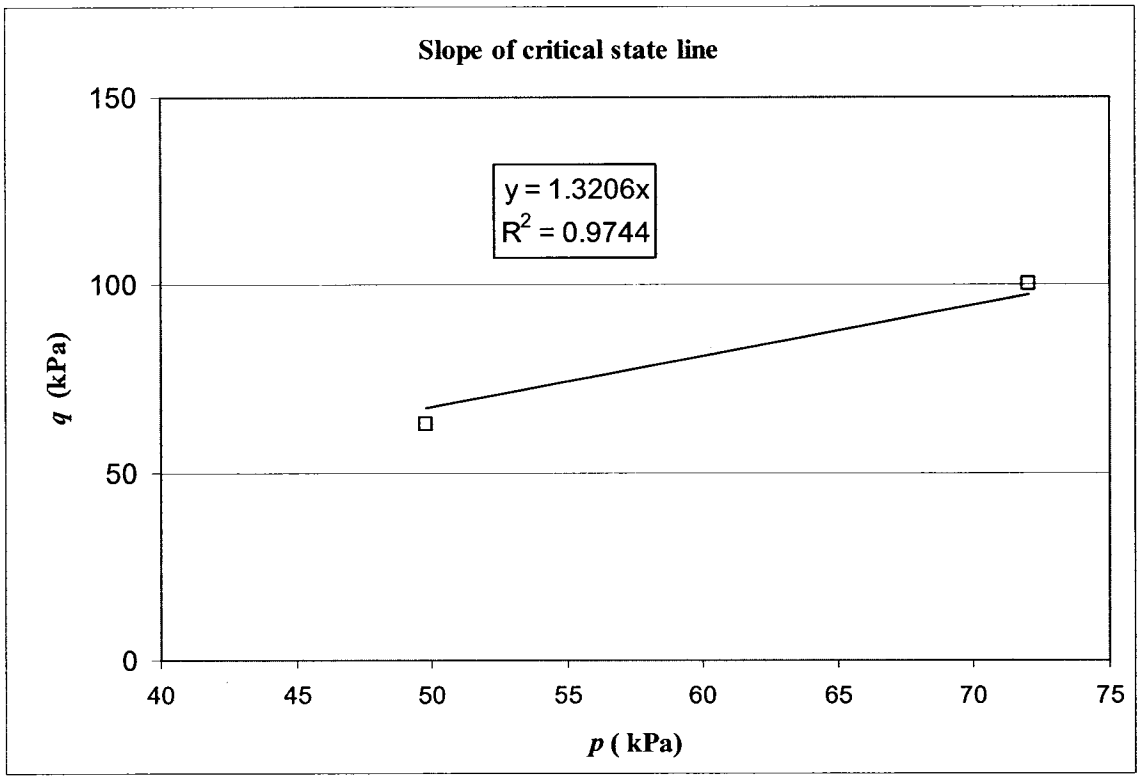

Figure 7.10 Determination of M, slope of critical state line by CU triaxial test

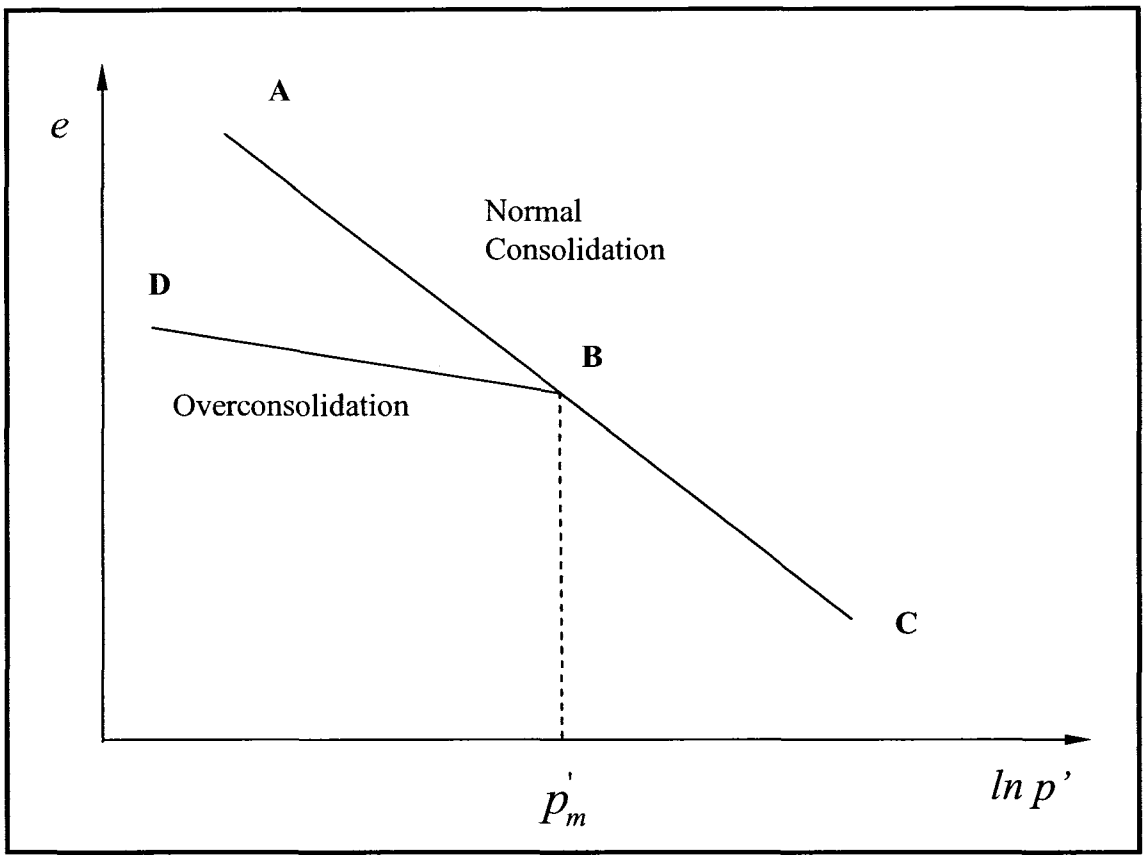

Figure 7.11 Normal consolidation and overconsolidation

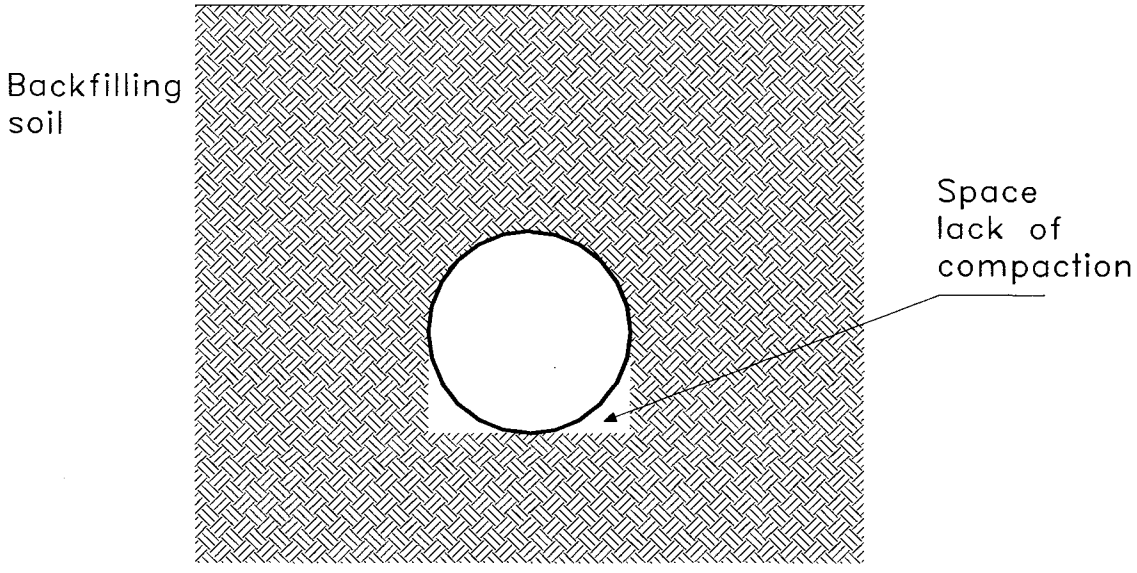

Figure 7.12 MPC around the circumferential direction

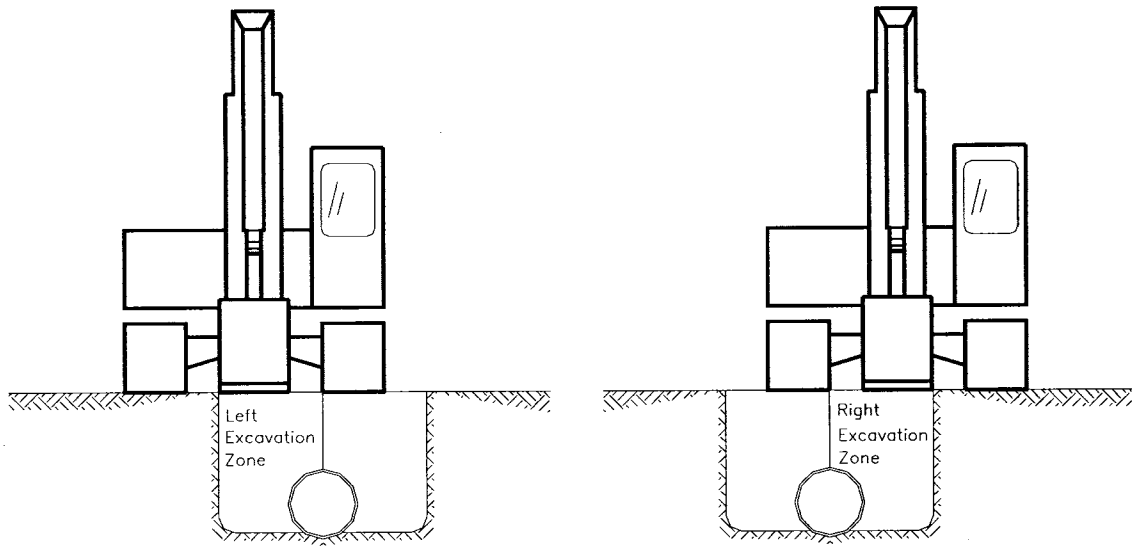

Figure 7.13 Excavator positions during excavation process

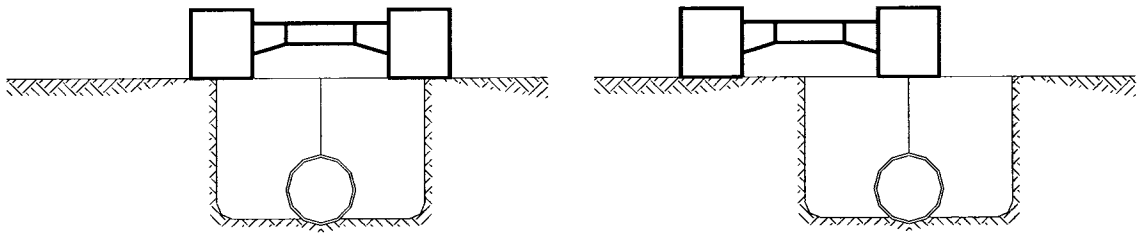

Figure 7.14 Critical positions of excavator during excavation process

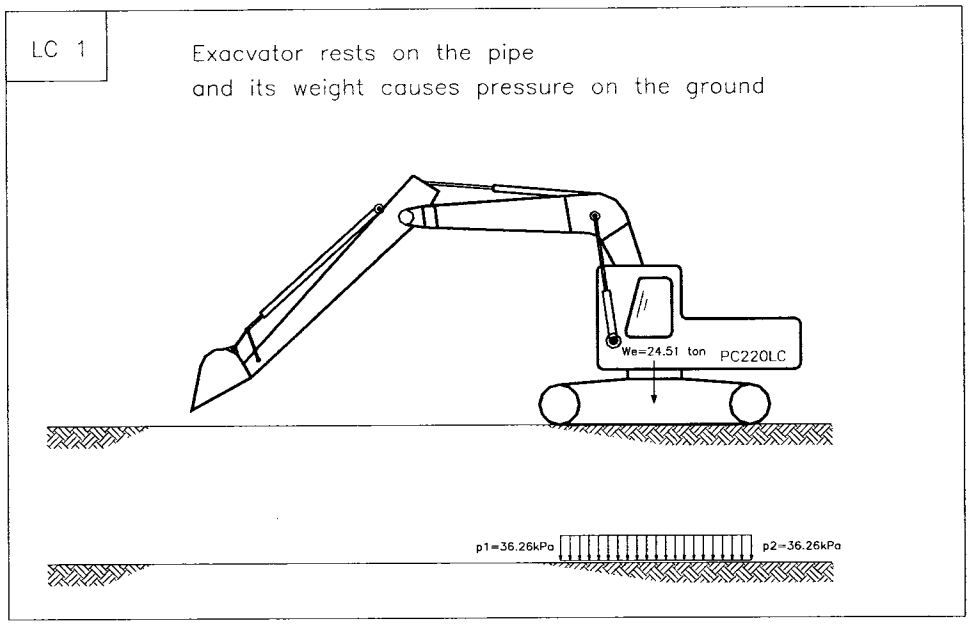

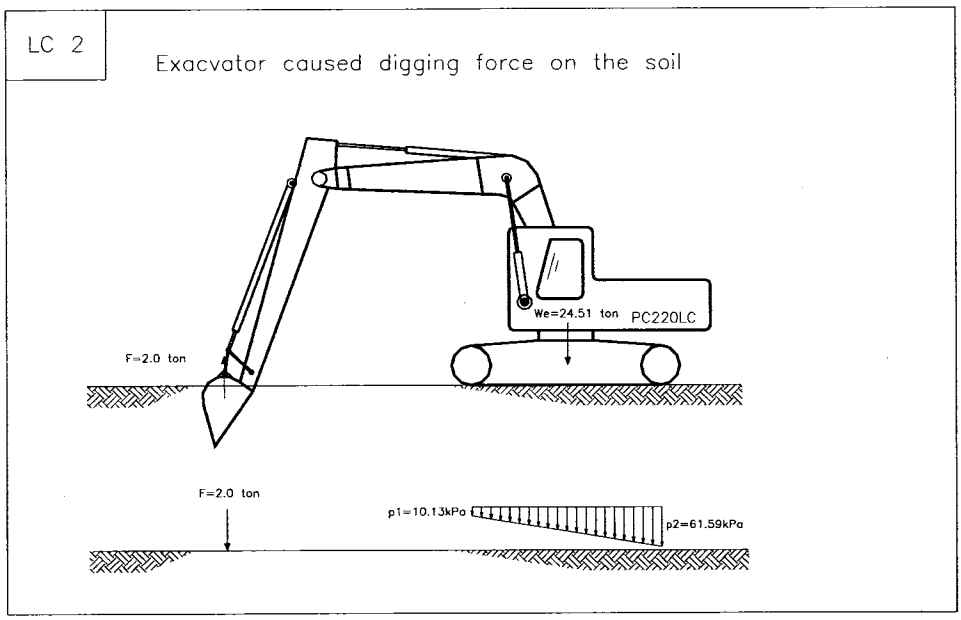

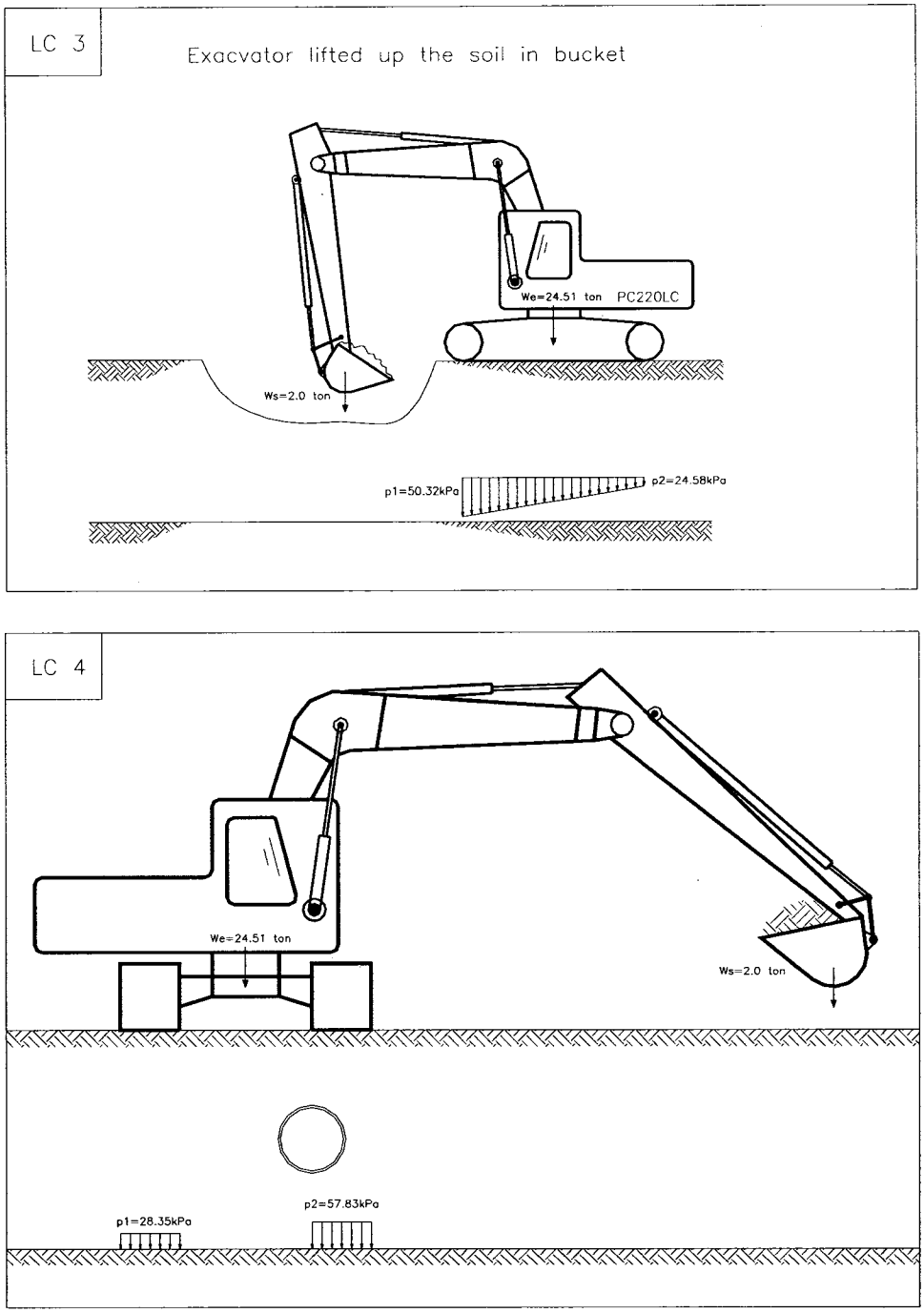

Figure 7.15 Four loading cases in a period of digging

8 DISCUSSION OF EXPERIMENTAL AND NUMERICAL RESULTS

The FEA model is validated with field test result. The summer un-pressurized test was chosen to compare with FEA results. The soil properties in the model are taken from the soil tests which can represent the soil in summer. The static analysis is performed in this model and the dynamic effects can be taken into account using impact factor.

8.1 Comparison of Test and FEA Results

The comparison of the result of summer un-pressurized test with FEA is presented from Figure 8.1 to Figure 8.21. The test data shown in the figures are approximately static by averaging the original test data in every 100 seconds to remove dynamic effect.

The trend of the result of test and FEA is very similar as shown in the figures. The typical process of deformation of the whole specimen is displayed in Figure 8.22.

8.2 Discuss of the Results of Test and FEA

8.2.1 Hoop Strain

The comparison of the maximum hoop strain of test and FEA is shown in Table 8.1 under the critical condition 1. The excavator is sitting on the section 3, 5, 6 and 7 and produced maximum hoop strain in these sections respectively. From the table it can be seen most of the ratio of FEA over Test (static) is close to 1.0 which represent the good agreement of FEA over test results. The ratio is a little bigger at 90° position and smaller at 270° position. This is because in the FEA model the position of excavator is located in the left side of the pipeline. In the test, the position of excavator may vary a little. The

hoop strain in the column of Test (dynamic) is the maximum in the original test which caused by the weight and rocking of excavator. In the last column is given the ratio of the maximum in the original test over the FEA. The ratio is between 0.95~2.20 with average of 1.28. The impact factor in the summer test varied from 1.14~2.0 with average 1.38. Therefore, the FEA result can give a good estimation of the maximum hoop strain using the impact factor.

When the section is exposed in the excavation process, in the figure we can see in the front section, mainly section 1 and 3, the sign of hoop strain changed sign both in the test and FEA results. This is the critical condition 2 to produce the maximum hoop strain. The hoop strain is caused by the release of gravity loads. As analyzed in the test results, the maximum hoop strain occurred at the bottom of the section. In the FEA analysis, the maximum hoop strain due to the application of gravity load is +108με and -104με at the bottom. In the test, the maximum hoop strain is +144με and -120με. The ratio of FEA over test is 0.75 and 0.87 respectively.

8.2.3 Deformation

From Figure 8.17, it can be the see the result of deformation in test and FEA agreed very well. The comparison of the maximum deformation of test and FEA is shown in Table 8.2 when the excavator is sitting on the section 6 and produced maximum deformation in this section. The ratio is between 0.96~0.97. Considering the dynamic response, the ratio of the maximum deformation in original test over FEA is from 1.23 to 1.28. The impact factor in the summer test varied from 1.16~1.27 with average 1.22. Therefore, the FEA result can give a good estimation of the maximum deformation using the impact factor.

8.2.3 Longitudinal Strain

The comparison of the maximum longitudinal strain of test and FEA is shown in Table 8.3 under the critical condition 1. The excavator is sitting on the section 2, 3, 4, 5 and 7 and produced maximum longitudinal strain in these sections respectively. From the table it can be seen most of the ratio of FEA over Test (static) is close to 1.0 which represent the good agreement of FEA over test results. The hoop strain in the column of Test (dynamic) is the maximum in the original test which caused by the weight and rocking of excavator. In the last column is given the ratio of the maximum in the original test over the FEA. The ratio is between 0.99~1.39 with average of 1.23. The impact factor in the summer test varied from 1.07~1.42 with average 1.27. Therefore, the FEA result can give a good estimation of the maximum longitudinal strain using the impact factor.

When the section is exposed in the excavation process, in the figure we can see in the front section, mainly section 1, 2 and 3, the sign of longitudinal strain changed sign both in the test and FEA results. This is the critical condition 2 to produce the maximum longitudinal strain. Under this condition the comparison of the maximum longitudinal strain of test and FEA is shown in Table 8.4. The ratio of FEA over Test (static) varied from 1.13 to 1.71 which means the FEA give a conservative prediction. Considering the dynamic effect, the ratio of FEA over Test (dynamic) is from 0.83 to 1.36. Therefore, the FEA analysis can still give a good estimation of maximum longitudinal strain under this condition.

8.3 Factors Influencing the Simulation in the FEA Model

As shown in the figures and discussed above, the FEA model established has the

ability to simulate the process of excavation. The FEA results agree well with the test results either in the trend and quantity. However, since the test is field test, some factors can't be controlled well as in the laboratory. These factors might be the compaction and loading of excavator. For example, the excavator's position is not obtained exactly relative to instrumented section in axial direction and to the central line (left and right). The good compaction can increase the soil stiffness, density and strength and therefore, decrease the strain level in the pipeline.

Table 8.1 Comparison of maximum hoop strain between test and FEA

Hoop Strain		FEA 1	Test(static) 2	Test(dynamic) 3	Ratio (1) / (2)	Ratio (1) / (3)	Ratio (3) / (1)
Section 3	0	-111	-117	-120	0.95	0.93	1.08
	90	120	105	118	1.14	1.02	0.98
		-135	-122	-134	1.11	1.01	0.99
	180	101	103	116	0.98	0.87	1.15
		-120	-118	-134	1.02	0.90	1.12
	270	54	92	111	0.59	0.49	2.06
		-73	-101	-118	0.72	0.62	1.62
Section 5	0	154	132	176	1.17	0.88	1.14
		-105	-107	-142	0.98	0.74	1.35
	90	121	101	116	1.20	1.04	0.96
		-137	-125	-143	1.10	0.96	1.04
	180	90	97	114	0.93	0.79	1.27
		-119	-123	-144	0.97	0.83	1.21
	270	50	88	110	0.57	0.45	2.20
		-71	-105	-134	0.68	0.53	1.89
Section 7	0	152	160	195	0.95	0.78	1.28
		-105	-97	-132	1.08	0.80	1.26
	90	120	93	118	1.29	1.02	0.98
		-137	-106	-130	1.29	1.05	0.95
	180	-124	-124	-140	1.00	0.89	1.13

Table 8.2 Comparison of maximum deformation between test and FEA

Deformation		FEA 1	Test(static) 2	Test(dynamic) 3	Ratio (1) / (2)	Ratio (1) / (3)	Ratio (3) / (1)
Section 6	V	-2.16	-2.26	-2.77	0.96	0.78	1.28
	H	2.12	2.19	2.60	0.97	0.82	1.23

Table 8.3 Comparison of maximum longitudinal strain between test and FEA under critical condition 1

Longitudinal Strain		FEA 1	Test(static) 2	Test(dynamic) 3	Ratio (1) / (2)	Ratio (1) / (3)	Ratio (3) / (1)
Section 2	Top	44	56	61	0.79	0.72	1.39
	Btm	-85	-79	-93	1.08	0.91	1.09
Section 3	Top	-86	-81	-85	1.06	1.01	0.99
Section 4	Top	48	40	56	1.20	0.86	1.17
	Btm	-85	-82	-108	1.04	0.79	1.27
Section 5	Top	-91	-108	-126	0.84	0.72	1.38
Section 7	Top	57	68	72	0.84	0.79	1.26
	Btm	-96	-113	-124	0.85	0.77	1.29

Table 8.4 Comparison of maximum longitudinal strain between test and FEA under critical condition 2

Longitudinal Strain		FEA	Test(static)	Test(dynamic)	Ratio	Ratio	Ratio
		1	2	3	(1) / (2)	(1) / (3)	(3) / (1)
Section 1	Top	49	33	36	1.48	1.36	0.73
	Btm	-58	-34	-37	1.71	1.57	0.64
Section 2	Top	53	47	52	1.13	1.02	0.98
	Btm	-49	-36	-59	1.36	0.83	1.20
Section 3	Top	54	44	48	1.23	1.13	0.89

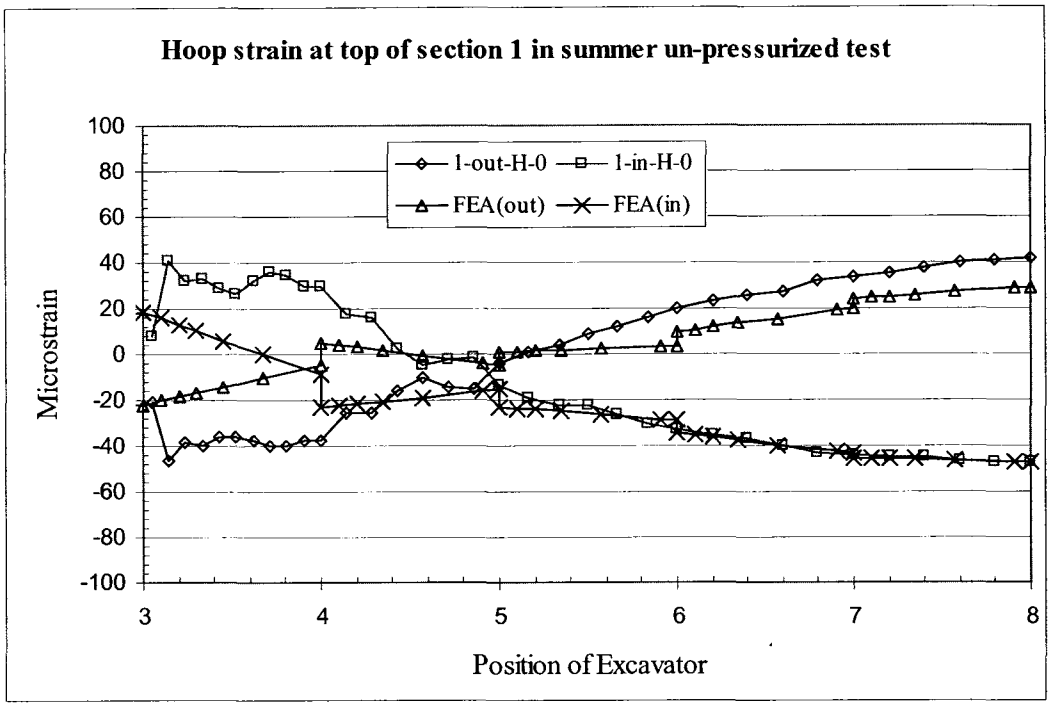

Figure 8.1 Comparison of hoop strain at top of section 1 between test and FEA results

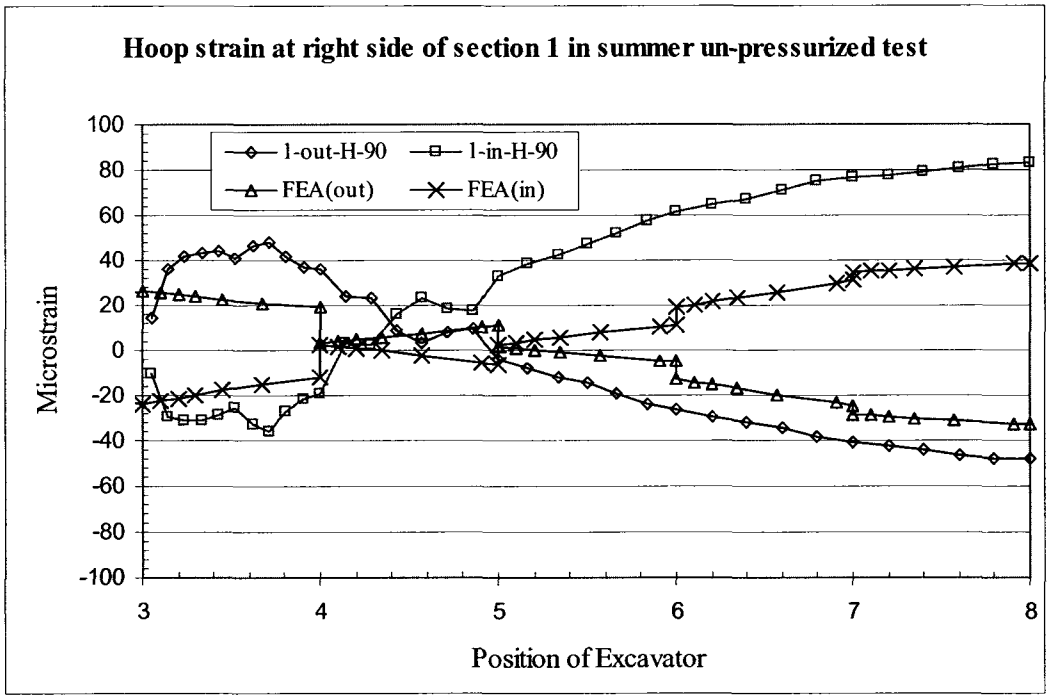

Figure 8.2 Comparison of hoop strain at right side of section 1 between test and FEA results

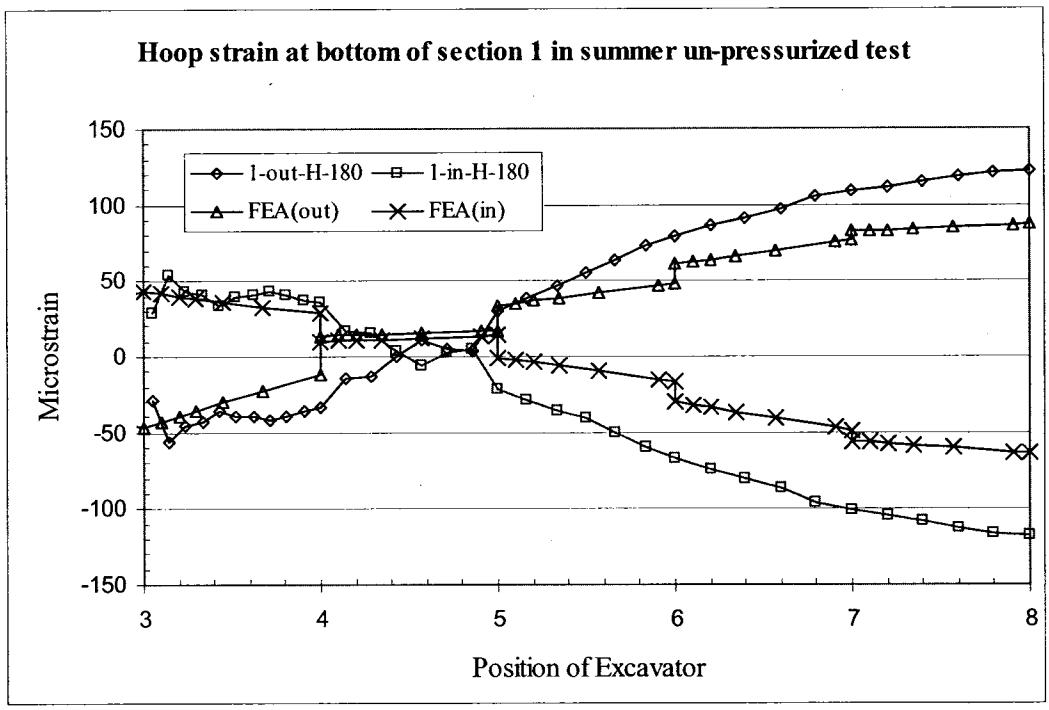

Figure 8.3 Comparison of hoop strain at bottom of section 1 between test and FEA results

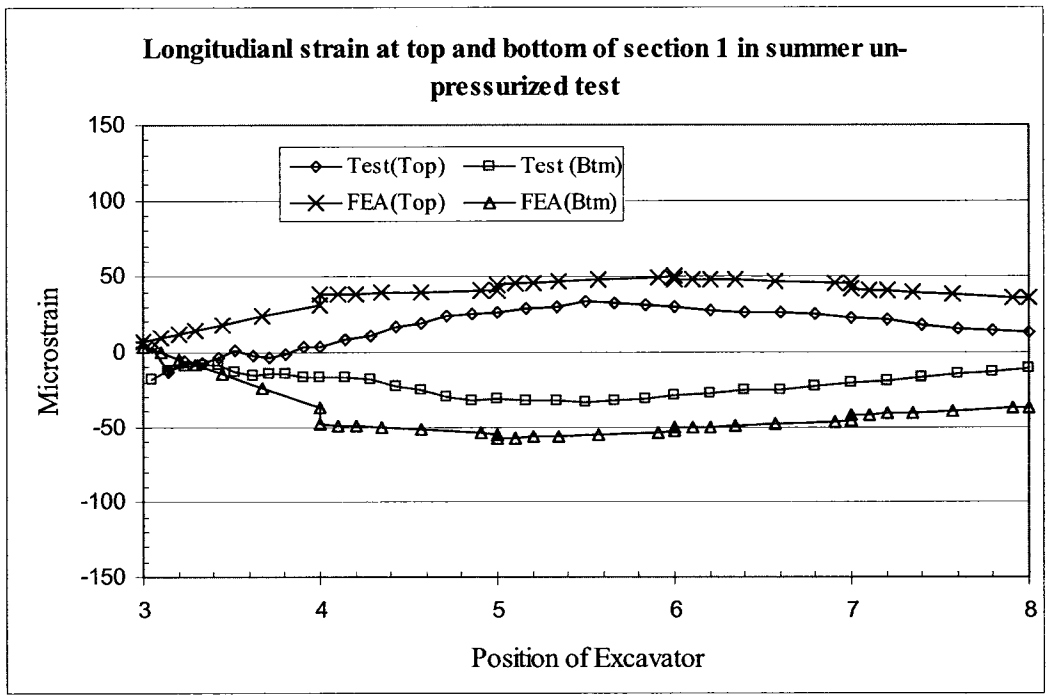

Figure 8.4 Comparison of longitudinal strain at top and bottom of section 1 between test and FEA results

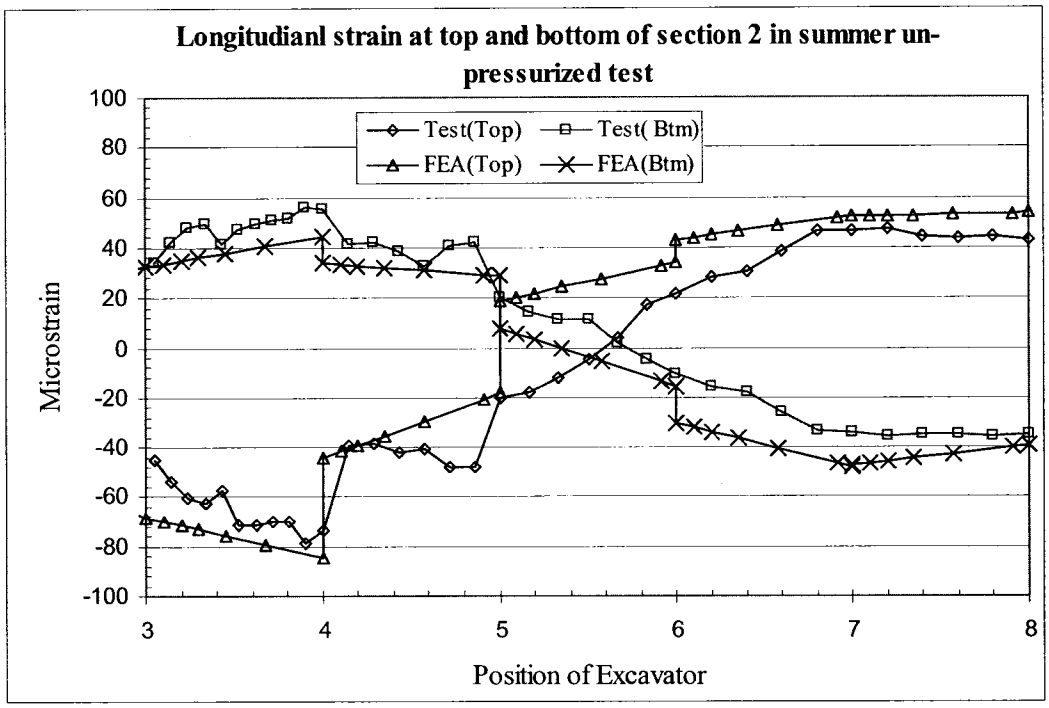

Figure 8.5 Comparison of longitudinal strain at top and bottom of section 2 between test and FEA results

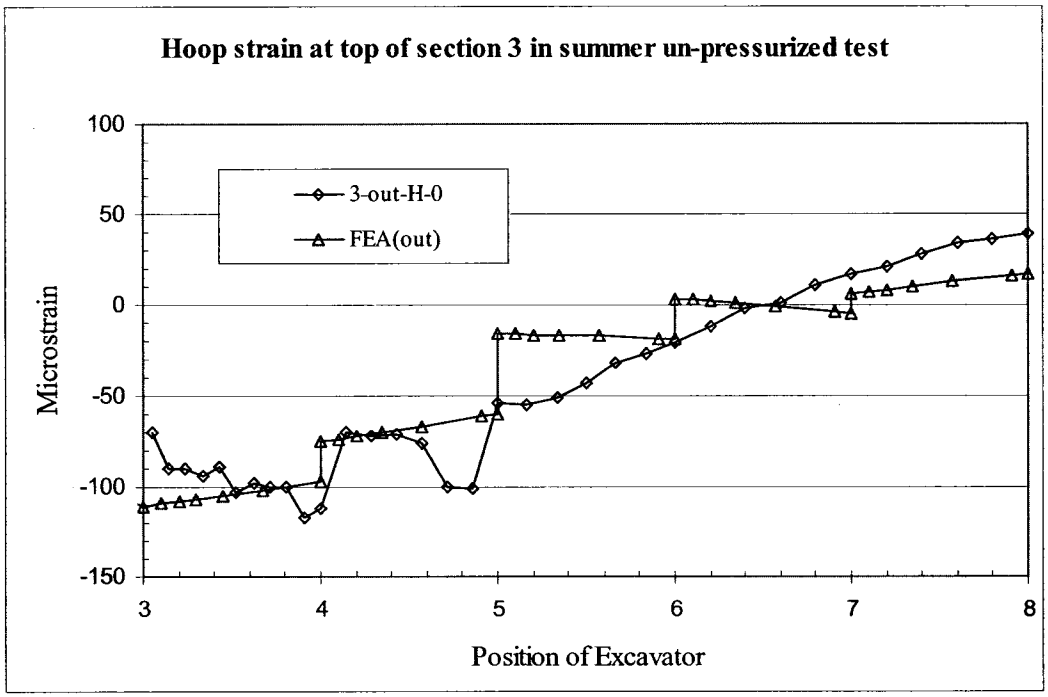

Figure 8.6 Comparison of hoop strain at top of section 3 between test and FEA results

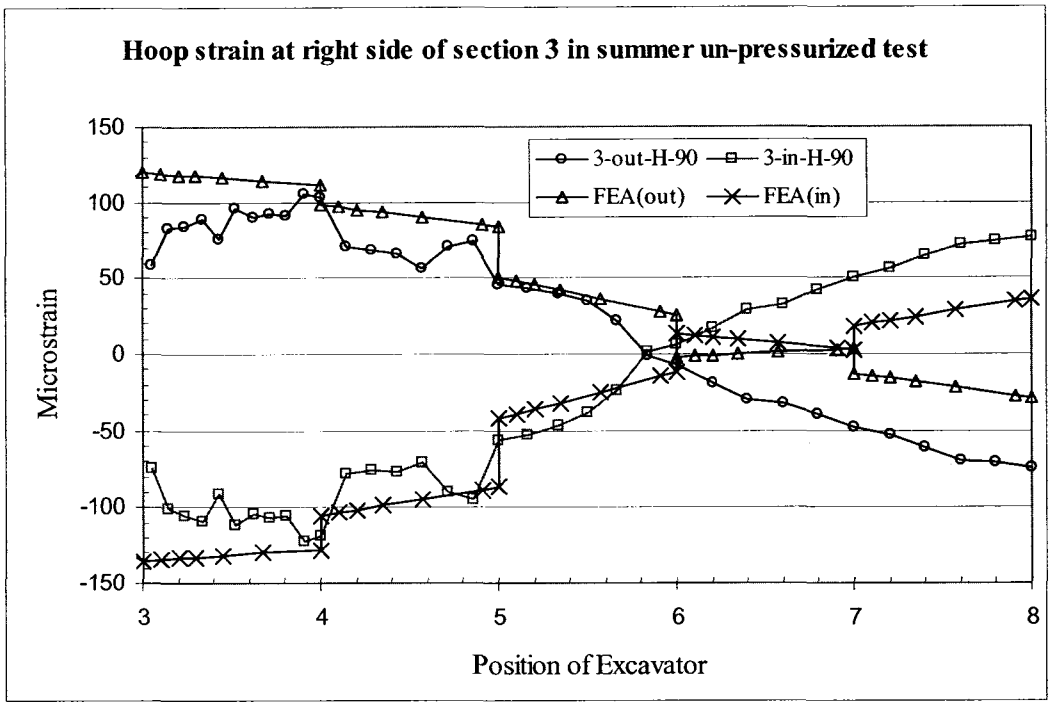

Figure 8.7 Comparison of hoop strain at right side of section 3 between test and FEA results

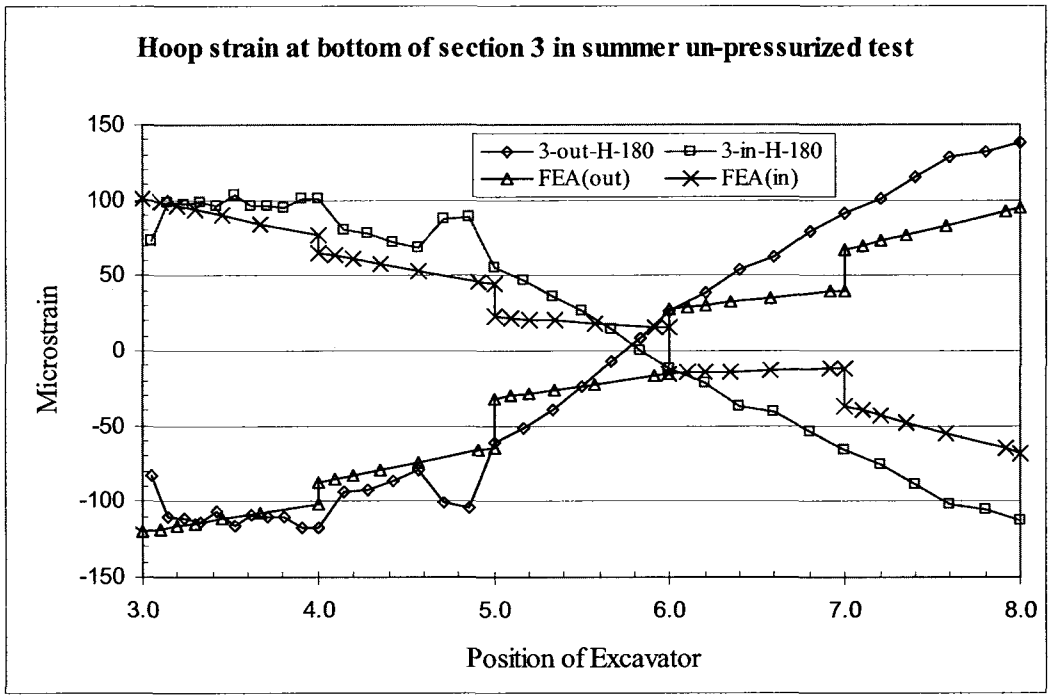

Figure 8.8 Comparison of hoop strain at bottom of section 3 between test and FEA results

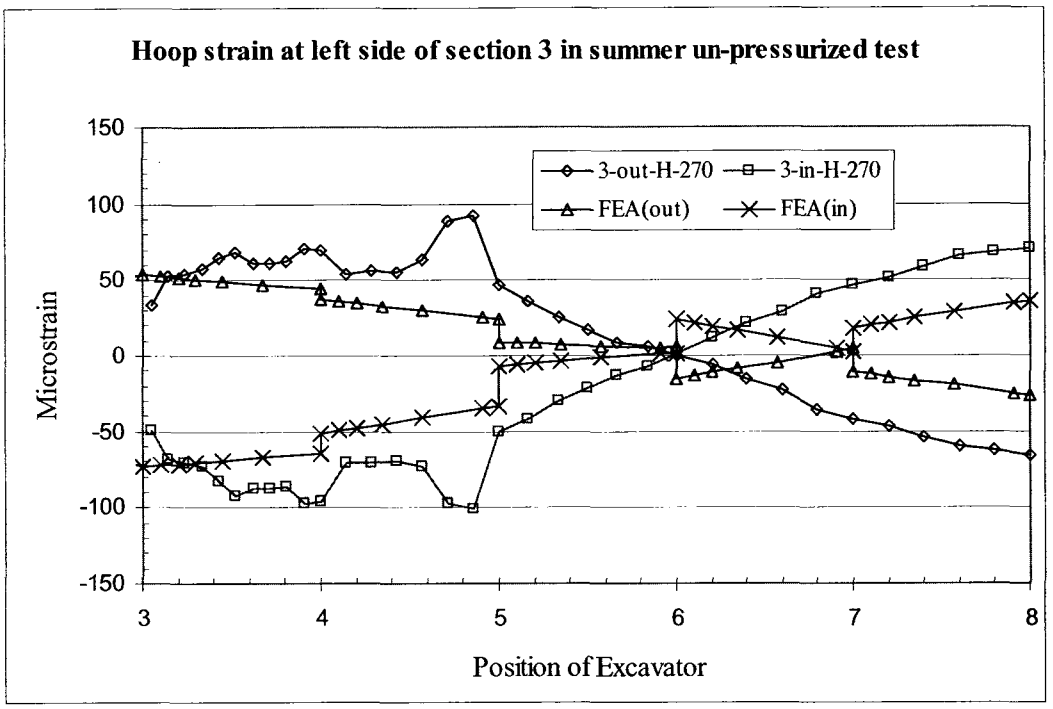

Figure 8.9 Comparison of hoop strain at left side of section 3 between test and FEA results

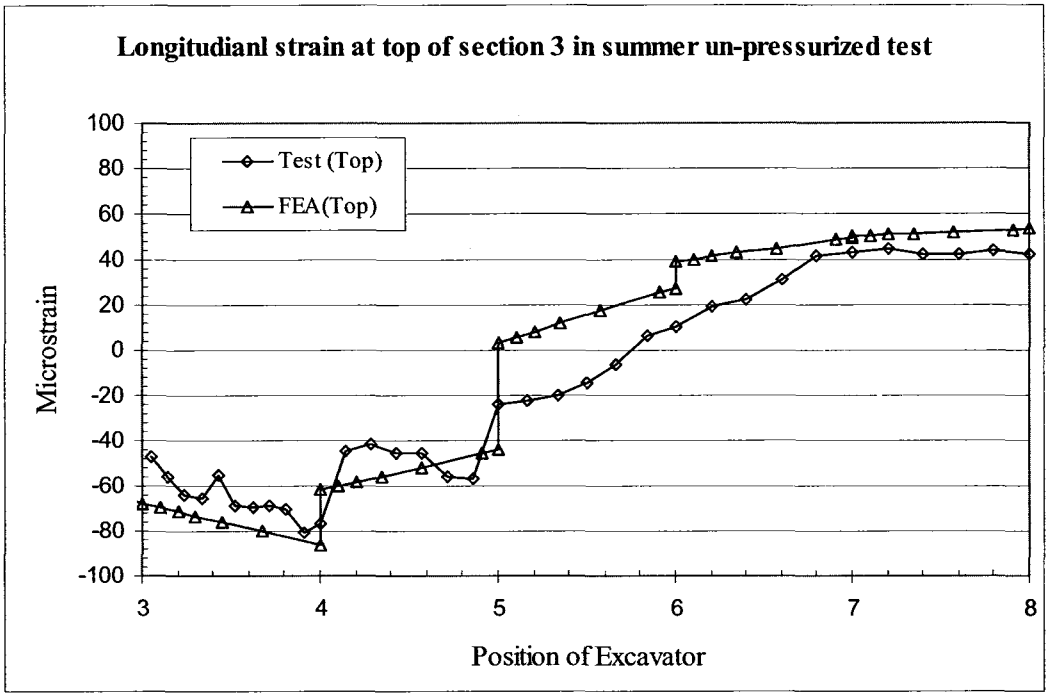

Figure 8.10 Comparison of longitudinal strain at top of section 3 between test and FEA results

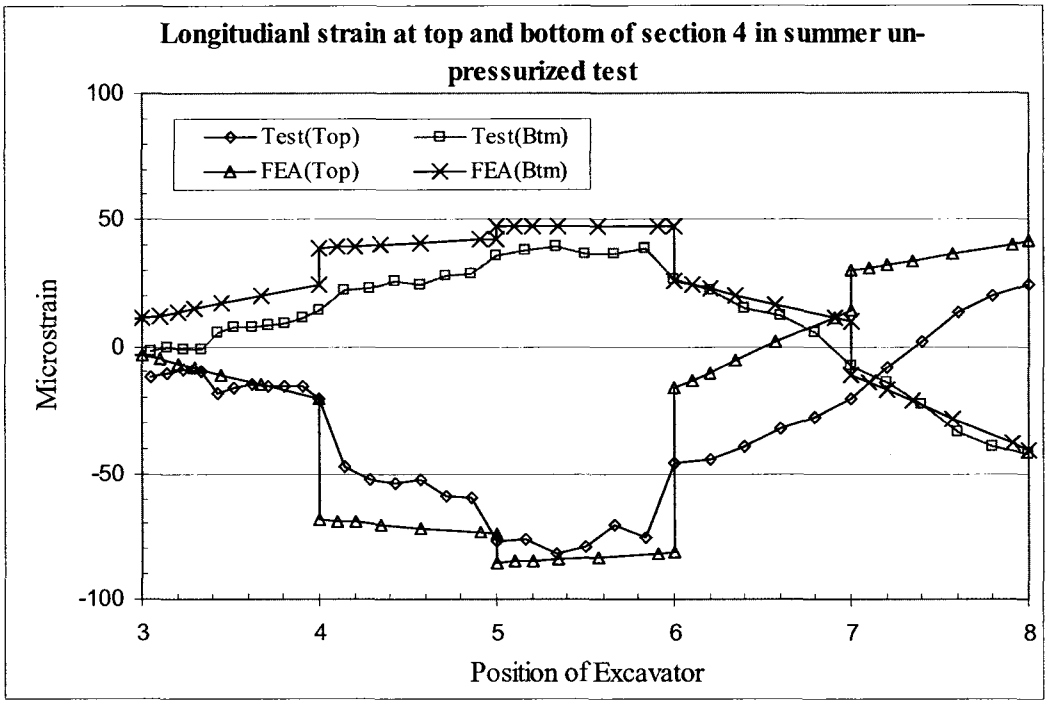

Figure 8.11 Comparison of longitudinal strain at top and bottom of section 4 between test and FEA results

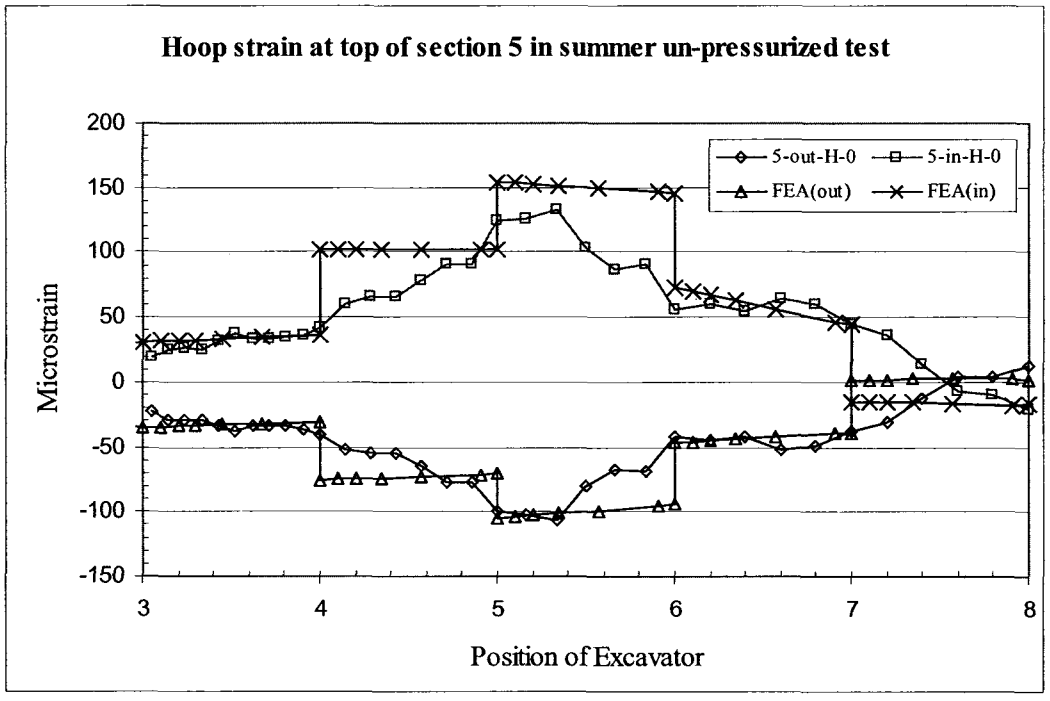

Figure 8.12 Comparison of hoop strain at top of section 5 between test and FEA results

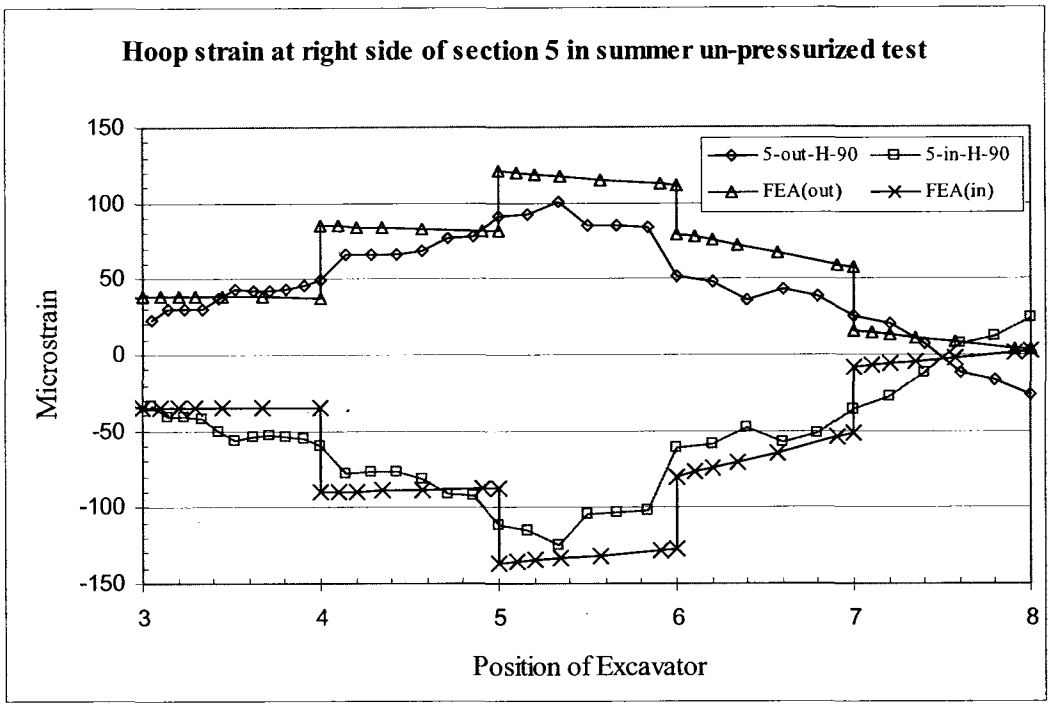

Figure 8.13 Comparison of hoop strain at right side of section 5 between test and FEA results

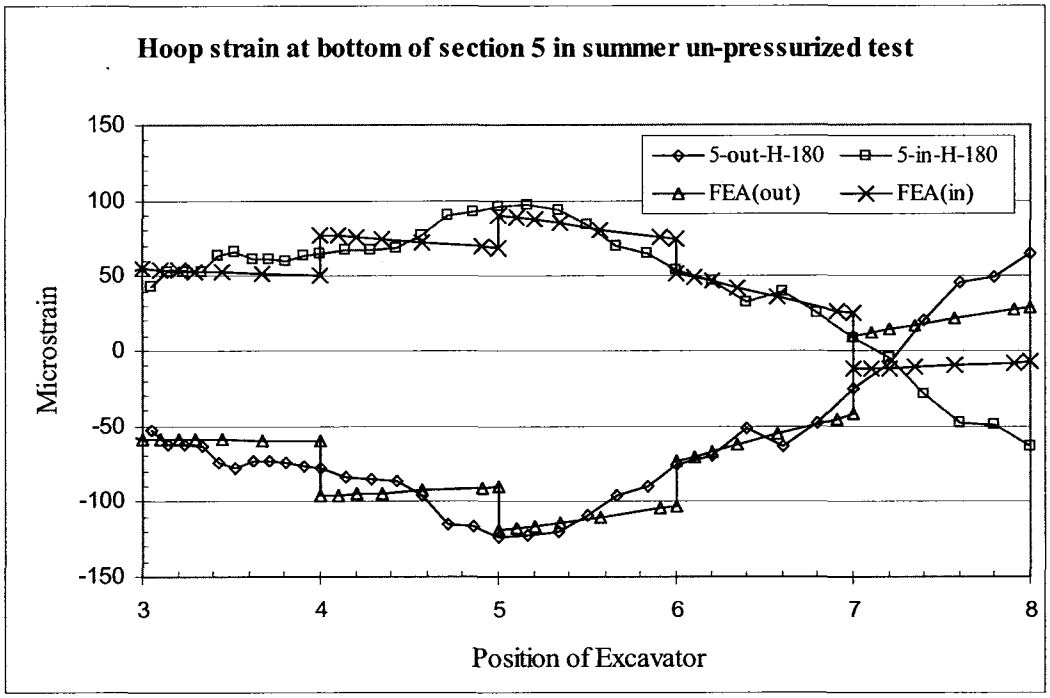

Figure 8.14 Comparison of hoop strain at bottom of section 5 between test and FEA results

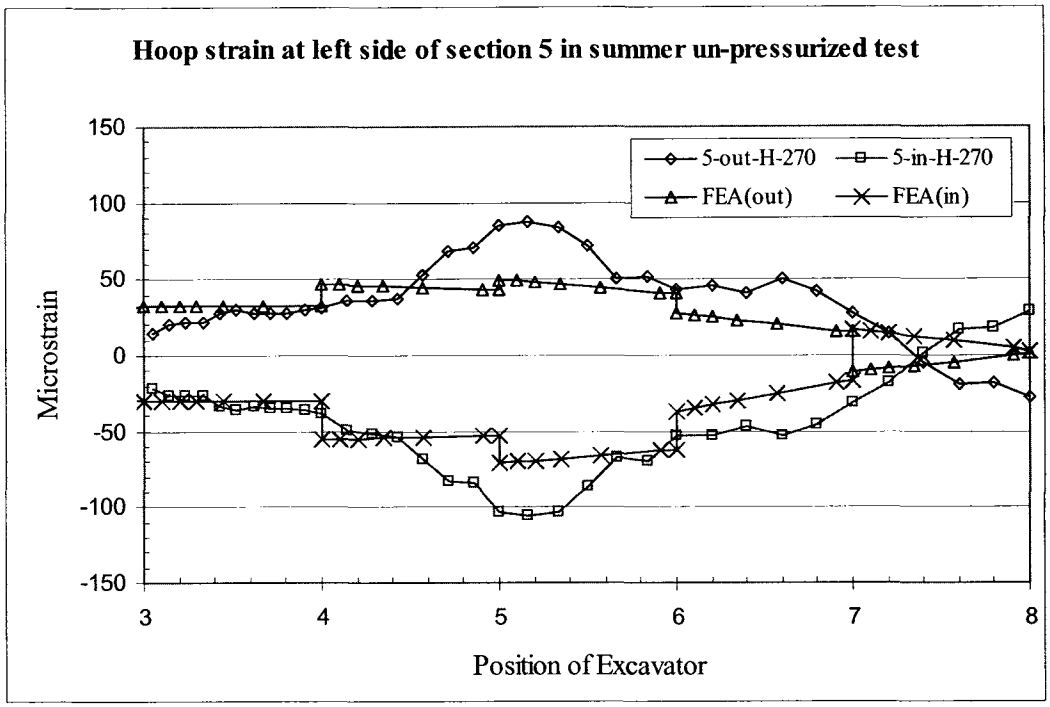

Figure 8.15 Comparison of hoop strain at left side of section 5 between test and FEA results

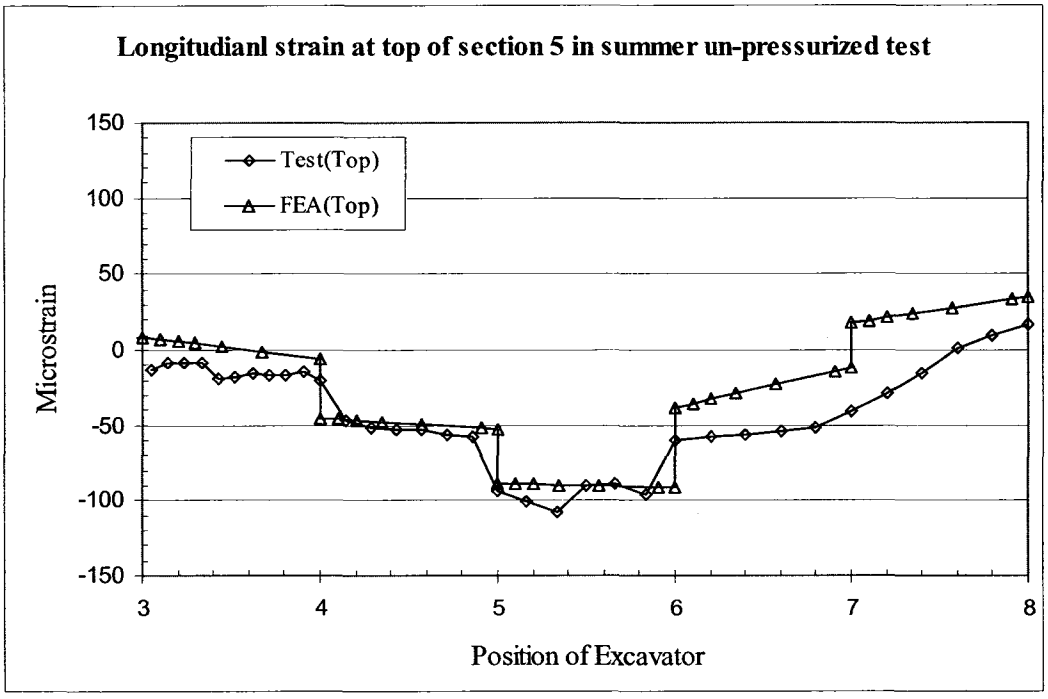

Figure 8.16 Comparison of longitudinal strain at top of section 5 between test and FEA results

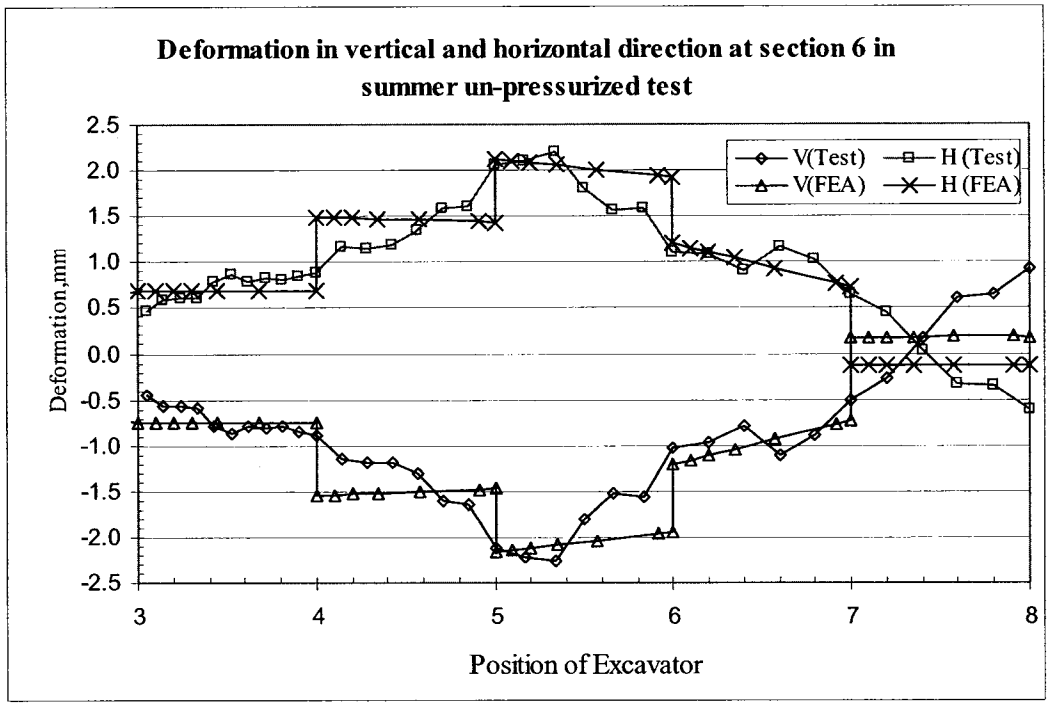

Figure 8.17 Comparison of deformation in vertical and horizontal direction at section 6 between test and FEA results

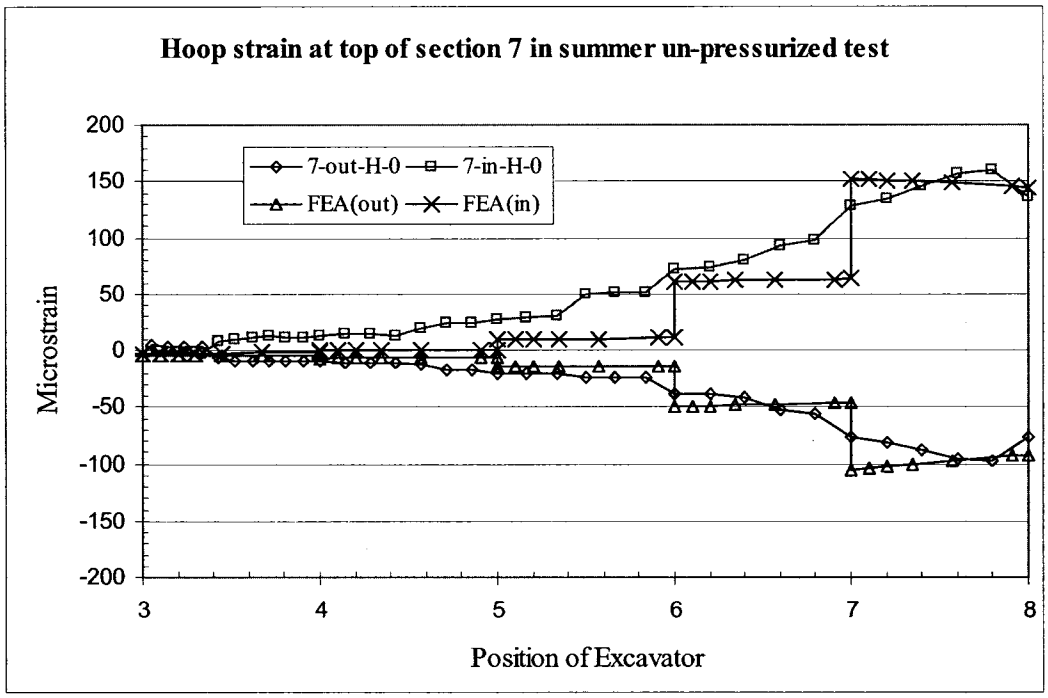

Figure 8.18 Comparison of hoop strain at top of section 7 between test and FEA results

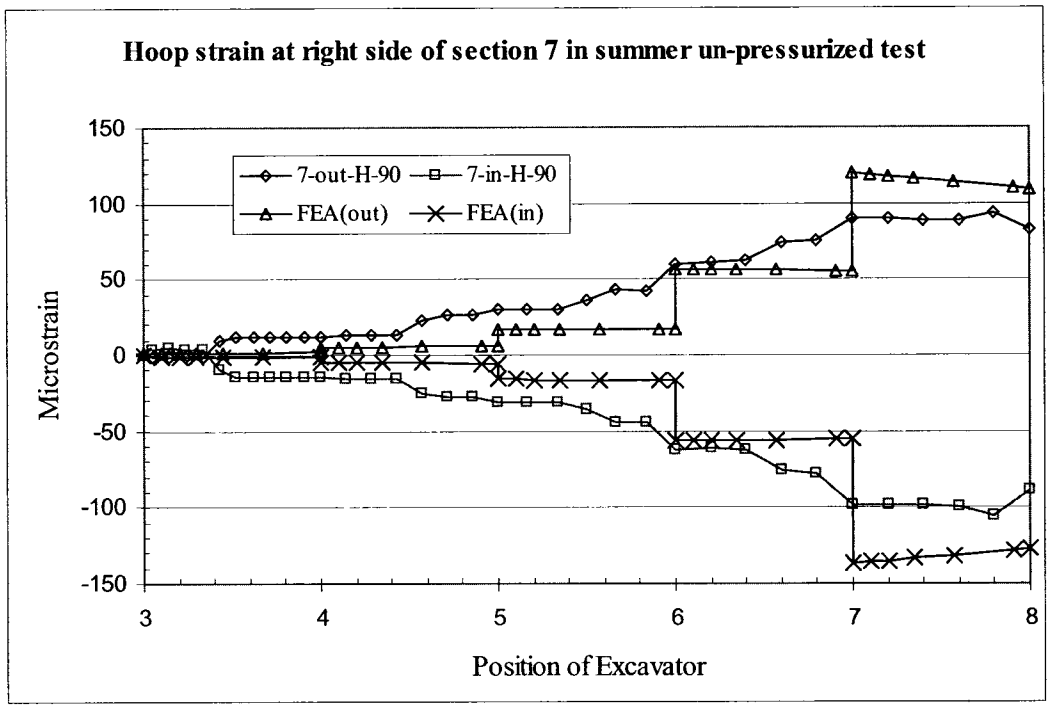

Figure 8.19 Comparison of hoop strain at right side of section 7 between test and FEA results

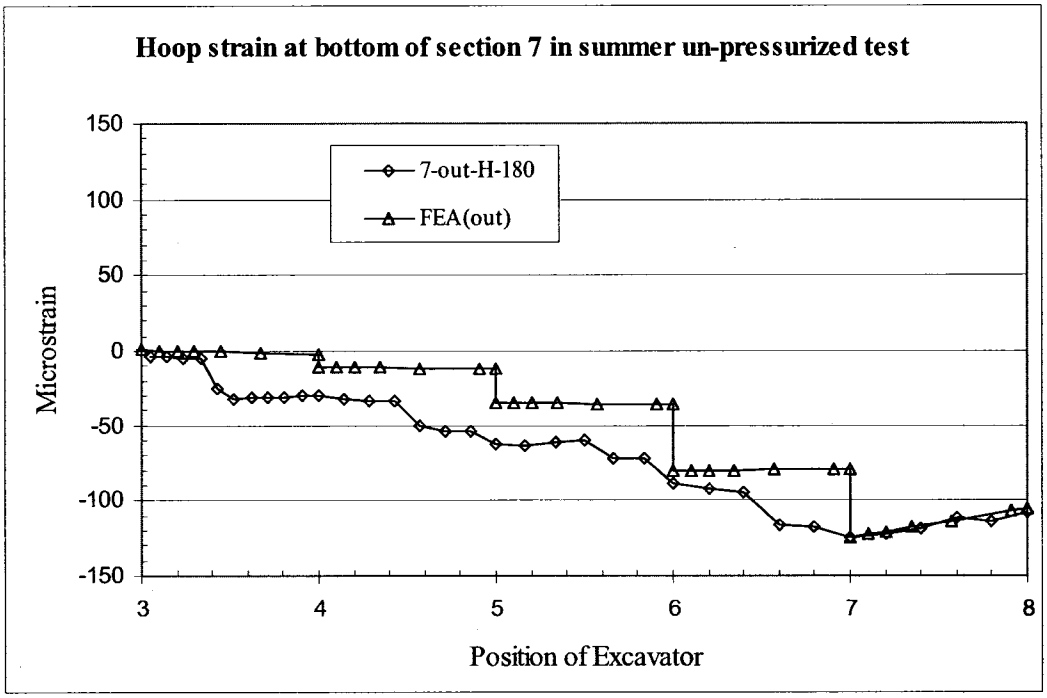

Figure 8.20 Comparison of hoop strain at bottom of section 7 between test and FEA results

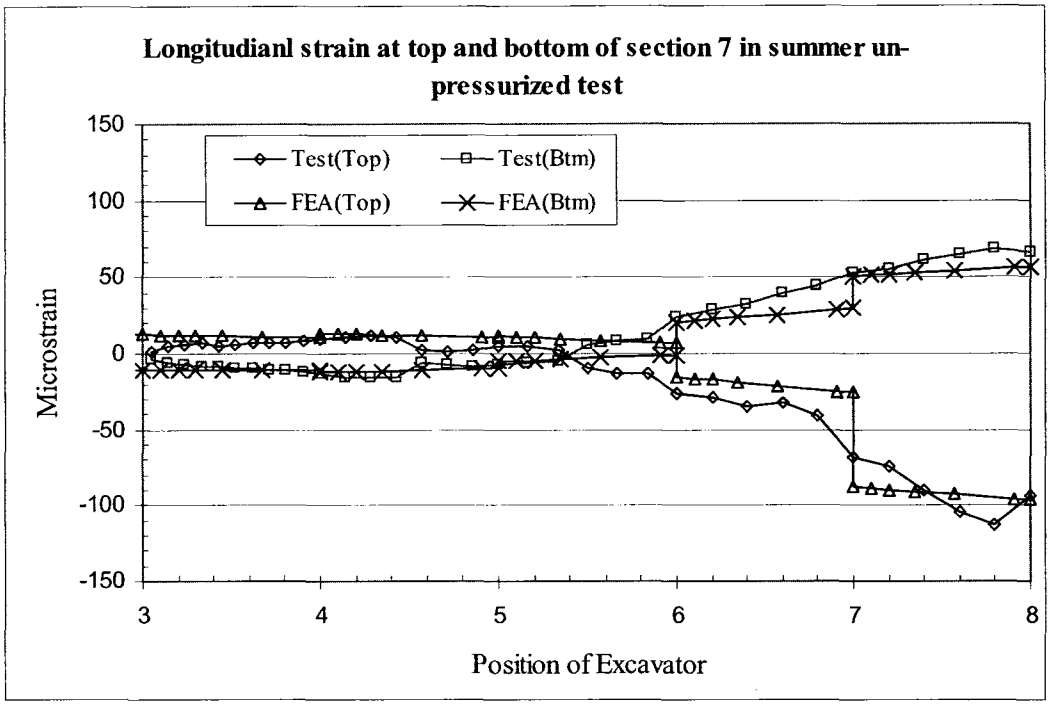

Figure 8.21 Comparison of longitudinal strain at top and bottom of section 7 between test and FEA results

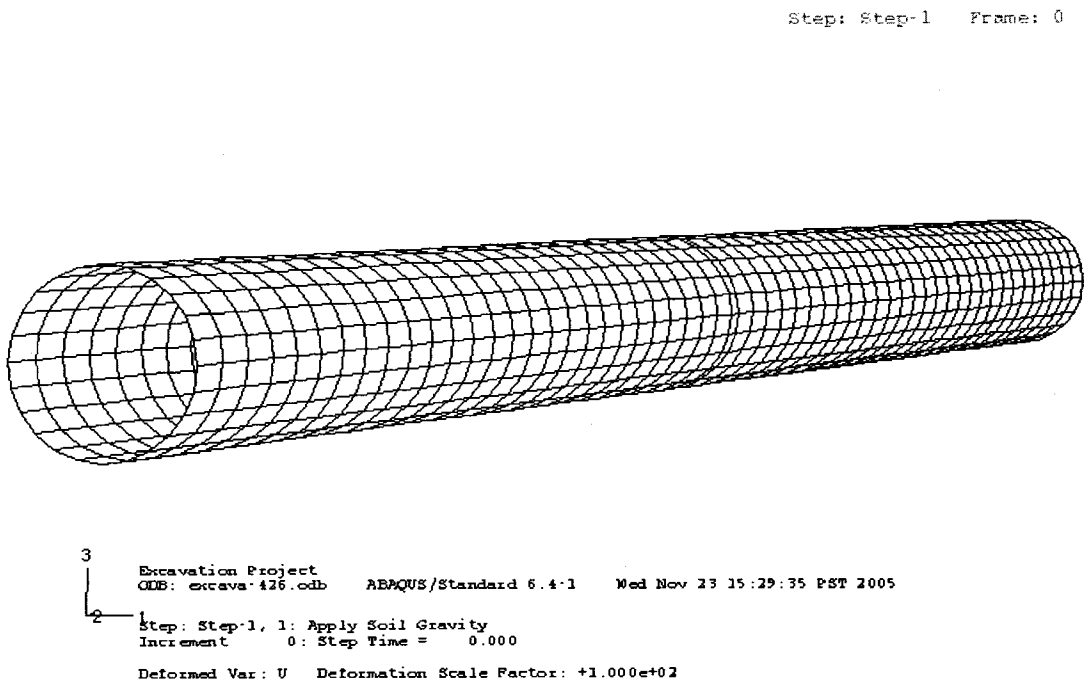

(1) Original state

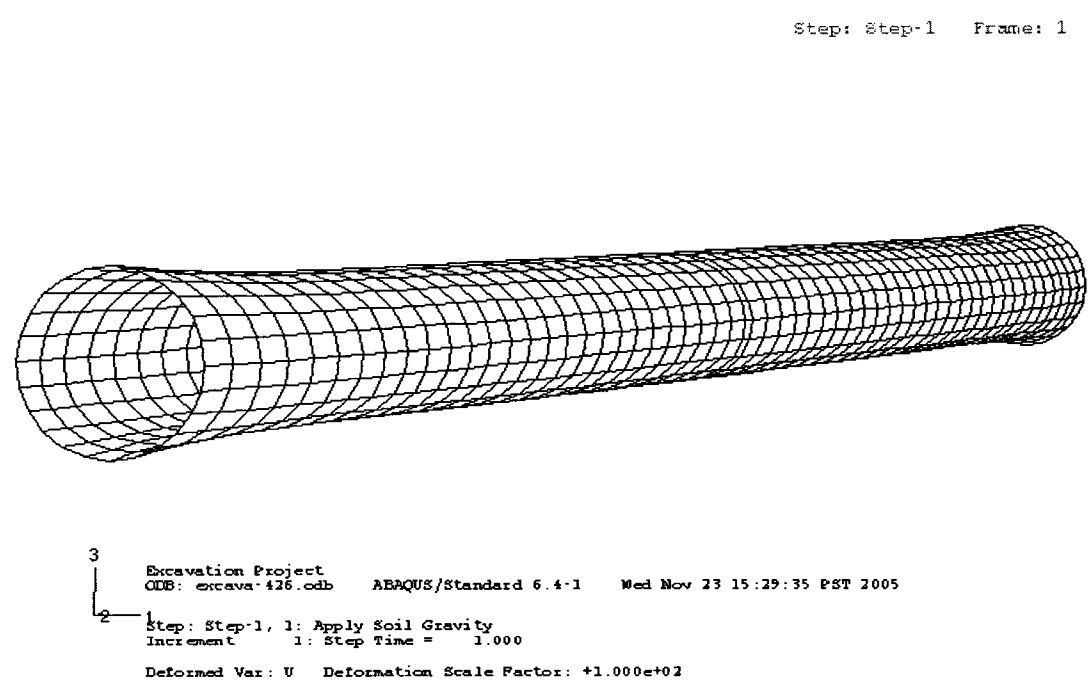

(2) Applied gravity loads

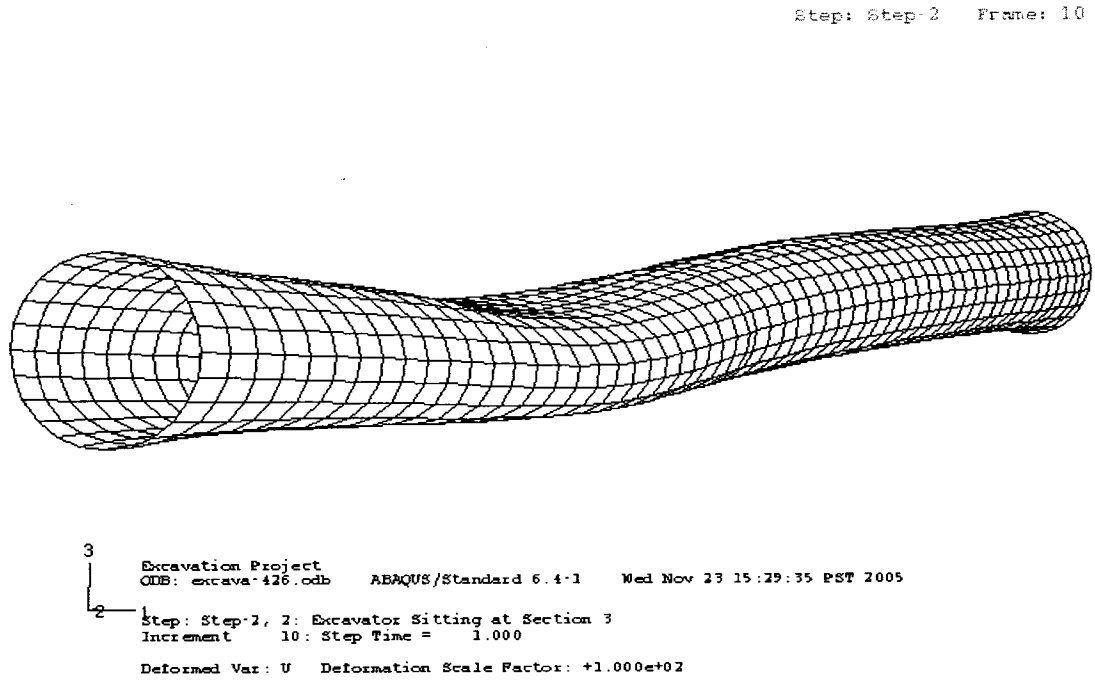

(3) Excavator sitting at section 3

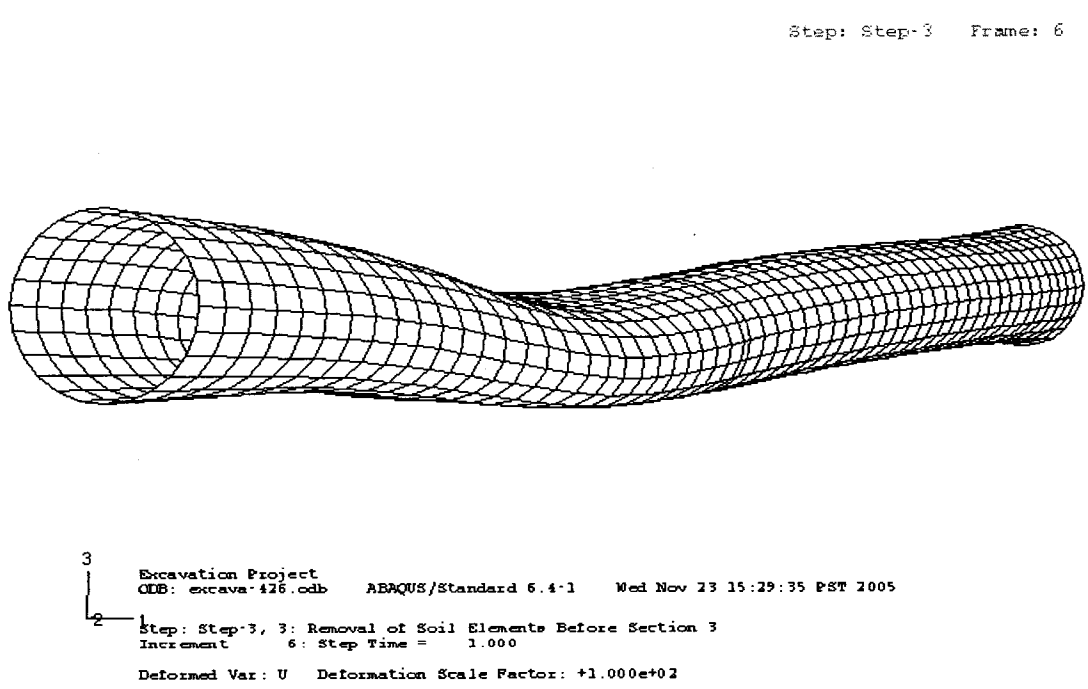

(4) Removal of soil before section 3

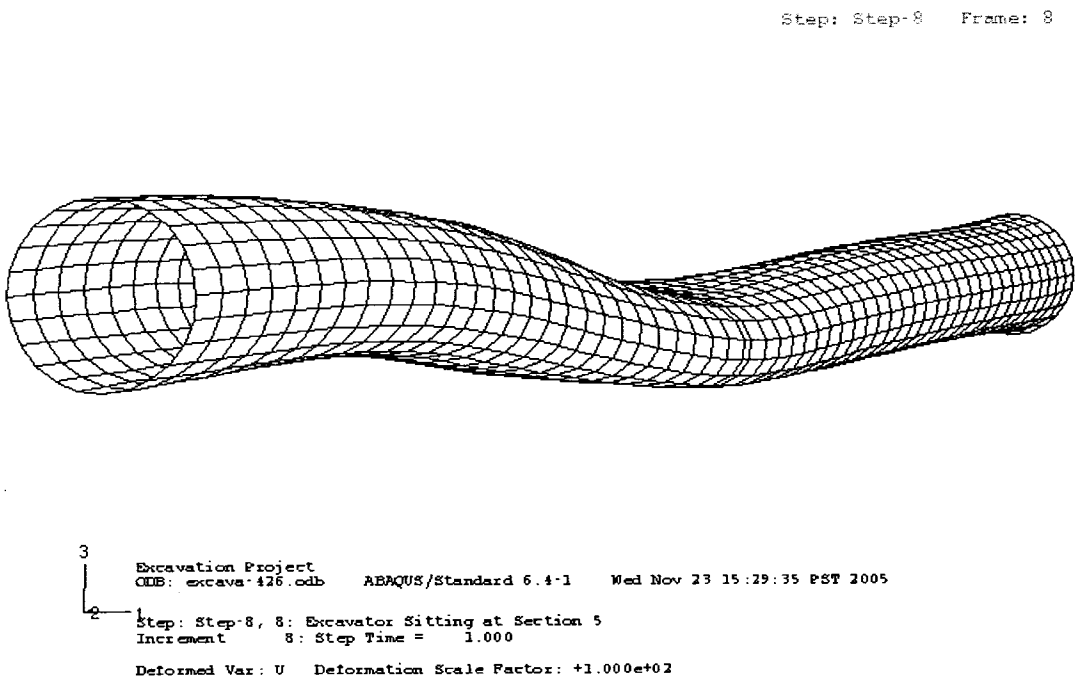

(5) Excavator sitting at section 5

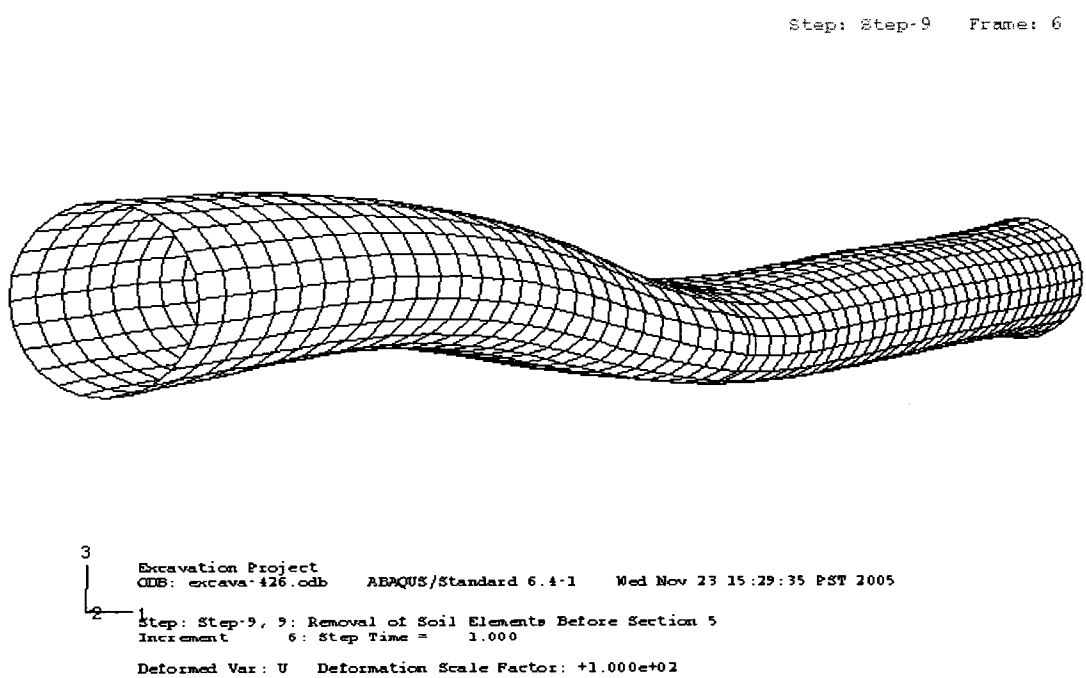

(6) Removal of soil before section 5

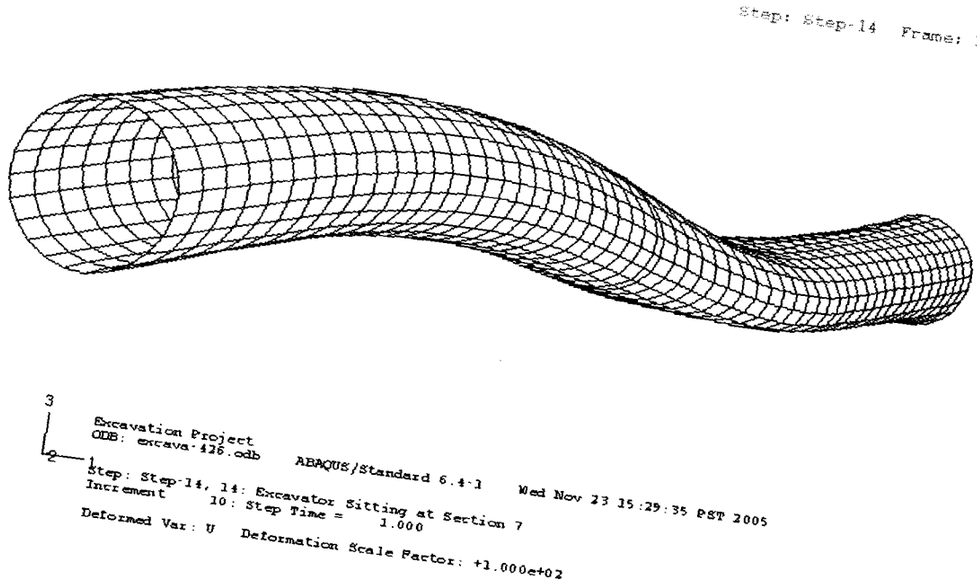

(7) Excavator sitting at section 7

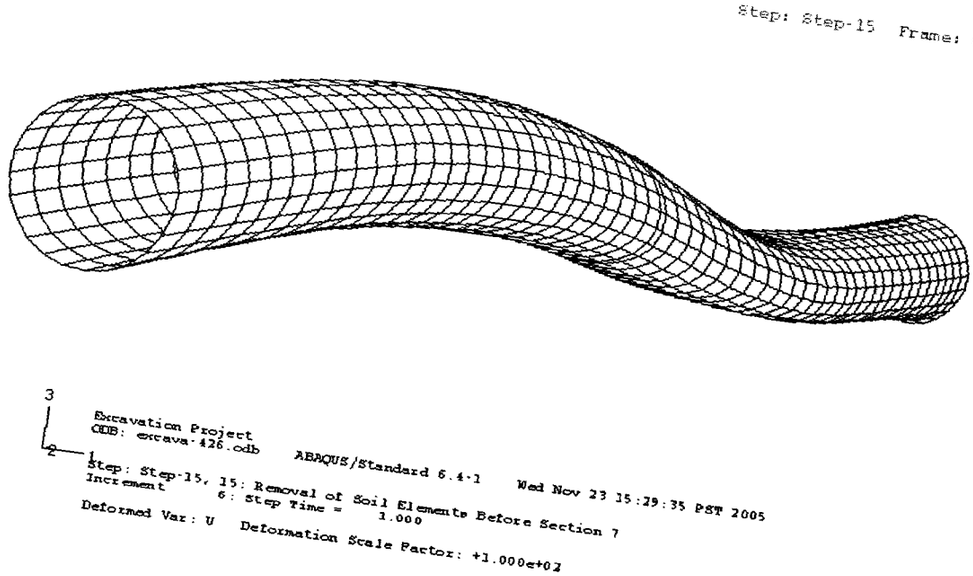

(8) Removal of soil before section 7

Figure 8.22 Typical process of deformation in excavation

9 SUMMARY, CONCLUSIONS AND RECOMMENDATIONS

9.1 Summary

The study and investigation of excavation effects on the buried pipeline are very important to the safety and maintenance of pipeline. A series of experiments were conducted in the field on a specimen to investigate the behavior of buried pipeline in the process of excavation. The main parameters were the soil conditions (unfrozen in summer and frozen in winter) and internal pressure (0% and 50%).

1) The maximum hoop strain, ovalization and longitudinal strain for the summer and winter pressurized (50%) and un-pressurized tests (0%) were obtained in the excavation process.
2) The critical condition to produce the maximum strain and deformation on the specimen were analyzed respectively.
3) The effects of internal pressure in summer and winter tests were investigated.
4) The effects of frozen soil were analyzed and compared with the unfrozen soil condition.
5) The impact factors were analyzed due to the weight and rocking of excavator on the instrumented section located under the excavator track shoes.
6) A series soil tests, classification tests and triaxial tests were conducted for the determination of soil parameters used in the soil material model in ABAQUS.
7) A finite element model was established using ABAQUS to simulate the excavation process and validated with field summer un-pressurized test.
8) The results of FEA model agreed very well with test results.

9.2 Conclusions

The following conclusions can be drawn from the analysis of the excavation field tests and FEA model.

1) The pipeline basically experienced through-wall or localized bending in the cross section by observing the inside and outside hoop strains. It also bent longitudinally or globally in the axial direction as evidenced by observing the top and bottom longitudinal strains.
2) In summer tests, the maximum strain and deformation happened in two critical conditions. Basically, the ring or portion of the pipeline under the excavator was flattened in hoop direction and bent downwards in longitudinal direction when the excavator was sitting on it. On the contrary, the ring or portion of the pipeline exposed due to the removal of soil was re-rounded in hoop direction and bent upwards in longitudinal direction.
3) In winter tests, the maximum strain and deformation occurred in four critical conditions. The first two critical conditions are the same as in the summer tests which are the basic behavior in the excavation process. The digging impact is significant and caused the maximum hoop strain on the ring or that portion of the pipeline being excavated before the excavator. In winter excavation test, the soil at the top of pipeline was left in place because of the need to protect the sealing glands and the difficulty in removing hard frozen soil. As a result, the loss of lateral soil support increased the deformation.
4) In the pressurized excavation test, the sections near the section which was under the excavator re-rounded because of the combining action of the internal pressure and rocking of excavator.

5) Internal pressure has the most significant effect on the reduction of the additional hoop strain caused by the action of excavator (critical condition 1). After the ring of pipeline was re-rounded due to the removal of soil around it (critical condition 2), the internal pressure can also reduced the maximum hoop strain and ovalization by about 50% in summer tests. This is because the pipeline section has already re-rounded by the internal pressure. The change of deformation under internal pressure is similar to the hoop strain. The effect of internal pressure is not as significant on the longitudinal strain as that on hoop strain in the tests.

6) In winter the maximum hoop strain and ovalization was caused by the digging of the excavator bucket. The impact of the bucket digging was proved to be the most critical condition to produce the maximum hoop strain (critical condition 3). In winter the maximum ovalization happened at the instrumented section being excavated by the excavator (critical condition 4). In the summer the maximum strain and ovalization occurred under critical condition 1 and 2.

7) In winter tests, the transient maximum strains were captured by high speed DAQ (100Hz) and the strain reversal was measured by either high speed (100Hz) or low speed DAQ (1 Hz). This resulted from the significant digging force because of the frozen soil in winter.

8) During excavation process, the temperature hardly changed and its effect on the pipeline was negligible.

9) A comparative study of the tests under same condition was performed in summer un-pressurized tests 1 and test 2. The strain history agreed well and the maximum strain was close. The slight difference in the results between test 1 and 2 resulted

from the variation of soil compaction and probably different excavation procedure in two tests.

10) Impact due to the rocking of excavator in the excavation process is significant under critical condition 1 and the impact factor was obtained by the analysis of test data. The digging impact can cause the hoop strain to increase by190με in winter un-pressurized test under critical condition 3.

11) The parameters of the soil material model were determined based on soil tests. The material model of soil used in the FEA model was the critical state (clay) plasticity model in ABAQUS.

12) The FEA model was established to simulate the excavation process. It can give the same trend of strain and deformation in the whole excavation process as in the test. The model can predict well the hoop strain, longitudinal strain and deformation while comparing with the test static values.

13) Using the impact factors based on tests and static values predicted by the FEA model, the maximum dynamic values (strain or deformation) can also be predicted well.

9.3 Recommendations

Based on the serial field excavation tests, the strain and deformation under specific condition were obtained and the critical condition was analyzed. The effects of internal pressure, soil condition and temperature were investigated based on the test results. A FEA model was established to simulate the excavation process and the results were validated with field test. The soil material model was determined and the parameters

of the model were based on the soil test results. The following recommendations are given for the future work:

1) It is recommended that a simulation of pressurized test to be performed to compare with the pressurized excavation test results.
2) In winter, the soil properties of frozen soil have changed. The consideration should be given to the future work.
3) Since the loading is a dynamic in nature, it is recommended to establish a dynamic model to simulate the excavating processes.

REFERENCES

American Lifeline Alliance, July, 2001, *Guideline for the Design of Buried Steel Pipe*, ASCE, American Society of Civil Engineers, USA.

Atkins, J.H. and Bransby, P.L., 1978, *The Mechanics of Soils, An Introduction to Critical State Soil Mechanics*, McGraw-Hill Book Company (UK) Limited, London.

Braun, Jill; Bukovansky, Michal; Major, Graeme and West, Donald O., 1998, "Geologic Hazards Reconnaissance and Mitigation, and Implications to Natural Gas Pipeline Operations and Risk Management", *Proceedings of the International Pipeline Conference*, Vol. 1, ASME, pp47~57.

Canadian Standards Association, 2003, *Oil and gas pipeline system*, 4th Edition, CSA Z662, Ontario, Canada

Das, Braja M., 1985, *Principles of Geotechnical Engineering*, PWS Engineering, Boston, MA, USA.

Desai, Chandrakant S. and Siriwardane, Hema J., 1984, *Constitutive Laws for Engineering Materials with Emphasis on Geologic Materials*, Prentice-Hall, Inc., Englewood Cliffs.

Duncan, J.M. and Chang, C.Y., 1970, "Nonlinear Analysis of Stress and Strain in Soils", *Journal of the Soil Mechanics and Foundations Division*, proceedings of the ASCE, September, pp1629-1653.

Hibbitt, Karlsson, & Sorenson, Inc., (HKS), 2004, *ABAQUS / Standard User's Manual*, Version 6.5, Hibbitt, Karlsson, & Sorenson, Inc., Pawtucket, Rhode Island.

Hibbitt, Karlsson, & Sorenson, Inc., (HKS), 2004, *ABAQUS Theory Manual*, Version 6.5, Hibbitt, Karlsson, & Sorenson, Inc., Pawtucket, Rhode Island.

Hibbitt, Karlsson, & Sorenson, Inc., (HKS), 2004, *ABAQUS Benchmarks*, Version 6.5, Hibbitt, Karlsson, & Sorenson, Inc., Pawtucket, Rhode Island.

Lambe, T. William and Whitman, Robert V., 1969, *Soil Mechanics,* John Wiley & Sons, Inc.

McCoy, Jackie and Ironside, Scott, 2004, "Dent Management Program", *Proceedings of the 5th Biennial International Pipeline Conference*, IPC, Vol. 2, pp 1211-1217.

Moser, A.P., 2001, *Buried Pipe Design*, 2nd Edition, McGraw-Hill.

Rizkalla, M., Turner, R.D., and Colquhoun, I.R., 1993, "State of Development of A Fibre Optic Technology-Based Pipeline Structural Integrity Monitoring System", OMAE, Vol. V, Pipeline Technology, pp295~302.

Schofield, A., and Worth, C., 1968, *Critical State Soil Mechanics*, McGraw-Hill, London

Wood, D. M., 1990, *Soil Behaviour and Critical State Soil Mechanics*, Cambridge University Press.